

**Part 1: A novel semi-synthetic approach to Taxol from
9-dihydro-13-acetylbaccatin III**

**Part 2: The rational design of a squaramide based hydrogen bond donor
organocatalyst**

by

David Norman

B.Sc. Honours, University of New Brunswick, 2000

A Dissertation Submitted in Partial Fulfillment

of the Requirements for the Degree of

Doctor of Philosophy

in the Graduate Academic Unit of Chemistry

Supervisor: Dr. G. Deslongchamps, Chemistry

Examining Board: Dr. Bryan Crawford, Biology

Dr. Larry Calhoun, Chemistry

Dr. James Tait, Chemistry

External Examiner: Dr. Pablo Ballester, ICREA Professor, Catalonia, Spain

This dissertation is accepted by the

Dean of Graduate Studies

THE UNIVERSITY OF NEW BRUNSWICK

February, 2010

©David Norman, 2010



Library and Archives
Canada

Published Heritage
Branch

395 Wellington Street
Ottawa ON K1A 0N4
Canada

Bibliothèque et
Archives Canada

Direction du
Patrimoine de l'édition

395, rue Wellington
Ottawa ON K1A 0N4
Canada

Your file Votre référence
ISBN: 978-0-494-87677-0

Our file Notre référence
ISBN: 978-0-494-87677-0

NOTICE:

The author has granted a non-exclusive license allowing Library and Archives Canada to reproduce, publish, archive, preserve, conserve, communicate to the public by telecommunication or on the Internet, loan, distribute and sell theses worldwide, for commercial or non-commercial purposes, in microform, paper, electronic and/or any other formats.

The author retains copyright ownership and moral rights in this thesis. Neither the thesis nor substantial extracts from it may be printed or otherwise reproduced without the author's permission.

AVIS:

L'auteur a accordé une licence non exclusive permettant à la Bibliothèque et Archives Canada de reproduire, publier, archiver, sauvegarder, conserver, transmettre au public par télécommunication ou par l'Internet, prêter, distribuer et vendre des thèses partout dans le monde, à des fins commerciales ou autres, sur support microforme, papier, électronique et/ou autres formats.

L'auteur conserve la propriété du droit d'auteur et des droits moraux qui protègent cette thèse. Ni la thèse ni des extraits substantiels de celle-ci ne doivent être imprimés ou autrement reproduits sans son autorisation.

In compliance with the Canadian Privacy Act some supporting forms may have been removed from this thesis.

While these forms may be included in the document page count, their removal does not represent any loss of content from the thesis.

Conformément à la loi canadienne sur la protection de la vie privée, quelques formulaires secondaires ont été enlevés de cette thèse.

Bien que ces formulaires aient inclus dans la pagination, il n'y aura aucun contenu manquant.

Canada

DEDICATION

For my daughter Annalise and son Aden

ABSTRACT

Taxol® has received considerable attention as an anticancer drug since it was first found to have antitumor properties some 30 years ago. Originally obtained from the bark of Pacific Yew trees, today all commercial sources are from partial synthesis procedures using easily obtainable and abundant intermediates. One of these intermediates, 9-dihydro-13-acetylbaccatin III, is found in yew trees in Eastern Canada and developing a new synthetic route to Taxol® from 9-dihydro-13-acetylbaccatin III would provide the opportunity of preparing anticancer compounds in Eastern Canada or more specifically New Brunswick from local biomass.

Given the length of time that Taxol has been investigated numerous methods of partial synthesis has been reported all of which entail multistep synthetic procedures. From the onset we too anticipated following similar but novel routes but later discovered a unique “one-pot” procedure where much of the chemistry is done in one reaction vessel without recourse to much chromatographic separation. After this one-pot procedure a single purification step provides material in high yield which can be potentially converted to Taxol® in 2 steps.

The second part of this thesis details work towards the design of a novel hydrogen bond squaramide-based organocatalyst. The design entailed introducing features to display the squaramide-based organocatalyst in a catalytically active conformation. Studies showed the catalyst to promote additions to carbonyl compounds but most interestingly

during investigation of promoting the Baylis-Hillman reaction we discovered that squaramides as monoanions could catalyze the aldol reaction.

Lastly, a new quantum mechanics method is introduced to study current organocatalytic reactions and assist in the development of new organocatalysts. The method is an extension of the valuable “reverse-docking” technique reported by G. Deslongchamps as a method to study enantioselective organocatalytic reactions.

ACKNOWLEDGEMENTS

First I would like to thank my supervisor, Dr. Ghislain Deslongchamps. Without the opportunity to work with him none of this would be possible. He is an exceptional teacher and mentor who has always allowed me to work independently and investigate my curiosities. Most importantly his door was always open to talk, whether it was about chemistry or life.

Second, I thank my parents David and Glenda. I am the person I am today because of them. From a very young age they instilled in me the importance to succeed academically and my dedication to learning has stemmed from that.

Lastly, I thank my wife Katherine. For the sacrifices you made to make this possible I will always be grateful.

Lay Summary

Chapter 1

Since the discovery of antitumor properties of Taxol®, there has been considerable effort towards the semi-synthesis of this molecule. Finding semi-synthetic routes has been important given the limited availability of Taxol® as a natural product. Fortunately, intermediates including baccatin III and 9-dihydro-acetyl-baccatin III are readily available natural products from renewable resources. Interestingly, 9-dihydro-acetyl-baccatin III is found in New Brunswick biomass and finding novel routes for the conversion to Taxol® would provide the opportunity to produce anticancer drugs here in New Brunswick.

Many of the methods used to convert either baccatin III or 9-dihydro-acetyl-baccatin III to Taxol® involve a multistep process of protection chemistry, performing the desired chemistry, and deprotection chemistry; resulting in procedures that are time consuming and costly. We looked to develop a process that through our protection/deprotection chemistry a key transformation (we call an ‘oxidative fragmentation’) would occur given us directly key intermediates to Taxol®.

Unfortunately, the oxidative fragmentation chemistry proved difficult to develop but through observations made during this investigation we developed novel chemistry which allowed us to perform 3 key steps in known Taxol® semi-synthetic procedures in one reaction providing a shorter synthetic route to Taxol®.

Chapter 2

Over the last decade a new field in organic chemistry has developed known as organocatalysis, the catalysis of asymmetric organic reactions by small organic molecules. Two common modes of catalysis are covalent and hydrogen bonding. For covalent catalysis, there is a covalent transition state intermediate formed between catalyst and reactant(s) while for hydrogen bonding catalysis hydrogen bonding is used to activate reactant(s) and stabilize transition states. A common hydrogen bond catalyst is thiourea. As will be detailed in this thesis we are of the opinion thiourea has disadvantages as an organocatalyst and a catalyst designed on a squaramide scaffold would be superior.

Efforts to develop squaramide as an organocatalyst entailed introducing functionality to control the conformation, a vital feature that we show important in the catalysis of the Diels-Alder reaction.

In testing the scope of reactions that our conformationally controlled squaramides could catalyze we inadvertently discovered that squaramide monoanions were effective catalysts for the aldol reaction. This is the first report of catalyzing the aldol reaction via hydrogen bonding and it is reminiscent of how nature catalyzes enolization reactions. This is a key discovery which will lead to the discovery of new catalysts using this novel mode of catalysis.

Lastly we investigate methods of designing organocatalyst assisted by computational chemistry and a significant contribution is made to the ‘reverse docking’ technique previously developed in the Deslongchamps research group. Also discussed is the importance of hydrogen bond strength for hydrogen bond catalysis and how computational methods can be used to analyze this feature and assist in catalyst design.

Table of Contents

Title Page	i
Dedication	ii
Abstract	iii
Acknowledgements	v
Lay Summary	vi
Table of Contents	ix
List of Tables	xii
List of Figures	xiv
List of Symbols, Nomenclature or Abbreviations	xx

Chapter 1. A novel semi-synthetic approach to Taxol from 9-dihydro-13-acetylbaccatin III.

1.1 Taxol and Taxotere

- | | |
|--|---|
| 1.1.1 Discovery and significance of Taxol | 1 |
| 1.1.2 Current synthetic approaches to biologically relevant taxane | 2 |

1.2 A novel semi-synthetic approach to taxane: A computational study

- | | |
|---|----|
| 1.2.1 Grob-type fragmentation to oxidize C-9 hydroxyl | 12 |
|---|----|

1.3 A novel semi-synthetic approach to taxane: Results and Discussion

- | | |
|-----------------------------|----|
| 1.3.1 Ketalization of 9-DHB | 22 |
| 1.3.2 Direct oxidation | 25 |

1.4 Potential alternative oxidants for the One-Pot procedure	
1.4.1 Pfitzner-Moffatt oxidation	39
1.4.2 Parikh-Doering oxidation	40
1.4.3 Other activated DMSO mediated oxidations	41
1.4.4 Corey-Kim oxidation	42
1.4.5 Pyridinium dichromate (PDC)	43
1.4.6 Pyridinium chlorochromate (PCC)	44
1.5 Conclusion	45

Chapter 2. The rational design of a squaramide based hydrogen bond donor organocatalyst.

2.1 Organocatalysis	
2.1.1 The beginnings of a new scientific field	46
2.1.2 Hydrogen bonding as a mode of activation by organocatalysts	49
2.2 The rational design of a new organocatalyst	
2.2.1 Squaramide as a functional organocatalyst	53
2.2.2 Testing squaramide's catalytic activity	66
2.2.3 Attempts towards the synthesis of 2 nd generation squaramides	68
2.2.4 Squaramide self-templated macrocyclization	70
2.2.5 Squaramide catalyzed enolate addition reactions	77
2.3 Computational chemistry	
2.3.1 Computational chemistry and organocatalysis	95

2.3.2 Hydrogen bonding and organocatalysis	100
2.3.3 Reverse docking and quantum mechanics	102
2.4 Future of organocatalyst design	
2.4.1 Future work towards the rational design of an organocatalyst	109
Chapter 3. Experimental procedures and spectral data	
3.1 General	
3.1.1 Conditions for the enhancement of the Diels-Alder reaction by conformationally controlled squaramides	114
3.1.2 General procedure for aldol using Baylis-Hillman conditions	114
3.1.3 Preparation of squaramide monoanion	114
3.1.4 Squaramide monoanion catalyzed enolization of d ₆ -acetone	114
3.1.5 General procedure for squaramide monoanion catalysis of the direct aldol reaction	115
3.2 Preparation of compounds	116
<i>References</i>	138
<i>Appendix</i>	
A1. ¹ H NMR spectra	144
A2. ¹³ C NMR spectra	166
Vitae	

List of Tables

Table 1 - Results of both the axial and equatorial epimers of bromoacetaldehyde 9-DHB 7,9-acetal analyzed by molecular dynamics	17
Table 2 - Results for the equatorial epimers of chloroacetaldehyde 9-DHB 7,9-acetal analyzed by molecular dynamics	18
Table 3 - Select results from a molecular dynamics (NVT, 300 K) simulation over a time of 5000 ps	21
Table 4 - Influence of solvent on the product ratios (determined by NMR) of the direct oxidation of 9-DHB with RuO ₄	29
Table 5 - Optimization of C7-mixed acetal formation	35
Table 6 - The 2-step, one-pot protection/oxidation reaction	37
Table 7 - Catalysis of the Diels-Alder reaction by thioureas	52
Table 8 - Major squaramide conformers from systematic conformational search. Relative energy of B3LYP/6-31G* optimized structures	61
Table 9 - The ¹ H NMR chemical shift of thioamide protons of the indicated compounds as a 10 mM solution in CDCl ₃	62
Table 10 - Ratio of free phosphine to betaine intermediate as a function of added squaramide catalysts. Values calculated by integration of ³¹ P-NMR signals	81
Table 11 - Squaramide catalyzed aldol reaction using Baylis-Hillman conditions	82
Table 12 - Rate of squaramide catalyzed enolization of acetone- <i>d</i> ₆	93
Table 13 - Squaramide monoanion catalysis of the direct aldol reaction	94
Table 14 - Correlation between the conversion in organocatalyzed Diels-Alder reactions and hydrogen bonding energies determined by	

Morokuma decomposition (HF/6-31G*). For catalyst structures, see Table 7	102
Table 15 - Comparison of calculated RESP charges compared to experimental pK _a values of the parent carboxylic acids	103
Table 16 - Catalysis of hetero Diels-Alder reaction with chiral oxazoline catalysts and the relationship between acidity, conversion and enantioselectivity, as reported by Sigman	105
Table 17 - Reverse-docking MM energies (five lowest energies) and hydrogen bonding type in the interaction of Sigman catalyst 1 to the “SR” hetero Diels-Alder transition state model and docking energies recalculated by quantum mechanics (HF/6-31G*)	107
Table 18 - Reverse-docking MM energies (five lowest energies) and hydrogen bonding type in the interaction of Sigman catalyst 1 to the “RS” hetero Diels-Alder transition state model and docking energies recalculated by quantum mechanics (HF/6-31G*)	108
Table 19 - The first five ranking AM1 minimized catalytic poses initially calculated by molecular mechanics and compared to rankings from QM calculations	109

List of Figures

Figure 1 - Structure of paclitaxel	1
Figure 2 - Chemical structures of two common metabolites used as intermediates in the semi-synthesis of paclitaxel	3
Figure 3 - Structure of baccatin III	4
Figure 4 - Greene/Potier paclitaxel semi-synthesis	5
Figure 5 - Synthetic work leading to the discovery of Taxotere®	6
Figure 6 - Holton/Ojima β -lactam approach	7
Figure 7 - Kingston oxazoline route	8
Figure 8 - Zamir conversion of 9-DHB into 7-protected baccatin III	9
Figure 9 - Liu conversion of 9-dihydro-13-acetylbaccatin III to 10-deacetylbaccatin III, baccatin III and paclitaxel	10
Figure 10 - Kasitu conversion of 9-dihydro-13-acetylbaccatin III to 9-oxo-13-acetylbaccatin III and subsequent conversion to 10-deacetylbaccatin III and baccatin III	11
Figure 11 - Findlay conversion of 9-dihydro-13-acetylbaccatin III to 10-deacetylbaccatin III	12
Figure 12 - Grob fragmentation showing the stereoelectronic requirement of the electrofuge (E) lone pair and nucleofuge about the C ₁ -C ₂ bond	12
Figure 13 - Grob fragmentation of (a) Wieland-Miescher ketone to Thapsigargin and (b) epoxy alcohol fragmentation in the synthesis of Taxol AB ring system	13

Figure 14 - Comparison of Grob fragmentation (below) to the proposed oxidative fragmentation of the 7,9-acetal (above). R ₂ is a suitable leaving group	14
Figure 15 - Possible fragmentation patterns of the 7,9-acetal via fragmentation initiated by elimination at C ₉ -H (left) or C ₇ -H (middle), or via 1,2-elimination (right)	14
Figure 16 - Bromo- and chloroacetaldehyde acetals can exist as (a) two epimers and (b) three different rotamers about the C _{acetal} -C bond	15
Figure 17 - The C ₉ hydrogen (pink) and acetal hydrogen (blue) in their respective steric environment	19
Figure 18 - Direct oxidation of 9-DHB	25
Figure 19 - Oxidation of unprotected 9-DHB	26
Figure 20 - A ruthenium catalysed regioselective monooxidation of a 1,2-diol	26
Figure 21 - Elimination of the ruthenium ester	27
Figure 22 - Direct oxidation of 9-DHB	27
Figure 23 - The competitive nucleophilic addition of water and Oxone® to the cyclic ruthenium-diol intermediate	28
Figure 24 - S _N 2-like addition of Oxone® to ruthenium-9-DHB cyclic intermediate and subsequent oxidation	30
Figure 25 - Influence of sterics on ruthenium mediated oxidation	30
Figure 26 - Solvation at the C ₇ hydroxyl resulting in preference for Oxone® approach on the C ₉ side of the ruthenium cyclic intermediate	31
Figure 27 - Templating effect promoting addition to the C ₉ side of the ruthenium cyclic intermediate	32

Figure 28 - Formation of mixed acetals when 9-DHB is treated with vinyl ethers	33
Figure 29 - Formation of the thermodynamic favored C7-mixed acetal	34
Figure 30 - Oxidation of 7-acetal	34
Figure 31 - The one-pot protection/oxidation/deprotection	38
Figure 32 - General procedure and proposed process for the Pfitzner-Moffatt oxidation	40
Figure 33 - General procedure and proposed process for the Parikh-Doering oxidation	41
Figure 34 - Formation of chlorodimethylsulfonium chloride described by Corey and Kim	42
Figure 35 - Corey-Kim oxidation	43
Figure 36 - Hajos-Parish reaction	46
Figure 37 - Hydrogen bonding catalyst of Jacobson (49), Corey (50), and Miller (51)	47
Figure 38 - Intermolecular aldol reaction catalyzed by L-proline	48
Figure 39 - Results of a Scifinder Scholar search of the keyword organocatalysis	49
Figure 40 - Reports of thiourea as an organocatalyst since 2003 report of noncovalent catalysis of the Diels-Alder reaction	54
Figure 41 - The major conformation of secondary squaramides that exist in solution	55
Figure 42 - Intermolecular assembly of secondary squaramides into oligomers (left) and dimers (right)	56
Figure 43 - ROESY contacts in squaramide 67	56

Figure 44 - Proposed squaramide conformation equilibrium shift upon intramolecular hydrogen bonding to squaramide carbonyls	57
Figure 45 - Synthesis of conformational controlled squaramides	58
Figure 46 - The sequential addition of amines to give either symmetrical or non-symmetric squaramides	59
Figure 47 - Barrier of rotation about squaramide C-N bond	60
Figure 48 - Serial dilution NMR study of squaramide 68	63
Figure 49 - X-ray structures of squaramides 68 , 69 , and 70	64
Figure 50 - VT- ¹ H NMR of squaramide 68	65
Figure 51 - Rate enhancement of Diels-Alder reaction by conformationally controlled squaramides 68 and 70	67
Figure 52 - Unsuccessful attempt of the synthesis of squaramides 74 and 75	68
Figure 53 - Proposed formation of compound 77	69
Figure 54 - Possible “ate” complexes in squaramide 78	69
Figure 55 - Synthesis of squaramide macrocycle 81	70
Figure 56 - Metal cation directed formation of 18-crown-6	71
Figure 57 - Synthesis of cyclic porphyrin oligomers templated by Bipy	72
Figure 58 - Examples of hydrogen bonded directed macrocyclization	73
Figure 59 - Molecular dynamics simulation (NVT ensemble, 600 K, 0.5 psec time step) of 80 demonstrating the propensity to self-fold	74
Figure 60 - Attempt towards the synthesis of 81	75
Figure 61 - Alternative synthesis of squaramide macrocycle precursor 79	76

Figure 62 - Squaramide macrocycle derivatives	77
Figure 63 - The Baylis-Hillman reaction and its potential rate-determining steps (RDS)	78
Figure 64 - The solvent dependence of the Baylis-Hillman reaction	79
Figure 65 - Solvent assisted elimination to give the Baylis-Hillman product	79
Figure 66 - The proposed role of the alcohol in the observed rate enhancement of the Baylis-Hillman reaction	80
Figure 67 - Squaramide catalyzed Baylis-Hillman reaction	81
Figure 68 - The requirement for enolization to give the aldol product	83
Figure 69 - Aldol reaction using LDA	83
Figure 70 - The Druckhammer enolization catalyst	84
Figure 71 - Proton shuffling via squaramide monoanion to catalyze enolization and then approximation of an electrophile for subsequent enolate addition	85
Figure 72 - Deprotonation of squaramide by the Baylis-Hillman betaine intermediate to form squaramide monoanion and the proposed subsequent catalytic cycle for the aldol reaction	86
Figure 73 - Incorporation of deuterium into cyclohexenone in the presence of squaramide 68 and n-tributylphosphine	87
Figure 74 - Squaramide monoanion and bound acetone enolization transition state (left) and bound acetone enolate to squaramide (right) optimized with B3LYP 6-31+G* in GAMESS	88
Figure 75 - Ammonia adding to acetaldehyde with two ammonium ions hydrogen bonded to both carbonyl lone pairs (left) and one ammonium group bound to a	

lone pair and one bound to the π -bond (right)	89
Figure 76 - B3LYP 6-31G* geometry optimization of acetaldehyde with ammonia and two ammonium molecules	90
Figure 77 - Reaction coordinate for the enolization of acetaldehyde and resultant positioning of ammonium molecules. Intermediate 1 (left), intermediate 2 (middle) and intermediate 3 (right)	91
Figure 78 - Reaction coordinate for the enolization of acetaldehyde and resultant positioning of tethered ammonium molecules. Intermediate 1 (left) and intermediate 2 (right)	92
Figure 79 - Squaramide 97 monoanion	95
Figure 80 - The Hajos-Parrish reaction and the transition state predicted computationally that gives the experimentally determined major product	96
Figure 81 - L-Proline catalyzed Mannich reaction leading to <i>syn</i> addition product	97
Figure 82 - Organocatalyzed Mannich reaction leading to <i>anti</i> addition product	97
Figure 83 - General illustration of the reverse-docking paradigm	99
Figure 84 - Comparing the transition state of an organocatalyzed reaction to the molecular complex obtained by reverse-docking. The example stems from Miller's peptide-catalyzed asymmetric azidation reaction	100
Figure 85 - A hydrogen bond catalyst designed by calculating interaction energies with catalyst and substrate	101
Figure 86 - Possible catalytic poses for the Sigman catalyst with the hetero Diels-Alder transition state with bifurcated (top) and cooperative hydrogen bonding (bottom)	106

List of Symbols, Nomenclature or Abbreviations

10-DAB	10-deacetylbaccatin III
9-DHB	9-dihydro-13-acetylbaccatin III
BINOL	1,1'-Bi-2-naphthol
Bipy	4,4'-bipyridyl
Bn	Benzyl
BTMA	Benzyltrimethylammonium
Bz	Benzoyl
CDI	<i>N,N'</i> -Carbonyldiimidazole
DCC	Dicyclohexyl carbodiimide
DDQ	2,3-Dichloro-5,6-dicyano-1,4-benzoquinone
DMAP	4-Dimethylaminopyridine
DMF	Dimethylformamide
DMP	Dess-Martin periodinane
DMSO	Dimethyl sulfoxide
EDC	1-ethyl-3-(3-dimethylaminopropyl) carbodiimide
ee	Enantiomeric excess
K	Kelvin
LUMO	Lowest unoccupied molecular orbital
MOM	Methoxymethyl
NCI	National Cancer Institute
NMO	<i>N</i> -Methylmorpholine- <i>N</i> -oxide
NMR	Nuclear magnetic resonance

NVT	Cononical ensemble
PCC	Pyridinium chlorochromate
PDC	Pyridinium dichromate
PMB	<i>p</i> -Methoxybenzyl
PPTS	Pyridinium <i>p</i> -Toluenesulfonate
ps	Picosecond
PTSA	<i>p</i> -Toluene sulfonic acid
Py	Pyridine
r.t.	Room temperature
RDS	Rate determining step
ROESY	Rotational nuclear Overhauser Effect Spectroscopy
TBAB	Tetrabutylammonium bromide
TESCI	Triethylsilylchloride
TFA	trifluoroacetic acid
THF	Tetrahydrofuran
THP	Tetrahydropyran
TPAP	Tetra- <i>n</i> -propylammonium perruthenate
Ts	Tosyl
VT	Variable temperature

Chapter 1. A novel semi-synthetic approach to Taxol from 9-dihydro-13-acetylbaccatin III.

1.1 Taxol and Taxotere

1.1.1 Discovery and significance of Taxol

In the late 1950's, bark extracts from the Pacific yew tree, *Taxus brevifolia*, were found to have antitumor activity by the National Cancer Institute (NCI) during a screening program of plant extracts. In 1969, Wall¹ in collaboration with NCI isolated paclitaxel (Figure 1) and showed it to be the most active ingredient. Two years later the structure of paclitaxel was elucidated from its ¹H-NMR spectrum and its structure and stereochemistry were confirmed by x-ray crystallography.¹

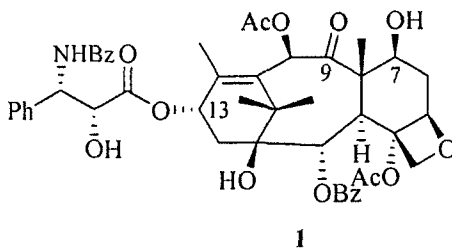


Figure 1. Structure of paclitaxel

Shortly after the structure elucidation, it was determined that the cellular target of paclitaxel was the protein tubulin, one of the two monomeric constituents of microtubules. However, the mode of action was found to be quite unique from other natural substances that were known at the time to interact with tubulin. Instead of preventing the self-assembly of microtubules, such as in the case of the action of

vinblastine, colchicine, and maytansine, paclitaxel promotes the assembly of tubulin into microtubules and prevents the disassembly.² Paclitaxel had little prospect to be used as a possible cancer drug because of its insolubility in water and the difficulty of obtaining it in large quantities from the *Taxus brevifolia* tree. Indeed, stripping the bark to extract paclitaxel results in the death of this slow-growing tree. However, after the discovery by Horwitz of the mode of action, paclitaxel quickly became a lead compound for further pharmacological studies. *In vivo* studies showed antileukemic and tumor inhibiting properties and phase I clinical investigation began in 1983 that showed activity of paclitaxel against ovarian cancers. Today paclitaxel, which is better known by its trademark name Taxol®, is used in the treatment of breast, lung and ovarian cancers and has been touted as the most important anticancer drug discovered in the last 30 years.

1.1.2 Current synthetic approaches to biologically relevant taxane

Given the biological importance and scarcity of paclitaxel as a natural product, synthesis via both total synthesis and semi-synthetic routes, has attracted much attention over the past 30 years. During the 1990s some 30 research groups worked on the total synthesis of Taxol®³ and to date 6 groups have reported successful syntheses. Despite the gratifying feeling for an organic chemist upon completing a complex synthesis and the development of new organic chemistry in the process, the total synthesis of a natural product such as paclitaxel has little value, at least from a commercial standpoint. Indeed, all the total syntheses to date involve extremely long and complex synthetic sequences, producing paclitaxel in extremely low yields, and as such are not

commercially viable. For this reason most efforts to produce paclitaxel in sufficient quantities for worldwide usage in the treatment of cancer have been directed toward semi-synthetic pathways targeting paclitaxel and other pharmaceutically important taxanes.

Two common intermediates used in the semi-synthesis of Taxol are 10-deacetylbaccatin III (10-DAB)⁴ and 9-dihydro-13-acetylbaccatin III^{5,6} (9-DHB) (Figure 2). Interestingly, both are found in the needles of *Taxus canadensis*, a yew bush, also known as ground hemlock, that is common in Eastern Canada and in the Northeastern US. 9-DHB is a major metabolite concentrated in the needles of *T. canadensis* while 10-DAB is a major metabolite found in the needles of *Taxus baccata* and in the bark of *Taxus brevifolia*.

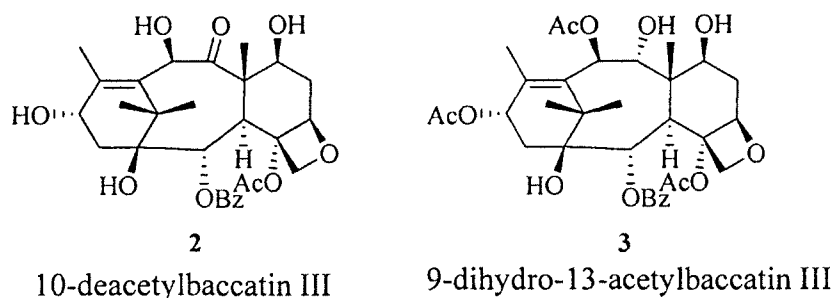


Figure 2. Chemical structures of two common metabolites used as intermediates in the semi-synthesis of paclitaxel.

In the first reported semi-synthesis of paclitaxel from 10-DAB, Greene and Potier⁷ initially attempted a selective acetylation at C10, to give baccatin III (Figure 3), but yielded acetylated product at C7 as the major product. As illustrated in Figure 4, the C7 hydroxyl showed similar selective reactivity towards TESCl yielding 7-triethylsilyl-10-

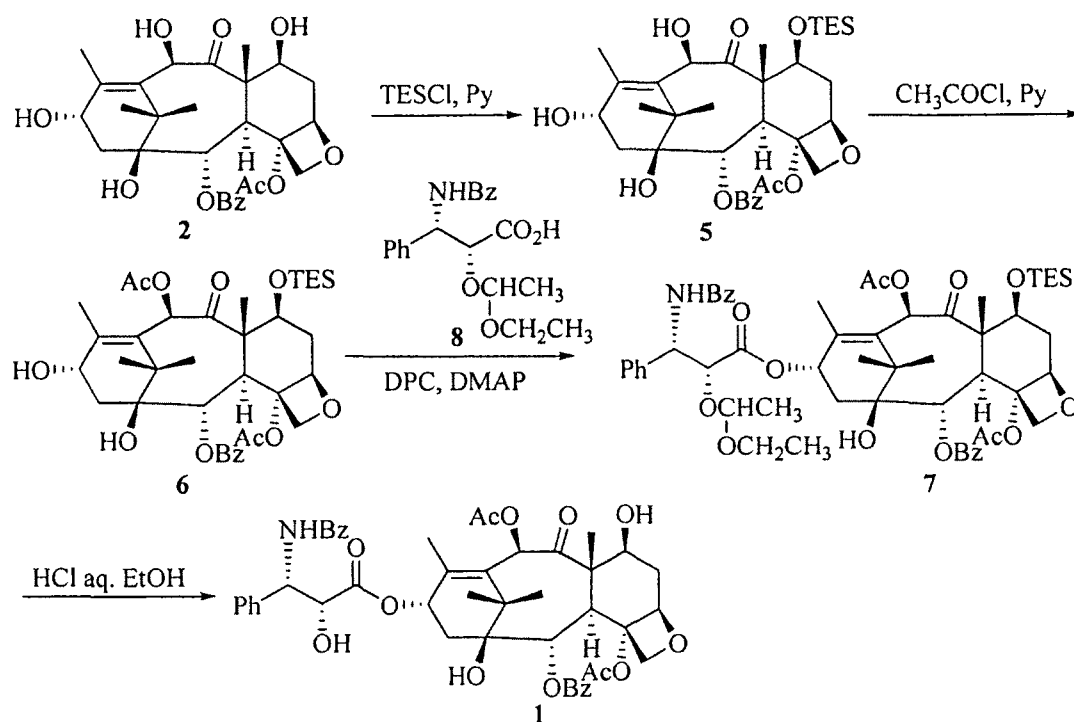


Figure 4. Greene/Potier paclitaxel semi-synthesis.

Although the Greene and Potier method converts 10-deacetylbaccatin III to paclitaxel the synthesis of the side chain is a multistep process with an overall yield of 23%.

Early investigations by Potier into side-chain attachment at C13 led to attempting the partial synthesis of paclitaxel from the more synthetically available 13-cinnamoyl derivative (9) and *tert*-butyl *N*-chloro-*N*-sodiocarbamate (10) using the Sharpless hydroxyamination procedure.⁸ There was no regioselectivity or diastereoselectivity observed in the hydroxyamination giving 4 isomers including 11 and after deprotection at C7 and C10 gave 12 which showed better activity on tubulin than paclitaxel (Figure 5).⁹ Compound 12 was later found to be more conveniently prepared in a similar

manner to the Greene/Potier paclitaxel semi-synthesis route and is now licensed and marketed by Sanofi Aventis as Taxotere®.

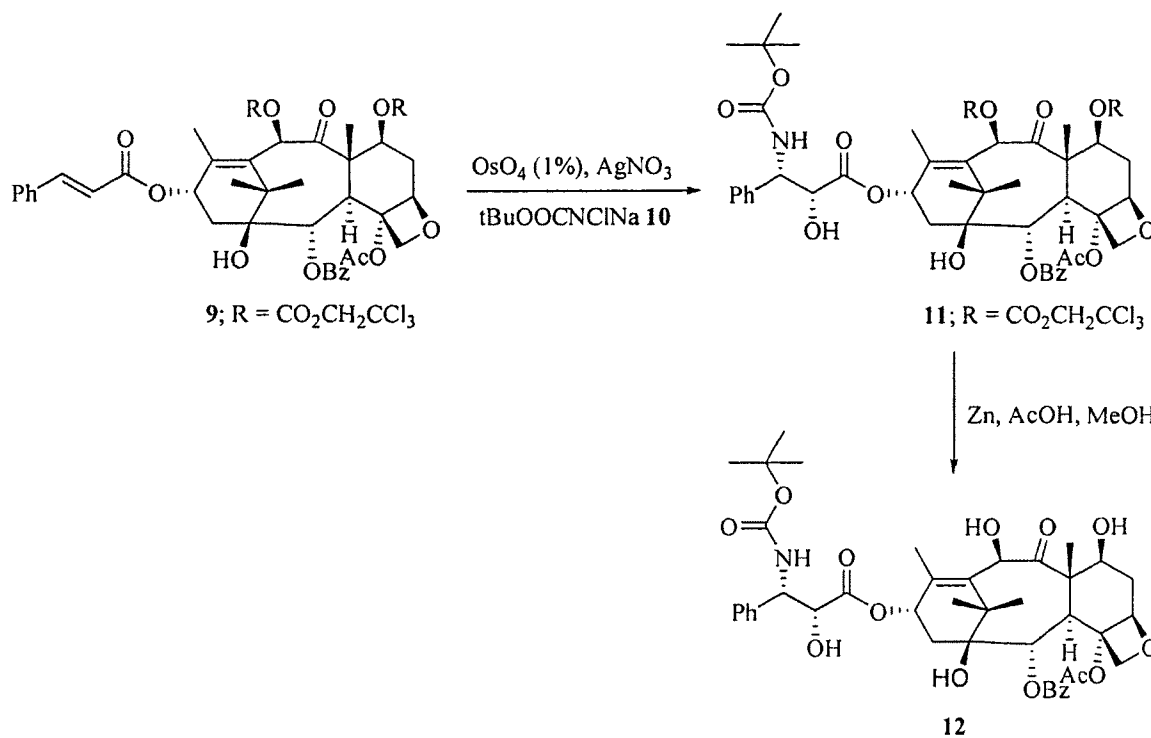


Figure 5. Synthetic work leading to the discovery of Taxotere®.

Recognizing the side chain synthesis as a disadvantage in the Greene and Potier method, Holton¹⁰ utilized a β -lactam¹¹ as a precursor to the paclitaxel side chain and the process was later licensed to Bristol-Myers Squibb (Figure 6). Although Holton describes the β -lactam approach as superior to the Greene and Potier approach, synthesis of the β -lactam is also a multistep procedure yielding only 26% of product.¹⁰

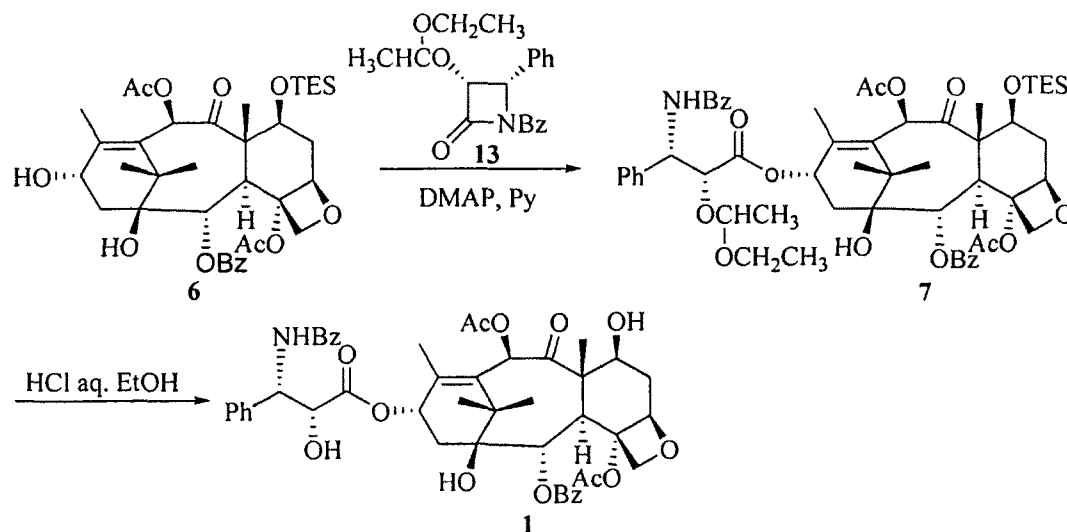


Figure 6. Holton/Ojima β -lactam approach.

Kingston¹² reported an oxazoline route which is derived from the starting material (+)-isobutyl-*trans*- β -phenyl glycidate that had been kinetically resolved via a lipase-mediated enantioselective transesterification of (\pm)-methyl-*trans*- β -phenyl glycidate.¹³ The oxazoline was obtained in a 40% yield from the glycidate which was when coupled to 7-triethylsilyl-10-deacetylbaccatin III (6). Subsequent acid hydrolysis of the oxazoline and C-7 protecting group yielded paclitaxel in a 71% yield (Figure 7).

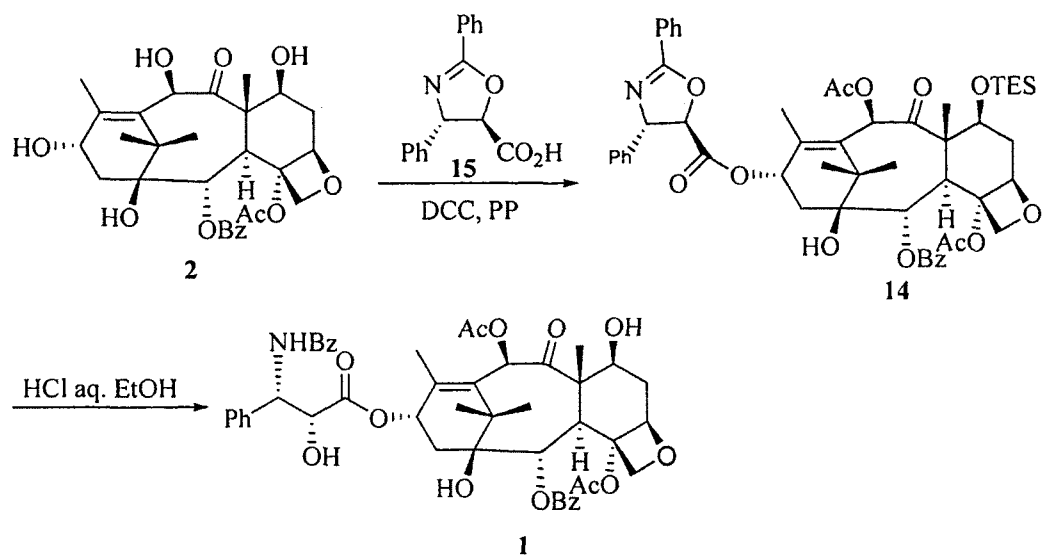


Figure 7. Kingston oxazoline route.

The above mentioned paclitaxel semi-synthetic examples all originate from the common precursor, 10-DAB. However, 9-DHB is also a plentiful metabolite, easily isolable from renewable biomass, which has also been used in the semi-synthesis of paclitaxel. Zamir,¹⁴ although on small scale and a 11% yield, converted 9-DHB to 7-protected baccatin III (**18**) via 3 steps (Figure 8). Subsequent side chain attachment and protecting group removal would then yield paclitaxel in 5 steps from 9-DHB.

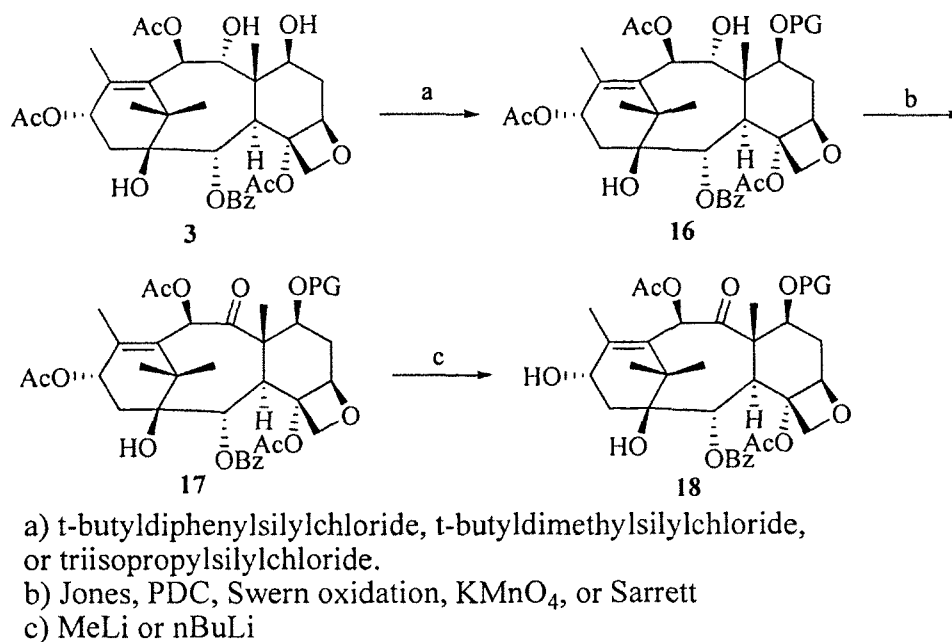


Figure 8. Zamir conversion of 9-DHB into 7-protected baccatin III.

Liu¹⁵ in 1999, filed a claim for the conversion of 9-DHB to 10-DAB and baccatin III using standard selective protection followed by oxidation and deprotection procedures (Figure 9). However, the choice of protecting group and oxidant is somewhat contentious given that a *p*-methoxybenzyl ether was used to mask the C7 hydroxyl followed by oxidation of the C9 hydroxyl with TPAP/NMO. It is strongly suspected that under these conditions the oxidant could oxidize the benzyl ether to the benzoate with subsequent hydrolysis. Also the feasibility of side chain attachment via an inactivated carboxylic acid as well as the selective removal of the C10 acetate with the use of hydride is questionable. Side chain attachment to C7 hydroxyl protected baccatin III was shown to be difficult via esterification of a phenyl isoserine derivative due to the steric environment of the C13 hydroxyl and its hydrogen bonding with the C4 acetate.⁷ It was found that DPC/DMAP and long reaction times were required for

efficient coupling giving yields of 80%.⁷ It is therefore surprising that Liu reported the esterification of inactivated phenyl isoserine. With regard to the removal of C10 acetate with hydride, Zamir reported the removal of the C13 acetate in the presence of C10 acetate using hydride with no influence on the C10 position.¹⁶

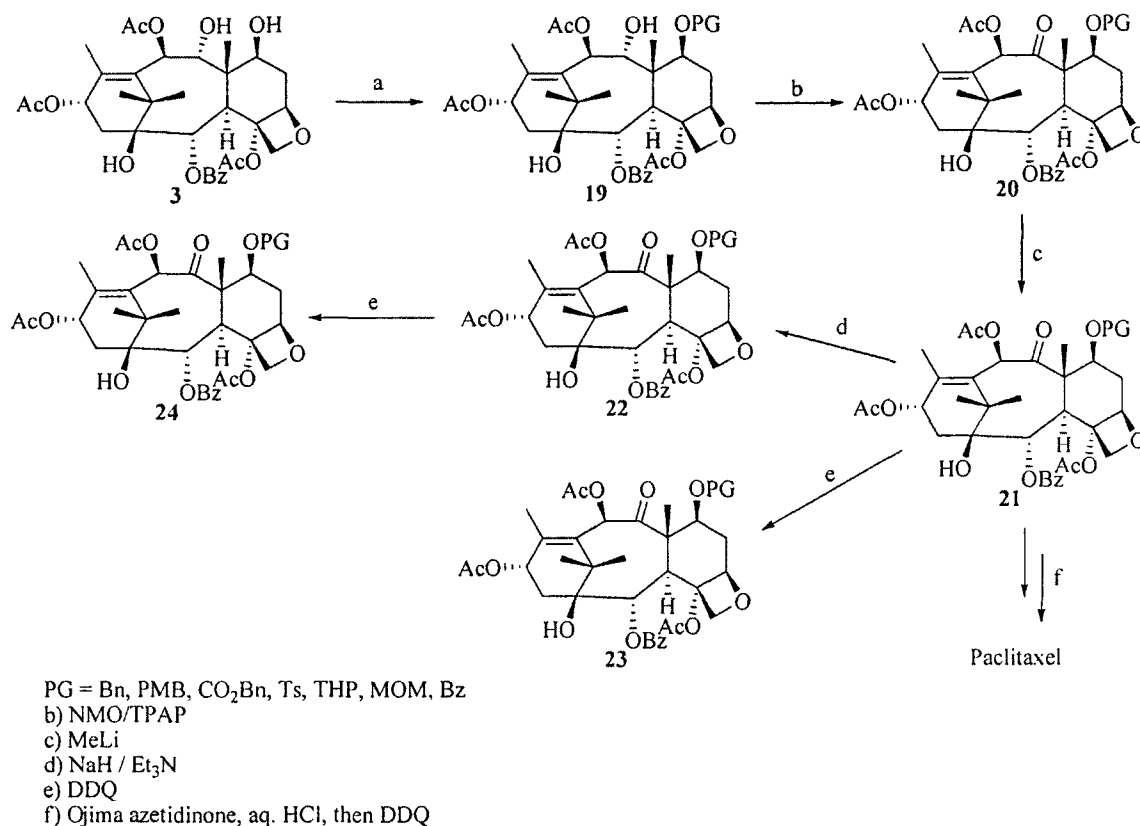


Figure 9. Liu conversion of 9-dihydro-13-acetylbaccatin III to 10-deacetylbaccatin III, baccatin III and paclitaxel.

Another report of the conversion of 9-dihydro-13-acetyl-baccatin III to 10-deacetylbaccatin III was by Kasitu¹⁵ where 9-dihydro-13-acetyl-baccatin III without the use of protecting groups is oxidized directly to 9-oxo-13-acetylbaccatin III (25) (Figure

10). This was surprising to us since until the report by Kasitu the precedent had been to protect the C7 hydroxyl followed by oxidation. Upon further examination by us of Kasitu's work and repeating some of his key reactions we determined that direct oxidation of the C9 hydroxyl in the presence of the C7 hydroxyl was unfounded and I discuss this to a further extent later.

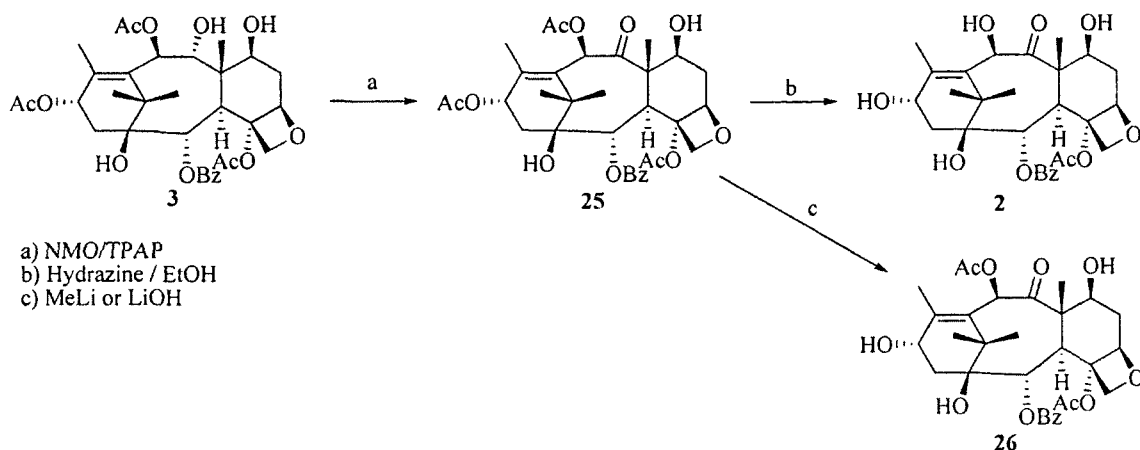


Figure 10. Kasitu conversion of 9-dihydro-13-acetylbaccatin III to 9-oxo-13-acetylbaccatin III and subsequent conversion to 10-deacetylbaccatin III and baccatin III.

Findlay *et al.*¹⁵ selectively protected the C7 hydroxyl of 9-dihydro-13-acetyl-baccatin III as acetate followed by oxidation of the C9 hydroxyl with chromium trioxide. Subsequent removal of acetates at C7, C10 and C13 with hydrazine in ethanol yielded 10-deacetylbaccatin III in an 80% overall yield on a multi-gram scale (Figure 11).

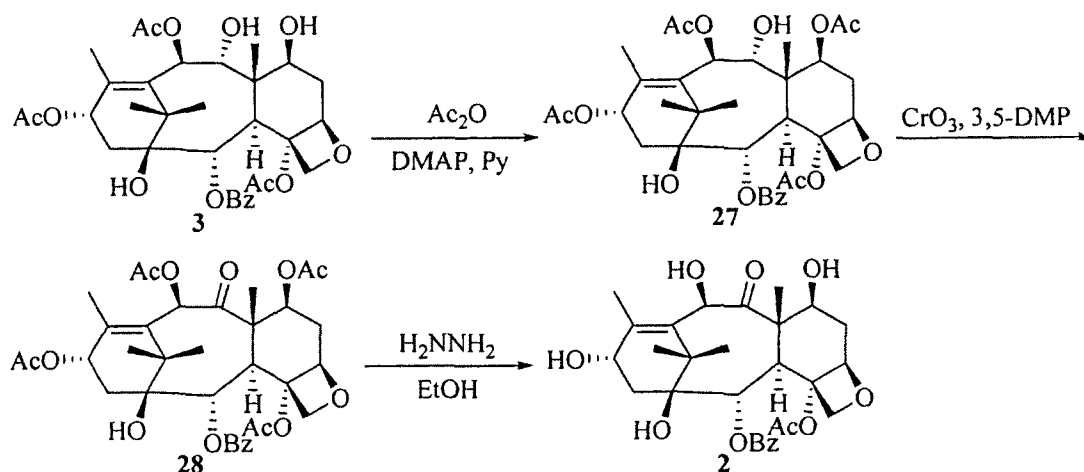


Figure 11. Findlay conversion of 9-dihydro-13-acetylbaccatin III to 10-deacetylbaccatin III.

1.2 A novel semi-synthetic approach to taxane: A computational study

1.2.1 Grob-type fragmentation to oxidize the C-9 hydroxyl group in 9-DHB

A Grob fragmentation, or 1,4 elimination reaction, first reported by Cyril A. Grob, occurs when an electrofuge and nucleofuge are situated in positions 1 and 3 of an aliphatic chain.¹⁷ The elimination is under strict stereoelectronic control where both the nucleofuge and a lone pair of the electrofuge are antiperiplanar to the $\text{C}_1\text{-C}_2$ bond (Figure 12).

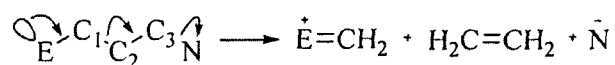


Figure 12. Grob fragmentation showing the stereoelectronic requirement of the electrofuge (E) lone pair and nucleofuge about the $\text{C}_1\text{-C}_2$ bond.

There are numerous examples of the Grob fragmentation in organic synthesis and two classic examples include the conversion of the Wieland-Miescher ketone to Thapsigargin, and an epoxy alcohol fragmentation in Holton's Taxol total synthesis (Figure 13).

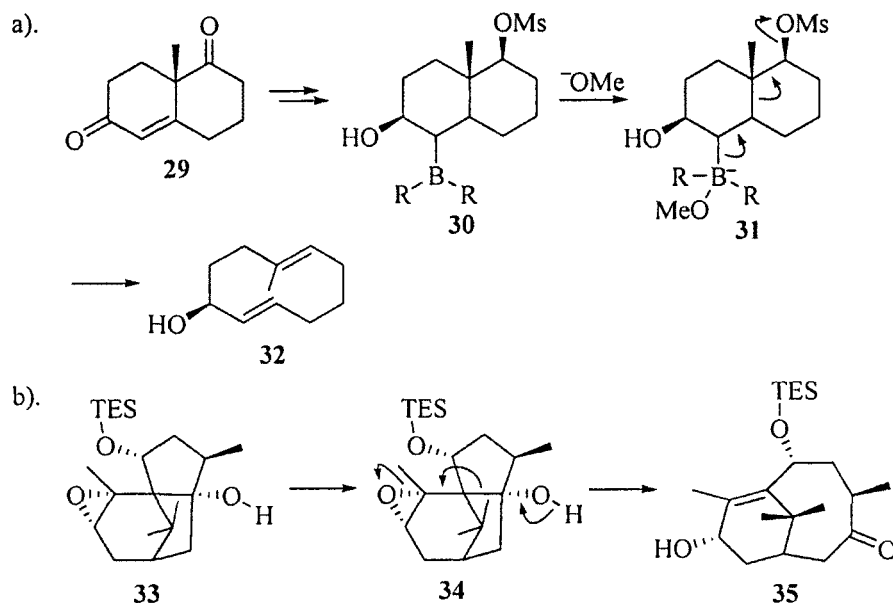


Figure 13. Grob fragmentation of (a) Wieland-Miescher ketone to Thapsigargin and (b) epoxy alcohol fragmentation in the synthesis of Taxol AB ring system.

Finding a new route for the conversion of 9-DHB to 10-DAB that circumvents all current processes described in the patent literature is no simple task. Thus, the use of a Grob-like fragmentation was envisioned as a first approach to the desired transformation based on an oxidative fragmentation of a cyclic acetal formed at the C7 and C9 hydroxyls of 9-DHB, which from this point will be referred to as the "7,9-acetal" (Figure 14). The R_2 substituent would, of course, have to be a leaving group suitable for

inducing fragmentation. Upon fragmentation, the critical C9-oxo group would be formed along with the C7 hydroxyl group now protected as an enol ether.

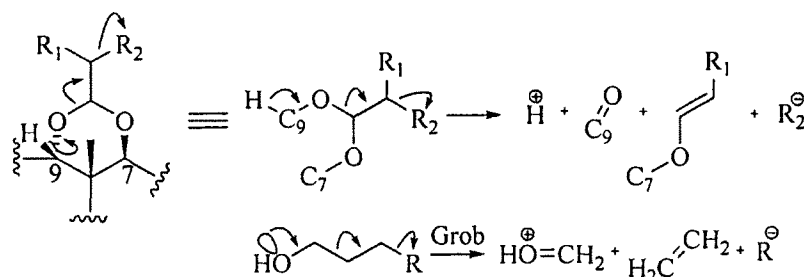


Figure 14. Comparison of Grob fragmentation (below) to the proposed oxidative fragmentation of the 7,9-acetal (above). R_2 is a suitable leaving group.

Of course one has to consider that elimination of the 7,9-acetal can initiate from 3 potential sites including the C_{acetal} -H leading to a 1,2-elimination and either the C_7 -H or C_9 -H position leading both to fragmentation (Figure 15).

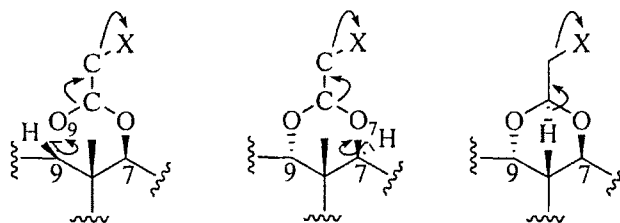


Figure 15. Possible fragmentation patterns of the 7,9-acetal via fragmentation initiated by elimination at C_9 -H (left) or C_7 -H (middle), or via 1,2-elimination (right).

1,2-Elimination at the acetal position, which would produce a ketene acetal product, is likely favored from the standpoint of the pK_a of the abstracted hydrogen. However like the Grob fragmentation, fragmentation of the 7,9-acetal would be subjected to strict

stereoelectronic control. It is accepted that, for a concerted 1,2-elimination of the E₂ type, the acidic hydrogen should be antiperiplanar to the leaving group.¹⁸ Syn elimination is also possible, but because it requires all the groups to be eclipsed, is usually observed only in conformationally rigid systems (i.e. bicyclo[2.2.1]heptanes). Similarly, for the fragmentation of the 7,9-acetal, either the C₇-H or C₉-H bond would have to be antiperiplanar to the scissile O-C_{acetal} bond and the leaving group would have to be antiperiplanar to the same O-C_{acetal} bond.

To assess the conformation of the 7,9-acetal and to determine if the correct stereoelectronic requirement for fragmentation from the C₉-H bond was attainable, a molecular dynamics computational study was initiated. Initial studies involved bromo- and chloroacetaldehyde 9-DHB acetal epimers, using molecular dynamics to assess their conformational preference in a dynamic equilibrium (Figure 16).

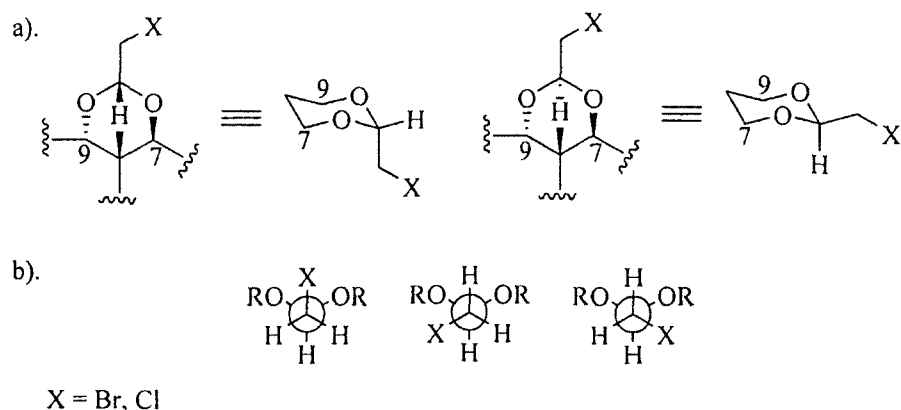
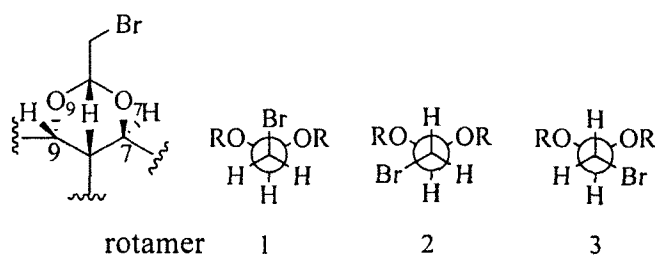
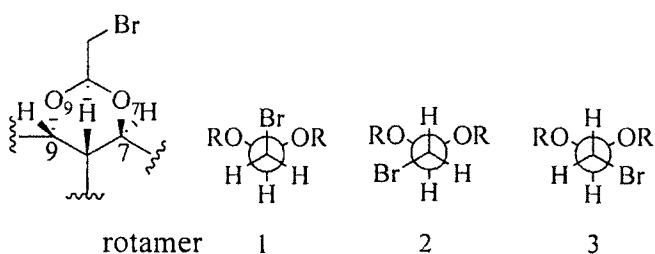


Figure 16. Bromo- and chloroacetaldehyde acetals can exist as (a) two epimers and (b) three different rotamers about the C_{acetal}-C bond.

Although the acetal epimer with the CH_2X group in the equatorial position is likely the lowest in energy, no assumptions were initially made about epimeric preference. Thus, all three staggered rotamers for both epimers of bromoacetaldehyde 9-DHB acetal epimers were studied (Table 1). It was necessary to analyze each rotamer since initial attempts at starting from one rotamer in the molecular dynamics run failed at generating the other possible rotamers. The results showed that, as expected, the barrier for rotation of the $(\text{RO})_2\text{CH}-\text{CH}_2\text{Br}$ bond is quite high and would require much longer molecular dynamics simulation times to observe the other rotamers. In retrospect, I would increase the simulation time not only to allow for sampling of all rotomers in a single run but to also sample the possible acetal conformations in addition to the chair conformation including the twist-boats, half-chairs and chair flips. Interestingly, with the simulation time used, the required stereoelectronic alignment is available for fragmentation of the 7,9-acetal from the $\text{C}_9\text{-H}$ bond with dihedral angles for $\text{H-C}_9\text{-O-C}_{\text{acetal}}$ and $\text{O-C}_{\text{acetal}}\text{-C-Br}$ of 168.8° and 167.0° (represents minimum energies of the conformations generated in the molecular dynamics simulation) respectively but that the correct stereoelectronic alignment does not exist for fragmentation from the $\text{C}_7\text{-H}$ bond. However, both epimers have a conformation conducive to a 1,2-elimination of the acetal which could compete with the 1,4-elimination, and possibly be the major pathway, since the $\text{p}K_{\text{a}}$ of the acetal hydrogen is likely lower than that of the C_9 hydrogen due to inductive effects.



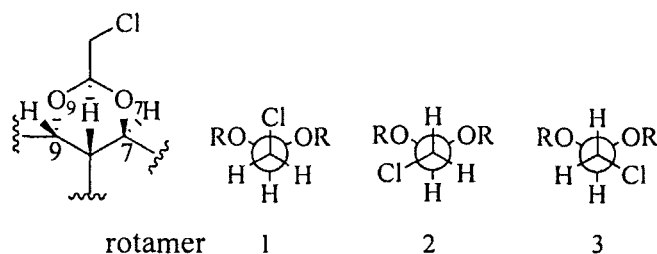
Starting rotamer	Dihedral angle H-C ₉ -O-C	Dihedral angle O ₉ -C-C-Br	Dihedral angle H-C ₇ -O-C	Dihedral angle O ₇ -C-C-Br	Dihedral angle H-C-C-Br	Energy (kcal/mol)
1	140.6	-63.0	140.7	62.6	179.7	189.7
2	160.7	156.6	63.5	-72.6	42.4	186.3
3	160.6	156.7	63.5	-72.6	42.5	186.3



1	168.8	167.0	60.9	74.6	-45.6	177.9
2	168.0	61.2	62.8	-61.2	-178.6	178.3
3	168.8	167.1	60.9	74.6	-45.7	177.9

Table 1. Results of both the axial and equatorial epimers of bromoacetaldehyde 9-DHB 7,9-acetal analyzed by molecular dynamics (NVT, 600 K, 5000 ps).

Next, a series of molecular dynamics simulations was carried out on equatorial chloroacetaldehyde 9-DHB 7,9-acetal giving the same lowest energy conformers as that of the equatorial bromoacetaldehyde 9-DHB 7,9-acetal (Table 2).



Starting rotamer	Dihedral angle H-C ₉ -O-C	Dihedral angle O ₉ -C-C-Cl	Dihedral angle H-C ₇ -O-C	Dihedral angle O ₇ -C-C-Cl	Dihedral angle H-C-C-Cl	Energy (kcal/mol)
1	168.7	170.2	60.9	71.3	-49.1	179.3
2	168.1	61.1	62.8	-60.9	178.5	179.7
3	168.7	170.2	60.8	71.3	-49.1	179.3

Table 2. Results for the equatorial epimer of chloroacetaldehyde 9-DHB 7,9-acetal analyzed by molecular dynamics (NVT, 600 K, 5000 ps).

In addition to the concern of a competing 1,2-elimination pathway, we were also mindful that the C₉ hydrogen would have to be accessible by an intermolecular base to initiate the requisite fragmentation. Analysis of molecular models shows that the C₉ hydrogen is in a fairly sterically crowded environment, due to methyls at C16 and C19, unlike the acetal hydrogen which is readily accessible (Figure 17). In fact, the successful C₉ oxidation in the Findlay/Deslongchamps process was attributed to the 3,5-dimethylpyrazine added to the CrO₃ oxidant, producing a base tethered intramolecularly via coordination to the chromium oxidant and more readily capable of abstracting the C₉ proton.

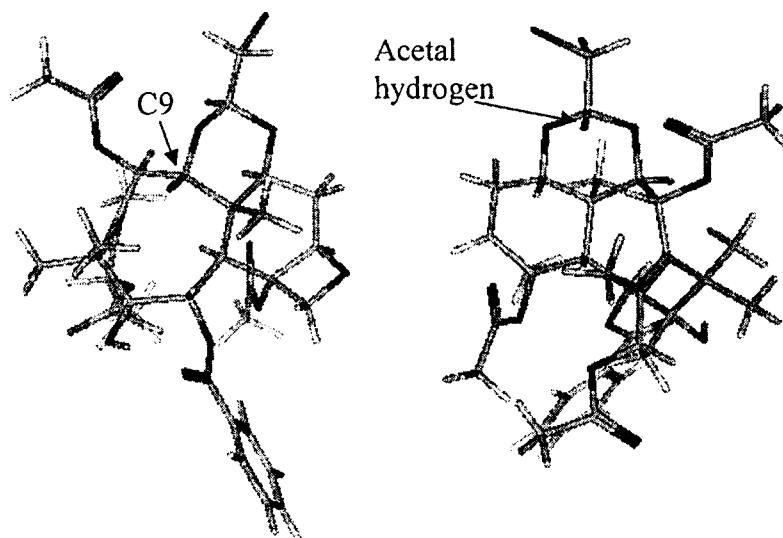
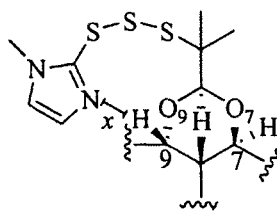


Figure 17. The C9 hydrogen and acetal hydrogen in their respective steric environment.

Since stereoelectronic and steric factors were deemed incompatible for overcoming the pK_a edge of the 1,2-elimination, the possibility of carrying out the fragmentation using a base tethered intramolecularly to the acetal was considered next. With a tethered base the fragmentation reaction would be a unimolecular process as opposed to bimolecular, thus more favorable. We imagined designing a tether which would allow the base to only approach the C₉-H bond thus eliminating any competing reactions from either the C₇-H bond or the acetal hydrogen.

Initial studies of using an intramolecular base were focused on tethering methylimidazole to the 7,9-acetal via an appropriate length tether and it was found that a trisulfide linkage would provide the conformational freedom for the base to reach the C₉-H bond for proton abstraction. Table 3 presents the results of the molecular dynamics simulation using methylimidazole as an intramolecular base. The simulation

suggest that methylimidazole can approach the C₉ hydrogen at a distance adequate for abstraction but the dihedral angle for elimination is not ideal. As already mentioned, fragmentation occurs most readily when the substituents at positions 1 and 2 are antiperiplanar to each other and when those at 3 and 4 are antiperiplanar as well. Here the substituents at positions 3 and 4 (acetal O₉ and S) have an average dihedral of 58.4° which may not be conducive to elimination. Although a dihedral of 180° is not possible in this system, upon extraction of the C₉ hydrogen the dihedral may rotate to 0° which would then be in proper alignment for a syn elimination albeit in a higher energy all-eclipsed conformation.



Structure #	Distance x (Å)	Dihedral $O_9-C_{acetal}-C-S$ (°)
1155	2.84	50.1
1156	2.78	56.6
1157	2.67	56.3
1158	2.67	60.2
1159	2.53	62.4
1160	2.78	57.1
1161	2.86	40.5
1954	2.82	56.9
3546	2.75	60.5
7703	2.88	70.0
7705	2.87	66.1
7706	2.80	64.1

Table 3. Selected results from a molecular dynamics (NVT, 300 K) simulation over a time of 5000 ps.

1.3 A novel semi-synthetic approach to taxane: Results and Discussion

1.3.1 Ketalization of 9-DHB

The computational studies suggested that the stereoelectronic requirements for a Grob-like fragmentation of our proposed 7,9-acetal from the C9 position was likely difficult to achieve, and that 1,2-elimination from the acetal hydrogen was a much more probable outcome. Nevertheless, a brief attempt was made to carry out the oxidative fragmentation experimentally. It was assumed that forming a suitably functionalized 7,9-acetal formation would be relatively trivial and that the difficulty would lie in promoting the proposed fragmentation chemistry.

Initial attempts of acetal formation involved reaction of tribromoacetaldehyde with 9-DHB in the presence of PPTS as acidic catalyst and molecular sieves to remove water as acetal formation proceeded. The reaction proceeded for 24 hours and was followed by TLC which indicated the formation of multiple products which were later shown by NMR to be unidentified degradation products of 9-DHB. Initial thoughts were that there was an unfavorable equilibrium for the formation of the 7,9-acetal and prolonged reaction with acid was leading to degradation of 9-DHB. The next attempt involved the use of bromoacetaldehyde dimethylacetal which should be able to undergo a trans ketalization reaction upon reaction with 9-DHB releasing methanol in the exchange. This process could be favorable due to the possible steric decompression of bromoacetaldehyde dimethylacetal upon exchange, water is not produced and is thus not necessary to remove, and the process is more entropically favourable. However, similar to initial attempts with tribromoacetaldehyde, reaction over a 48 hour period showed

degradation products with no indication of 7,9-acetal formation. Assuming that PPTS may be too mild of an acid catalyst, the reaction using bromoacetaldehyde dimethylacetal was repeated with PTSA. Again, over prolonged reaction times degradation of starting material was the only outcome.

The possibility that the acid catalyst was involved in an acid promoted degradation of 9-DHB was next addressed by simply treating 9-DHB in CH_2Cl_2 with a catalytic amount of either PPTS or PTSA. Reaction over 24 hours showed no degradation of 9-DHB when treated with PPTS but rapid degradation occurred upon treatment with PTSA. It then became apparent that the degradation being observed was acid promoted and HBr likely present in tribromoacetaldehyde and bromoacetaldehyde dimethylacetal could be a contributing factor.

With the unsuccessful attempts at acetal formation, the literature was reassessed for finding a reliable precedent for 7,9-acetal formation. Klein¹⁹ had reported the formation of the 9-DHB 7,9-acetonide in quantitative yield using excess dimethoxypropane in acetone with catalytic CSA but found that the formation of other acetals and ketals were difficult due to the acid-sensitive nature of the 4-membered oxetane ring present in 9-DHB and therefore had to resort to short reaction times to avoid degradation of product and starting material. We were able to repeat Klein's work in our own lab producing the 7,9-acetonide of 9-DHB quantitatively in 1 hour.

With an understanding that 9-DHB is acid-sensitive resulting in degradation upon prolonged reaction time we next accessed its stability in solvents other than CH_2Cl_2 . The initial choice of CH_2Cl_2 was due to the solubility of 9-DHB in this solvent. Upon testing diethyl ether, dimethoxyethane and tetrahydrofuran as suitable solvents for solubility and acid stability of 9-DHB we found that diethyl ether didn't provide the desired solubility but that dimethoxyethane and tetrahydrofuran did and that there was no evidence of 9-DHB degradation upon treatment with CSA for up to 3 hours. However, upon attempting acetal formation using bromoacetaldehyde dimethyl acetal, degradation products began to appear at 24 hours, with complete degradation of starting material over 5 days with no evidence of acetal formation over that time. Attempts at forming the acetonide using dimethoxyethane in THF with catalytic CSA gave a 68.6% yield over 50 hours giving us an indication that acetal formation in THF is sluggish at best.

After numerous other attempts at forming related acetals and ketals, all of which gave poor yields or no product at all, it started to become apparent that our attempts were becoming futile. In assessing possible other routes to convert 9-DHB to 10-deacetylbaccatin III we were aware that our options were limited as the patent literature covered most if not all of the standard protection/oxidation procedures that we viewed as feasible or competitive. We were intrigued though with the possibility of selectively oxidizing the C9 hydroxyl in the presence of the C7 hydroxyl, though we were aware of the difficulty in attaining such a conversion given that the C9 hydroxyl is more sterically

hindered than the C7 hydroxyl and that the strategy precedent had been to first protect the C7 hydroxyl before oxidizing at the C9 position.

1.3.2 Direct oxidation

Understanding the inherent difficulties of performing a regioselective oxidation of the C9 position over C7 we were somewhat surprised of a report by Kasitu for the direct oxidation of 9-DHB into the 9-oxo counterpart (Figure 18).

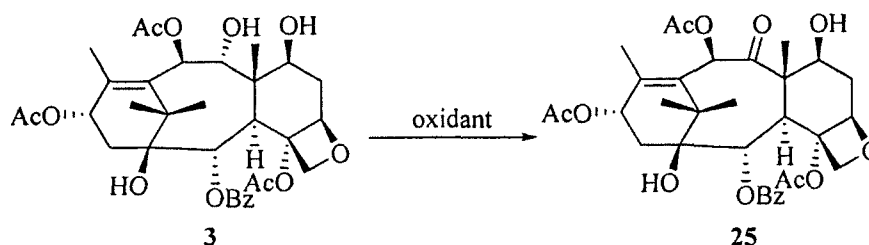


Figure 18. Direct oxidation of 9-DHB

Indeed, Kasitu had reported an 80% yield of C9 oxidized product with a 17% recovery of 9-DHB. In our hands, repeating the Kasitu procedure, led consistently to the conversion of 9-DHB to 7-oxo-oxetane ring-opened (**36**) and 9-oxo-13-acetyl-baccatin III (**25**) in yields of 79% and 17% respectively (Figure 19). It is clear to us that the Kasitu patent erroneously identified the major product as the 9-oxo product where in fact the principal oxidation occurred at C7, followed by a now facilitated beta-elimination and opening of the oxetane ring. In hindsight, the Kasitu claims were quite controversial in light of the overwhelming literature precedent for first protecting C7 prior to attempting C9 oxidation. Admittedly we were somewhat relieved that Kasitu's patent was in error as it opened up the possibility for us to develop a direct oxidation strategy.

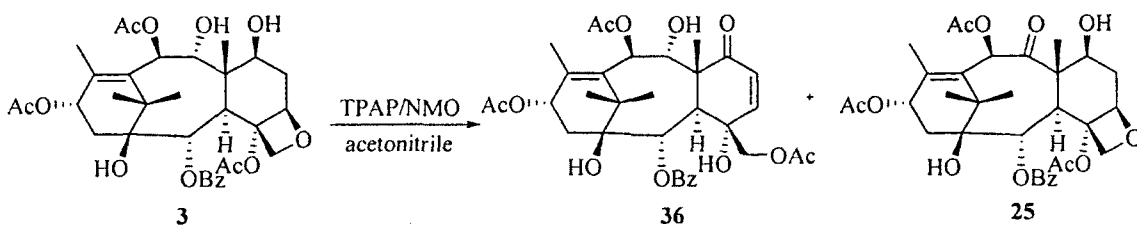


Figure 19. Oxidation of unprotected 9-DHB.

During our investigation of a potential direct oxidation of the C9 position there was a report of a general method for the regioselective monooxidation of 1,2-diols with RuO_4 and Oxone® as a nucleophilic reoxidant²⁰ (Figure 20).

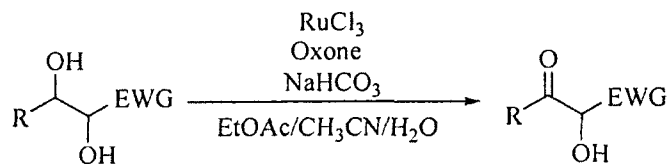


Figure 20. A ruthenium catalysed regioselective monooxidation of a 1,2-diol.

Mechanistically, it is believed that RuCl_3 is oxidized to RuO_4 by Oxone® ($2\text{KHSO}_5 \cdot \text{KHSO}_4 \cdot \text{K}_2\text{SO}_4$), then transforms diol **37** into cyclic ruthenium intermediate **38**, (Figure 21). Subsequent nucleophilic addition of re-oxidant HSO_5^- to the strongly electron-withdrawing ruthenium leads to cleavage of the less electron-rich Ru-O bond in **38** leading to the ruthenium peroxo ester **39**. A beta-elimination of **39** gives α -hydroxy ketone **40** and regeneration of RuO_4 .

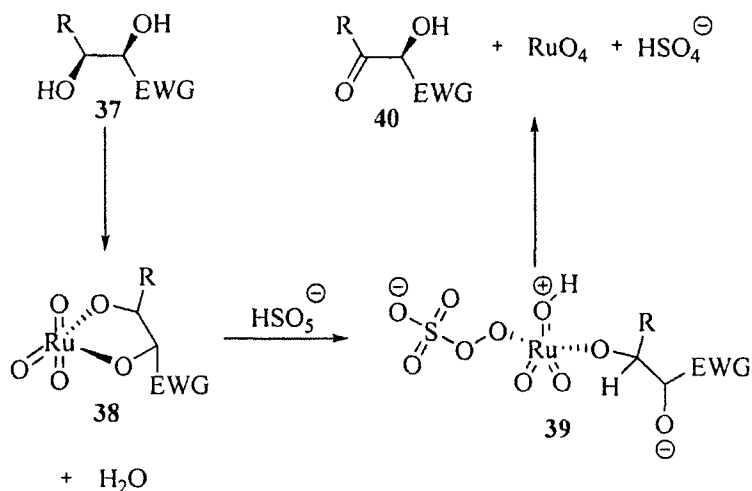


Figure 21. Elimination of the ruthenium ester.

Although there is little difference in the electronic character of the C7-O and C9-O bonds in 9-DHB, we nevertheless attempted a direct oxidation with RuO_4 . Surprisingly, in our first attempt the ratio of C9 oxidized product to C7 and C7,C9 oxidized product was 1:1.6, determined by NMR of the crude product (Figure 22).

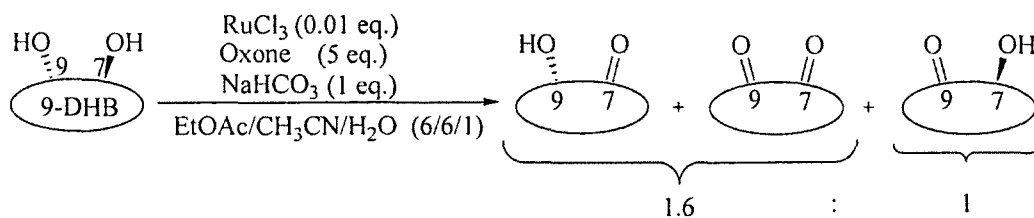


Figure 22. Direct oxidation of 9-DHB.

Attempts to optimize the procedure by changing the re-oxidant, base and solvent were for the most part unfruitful. Oxone® was substituted with either NaIO_4 , KBrO_3 , or $\text{K}_2\text{S}_2\text{O}_8$ resulting in ratios of C9 oxidized product to C7 and C7,C9 of 2.3:1, 4.8:1 for NaIO_4 and KBrO_3 respectively and there was no reaction when $\text{K}_2\text{S}_2\text{O}_8$ was used as re-

oxidant. As the reaction progressed there was an increase in the acidity and a slowing of the rate of reaction. We were limited in the buffering capacity of the added base due to persistent solubility problems. Increasing the amount of water to increase the solubility of the base in the reaction mixture only slowed the reaction rates resulting in poorer oxidized product ratios. Water is known to hydrolyze the cyclic ruthenium-diol intermediate back to RuO_4 and diol and therefore by increasing the amount of water in the reaction mixture, likely competed with Oxone® for nucleophilic attack (Figure 23).

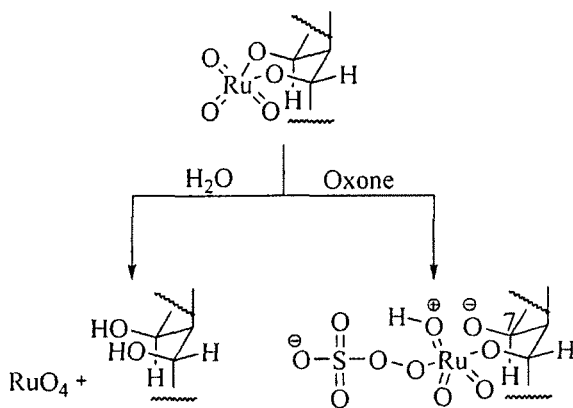
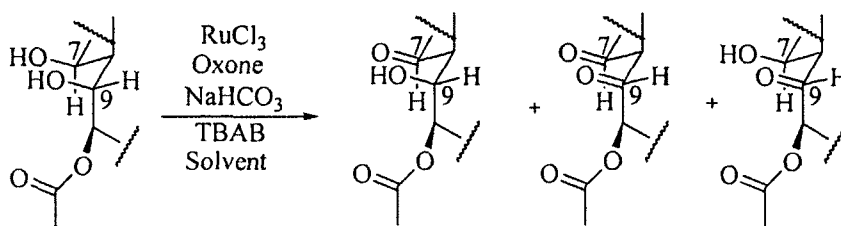


Figure 23. The competitive nucleophilic addition of water and Oxone® to the cyclic ruthenium-diol intermediate.

Although water could slow the rate of the reaction by competing with Oxone® it was necessary in the reaction mixture not only for solubilizing the base but also the Oxone®. Given that water was needed in the solvent mixture, we kept that constant and tried water in combination with other organic solvents to check the influence of solvent on the selectivity of oxidation. Various solvent mixtures were tried but a mixture of *tert*-butyl alcohol/water gave the most favorable results (Table 4). To assist in the transfer of

Oxone® across the aqueous-organic interface we began to use tetrabutylammonium bromide as a phase transfer agent.



Solvent	C7 + C7,C9 : C9 oxidized products
EtOAc/ $\text{CH}_3\text{CN}/\text{H}_2\text{O}$ (6/6/1)	1.9:1
<i>t</i> -butyl alcohol/ $\text{CH}_3\text{CN}/\text{H}_2\text{O}$ (6/6/1)	1.3:1
THF/ H_2O (12/1)	1.3:1
$\text{CHCl}_3/\text{H}_2\text{O}$ (1/1)	6.2:1
$\text{CH}_3\text{CN}/\text{H}_2\text{O}$ (12/1)	1.5:1
<i>t</i> -butyl alcohol / H_2O (12/1)	1:1

Table 4. Influence of solvent on the product ratios (determined by NMR) of the direct oxidation of 9-DHB with RuO_4 .

Despite the respectable product ratios using our direct oxidation procedure the reaction was still plagued with slowing reaction rates as the reaction progressed resulting in 50 percent conversion of starting material at best. Further attempts to optimize the procedure failed likely in part due to the lack of understanding of why the reaction rate slowed and the complexity of the mechanism of this selective oxidation.

Mechanistically there is likely a bias present in the ruthenium-9-DHB cyclic intermediate that favors the addition of the nucleophilic oxidant to the C9 side leading to opening of the cyclic intermediate, if addition is S_N2-like, on the C7 side and resulting in subsequent oxidation at C9 (Figure 24). Plietker showed, using trans-cyclohexenyl diacetate (**41**), that sterics influence the addition of Oxone® to cyclic ruthenium diol intermediate **42**.²¹ Addition of Oxone® along path **a** is sterically disfavored giving product **43a** while approach along path **b** is favored leading to product **43b** as the major product (Figure 25).

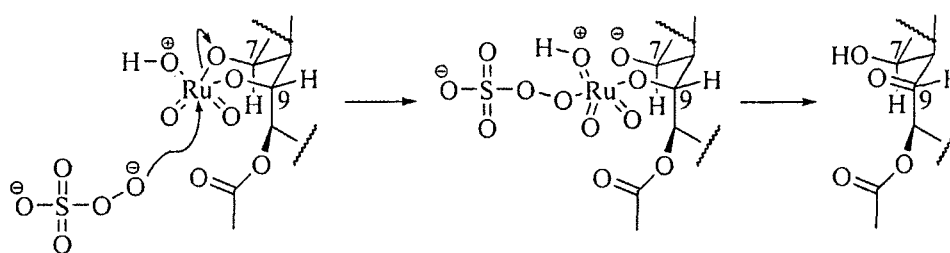


Figure 24. S_N2-like addition of Oxone® to ruthenium-9-DHB cyclic intermediate and subsequent oxidation.

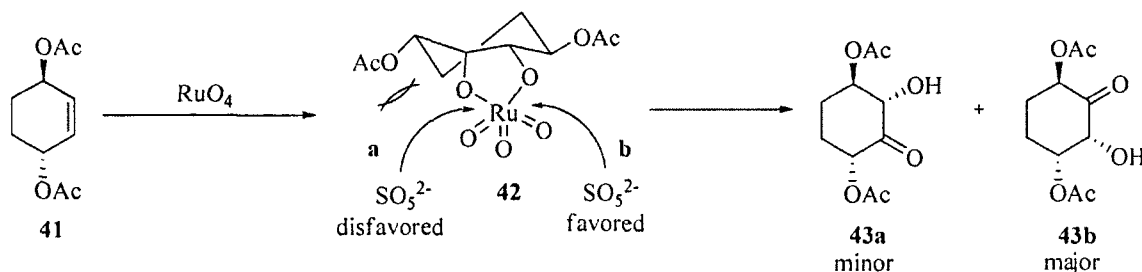


Figure 25. Influence of sterics on ruthenium mediated oxidation.

The results of Plietker showing the regioselective preference for diol oxidation is favored towards the alcohol in the least sterically crowded environment go against what

we observed in the selective oxidation of 9-DHB given that the C9 alcohol is more sterically crowded than the C7 alcohol. Therefore it is apparent that some other factor may bias oxidation at C9. One possibility is that the C7 oxygen is solvated in the ruthenium cyclic intermediate thus favouring Oxone® approach on the C9 side (Figure 26). Alternatively, if SO_5^{2-} is not approaching the ruthenium intermediate but rather HSO_5^- the C10 acetate may provide a templating affect and promote addition to the C9 side (Figure 27).

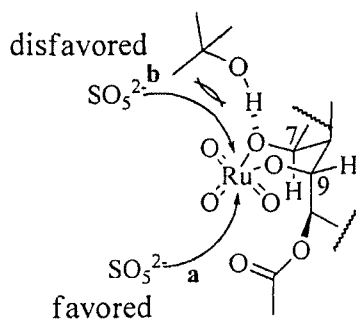


Figure 26. Solvation at the C7 hydroxyl resulting in preference for Oxone® approach on the C9 side of the ruthenium cyclic intermediate.

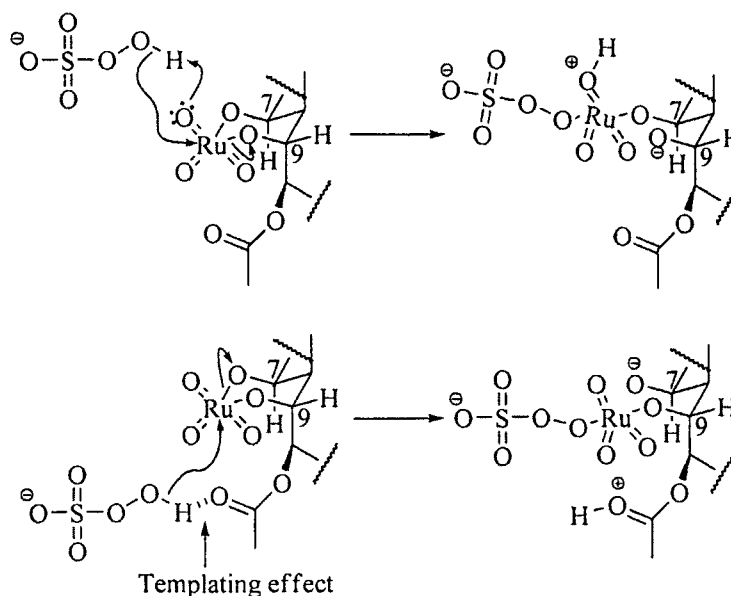


Figure 27. Templating effect promoting addition to the C9 side of the ruthenium cyclic intermediate.

1.3.3. One-Pot Oxidation

Since our multiple attempts at carrying out the direct oxidation beyond what is reported in Table 4 could not be improved and due to the complexity of the oxidation reaction conditions and not understanding the mechanism beyond what is presented here we decided to investigate an alternative approach to the direct oxidation. Our thinking was to temporarily protect the C7 hydroxyl, oxidize the C9 hydroxyl and then remove the protecting group at C7 all in one reaction vessel without purification of intermediates to give what we termed the “one-pot oxidation.”

While working on the chemistry of forming 7,9-acetals we had observed that when vinyl ethers were reacted with 9-DHB in the presence of catalytic acid, mixed acetals at C7 and C9 rather than cyclic C7, C9 acetals were sometimes observed (Figure 28).

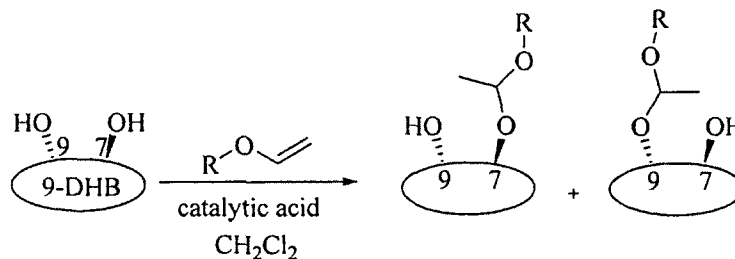


Figure 28. Formation of mixed acetals when 9-DHB is treated with vinyl ethers.

At the time, these results were set aside as all the synthetic efforts were focused on obtaining cyclic acetals that would be conducive to our proposed oxidative fragmentation strategy. However, the observation of mixed acetals would later on prove to be a pivotal point in the development of the one-pot procedure. Indeed, these mixed acetals could potentially be produced *in situ* and, if capable of surviving the subsequent oxidation chemistry to produce a C9-oxo group, could be easily removed perhaps even during acidic work-up. To test the validity of this approach would at least require a demonstration that 1- a C7-mixed acetal could be installed selectively over a C9-mixed acetal and 2- that oxidation of the C9-hydroxyl could be achieved without loss of the C7-mixed acetal.

Careful reinvestigation of the chemistry for forming mixed acetals using alkyl vinyl ethers showed that the C7-mixed acetal was a thermodynamic product generated almost exclusively over a prolonged reaction time (Figure 29). After an optimization of the reaction conditions it was found that the C7-mixed acetal could be formed reliably in 90% yield (Table 5).

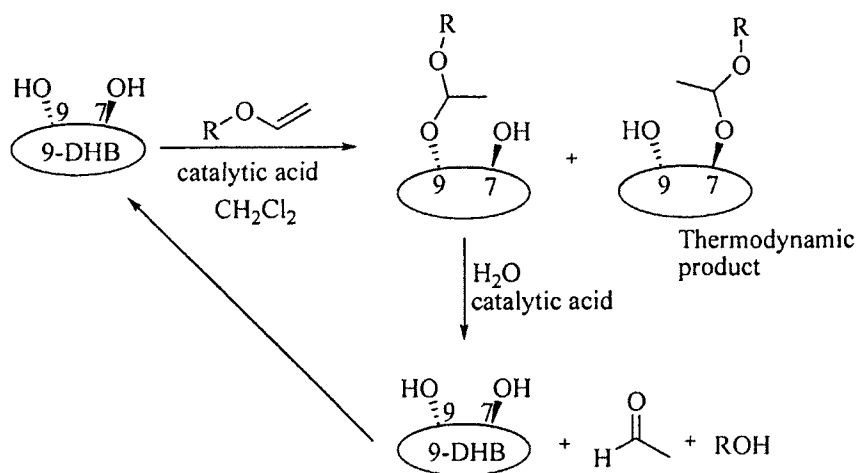


Figure 29. Formation of the thermodynamic favored C7-mixed acetal.

As for the oxidation step, a series of experiments were carried out with oxidants that were non-acidic and that could leave the C7-mixed acetals intact. As shown in Figure 30 use of the Dess-Martin periodinane in the presence of pyridine to maintain a basic solution yielded 7-acetal-9-oxo in 86% yield from the purified C7-mixed acetal product.

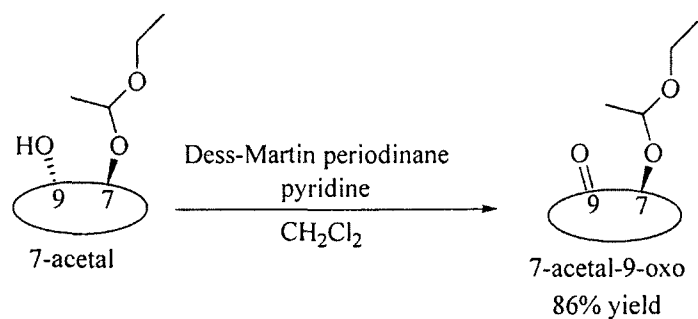
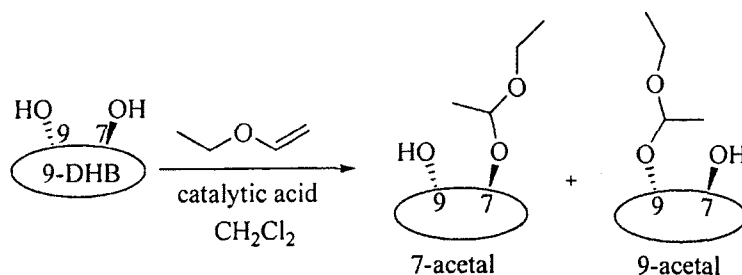


Figure 30. Oxidation of 7-acetal.



Entry	Conditions	Products ^{a,b}
1	9-DHB (50 mg), ethyl vinyl ether (10 eq), PTSA (0.5 mg), CH ₂ Cl ₂ (5 mL), r.t.	7-acetal + minor contaminant (37.5mg), 9-DHB (7.4mg)
2	9-DHB (50 mg), ethyl vinyl ether (2 eq), PTSA (0.5 mg), CH ₂ Cl ₂ (5 mL), -15°C	7-acetal + minor contaminant (38.6mg), 9-DHB (6.1mg)
3	9-DHB (50 mg), ethyl vinyl ether (2 eq), PPTS (1 mg), CH ₂ Cl ₂ (5 mL), -15°C (30 min), r.t. (24 hrs)	No Reaction
4	9-DHB (50 mg), ethyl vinyl ether (2 eq), PTSA (0.5 mg), CH ₂ Cl ₂ (5 mL), -15°C	7-acetal + minor contaminant (39.1mg)
5 ^c	9-DHB (50 mg), ethyl vinyl ether (4 eq.) PPTS (5 mg), CH ₂ Cl ₂ (5 mL), r.t.	7-acetal - 37.9mg 9-acetal - 11.2mg
6 ^d	9-DHB (50 mg), ethyl vinyl ether - 4eq, PPTS (1 mg), CH ₂ Cl ₂ (5 mL), r.t.	7-acetal - 49.8mg 9-acetal - 4.8mg 9-DHB - 1.1mg

^a Theoretical yield (T.Y.) of 7-acetal - 55.5mg based on 50mg of 9-DHB

^b Minor contaminant was later separated from 7-acetal and found to be 9-acetal. Experiments in entries 1,2 and 4 were performed without successful chromatographic separation of 7-acetal and 9-acetal.

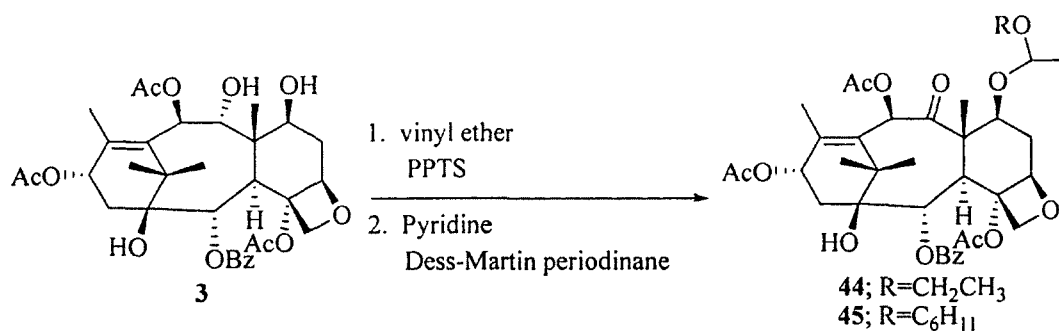
^c Ethyl vinyl ether was freshly distilled and PPTS was dried by azeotropic distillation.

^d 9-DHB was dried under vacuum over toluene reflux and P₂O₅. 2 mole equivalents of H₂O removed.

Table 5. Optimization of C7-mixed acetal formation.

With the selective protection of the C7-hydroxyl and subsequent oxidation giving a 77% overall yield in 2 steps, we then tested the protocol in a one-pot procedure on scales

ranging from 50 mg to 600 mg and obtained overall yields of 7-acetal-9-oxo up to 79% (Table 6).



Entry	Conditions	Products
1	Protection: 9-DHB (50 mg), ethyl vinyl ether (4 eq), PPTS (5 mg), CH ₂ Cl ₂ (5 mL), r.t., 20 hrs Oxidation: DMP – 2.5eq (0.06 M soln in CH ₂ Cl ₂ + 6 eq. of pyridine) added to reaction mixture. r.t., 24 hrs.	7-acetal-9-oxo : 43.2 mg (78.5%)
2	Protection: 9-DHB (50 mg), cyclohexyl vinyl ether (2.8 eq) added over 4.5 hrs. PPTS (1 mg), CH ₂ Cl ₂ (2.6 mL), r.t., quenched with pyridine (30 eq) at 4.5 hrs Oxidation: DMP – 5 eq. (0.2 M soln in CH ₂ Cl ₂ (2 mL)) added to reaction mixture. r.t., 10 hrs.	7-acetal-9-oxo : 46.3 mg (77.2%)
3	Protection: 9-DHB (500 mg), ethyl vinyl ether (4 eq), PPTS (catalytic), CH ₂ Cl ₂ (26.3 mL), r.t., quenched with pyridine (30 eq) at 7.5 hrs Oxidation: DMP – 5 eq. (0.2 M soln in CH ₂ Cl ₂ (20 mL)) added to reaction mixture. r.t., 10 hrs.	7-acetal-9-oxo : 439.1 mg (79.7%)
4	Protection: 9-DHB (600 mg), cyclohexyl vinyl ether (2.3 eq) added over 2.5 hrs, PPTS (catalytic), CH ₂ Cl ₂ (31.7 mL), r.t., quenched with pyridine (30 eq) at 4.5 hrs. Oxidation: DMP (5 eq) (0.2 M soln in CH ₂ Cl ₂ (23.8 mL)) added to reaction mixture. r.t., 10 hrs.	7-acetal-9-oxo : 537.0 mg (75.0%)

Table 6. The 2-step, one-pot protection/oxidation reaction.

Finally, once proof-of-concept for the selective ketalization step and for the oxidation step had been achieved, the complete one-pot protection/oxidation/deprotection procedure was tested on 1.0 g scale of 9-DHB, yielding the anticipated 9-oxo product **25** in 79% yield (Figure 31).

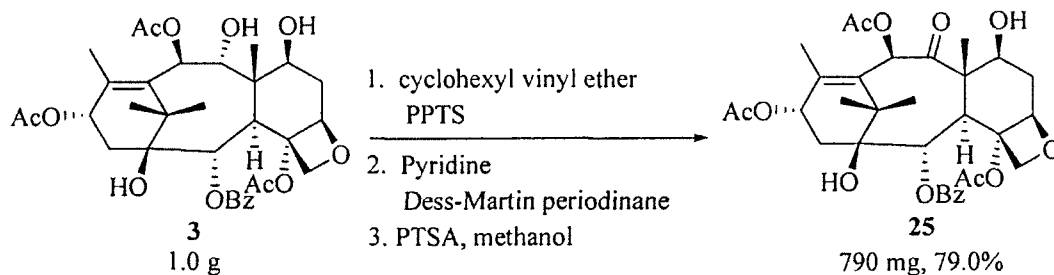


Figure 31. The one-pot protection/oxidation/deprotection.

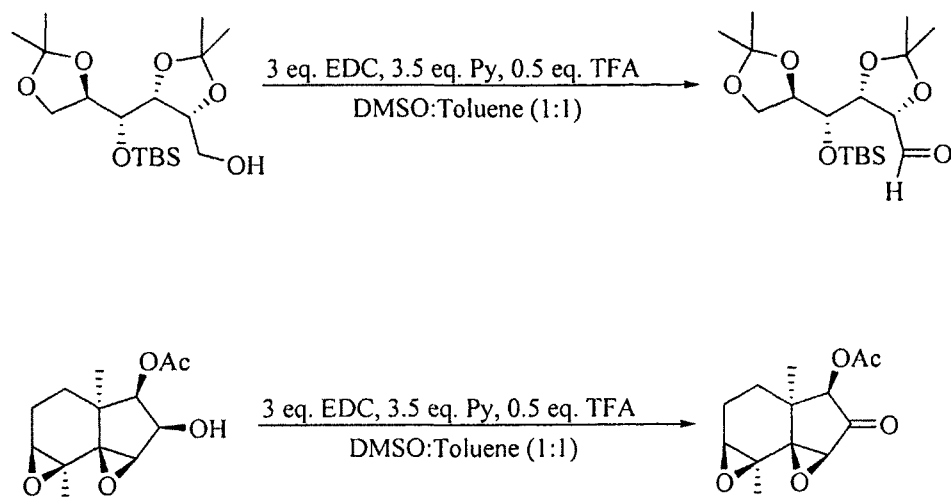
The successful one-pot conversion of 9-DHB to **25** opens up a simple and efficient route to the production of 10-deacetylbaccatin III, the key synthetic intermediate for all commercially important processes of semi-synthetic paclitaxel and docetaxel worldwide. Moreover, it should be noted that selective deprotection of the C13 acetate of either intermediate **44** or **45** would give an even quicker access to paclitaxel in only 2 steps. Perhaps the only remaining obstacle to the large-scale production of pharmaceutically important taxanes by the one-pot route is the oxidant used in the proof-of-concept stage. The Dess-Martin periodinane is used in excess and may not be optimal for a commercial scale reaction. The last section of this chapter outlines several possible alternative oxidants that could be investigated for the one-pot oxidation procedure that may be compatible with the transient mixed acetal protecting group of this novel route.

1.4 Potential alternative oxidants for the One-Pot procedure

1.4.1 Pfitzner-Moffatt oxidation

Originally developed by Moffatt and Pfitzner²² utilizing dicyclohexylcarbodiimide (DCC) to activate DMSO in the presence of a mild acid, this reaction is often referred to as a Pfitzner-Moffatt oxidation.

General Procedure: Three equivalents of a carbodiimide are added to a solution of 1 equivalent of the alcohol and 0.5 equivalents of pyridinium trifluoroacetate in neat dry DMSO or a mixture of DMSO and benzene at room temperature (Figure 32). A quantity of DMSO above 6 equivalents has minimal influence on yield, although most procedures utilize a 1:1 ratio of DMSO and benzene. Benzene has been substituted with toluene or methylene chloride with success.



Proposed process:

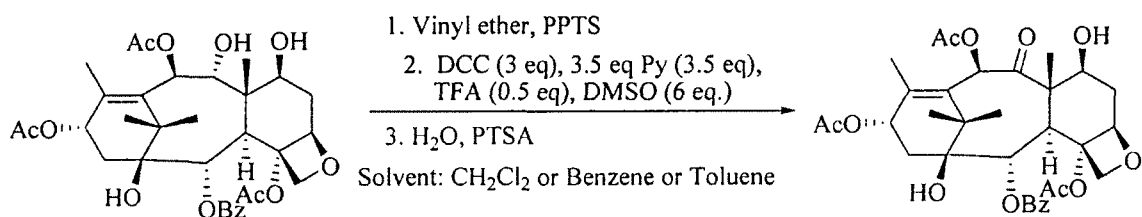
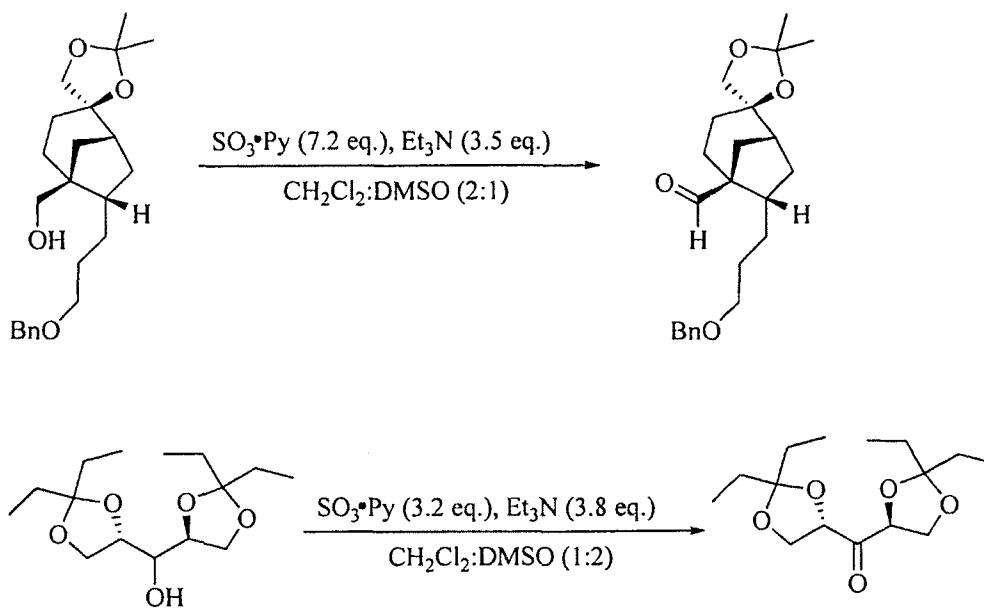


Figure 32. General procedure and proposed process for the Pfitzner-Moffatt oxidation.

1.4.2 Parikh-Doering oxidation

Parikh and Doering in 1967 described the procedure²³ for the oxidation of alcohols with DMSO activated using sulfur trioxide and complexed with pyridine (Figure 33). Originally performed in DMSO, subsequent investigators have modified the original procedure utilizing CH_2Cl_2 , THF or CHCl_3 as a co-solvent with as little as 3 equivalents of DMSO.

General procedure: Between 2 and 9 equivalents of the complex $\text{SO}_3\cdot\text{Py}$ in dry DMSO are slowly added to a 0.2-0.6 M solution of 1 equivalent of alcohol in DMSO, CH_2Cl_2 , THF or CHCl_3 containing 7-17 equivalents of Et_3N . When the starting material is consumed water is added and the organics are extracted into a suitable organic solvent.



Proposed process:

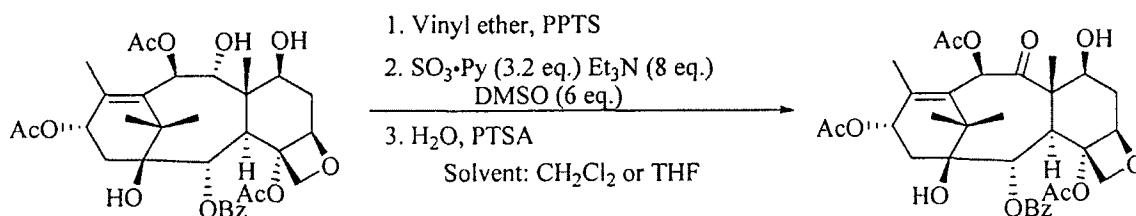


Figure 33. General procedure and proposed process for the Parikh-Doering oxidation.

1.4.3 Other activated DMSO mediated oxidations

The Omura-Sharma-Swern oxidation²⁴ and the Swern oxidation²⁵ have been successfully used in oxidizing substrates with acid-sensitive functional groups including acetals. However, due to the inherent explosive nature of reacting intermediates and the side reactions encountered when using these two methods it is anticipated that it would not be appropriate for the conversion of 9-DHB to 13-acetylbaccatin III on a commercial scale.

1.4.4 Corey-Kim oxidation

Prior to Swern, in 1978, disclosing the process of activating DMSO with oxalyl chloride Corey and Kim, in 1972, described the reaction²⁶ of dimethyl sulfide with chlorine to yield chlorodimethylsulfonium chloride (Figure 34), the activated DMSO species generated in the Swern oxidation.

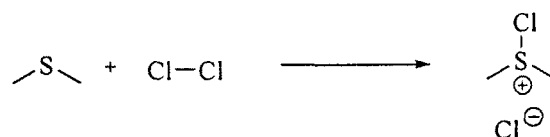


Figure 34. Formation of chlorodimethylsulfonium chloride described by Corey and Kim.

Since gaseous chlorine is inconvenient to work with, Corey-Kim oxidations are often performed by oxidation of dimethyl sulfide with *N*-chlorosuccinimide (Figure 35). Although dimethyl sulfide and *N*-chlorosuccinimide does not react in an explosive nature when generating the activated DMSO species, it is not often used as an alternative to the Swern oxidation. Hence, due to the limited reports of the Corey-Kim oxidation there have been no reports of its use on substrates containing the acetal functional group.

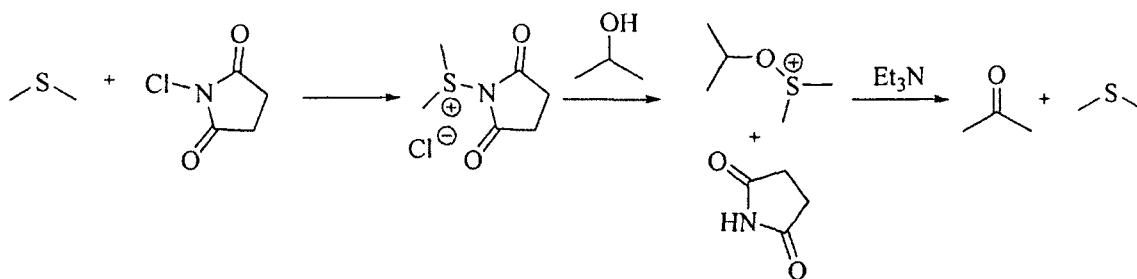


Figure 35. Corey-Kim oxidation.

1.4.5 Pyridinium dichromate (PDC)

The presence of pyridinium cations makes PDC slightly acidic but sensitive functionalities, including acetals, are able to withstand the action of PDC. The acidity can be buffered with sodium acetate and other bases including pyridine have been used in some instances. The presence of PPTS from the first step of the One-Pot procedure is unlikely to hinder the action of PDC since PPTS is sometimes used to accelerate PDC mediated oxidations. Molecular sieves are also used to accelerate these reactions.

Although commercially available, best reports have been made when PDC was freshly prepared. Preparation involves the slow addition of one equivalent of pyridine to a concentrated solution of CrO_3 leading to PDC that can be precipitated by the addition of acetone. Explosion can occur during preparation but can be avoided by insuring the chromium trioxide is completely dissolved in the aqueous solution and the temperature maintained below 25°C .

1.4.6 Pyridinium chlorochromate (PCC)

Similar to PDC the slightly acidic nature can be buffered. Common buffers include NaOAc, KOAc, CaCO₃, BaCO₃, NaHCO₃, Na₂HPO₄, pyridine, and Na₂CO₃. Molecular sieves are sometimes used to accelerate PCC mediated oxidations.

1.5 Conclusion

Initial work towards acetal formation and subsequent Grob-like fragmentation to oxidize the C9 position of 9-DHB was unsuccessful due to failed attempts to form 7,9-acetals. As an alternative, methods of directly oxidizing the C9 position without protection at C7 proved futile due to poor yields, despite favorable ratios of C7 to C9 oxidation. Attempts at optimization failed to improve yields and the method was abandoned. Finally, the observation that mixed acetals could be selectively formed at C7 led to the successful development of a “one-pot” procedure for the protection of C7 and subsequent oxidation of C9 in yield near 80% giving us a competitive procedure to already known processes. Further optimization of the procedure by finding alternative oxidants can make the process cheaper and an attractive process to make anticancer drugs from New Brunswick biomass.

Chapter 2. The rational design of a squaramide based hydrogen bond donor catalyst

2.1 Organocatalysis

2.1.1 The beginnings of a new scientific field

The asymmetric catalysis of organic reactions by small organic molecules entered its infancy in the late 1990s with a spattering of interest dating back to 1969 in a field which had yet to be named and known today as organocatalysis. Hajos and Parrish²⁷ reported the first example of organocatalysis when they showed the asymmetric intramolecular aldol cyclization of triketone **46** catalyzed by only 3 mol % of proline (Figure 36), which was later proposed to proceed via an enamine intermediate.²⁸ Simultaneous to Hajos and Parrish, Wiechert and co-workers²⁹ reported the same reaction but under harsher conditions giving the condensation product rather than bicyclic ketol **48**.

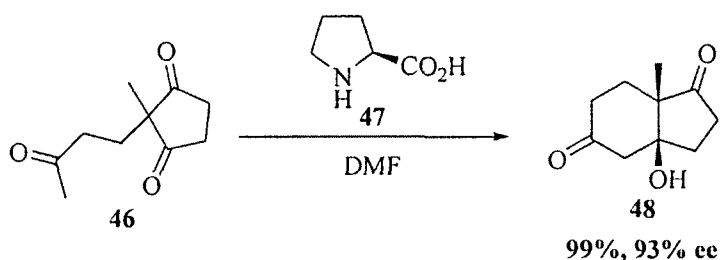


Figure 36. Hajos-Parish reaction.

An interesting observation was that the Hajos-Parish reaction was proceeding through an enamine intermediate, which in some sense is biomimetic to the way Nature catalyzes aldol reactions. Indeed class I aldolases catalyze their respective aldol reactions via an enamine intermediate. The Hajos-Parish reaction was unique since in

traditional asymmetric synthesis, aldol type C-C bond forming reactions typically proceed via some metal enolate nucleophilic counterpart with the aid of a chiral ligand and Lewis acid. Despite the Hajos-Parish reaction being a new mode of catalyzing the asymmetric aldol reaction chemically, it did not receive much attention because of the perceived narrow scope of the reaction. Expansion of the asymmetric organocatalysis concept and realization of its generality for other substrates and reactions would not be recognized until decades later.

From 1969 to the late 1990s there was little interest in utilizing small organic molecules to catalyze asymmetric reactions and then in 1998 and 1999 there were three separate reports of using small organic molecules as non-covalent hydrogen bonding catalysts, yet another mode of biomimetic activation in catalysis. Eric Jacobson³⁰ in 1998 and E.J. Corey³¹ in 1999 each described the first examples of hydrogen bonding catalysis in an asymmetric Strecker reaction. Also in 1998, Scott Miller³² used tripeptides as chiral hydrogen bond donors for the kinetic resolution of alcohols (Figure 37). Despite these reports the field still did not generate much interest until two simultaneous reports by Benjamin List³³ and David MacMillan³⁴ of enamine and iminium catalysis.

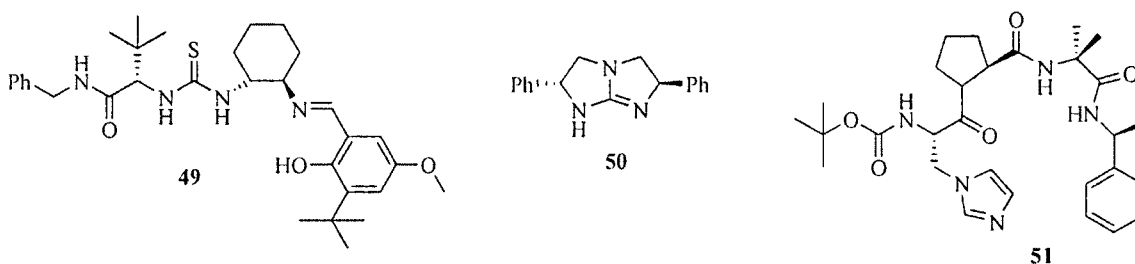


Figure 37. Hydrogen bonding catalyst of Jacobson (49), Corey (50), and Miller (51)

The report by List described an enamine-catalyzed reaction that was an intermolecular version of the Hajos-Parish reaction where a ketone was activated via enamine formation and followed by reaction with an aldehyde in bimolecular fashion (Figure 38).

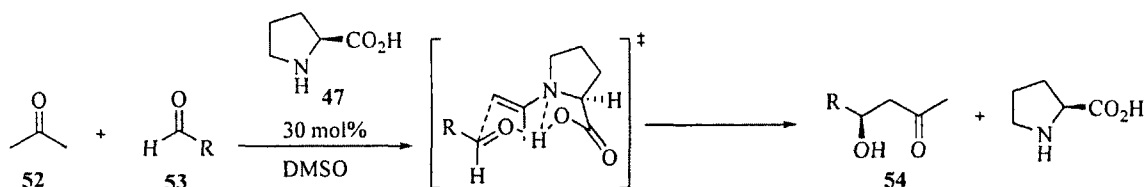


Figure 38. Intermolecular aldol reaction catalyzed by L-proline.

Reaction of acetone with *p*-nitrobenzaldehyde gave aldol addition product in a 68% yield with 76% ee. David MacMillan's group utilized cyclic secondary amines to catalyze Diels-Alder reactions. It was proposed the amine formed an iminium ion with the dienophile, thus lowering the LUMO for reaction with the HOMO of the incoming diene. It has been suggested that these two simultaneous reports, along with those in the late 1990s, marked the infancy of organocatalysis. Interest grew at a rapid pace as it was recognized that the modes of activation via organocatalysis could be extended over a wide range of organic reactions (Figure 39).

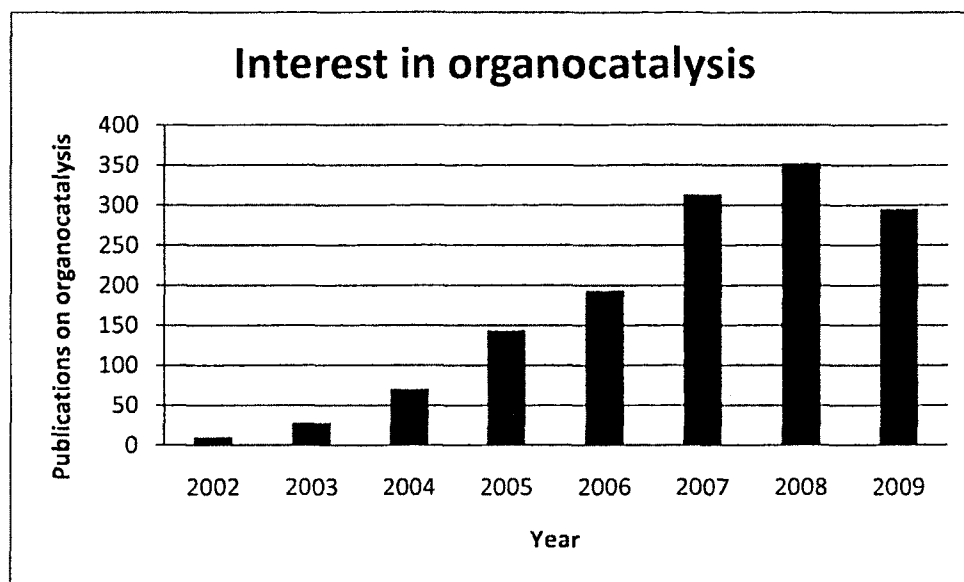


Figure 39. Results of a Scifinder Scholar search of the keyword organocatalysis.

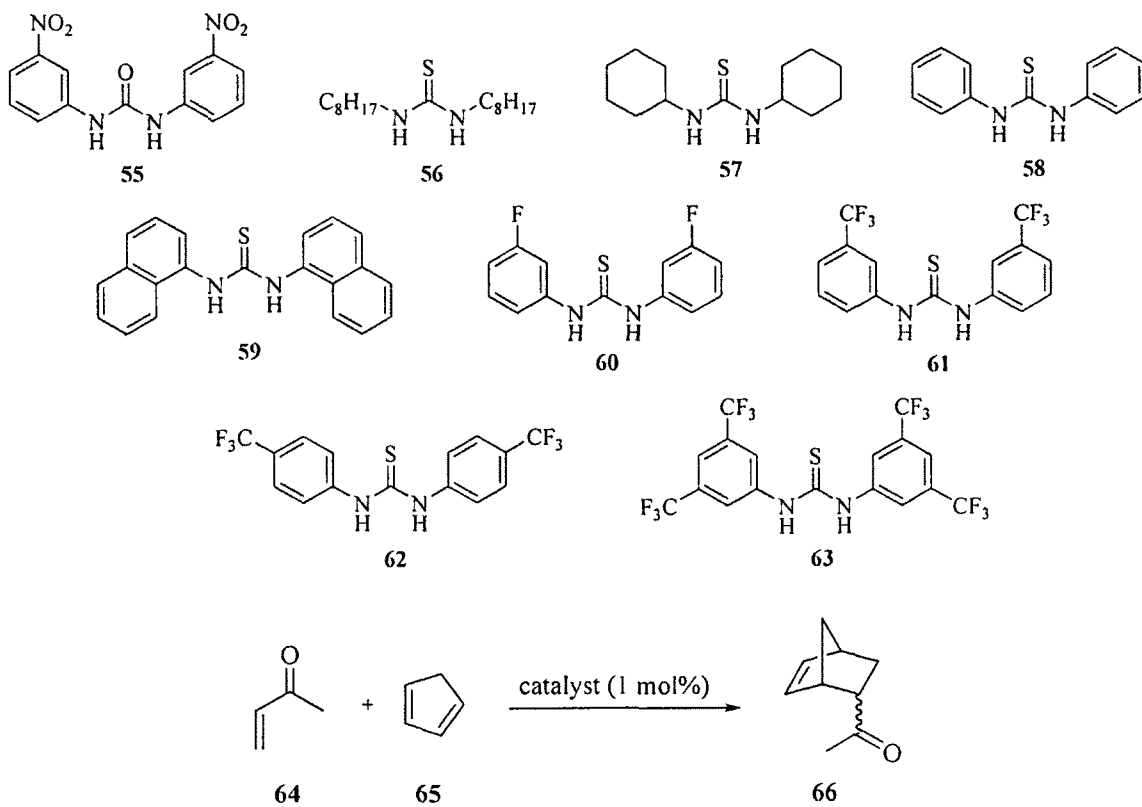
2.1.2 Hydrogen bonding as a mode of activation by organocatalysts

The emergence and success of organocatalysis is attributed to the general modes of activation that can be extended over a wide range of organic reactions. In many respects, asymmetric organocatalysis can be viewed as the biomimetic equivalent of metal-free enzyme catalysis; one need only consider the broad range of reactions catalyzed by such enzymes to appreciate the potential scope of this methodological approach. Since the initial report of the Hajos-Parish reaction numerous modes of activation used in organocatalysis have been reported to be useful including enamine, iminium, SOMO, counterion and hydrogen bonding catalysis all of which have shown success.³⁵ However this work entailed the development of hydrogen bonding organocatalysis and it is this mode of activation that will be discussed in detail throughout this thesis.

Important to the chemistry of carbonyl compounds is the activation of the carbonyl functionality for addition to a nucleophile. The carbonyl lone pairs are considered hard Lewis basic sites making coordination of Lewis acids to a carbonyl lone pair an efficient mode of activation. Coordination of a Lewis acid withdraws electron density away from the carbonyl lowering the energy of the LUMO, which corresponds to the C=O π^* orbital in the localized molecular orbital view, thereby activating the carbonyl carbon toward nucleophilic attack. A hard Lewis acid, the proton, is effective for activating the carbonyl towards carbonyl attack but at the same time can lead to many unwanted reactions. Therefore, typical Lewis acids used have been metals instead of the proton in specific acid catalysis. However, enzymes use general acid catalysis or hydrogen bonding to catalyze a variety of organic transformation where acidic side-chains and hydrogen bonding are used to stabilize transition states. This observation has been used to develop organocatalysts with a mode of activation utilizing hydrogen bonding to lower the carbonyl LUMO and stabilize developing charge in the transition state.

As mentioned earlier, the first hydrogen bonding organocatalysts were those of Jacobson, Corey and Miller and these studies paved the way for the development of other hydrogen bonding organocatalysts. The thiourea group has received considerable attention as a functional scaffold for organocatalysts since the work of Peter Schreiner³⁶ that developed from the observation of Margaret Etter and co-workers³⁷ that urea **55** (Table 7) co-crystallized with a variety of hydrogen bonding acceptors, including carbonyls. This observation led to the development by Schreiner of a series of thiourea organocatalysts **56** - **63** and a demonstration that the most electron deficient thioureas

could catalyze the Diels-Alder reaction between dienophile **64** and diene **65** presumably because of their superior hydrogen bond donating potential (Table 7).



Catalyst	% Conversion over 60 min.
56	27
57	30
58	33
59	33
60	37
61	45
62	55
63	75

Table 7. Catalysis of the Diels-Alder reaction by thioureas.

2.2 The rational design of a new organocatalyst

2.2.1 Squaramide as a functional organocatalyst

It is accepted that preorganization of the enzyme active site is an important contributing factor to the efficiency of enzyme catalyzed reactions. Similarly, in organocatalysis, it is important that the catalyst be predisposed to approximate the incoming reactants and stabilize reactive intermediates along the reaction coordinate. Two examples of the importance of preorganization in organocatalysis include the thiourea-catalyzed Diels-Alder reaction³⁶ and the Bronsted acid/base catalyzed enolization reaction.³⁸ This represents only two examples but a survey of all known asymmetric organocatalysts reveals that the majority are built from preorganized scaffolds such as proline, quinine, BINOL, and thiourea as can be seen in the comprehensive database of asymmetric organocatalysis by Lambropoulos and Deslongchamps (unpublished results). Recently, it has been reported that squaramide can serve as a non-classical isostere of thiourea as it was shown to effectively catalyze the asymmetric addition of 1,3-diketones to nitro olefins.³⁹ Shortly thereafter appeared a report of squaramide catalyzed Mukaiyama aldol and Michael reactions.⁴⁰ Two years prior to these reports our group had been investigating the rational design of an organocatalyst based on the squaramide functional scaffold. These reports certainly prompted us to disclose our results, the bulk of which are reported in this thesis chapter.

Thiourea has received incredible attention since the first report of thiourea as an efficient hydrogen bond donor catalyst³⁶ in 2003 as evidenced by a recent survey of the literature (Figure 40).

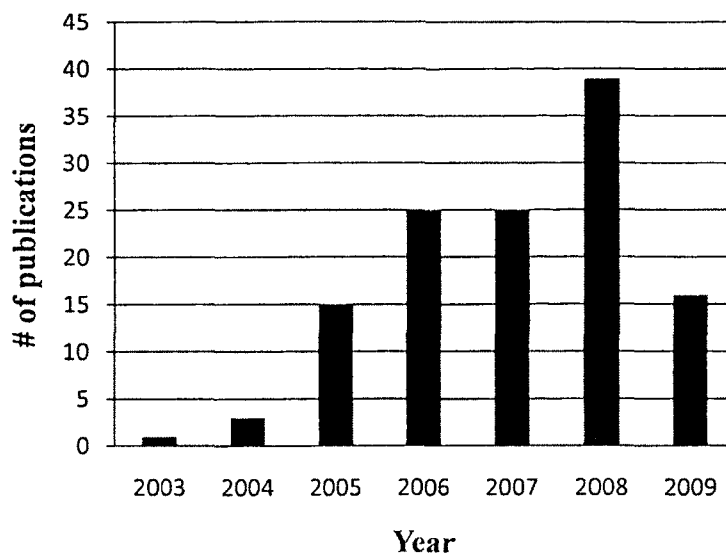


Figure 40. Reports of thiourea as an organocatalyst since 2003 report of noncovalent catalysis of Diels-Alder Reaction.

The squaramide moiety can be easily recognized as an isostere of urea but, despite the two recent reports of squaramide-based organocatalysts, it is our firm belief that key issues must first be addressed in order for the squaramide group to receive equal attention and success as the thiourea group for organocatalysis applications. The first issue relates to the preferred conformation of squaramides, especially secondary squaramides, which are known to exist in two major conformations in solution, anti/anti and syn/anti⁴¹ (Figure 41). Evidently, only the anti/anti conformation is appropriate for the display of two convergent hydrogen bond donors, similarly to urea derivatives, for nucleophilic activation of carbonyl compounds.

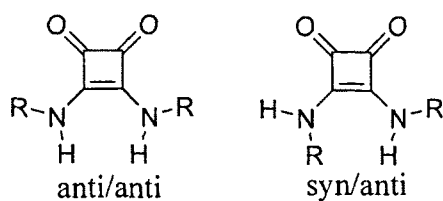


Figure 41. The major conformation of secondary squaramides that exist in solution.

Unfortunately, from the perspective of the design of a bidentate organocatalyst, the equilibrium lies toward the syn/anti conformation⁴¹ for simple secondary squaramide derivatives. The second issue has to do with the fact that secondary squaramides have two excellent hydrogen bond donors (N-H) and two hydrogen bond acceptors (C=O) affording squaramides the propensity to self-assemble into aggregates, including oligomers and dimers, contributing to poor organic solvent solubility and low effective monomer availability for organocatalysis (Figure 42). Herein we report the design of a conformationally controlled squaramide organocatalyst and demonstrate the importance of preorganization for squaramides to serve as effective bidentate hydrogen bond donors and, by the same token, efficient organocatalysts.

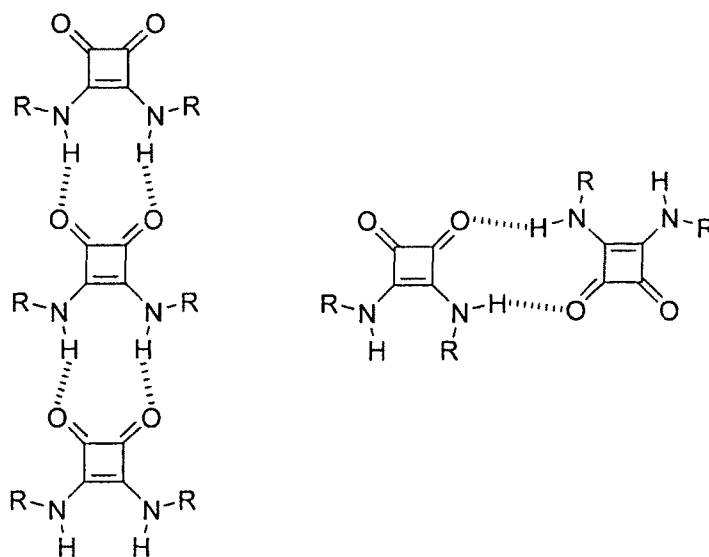


Figure 42. Intermolecular assembly of secondary squaramides into oligomers (left) and dimers (right).

Early into our investigation of utilizing squaramides as bidentate hydrogen bond donors we realized the magnitude of the conformation and solubility problem after many squaramide derivatives failed to exhibit appreciable solubility in CDCl_3 while the single secondary squaramide that displayed adequate solubility was shown to exist predominantly in a syn/anti conformation by NMR ROESY analysis (Figure 43).

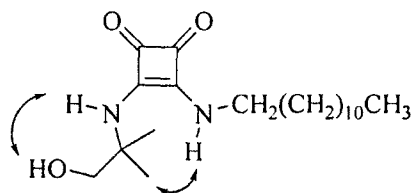


Figure 43. ROESY contacts in squaramide **67**.

The first challenge for us to tackle would be to impart conformational control in a series of secondary squaramides that would exist predominantly in the catalytically relevant anti/anti conformation. This would also entail that some sort of impediment to aggregation be incorporated into the molecular design to improve solubility in organic solvents. Our first design strategy entailed the judicious use of the squaramide carbonyl groups to control the conformation about the rotatable C-N bond via a molecular recognition event through intramolecular hydrogen bonding, hoping for a shift of the conformation equilibrium toward anti/anti (Figure 44). One could also anticipate that hydrogen bonding to the squaramide carbonyls would decrease the basicity of the remaining carbonyl lone pairs while, at the same time, lowering the pK_a of the conjugated NH groups and perhaps improving their hydrogen bond donating propensity.

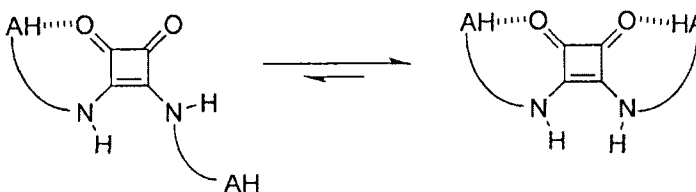


Figure 44. Proposed squaramide conformation equilibrium shift upon intramolecular hydrogen bonding to squaramide carbonyls.

Overall, reducing the propensity for the squaramide molecules to self-assemble while simultaneously increasing the Bronsted acidity of the squaramide NH groups is a most enticing proposition. Our design criteria of using simple and easily obtainable chiral building blocks led us to make use of amino acids coupled to primary amines in our original squaramide design (Figure 45).

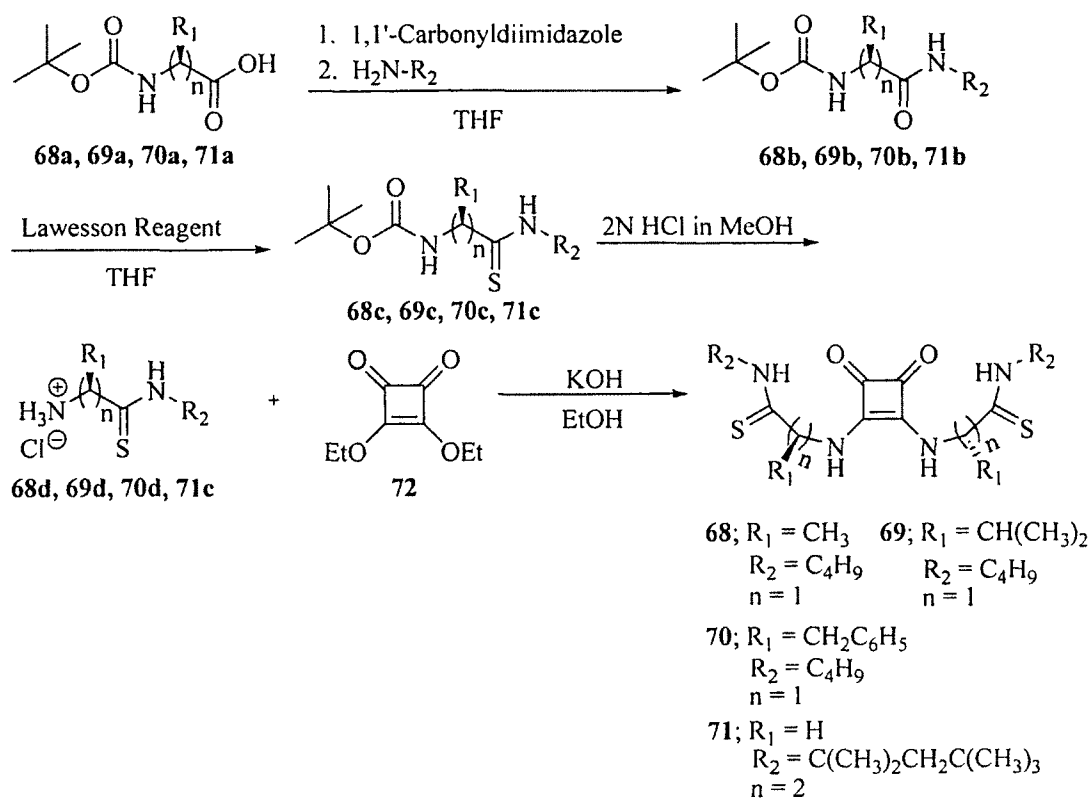


Figure 45. Synthesis of conformational controlled squaramides.

Amines condense with diethyl squarate (**72**) to give squaramides and adding one equivalent of amine gives quantitatively monosquaramide **73**, which when followed by the addition of an excess of amine gives bis-squaramide. This sequential addition allows us to be able to make either symmetrical (**74**) or non-symmetric squaramides (**75**) (Figure 46).

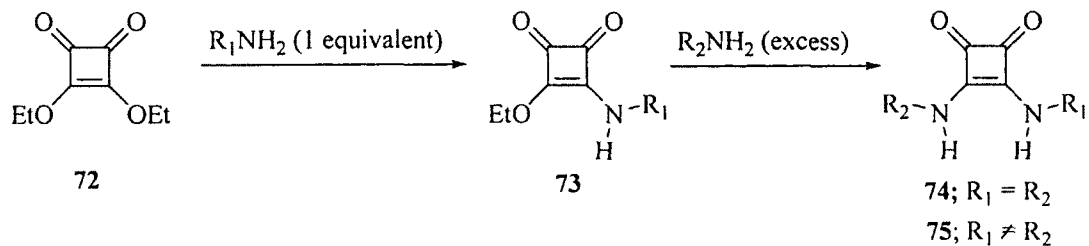


Figure 46. The sequential addition of amines to give either symmetrical or non-symmetric squaramides.

Despite the ability to form both symmetrical and non-symmetric squaramides we favored designing an organocatalyst using symmetrical squaramides because of the advantages of using a C₂-symmetric molecule as an organocatalyst. C₂-symmetry is favorable in an organocatalyst because, similar as in the design of chiral ligands⁴², the number of possible catalyst-substrate interactions are limited which can have a beneficial effect on enantioselectivity by eliminating possible less selective reactive pathways. Also, by reducing the number of possible catalyst-substrate interactions computational led studies of organocatalyzed reaction mechanisms are simplified.

As a chiral source for our squaramide based organocatalyst we made use of amino acids. Initially, amino acids end-capped at their carboxyl group with simple amide functionalities were condensed with diethyl squarate but the resulting squaramides showed poor solubility in organic solvent. The end-cap amide NHs in the arms are likely to hydrogen bond intramolecularly to their nearest neighbor squaramide carbonyl but not very strongly in light of the relatively high pK_a of the amide NH group, while the end-cap amide carbonyls are apt to hydrogen bond intermolecularly and contribute to aggregation. Ultimately, introducing additional amide groups in the squaramide arms

may have led to more self-assembly and less than ideal conformational control. However, simply replacing the amide end-capping group with a thioamide can address both issues. Indeed, the thiocarbonyl group is a softer base and thus a poorer hydrogen bond acceptor while the NH group is more acidic. Both of these factors would likely aid in the conformational preference and molecular recognition propensities of the squaramide catalysts.

To study the accessible conformational space of our squaramide derivatives, a scan of the potential energy surface for rotation about the squaramide C-N bond, starting from the anti/anti conformation was performed. Using B3LYP/6-31G* results show a barrier of rotation of 7 kcal/mol for the squaramide C-N bond of squaramide **68** compared to N,N'-dimethyl squaramide (Figure 47).

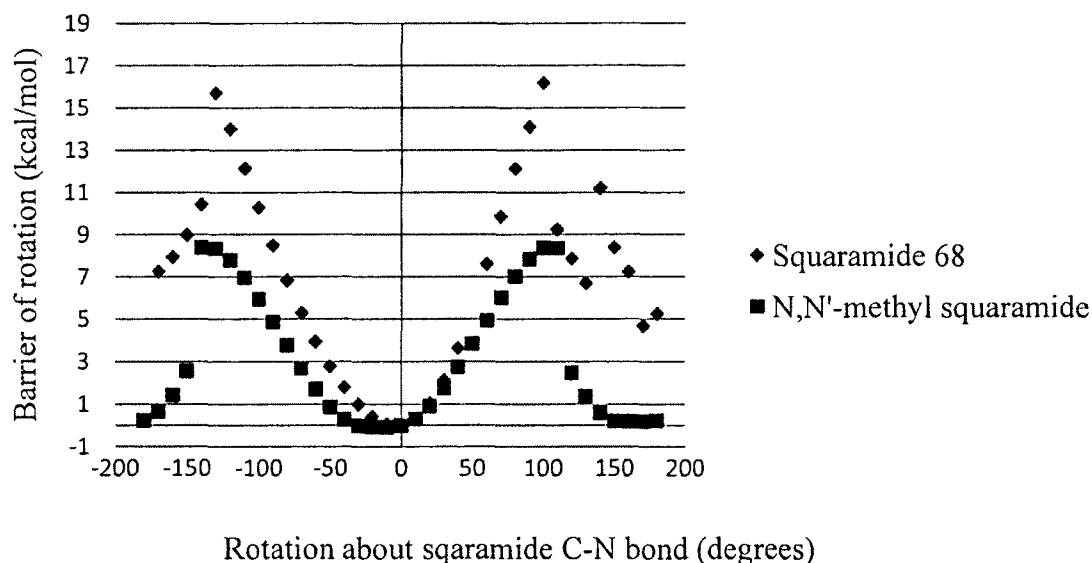


Figure 47. Barrier of rotation about squaramide C-N bond.

A systematic molecular mechanics conformational search of squaramide **68** using the MMF94x forcefield was carried out after which the resultant conformers were geometry re-optimized using B3LYP/6-31G*. The results show that, at least in the gas phase, the anti/anti conformation with intramolecular hydrogen bonded thioamides to the squaramide carbonyls corresponds to the global minimum (Table 8).

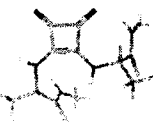
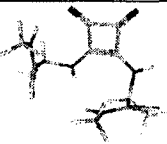
Squaramide conformer	Energy (kcal/mol)
	0.00
	2.72
	3.22
	4.60
	4.86

Table 8. Major squaramide conformers from systematic conformational search.

Relative energy of B3LYP/6-31G* optimized structures.

Despite the computational support that our squaramide derivatives should exist in the desired anti/anti conformation, the experimental evidence, including NMR and x-ray, is somewhat inconclusive. By ^1H NMR, acidic protons typically exhibit downfield shifts when hydrogen bonded; comparing the ^1H NMR chemical shifts of the thioamide N-H in squaramides **68**, **69** and **70** to that of *N*-methylthioacetamide, it appears that the thioamide is hydrogen bonded in squaramides **68** and **69** but not in squaramide **70** (Table 9).

Thioamide N-H	^1H -NMR Chemical Shift (ppm)
<i>N</i> -methylthioacetamide	7.81
Squaramide 68	8.79
Squaramide 69	8.76
Squaramide 70	8.00

Table 9. The ^1H NMR chemical shift of thioamide protons of the indicated compounds as a 10 mM solution in CDCl_3 .

A serial dilution NMR experiment of compounds exhibiting either intermolecular or intramolecular hydrogen bonding is useful in assessing the type of hydrogen bond since intermolecular hydrogen bonds are concentration dependant unlike their intramolecular counterparts. Serial dilution of a CDCl_3 solution of squaramide **68** with CDCl_3 gave no information as there was insignificant change in the chemical shift of either the squaramide N-H or the squaramide thioamide N-H. Repeating the experiment starting

with a $CDCl_3$ solution of squaramide **68** but diluting it with CD_3CN , a much more competitive solvent, resulted in a more noticeable concentration dependence for the chemical shift of the squaramide N-H rather than the squaramide thioamide N-H supporting the notion that the squaramide thioamide N-H is involved in an intramolecular hydrogen bond (Figure 48).

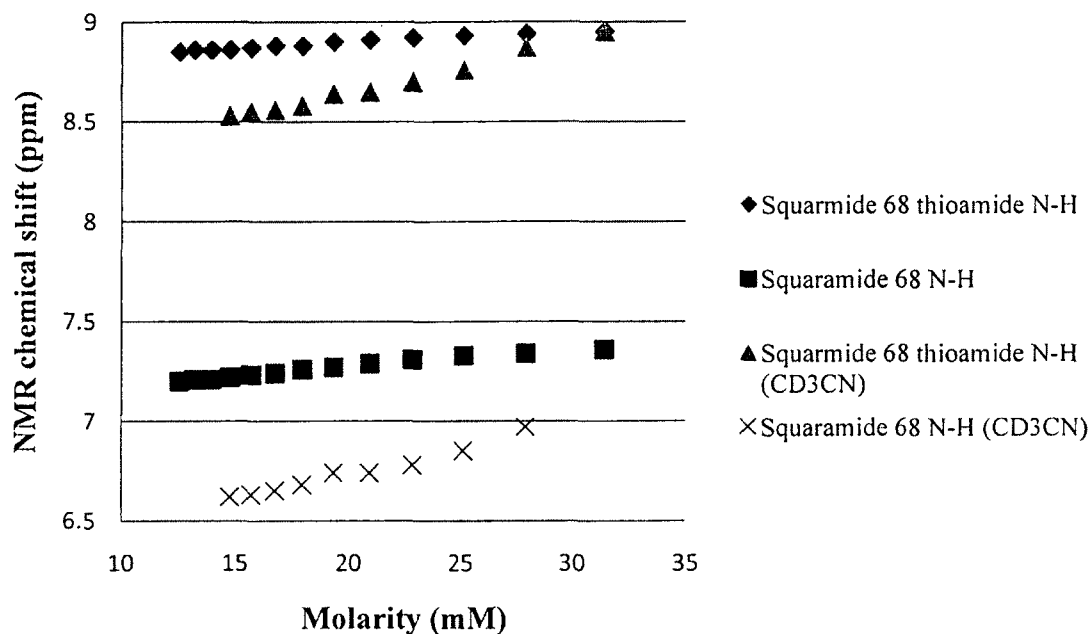


Figure 48. Serial dilution NMR study of squaramide **68**.

Unlike the NMR evidence that suggests that squaramides **68** and **69** have intramolecular hydrogen bonded thioamides (but that squaramide **70** does not), x-ray data shows the thioamides of squaramide **70** hydrogen bonded to the squaramide carbonyls while the thioamides for squaramides **68** and **69** are not (Figure 49). The contradictory results seen in the x-ray data may not be all that surprising as conformational changes upon crystal lattice packing are very common in oligoamide compounds.⁴³

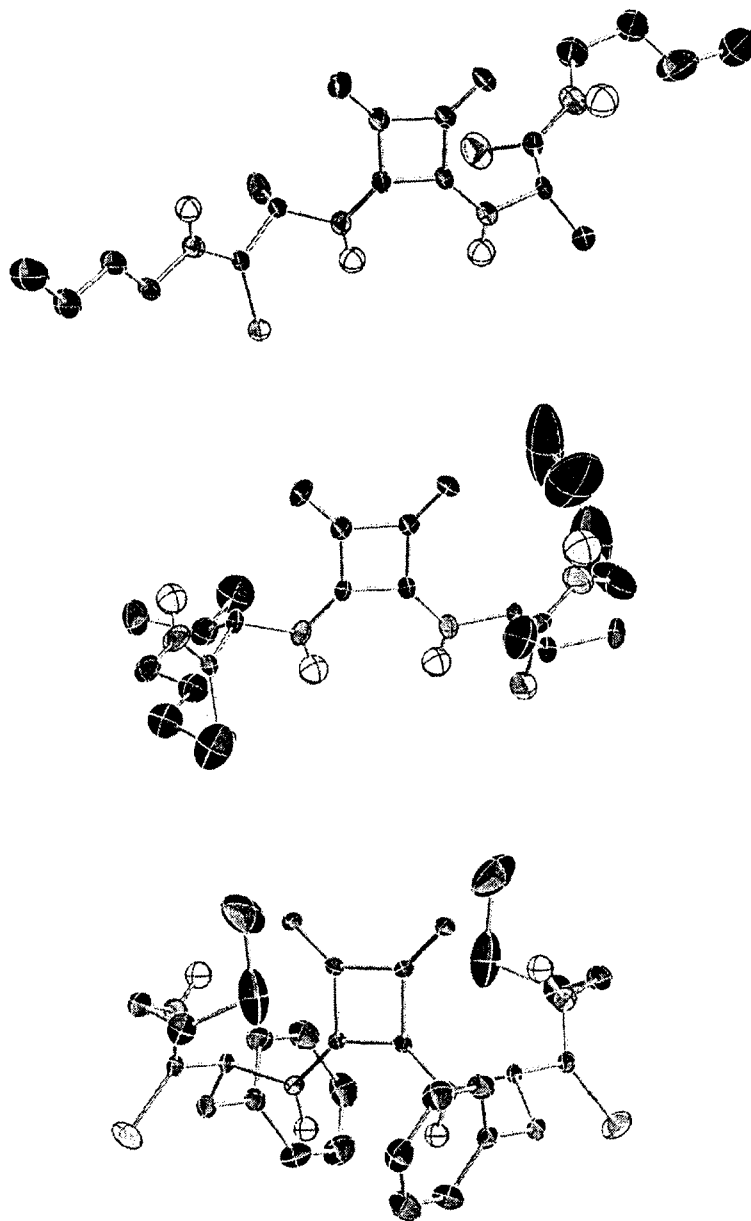


Figure 49. X-ray structures of squaramides 68, 69, and 70.

We attempted to detect a heteronuclear nOe between the squaramide thioamide N-H and the squaramide carbonyl carbon but failed to observe such an interaction. We were unclear of the heteronuclear nOe sensitivity at the concentrations of squaramides we

tested so we couldn't conclude that the intramolecular hydrogen bond didn't exist. However, it was discouraging that we couldn't find conclusive evidence for the conformation of our squaramide derivatives. In one final attempt to elucidate the conformation we attempted VT-NMR of squaramide **68**. At 25°C, the proton alpha to the squaramide N-H is broad, while one would expect that it should appear as a sharp multiplet in a rigid structure. At -25°C, the alpha proton signal begins to sharpen but additional signals appear for protons a, b and c indicative of squaramides existing in multiple conformations that interconvert quickly on the NMR time scale (i.e. faster than a millisecond) at higher temperatures (Figure 50). Attempts to go to lower temperatures failed as squaramide solubility became an issue.

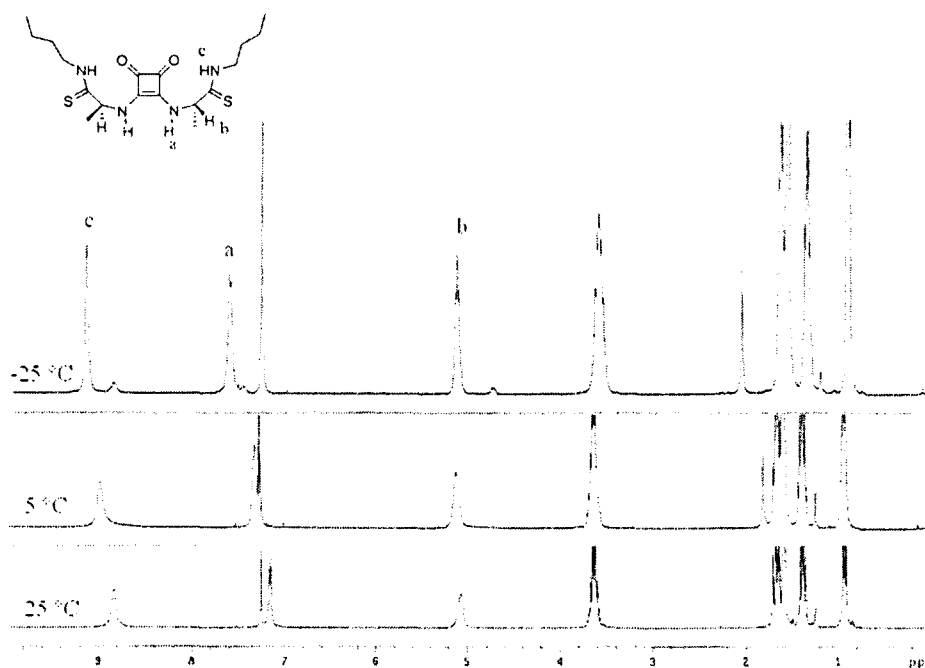


Figure 50. VT ¹H-NMR of squaramide **68**.

2.2.2 Testing squaramides catalytic activity

By all accounts, it appears that the squaramide derivatives exist in solution as a dynamic population of conformations, including both intramolecularly and intermolecularly hydrogen bonded thioamide arms. Perhaps the population of anti/anti conformers is nevertheless adequate for organocatalysis applications. Thus, we decided to test their ability to catalyze the Diels-Alder reaction (Figure 51). The Diels-Alder reaction was chosen as a test experiment because it has been shown to be accelerated by bidentate hydrogen bonding in the now famous *Nature* paper published by Rawal in 2003;^{44, 45} it has also been used as a method to assess the ability of organocatalysts to accelerate reactions via hydrogen bonding.^{46, 47}

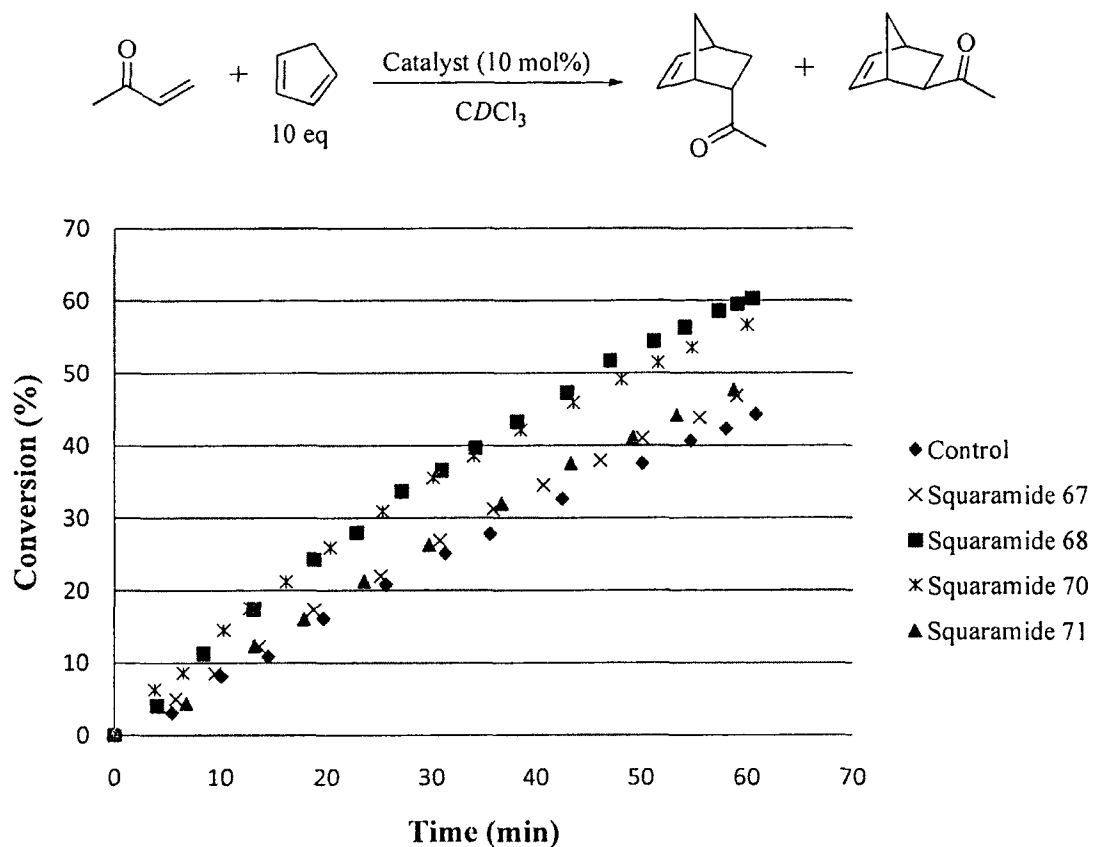


Figure 51. Rate enhancement of the Diels-Alder reaction by conformationally controlled squaramides **68** and **70**.

Given the rate enhancement of the above Diels-Alder reaction, it is apparent that when catalyzing reactions using squaramide as a functional scaffold, it is important to present preorganized bidentate hydrogen bonds. Indeed, squaramides **68** and **70** were able to catalyze the Diels-Alder reaction but squaramide **70** did not have catalytic activity; the failure of **71** is likely due to the fact that β -alanine has more conformational freedom and the entropy loss upon preorganization is not compensated by the gain in enthalpy through hydrogen bonding to the squaramide carbonyls.

2.2.3 Attempts towards the synthesis of 2nd generation squaramides

Encouraged by the Diels-Alder reaction results, we next directed our attention towards more specifically functionalized squaramide derivatives, which would be more conformationally preorganized, presenting multiple hydrogen bonds for intramolecular hydrogen bonding to the squaramide carbonyl, anticipating that the resultant structures would generally be more conducive to organocatalysis. Initially, we attempted the syntheses of squaramides **74** and **75** both of which present two intramolecular hydrogen bonding interactions per squaramide carbonyl (Figure 52). However, the coupling of the amino acid derivatives **72** and **73** to diethyl squarate proved to be very difficult, leading to multiple unidentified products.

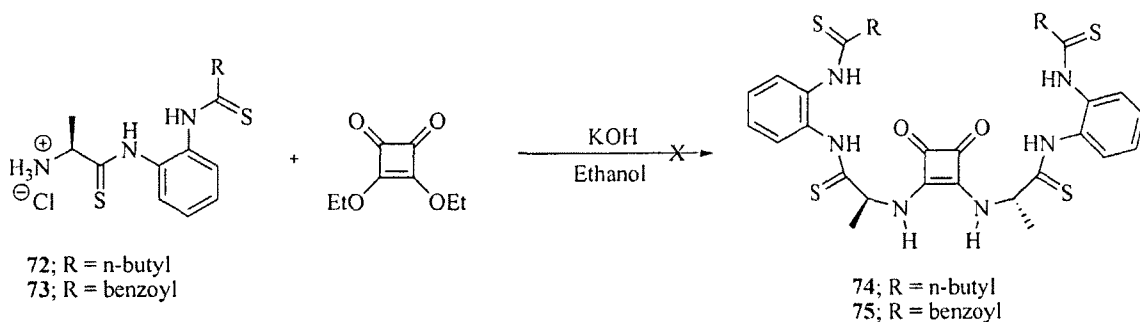


Figure 52. Unsuccessful attempt of the synthesis of squaramides **74** and **75**.

Crystals harvested from a crude reaction mixture of an attempt to prepare **74** by the coupling method shown above were determined by x-ray to correspond to benzamidine by-product **77**! A proposed route to its formation is shown below (Figure 53), based on an intramolecular thioacyl transfer, followed by intramolecular condensation to generate the observed benzamidine.

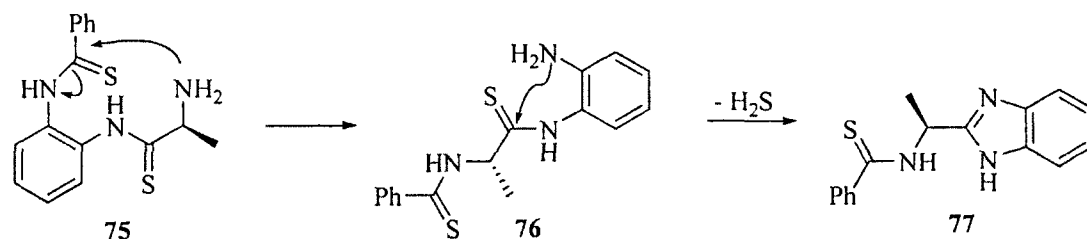


Figure 53. Proposed formation of compound 77.

Another squaramide derivative we investigated is squaramide 78. We envisioned the boronate esters either forming an “ate” complex with the squaramide carbonyls or with the aniline derived amide thus increasing the amides acidity and therefore enabling a stronger interaction with the squaramide carbonyls (Figure 54).

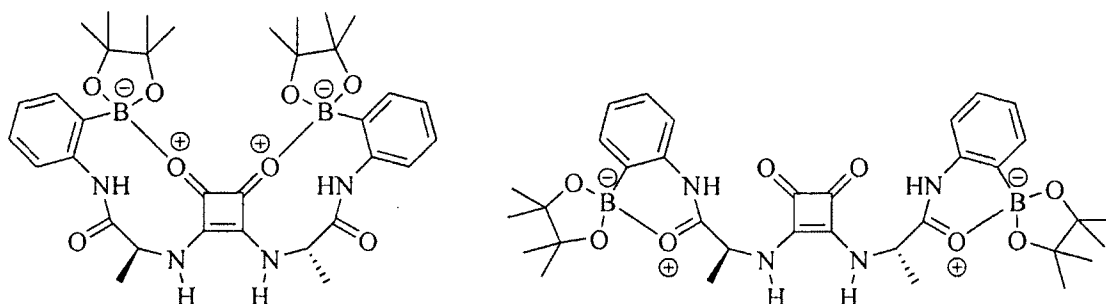


Figure 54. Possible “ate” complexes in squaramide 78.

Compound 78 was synthesized successfully, however it was later shown to be catalytically inactive toward the Diels-Alder reaction described in Figure 50, and was not pursued further.

2.2.4 Squaramide self-templated macrocyclization

Lastly, we envisioned using the squaramide core to template a macrocyclization reaction to give fully preorganized squaramide **81** from precursor **79** (Figure 55).

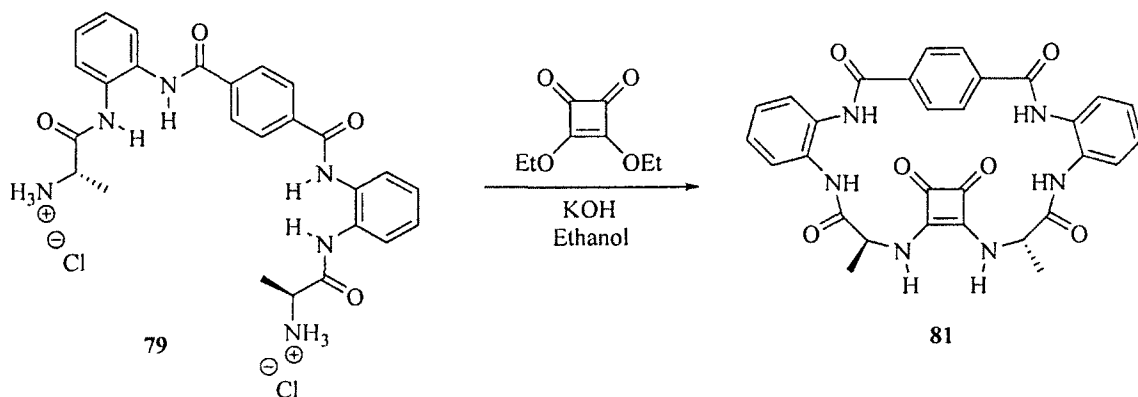


Figure 55. Synthesis of squaramide macrocycle **81**.

In general, macrocycles are difficult to obtain because the formation of medium to large rings is entropically unfavorable and unwanted side-reactions, especially oligomerization, become dominant. Likewise, the geometry for intramolecular cyclization must be energetically favorable or else the reaction will fail due to enthalpic strain. The formation of oligomers results from intermolecular reactions and can sometimes be mitigated by using high dilution conditions for the cyclization reaction. Proper macrocyclization can also be promoted by a template-directed reaction where the acyclic macrocyclic precursor interacts with some template through non-covalent interactions. A classic example of template-directed macrocyclization is the metal cation directed formation of crown ethers⁴⁸ (Figure 56).

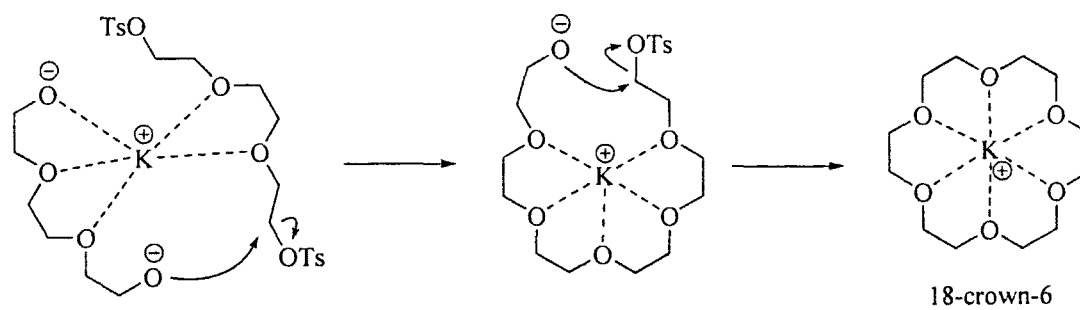


Figure 56. Metal cation directed formation of 18-crown-6.

A more elegant example is the synthesis of cyclic porphyrin oligomers using a Glaser alkyne coupling templated by 4,4'-bipyridyl (Bipy)⁴⁹ (Figure 57).

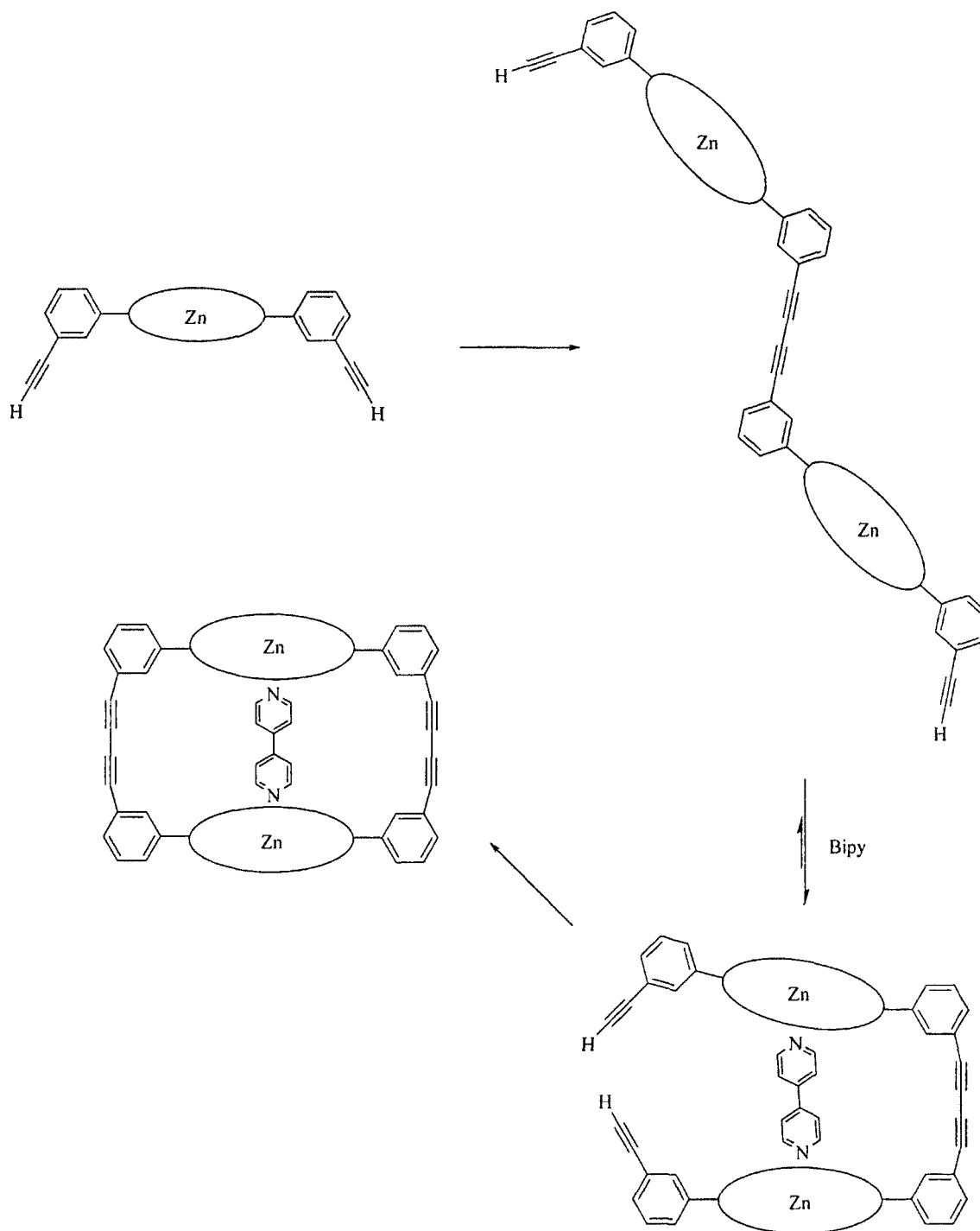


Figure 57. Synthesis of cyclic porphyrin oligomers templated by Bipy.

The above macrocyclization reactions were template-directed using metal cations but hydrogen bonding too has been utilized in macrocyclization reactions^{41, 50} (Figure 58).

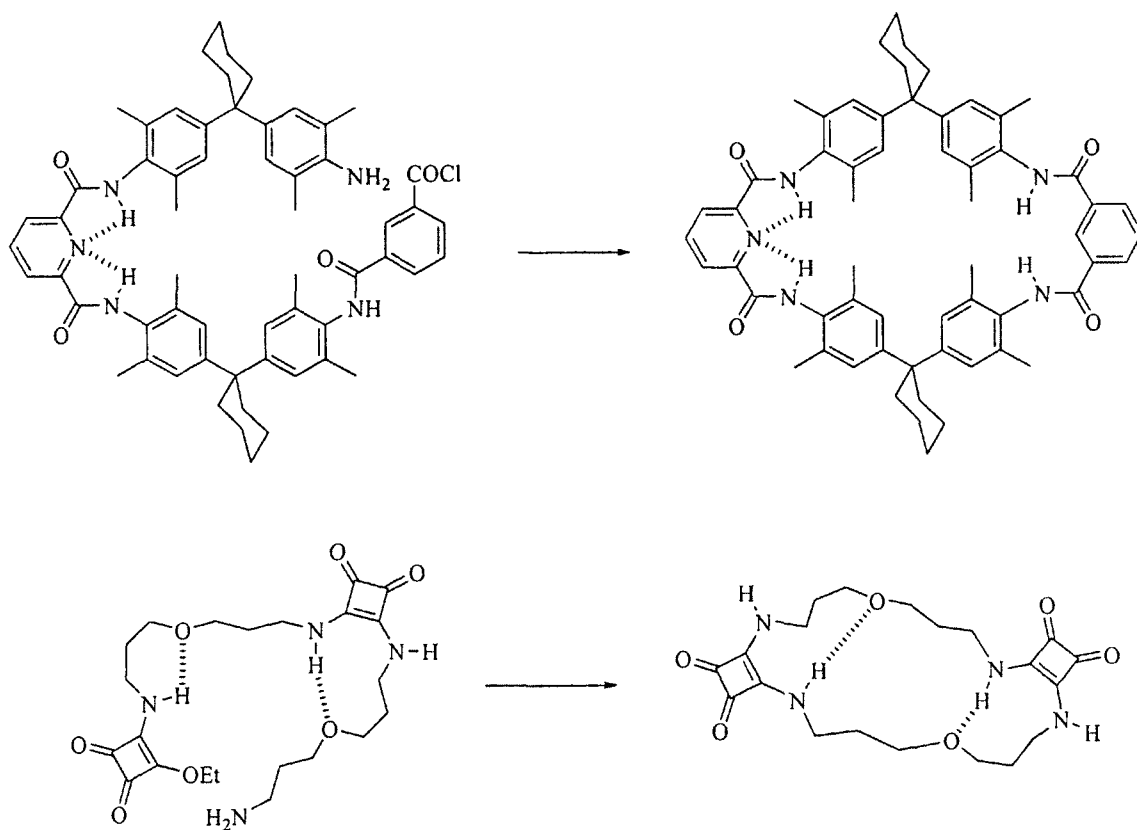


Figure 58. Examples of hydrogen bonded directed macrocyclization.

Our pre-laboratory investigation into forming squaramide macrocycles started with performing a molecular dynamics simulation of macrocyclic precursor **80**. Simulation over a 350 picosecond period shows folding of **80** mediated by hydrogen bonding between the squaramide carbonyls and the aryl amides (Figure 59) which may promote the macrocyclization of **80** to **81**.

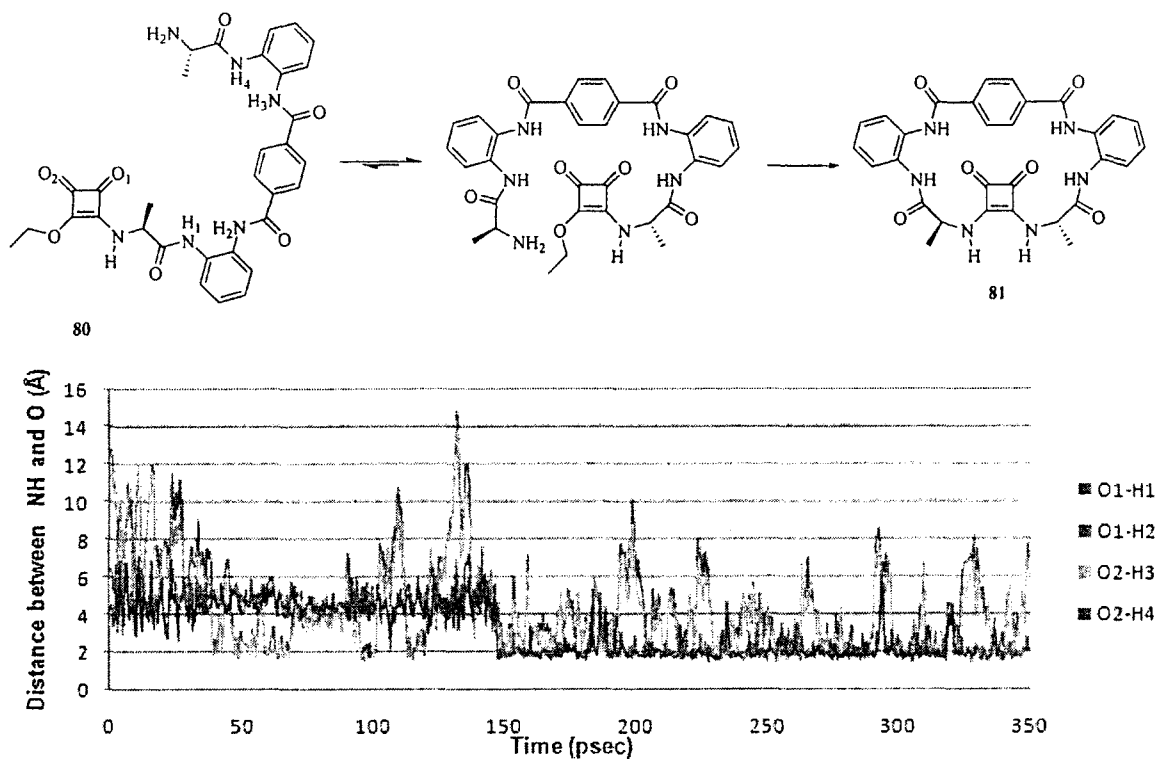


Figure 59. Molecular dynamics simulation (NVT ensemble, 600 K, 0.5 psec time step) of **80** demonstrating the propensity to self-fold.

Encouraged by the molecular dynamics results, the synthesis of **81** was attempted by first coupling nitroaniline **82** with terephthaloyl chloride **83** giving **84** in a 61.8% yield which then was reduced to give diamine **85** in a 71.5 % yield (Figure 60).

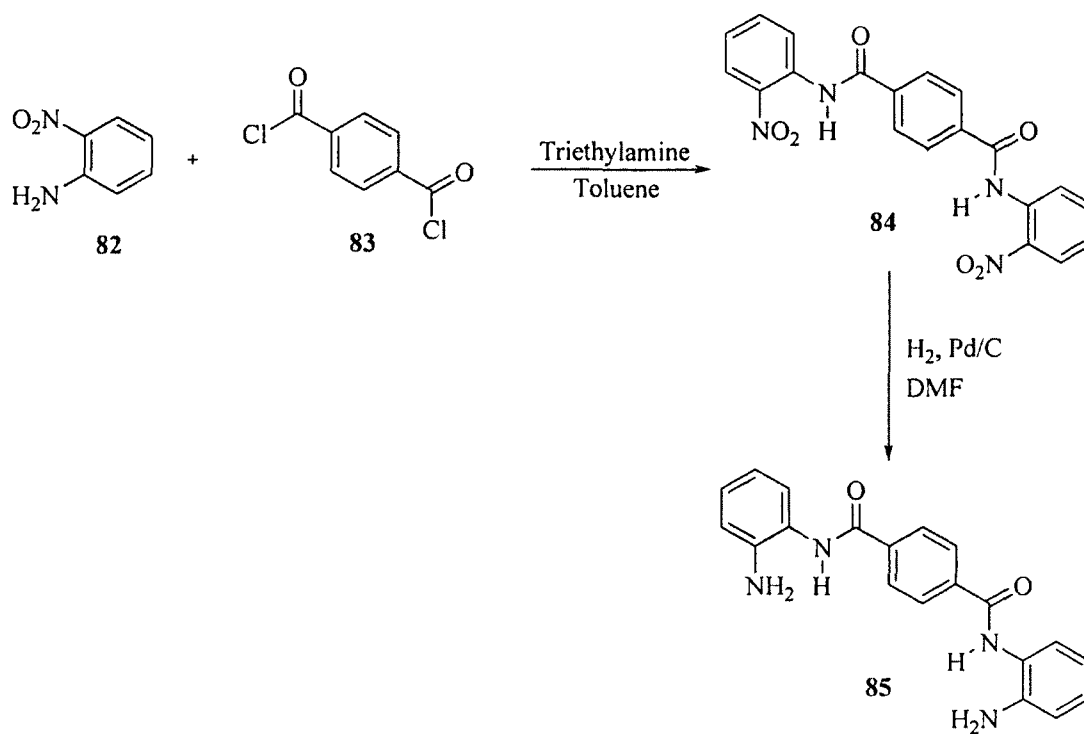


Figure 60. Attempt towards the synthesis of **81**.

Compounds **84** and **85** displayed poor solubility in a wide range of organic solvents so an alternative synthetic route to macrocyclic precursor **79** was attempted, starting from diamine **86** and amino acid **68a** (Figure 61).

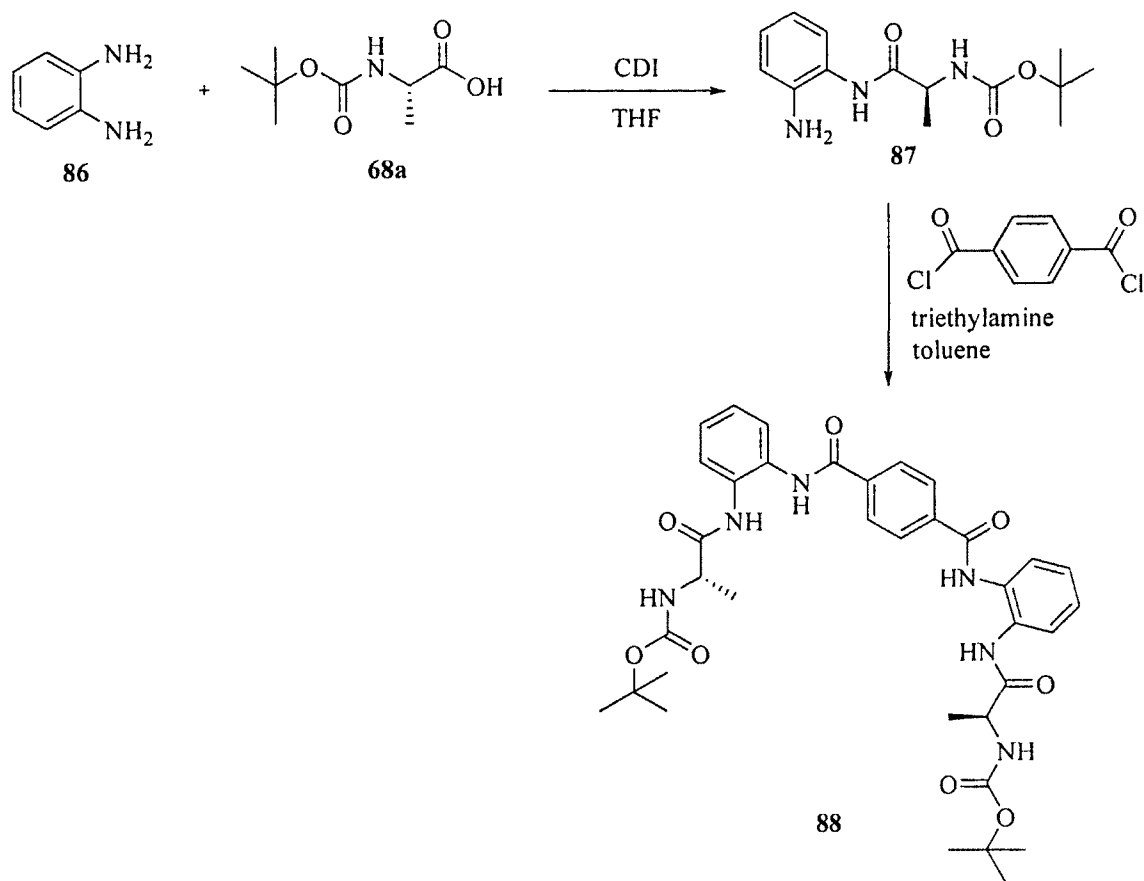


Figure 61. Alternative synthesis of squaramide macrocycle precursor 79.

The CDI promoted coupling of **68a** to **86** gave **87** in a 66.2% yield. Compound **87** was then added to terephthaloyl chloride to give **88** in a 79.4% yield which was then treated in 2 M HCl in methanol to give **79** which after work-up was then added to diethyl squarate. After 60 hours the reaction was concentrated yielding a white solid which was only soluble in DMSO. Addition of water precipitated a white solid which is believed to be squaramide macrocycle **81** shown by $^1\text{H-NMR}$ (disappearance of diethyl squarate OCH_2CH_3 proton signals and appearance of alanine alpha proton signal) and MS. Attempts were made at synthesizing derivatives **89** and **90** (Figure 62) but the crude reaction mixtures had multiple products that could not be isolated, with solubility again

an issue so macrocyclization was abandoned. Initially we believed that introducing alkyl groups into diamine **86** would increase organic solvent solubility but proved not to be the case. The *t*-butyl group may not have been sterically bulky enough to prevent self-assembly and the *n*-heptyl alkyl chain likely promoted self-assembly through hydrophobic interactions between alkyl chains of adjacent molecules.

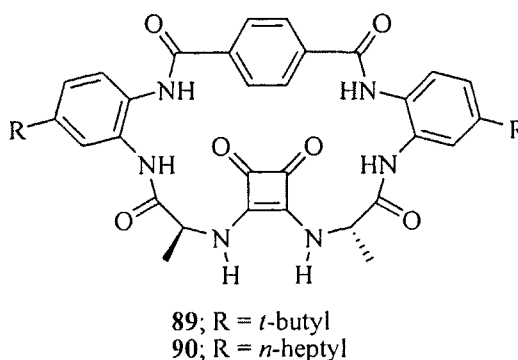


Figure 62. Squaramide macrocycle derivatives.

2.2.5 Squaramide catalyzed enolate addition reactions

Despite three failed attempts at making ‘second generation’ squaramide derivatives, our ‘first generation’ squaramides were at hand and had shown catalytic activity toward the Diels-Alder reaction. We decided to test these squaramides as Bronsted acid catalysts for the Baylis-Hillman reaction (Figure 63). The Baylis-Hillman reaction is extremely useful in synthesis but it is known to be notoriously slow and often low-yielding. Relevant to our studies of asymmetric organocatalysis was the demonstration that this reaction could be accelerated by BINOL,⁵¹ a ditopic Bronsted acid, and that numerous other organocatalyzed examples had been subsequently reported.⁵²⁻⁵⁸ It is thought that a bidentate hydrogen bond donor, present in the C₂-symmetric arrangement of the two

phenol groups of BINOL could stabilize both the nucleophilic betaine intermediate and activate the aldehyde component.⁵⁷ It has also been suggested that a hydrogen bond donor catalyst may assist in the elimination of the intermolecular base to give the Baylis-Hillman product⁵³ and that the elimination is possibly the rate-determining step rather than the addition of the betaine intermediate to the aldehyde.⁵⁹

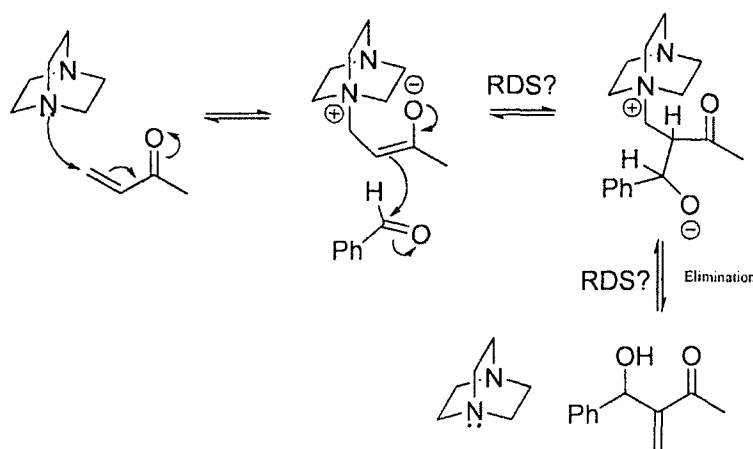


Figure 63. The Baylis-Hillman reaction and its potential rate-determining steps (RDS).

The observation that the reaction has a solvent dependence has been proposed as evidence that the final elimination of the nucleophilic base catalyst is the rate-determining step in some cases. For instance, the addition of cyclohexenone **91** to p-nitrobenzaldehyde (**92**) in the presence of n-butylphosphine as the nucleophilic catalyst runs smoothly in THF but does not lead to any product formation in CH_2Cl_2 (Figure 64).

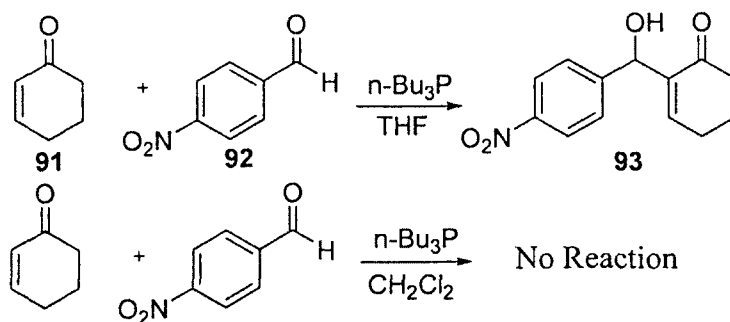


Figure 64. The solvent dependence of the Baylis-Hillman reaction.

The difference in reactivity was attributed to the fact that THF may function as a Bronsted base and to assist in the elimination (Figure 65).

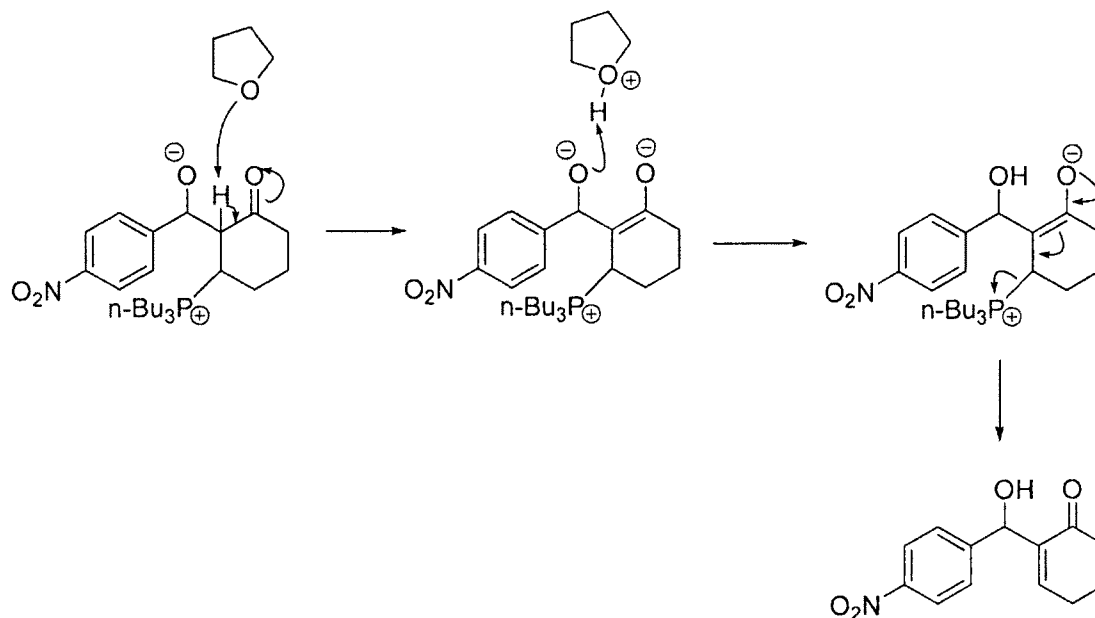


Figure 65. Solvent assisted elimination to give the Baylis-Hillman product.

It has also been shown that there is a rate enhancement in the Baylis-Hillman reaction in the presence of alcohol. One of the proposed explanations put forth to account for the

rate enhancement was that the alcohol could assist in the elimination step through a bimolecular hydrogen bonded six-membered ring transition state⁶⁰ (Figure 66).

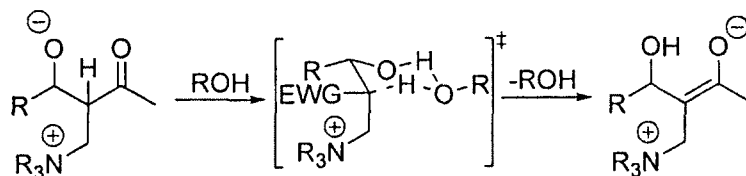
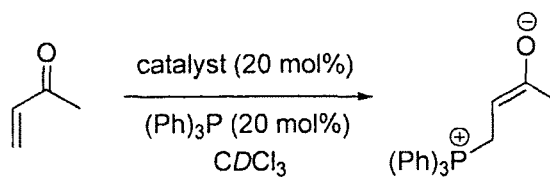


Figure 66. The proposed role of the alcohol in the observed rate enhancement of the Baylis-Hillman reaction.

Given the past success of Bronsted acid catalyzed Baylis-Hillman reactions, we anticipated that squaramides could serve as favourable catalysts. For instance, their complexation to the carbonyl group of the alpha,beta-unsaturated component via hydrogen bonding could facilitate the formation and/or stabilize the betaine intermediate produced by the initial conjugate addition of amine or phosphine. Likewise, the squaramides could potentially activate the aldehyde component toward addition of the enolate group of the betaine intermediate. The squaramides could potentially also assist in the elimination step to give the final product.

If some intermolecular factor were capable of stabilizing the betaine intermediate, the result should be a higher concentration of that betaine in solution and one might be able to observe it by NMR.⁶¹ Indeed, ³¹P-NMR showed the presence of two ³¹P signals, corresponding to free phosphine (-5.3 ppm) and the betaine intermediate (25.2 ppm), when triphenylphospine was added to methyl vinyl ketone in the presence of squaramide **68** (Table 10).



Catalyst	(Ph) ₃ P : betaine
none	96.2 : 3.8
67	96.6 : 3.4
68	85.5 : 14.5
78	81.6 : 18.4

Table 10. Ratio of free phosphine to betaine intermediate as a function of added squaramide catalysts. Values calculated by integration of ³¹P NMR signals.

Intrigued by these results, a simple Baylis-Hillman electrophile, p-nitrobenzaldehyde, was added to assess whether the betaine intermediate could be trapped and result in the formation of at least some of the Baylis-Hillman product. Gratifyingly, the Baylis-Hillman product **95** was formed in a 54.4% yield, calculated by NMR, along with other unidentified products (Figure 67).

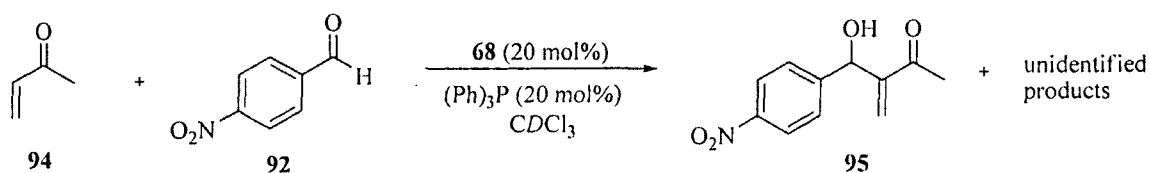


Figure 67. Squaramide catalyzed Baylis-Hillman reaction.

To minimize side-reactions due principally to its high reactivity, methyl vinyl ketone was replaced by cyclohexenone, a less reactive enone still known to react in a Baylis-Hillman reaction, however no reaction occurred in the presence of triphenylphosphine as the nucleophilic catalyst. However, using the more reactive *n*-tributylphosphine as nucleophilic catalyst, a reaction did take place but we were surprised to obtain solely aldol products instead of Baylis-Hillman products (Table 11)!

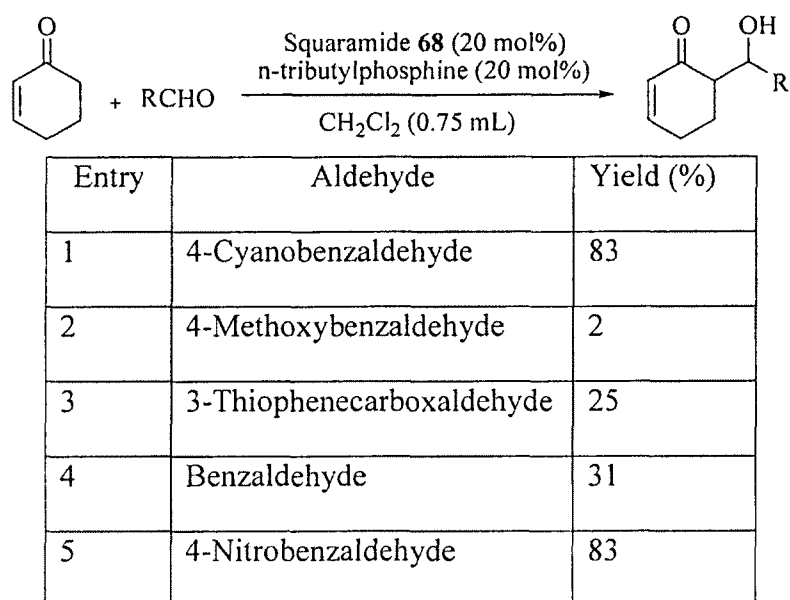


Table 11. Squaramide catalyzed aldol reaction using Baylis-Hillman conditions.

This turned out to be a most interesting outcome. To obtain aldol products via an enolization mechanism would require that cyclohexenone be able to somehow enolize at the α -CH₂ position of cyclohexenone first, then add to the aldehyde (Figure 68).

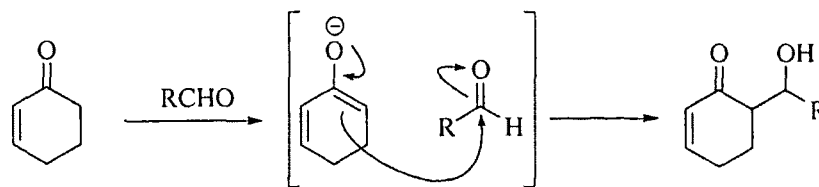


Figure 68. The requirement for enolization to give the aldol product.

Aldol products formed via enolate addition to the electrophile are normally Bronsted base promoted and a metal-based Lewis acid is typically used to stabilize the enolate and to approximate the enolate to the electrophile (Figure 69).

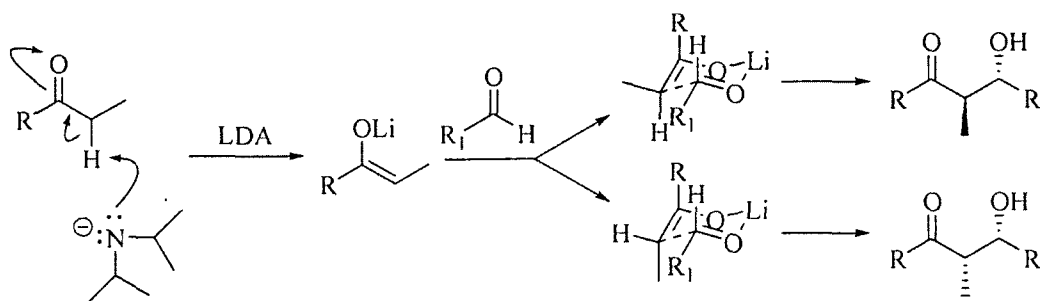


Figure 69. Aldol reaction using LDA.

Although Bronsted bases and Lewis acids are typically used to form and stabilize enolates, hydrogen bonding too has been shown to promote enolate formation by increasing the acidity of carbon acids through stabilization of the corresponding enolate.⁶² Furthermore, it has been shown that the catalyzed rate can be further increased if the Bronsted acid and base are preorganized by scaffolding to activate the carbonyl group and abstract the alpha hydrogen with proper geometric and stereoelectronic alignment³⁸ (Figure 70). However, to the best of our knowledge, there

are no reported examples of a Bronsted acid/base catalyzed direct aldol reaction using unactivated ketones or enolates not stabilized by intramolecular hydrogen bonding.⁶³

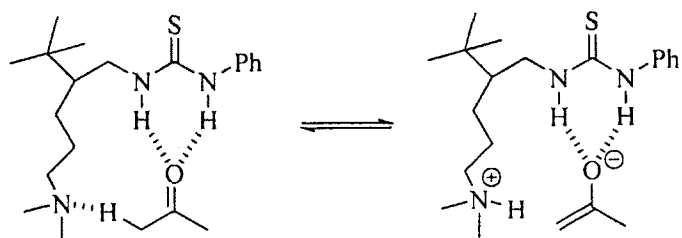


Figure 70. The Druekhammer enolization catalyst.

We were therefore extremely pleased and surprised to observe the formation of aldol product in the presence of squaramide. It didn't appear that a preorganized Bronsted acid/base system existed in our squaramide/tributylphosphine system to effectively catalyze enolization; likewise it was extremely unlikely that in our system, free squaramide and tributylphosphine (pKa 8.43)⁶⁴ would promote enolization (and subsequent aldol) given that thiourea (pKa 21)⁶⁵ and free dimethylbutylamine (pKa 10.06)⁶⁶ were shown previously to be inadequate for rate enhancements of enolization.³⁸ The other base in our system, the Baylis-Hillman betaine intermediate, was as well presumably lacking preorganization with the squaramide Bronsted acid despite the fact that the enolate present could be basic enough to enolize a second enone molecule.

Upon considering a wide range of potential reaction pathways, all our analyses eventually converged on a most alluring scenario that could account for the observed catalytic activity of the squaramide/phosphine system: It is clear that the conjugate

addition of phosphine produces a betaine that is fairly basic and, although it could deprotonate directly at the methylene position of another cyclohexenone molecule to catalyze the aldol, the betaine would be much more likely to deprotonate the squaramide based on simple pK_a arguments. The resulting squaramide monoanion represents a unique form of preorganized Bronsted acid/base that fulfills all the requirements for an effective enolization organocatalyst (Figure 71).

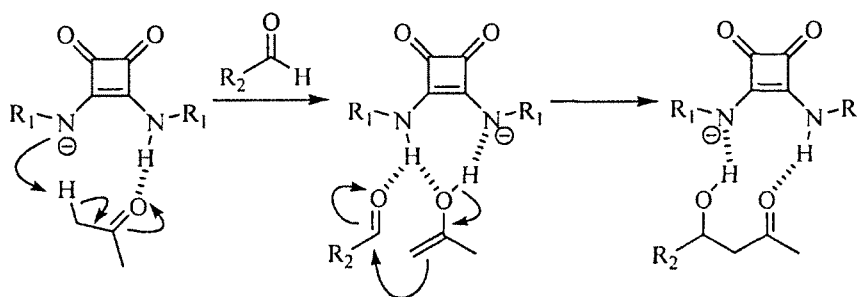


Figure 71. Proton shuffling via squaramide monoanion to catalyze enolization and then approximation of an electrophile for subsequent enolate addition.

The squaramide monoanion is certainly easy to form and is quite stable; its geometry appears to be well-disposed to simultaneously activate the carbonyl “substrate” via hydrogen bonding and abstract the alpha hydrogen to form the enolate. The activation barrier for proton shuffling between the two squaramide nitrogens during proton transfer is likely very low due to the electron delocalization between the two nitrogens inherent in the squaramide moiety. Integrating the squaramide monoanion into a complete catalytic cycle is illustrated in Figure 72. After deprotonation of squaramide by betaine, cyclohexenone can bind in a geometry as discussed above conducive to enolization. Subsequent proton transfer to squaramide then allows bifurcated H-bonding to the

enolate oxygen and hydrogen bonding to the incoming electrophile approximates it to the enolate for subsequent addition. Alternatively, one squaramide NH can hydrogen bond to the enolate while the second squaramide NH can possibly approximate and activate the electrophile for enolate addition. The final aldol addition product is formed after transfer from squaramide a NH proton to the oxygen anion and thus regeneration of squaramide monoanion to reenter the catalytic cycle.

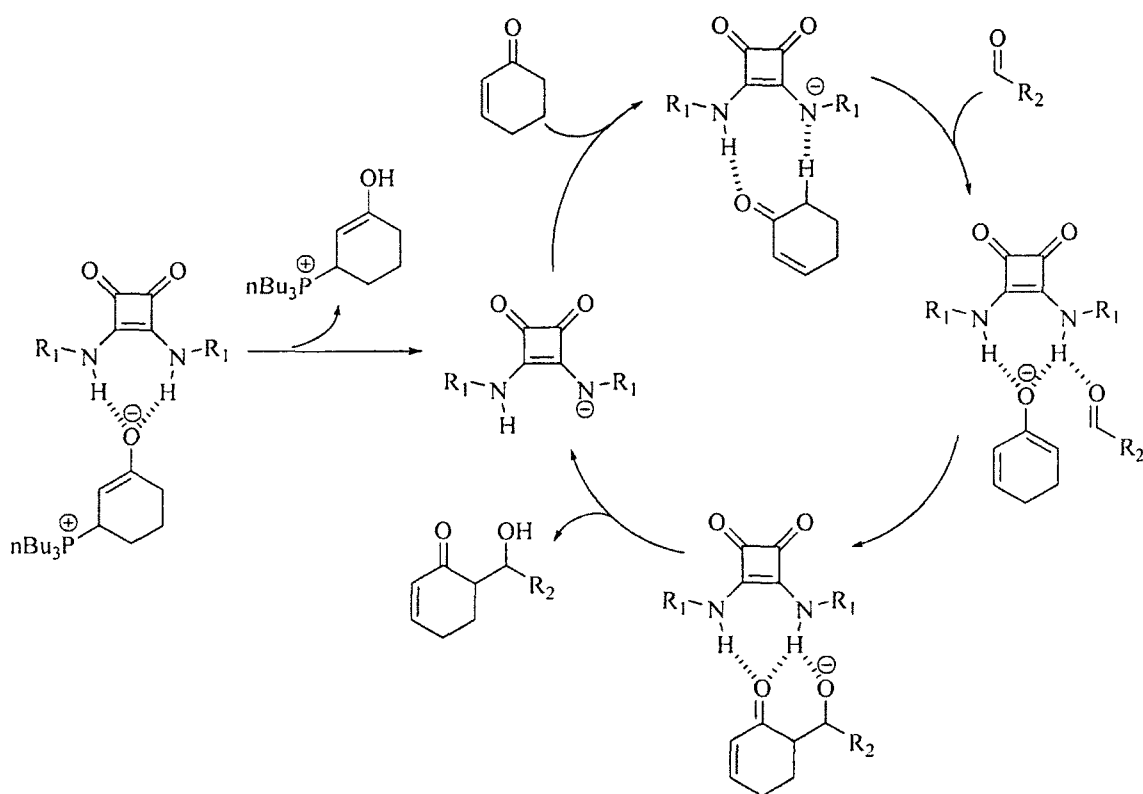


Figure 72. Deprotonation of squaramide by the Baylis-Hillman betaine intermediate to form squaramide monoanion and the proposed subsequent catalytic cycle for the aldol reaction.

Of course, proposing such a catalytic cycle requires at least some experimental backing. First, a test was designed to assess experimentally whether enolization was occurring at the α -CH₂ position of cyclohexenone under the reaction conditions. Accordingly, a deuterium incorporation experiment reacting cyclohexenone in the presence of squaramide **68** and *n*-tributylphosphine, using acetone-*d*₆ as a deuterium source was carried out (Figure 73).

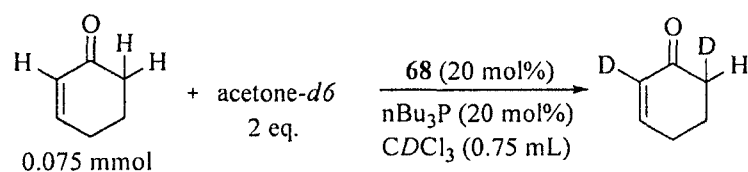


Figure 73. Incorporation of deuterium into cyclohexenone in the presence of squaramide **68** and *n*-tributylphosphine.

Incorporation of deuterium at the α -CH position was 57% while at the α -CH₂ position incorporation was 21%. Thus, the betaine is indeed forming, which explains deuterium exchange at the vinylic CH position (deprotonating at the gamma carbon followed by deuterium quench seems unlikely under the reaction conditions). However, deprotonation is also observed at the α -CH₂ as shown above. To gain more insight into the ability of the squaramide monoanion to enolize ketones a computation study was initiated. Modeling the squaramide monoanion with bound acetone indicates a ground-state binding geometry that allows the alpha CH bond perpendicular to the carbonyl group to hydrogen bond effectively to the amide anion while the carbonyl group interacts with the opposing amide NH hydrogen bond donor; this is a

stereoelectronically preferred geometry allowing for proper overlap of the scissile C-H sigma bond with the carbonyl π^* orbital during the course of enolization (Figure 74).

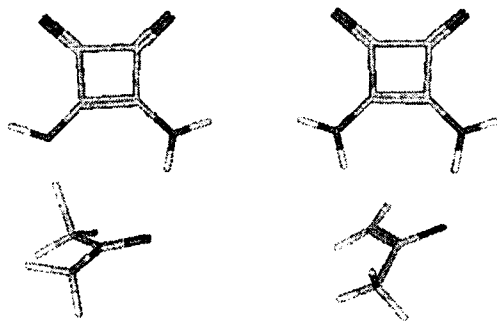


Figure 74. Squaramide monoanion and bound acetone enolization transition state (left) and bound acetone enolate to squaramide (right) optimized with B3LYP 6-31+G* in GAMESS.

Interestingly, the squaramide N-H is hydrogen bonded to the π -system of the carbonyl group instead of one of the lone pairs of the acetone oxygen. It has in fact been suggested that a Bronsted acid hydrogen bonded to the π -system of a carbon acid has a greater effect on carbon acidity than if hydrogen bonded to the lone pair electrons.⁶⁷ In hindsight, this is perfectly logical since, at first approximation, the oxygen lone pairs are orthogonal to the π -system of the carbonyl group. Protonating at the π -system of the carbonyl rather than at one of the oxygen lone pairs should induce enolization more readily.

A quantum mechanical study was then carried out to show that at least one hydrogen bond to the π -system has a stabilizing effect on enolates. Initially, two molecular

systems were created using acetaldehyde and $\text{NH}_3/\text{NH}_4^+$ where ammonia models the Bronsted base. In one molecular system, two ammonium ions were used as hydrogen bond donor surrogates interacting with both carbonyl lone pairs of the acetaldehyde. In the other molecular system, one ammonium group was bound to a lone pair while the other one interacted with the π -system (Figure 75).

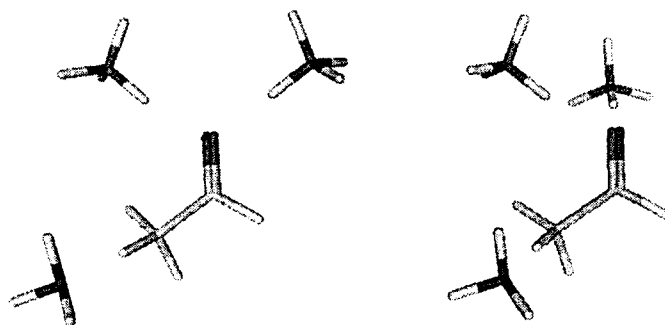


Figure 75. Ammonia adding to acetaldehyde with two ammonium ions hydrogen bonded to both carbonyl lone pairs (left) and one ammonium group bound to a lone pair and one bound to the π -bond (right).

Anticipating that if both systems in Figure 67 were geometry optimized while lengthening the alpha C-H bond in gradual increments, two different binding geometries to the enolate would be obtained, providing some insight into whether hydrogen bonding to the carbonyl π -bond helps to stabilize the incipient negative charge on the developing enolate. Interestingly, during geometry optimization both complexes optimized to the same geometry with the ammonium ion originally H-bonded to the π -bond rotated out onto the lone pair (Figure 76).

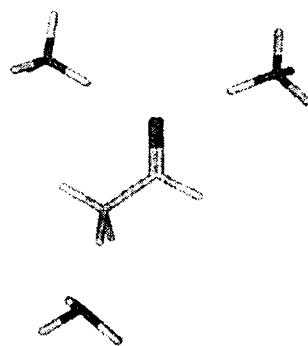


Figure 76. B3LYP 6-31G* geometry optimization of acetaldehyde with ammonia and two ammonium molecules.

After numerous attempts at obtaining geometry optimized structures with ammonium ions directed toward the carbonyl π -bond, the approach was modified and instead worked directly from the optimized complex with hydrogen bonding to the carbonyl lone pairs. We anticipated that if hydrogen bonding to the carbonyl π -bond was important for stabilization of the developing negative charge during enolate formation, at least one of the ammonium molecules would rotate away from the lone pair and towards the developing enolate π -system. Results show that one ammonium molecule rotates away from a lone pair as enolization occurs resulting in a bound enolate that is 1.54 kcal/mol less stable than bound acetaldehyde and bound enol that is 0.86 kcal/mol less stable than bound acetaldehyde (Figure 77).

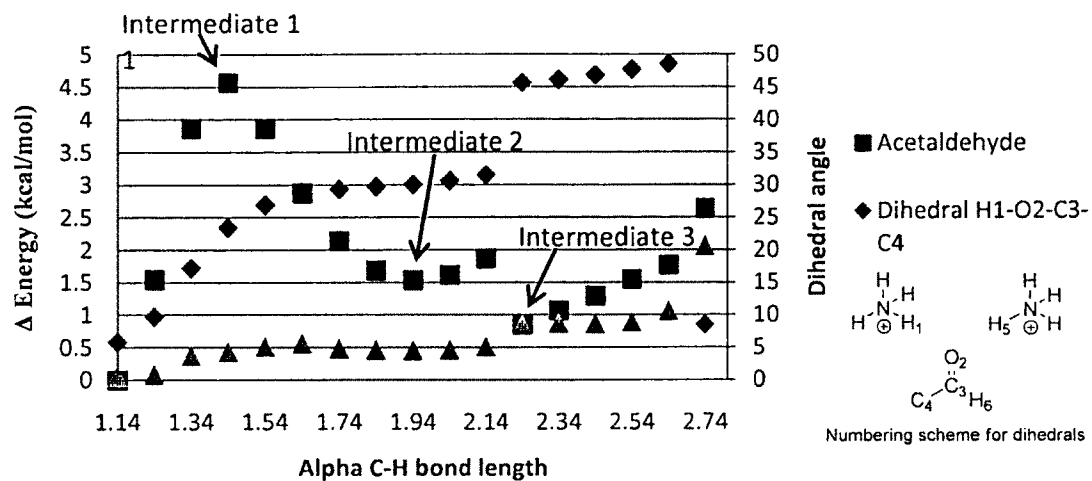


Figure 77. Reaction coordinate for the enolization of acetaldehyde and resultant positioning of ammonium molecules. Intermediate 1 (left), intermediate 2 (middle) and intermediate 3 (right).

When both ammonium ions are tethered together the reaction coordinate is considerably different with both the enolate and enol existing in a higher energy state. Presumably, as the hydrogen bond donor is rotating away from one of the carbonyl lone pairs, there is strain created in the linker as the other hydrogen bond donor attempts to remain hydrogen bonded to a lone pair resulting in intermediates along the reaction coordinate that are significantly less stable than the starting structure (Figure 78).

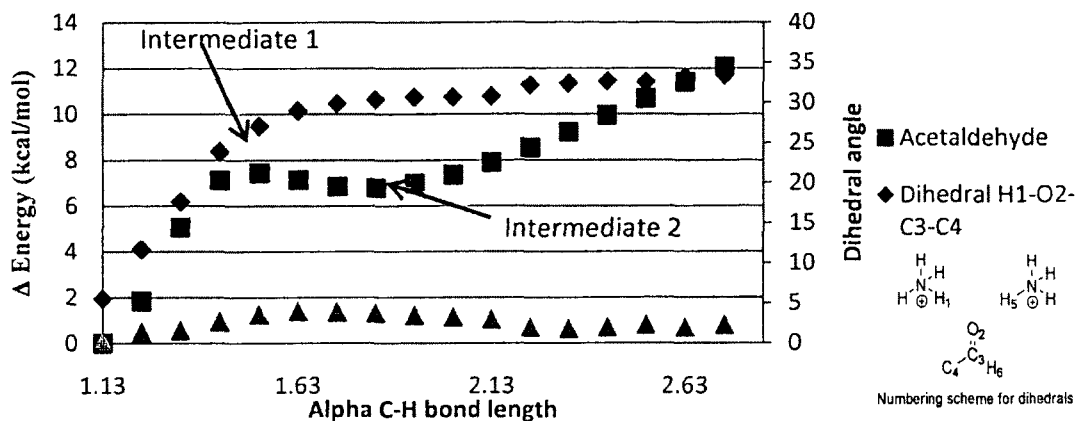
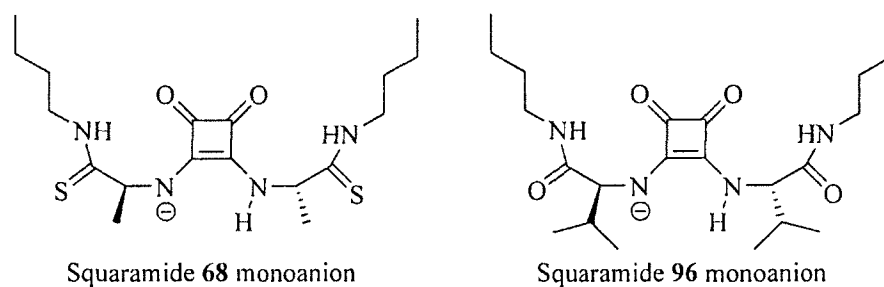


Figure 78. Reaction coordinate for the enolization of acetaldehyde and resultant positioning of tethered ammonium molecules. Intermediate 1 (left) and intermediate 2 (right).

An interesting experiment to test much more directly the catalytic propensity of squaramide monoanion would be to prepare it in a straightforward and controlled manner without resorting to the *in situ* formation of a Baylis-Hillman betaine as the base to deprotonate squaramide. It could then, be determined if squaramide monoanion, on its own, acts as a competent enolization and direct aldol catalyst? To this effect benzyltrimethylammonium (BTMA) squaramide monoanion was prepared and the rate of

enolization of acetone-*d*6 was determined experimentally. The BTMA cation was chosen as a non-interacting counteranion, incapable of acting as a Lewis acid, which could potentially complicate the outcome of the reaction. In fact, BTMA alkoxides have been shown previously to cleanly catalyze the alpha alkylation of aldehyde enolates with little or no aldol by-products, in the absence of chelating cations.⁶⁸ Previous studies using a well-tuned thiourea based enolization catalyst showed a rate constant of 0.05 min⁻¹ representing a 5x rate enhancement over uncatalyzed enolization.³⁸ Using BTMA squaramide monoanion, we found up to a 14x rate enhancement (Table 12).

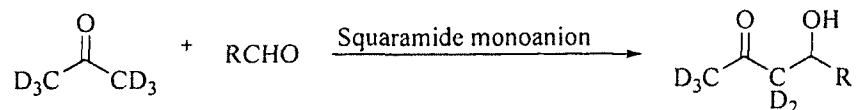


Catalyst	Rate (min ⁻¹)
68	0.084
96	0.123

Table 12. Rate of squaramide catalyzed enolization of acetone-*d*6.

The ability of squaramide monoanion to catalyze the direct aldol reaction was then studied experimentally; initial experiments show promise with high yielding reactions (Table 13). NMR tube experiments showed that acetone-*d*6 undergoes clean aldol condensation to a range of aldehyde electrophiles, in the presence of 20 mol% of

squaramide monoanions **68** or **96**. The neutral squaramide themselves did not catalyze any reaction. The near-quantitative aldol condensation of acetone with 4-nitrobenzaldehyde in the presence of 20 mol% of BTMA squaramide monoanion derived from **96** is certainly noteworthy.



Catalyst	Aldehyde	Time (min)	Yield %
None	4-Nitrobenzaldehyde	60	0
68	4-Nitrobenzaldehyde	60	91.5
96	4-Nitrobenzaldehyde	5	100
96	Benzaldehyde	60	70.8
96	Isobutyraldehyde	60	56.2

Table 13. Squaramide monoanion catalysis of the direct aldol reaction.

It has been suggested that enzymes catalyzing enolization reactions stabilize the enolate as an enolic intermediate through a partial proton transfer from the acid catalyst to the enolate oxygen.⁶⁹ Organocatalysts may also stabilize reactive intermediates⁷⁰ and it is possible that squaramide is stabilizing and displaying an enolic intermediate which undergoes subsequent aldol addition in the presence of aldehyde. Current computational studies are ongoing to assist in the understanding of the exact mechanism and of the

requirements for regioselective and enantioselective squaramide monoanion catalyzed direct aldol reactions.

Finally, we found experimentally that the reaction of benzaldehyde with 2-butanone catalyzed by either squaramide **96** or **97** (Figure 79) BTMA monoanion shows regioselectivity towards the thermodynamic enolate over the kinetic by a ratio of up to 8:1 based on the *syn* / *anti* aldol product ratio when reacted in toluene at room temperature. Investigation of enantioselectivity shows a 0% ee for the *syn* product at room temperature but at 4°C has a 22% ee. Chiral HPLC baseline separation was not achievable for the *anti* product and thus enantiomeric excess was not calculated.

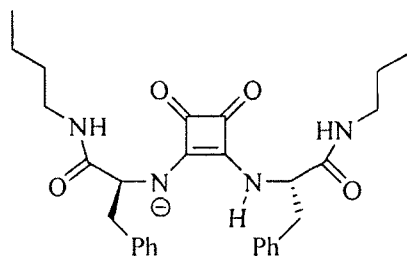


Figure 78. Squaramide **97** monoanion.

2.3 Computational chemistry

2.3.1 Computational chemistry and organocatalysis

Throughout the development of a squaramide organocatalyst we utilized computational chemistry to assist in the better understanding of experimental results and proved to be a valuable tool in our research. However, while the experimental developments in organocatalysis have advanced rapidly over the last decade, specific computational studies of organocatalysis are still in their infancy with only a few groups active in the area worldwide. Nevertheless, some investigators have shown the usefulness of

computational chemistry to predict reactivity, to provide insight into the mechanisms of organocatalyzed reactions, and to suggest general design principles. Not surprisingly, and perhaps somewhat fitting, the first organocatalyzed reaction to be studied computationally was the Hajos-Parrish reaction.^{27,71-73} Computational studies by the Houk group supported an enamine mechanism and also predicted the experimentally observed product (Figure 80).

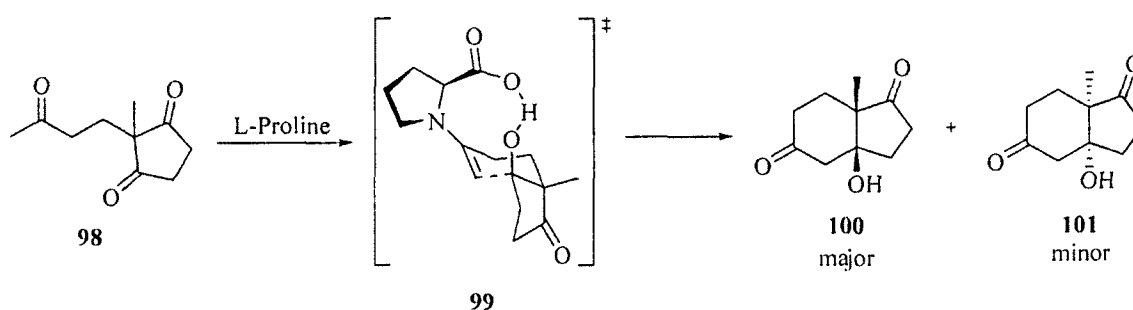


Figure 80. The Hajos-Parrish reaction and the transition state predicted computationally that gives the experimentally determined major product.

The above example verified an experimental observation but the work was also directed toward designing a catalyst to give a desired stereochemical outcome.⁷⁴ L-proline organocatalyzed Mannich reactions give products with a *syn* configuration (Figure 81) but an experimental observation that pipercolic acid gave a mixture of *syn* and *anti* addition products led to the computational design of an organocatalyst to give *anti* addition Mannich products⁷⁵ (Figure 82).

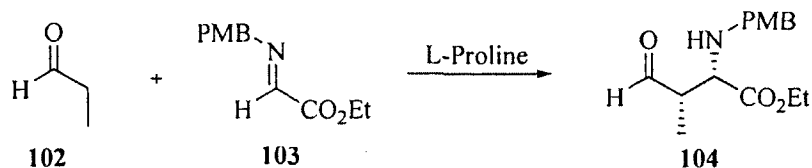


Figure 81. L-Proline catalyzed Mannich reaction leading to *syn* addition product.

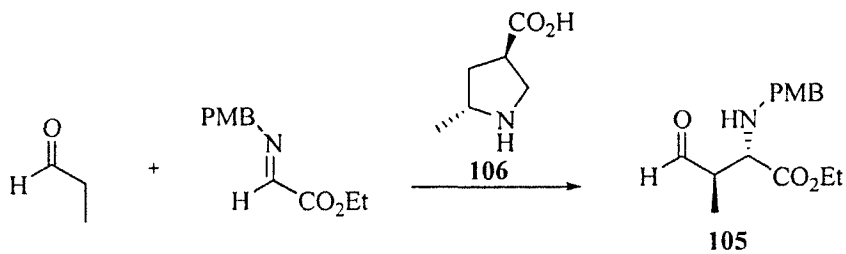


Figure 82. Organocatalyzed Mannich reaction leading to *anti* addition product.

The above examples demonstrate the utility of using quantum mechanics to help understand organocatalyzed mechanisms and to tune the stereochemical outcome of asymmetric reactions. Numerous examples of organocatalyzed reactions studied through quantum mechanics continue to emerge and will continue to represent an important area of research in the field.

However, a survey of the literature for computational studies of organocatalysis reveals that the vast majority of catalytic systems studied to date involve either covalently bound catalysts, such as the enamine intermediates formed by condensation of a proline catalyst to a carbonyl substrate, or reactions where more than one bond is formed, such as the Diels-Alder reaction. For both these types of reactions, modeling the kinetically relevant transition states is fairly straightforward because there are actually very few degrees of freedom to consider for generating the possible transition state geometries.

Using chemical intuition, a good knowledge of conformational analysis, and a clear understanding of the reaction mechanism allows one to home in on the appropriate transition state geometry for subsequent high-level quantum mechanical modeling. However, much of the developing methodologies in asymmetric organocatalysis involve non-covalent catalysis, such as in the case of Bronsted acid organocatalyzed reactions, and organocatalysts that have considerable conformational flexibility. Thus, the challenge of identifying and modeling the most kinetically relevant transition state model for a given reaction becomes a nearly intractable problem, as one may need to consider thousands of potential transition state geometries for further consideration for quantum mechanical calculation.

A significant contribution to the area of computational chemistry and organocatalysis has been from the research group of Ghislain Deslongchamps who introduced and used the concept of “reverse docking” to study the mechanisms and stereochemical outcomes of asymmetric organocatalyzed reactions.^{76, 77} Unlike the quantum mechanics work of others, Deslongchamps uses molecular mechanics and a stochastic approach to dock large databases of catalyst conformations around rigid transition state models of the uncatalyzed reactions to identify favorable catalytic poses between organocatalyst and transition state (Figure 83).

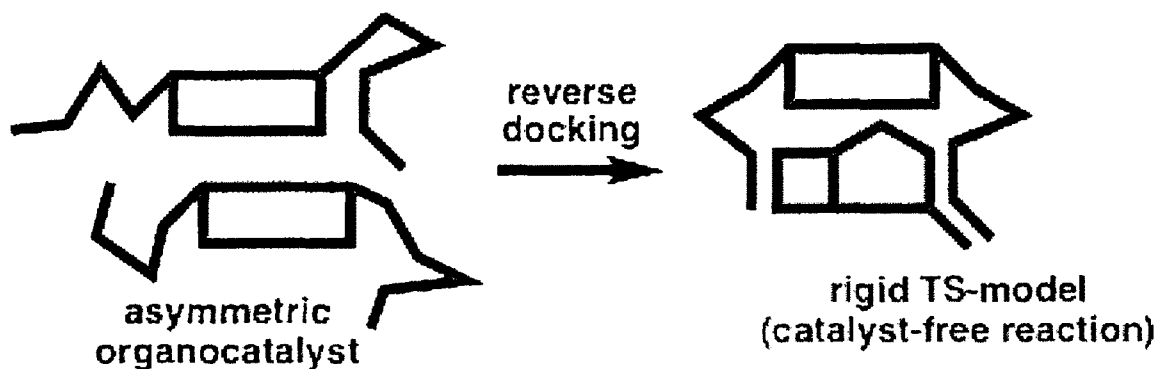


Figure 83. General illustration of the reverse-docking paradigm.

The basic hypothesis is that docking a chiral organocatalyst to rigid transition state models of an uncatalyzed asymmetric reaction (both enantiomers), and analyzing the relative docking energies, should allow one to correlate the preferred enantioselectivities, perhaps even correlate experimental ee's, and provide useful 3D models of the catalyzed reactions for further catalyst design and development. The reverse-docking paradigm assumes several simplifications, for example it assumes that the transition state of the uncatalyzed reaction is the same as the catalyzed one, and that the catalytic core, excluding the catalyst itself, is essentially enantiomeric. Moreover, in its early inception, docking scores were obtained by a molecular mechanics force field. (Figure 84).

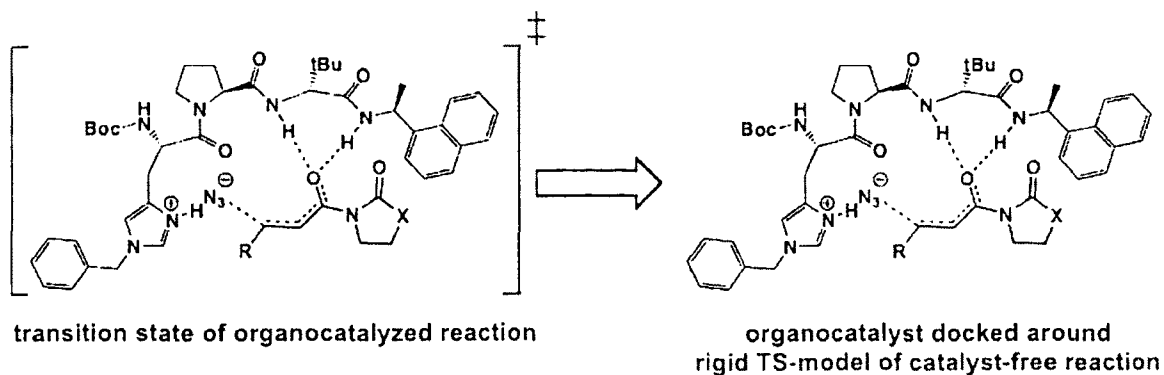


Figure 84. Comparing the transition state of an organocatalyzed reaction to the molecular complex obtained by reverse-docking. The example stems from Miller's peptide-catalyzed asymmetric azidation reaction.

Nevertheless, the reverse-docking method has been successfully applied to the study of Miller's peptide-catalyzed conjugate azide addition,⁷⁶ Rawal's TADDOL catalyzed hetero-Diels-Alder reaction,⁷⁷ Jacobsen's asymmetric Strecker reaction⁷⁸ and, most recently, Rawal's cinchona-tethered squaramide Diels-Alder catalyst. In all cases, the reverse-docking method correctly explained the preferred product enantiomers and, in later work, gave some promising signs of correlation with enantiomeric excess.

2.3.2 Hydrogen bonding and organocatalysis

Most computational work towards organocatalysis has focused on calculating total energies of substrate-catalyst complexes and little focus has been toward calculating energies of interactions between substrate and catalyst. Hydrogen bonding offers a significant mode of catalysis in organocatalysis owing to the ability to activate reactant(s)⁷⁹ and stabilize developing charge in transition states.⁸⁰ Fleming⁷⁹ calculated interaction energies using B3LYP/6-31G* between epoxides and numerous

hydrogen bond donor catalysts and used the catalyst with the highest interaction energy to the substrate as an organocatalyst for addition reactions to epoxides (Figure 85).

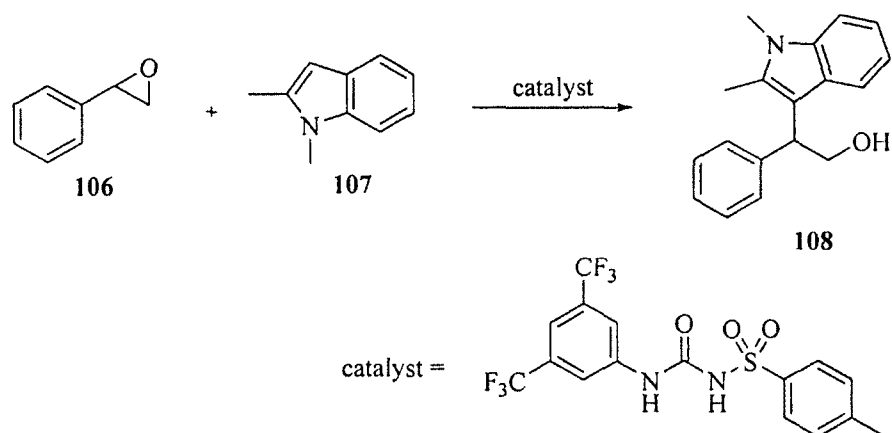


Figure 85. A hydrogen bond catalyst designed by calculating interaction energies with catalyst and substrate.

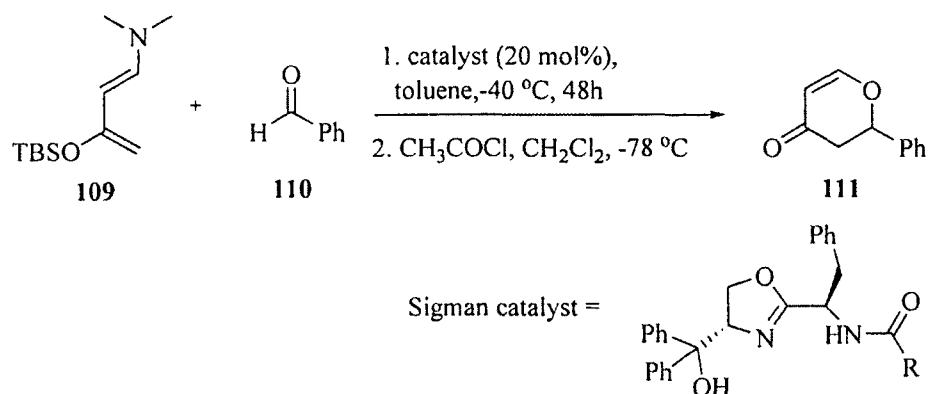
For our purposes we made use of a quantum mechanics method, the Morokuma energy decomposition,⁸¹ which is a Hartree-Fock based method that decomposes quantitatively the various energetic components of intermolecular interactions. Using the Morokuma method, we found a correlation between the rates of organocatalyzed Diels-Alder reactions and the strength of the hydrogen bond between the particular hydrogen bonding catalyst and the dienophile of the reaction (Table 14). This work has yet to be published but we believe this is a rare demonstration of correlation between hydrogen bonding strength between a Bronsted organocatalyst and reaction substrate. This work along with the pioneering work of Flemming should lay a solid foundation for using calculated interaction energies to modify existing catalysts and develop new ones.

method. Inaccuracies in the molecular mechanics approach are typically due to the force field parameterization and to the way that electrostatics are treated. Indeed, most molecular mechanics force fields utilize a non-polarizable electrostatic model dependent on the assignment of partial charges on all the atoms and a pairwise sum of all Coulombic interactions between those partial charges. The RESP method for assigning atomic partial charges is still the state-of-the-art but still has inaccuracies inherent to the method. For example, RESP charges calculated for a series of secondary amides do not correlate with the pK_a of the NH groups. One would naively assume that the RESP charges on the nitrogen to become more negative as the NH acidity increases but this is not the case (Table 15). What is more alarming is that there is not even a trend and that partial charges on nitrogen fluctuate up and down as the pK_a of the parent carboxylic acids increases systematically.

R	pK_a of RCO_2H	RESP charge on N of $RCONHCH_3$
CF_3	-0.25	-0.381
CCl_3	0.65	-0.639
$CHCl_2$	1.29	-0.429
CH_2F	2.66	-0.527
CH_2Cl	2.86	-0.431

Table 15. Comparison of calculated RESP charges compared to experimental pK_a values of the parent carboxylic acids.

Quantum mechanical calculations, on the other hand, are not dependent on the assignment of somehow artificial atomic partial charges and do give more accurate energies and geometries than what one obtains by molecular mechanics. Unfortunately, when the reverse docking method was first developed and implemented, the computational power available limited the technique to the use of molecular mechanics. In 2008, the Deslongchamps group became a member of the ACEnet high-performance computing consortium and was able to install MOE (Molecular Operating Environment), the computing platform on which was developed their reverse-docking program EM-Dock, on one hundred computing nodes of UNB's local ACEnet cluster (Fundy). In addition, the Gaussian 03 and GAMESS quantum mechanical packages were available on the ACEnet network. Now with the availability of increased computational power, we took the opportunity to augment the reverse docking method by computing the energies of docking poses by full quantum mechanics. As an initial study, the recent computational study by Sigman⁸² on the experimental observations made on the organocatalyzed hetero Diels-Alder reaction were examined by our group. Sigman developed organocatalysts based on an oxazoline core capable of displaying two convergent hydrogen bond donors and found a relation between catalyst acidity, reaction rates, and enantioselectivity (Table 16).



Catalyst	R	pK _a of RCO ₂ H	Yield (%)	e.r. (S/R)
1	CF ₃	-0.25	67	20
2	CCl ₃	0.65	61	9.6
3	CHCl ₂	1.29	53	7.0
4	CH ₂ F	2.66	17	4.3
5	CH ₂ Cl	2.86	32	3.1

Table 16. Catalysis of hetero Diels-Alder reaction with chiral oxazoline catalysts and the relationship between acidity, conversion and enantioselectivity, as reported by Sigman.

As in any computational study into the mechanism of an organocatalyzed reaction, elucidating an accurate 3D model of the transition state is extremely valuable. In many catalytic systems, not unlike the Sigman system, the number of possible poses is significant and locating the lowest energy pose manually is a difficult task. Figure 86 shows just three possible poses, of many, between rigid hetero Diels-Alder transition states and Sigman catalyst.

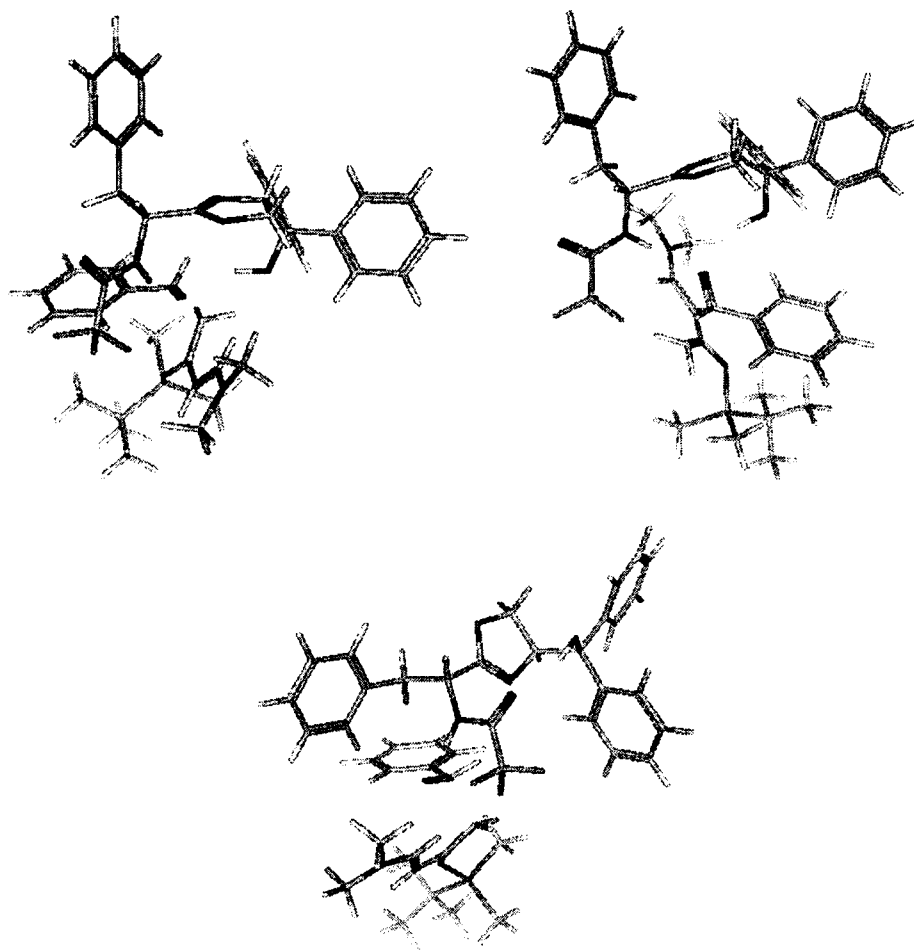


Figure 86. Possible catalytic poses for the Sigman catalyst with the hetero Diels-Alder transition state with bifurcated (top) and cooperative hydrogen bonding (bottom).

It has been shown previously that the Diels-Alder and hetero Diels-Alder reactions can be catalyzed by either a bifurcated or cooperative mode of hydrogen bonding as seen in Figure 75. To help elucidate the predominant catalytic poses in the Sigman catalytic system, reverse-docking was utilized to scan the catalyst conformations space about a rigid hetero Diels-Alder transition state. However, unlike previous reverse-docking work where only molecular mechanics was used to calculate the energies of the reverse-

docking poses, poses were now re-optimized using quantum mechanics (HF/6-31G*). The difference in energies calculated and the conformation of poses using the two methods is significant (Tables 17 and 18).

MM ranking	Relative MM energy (kcal/mol)	Hydrogen bonding type	QM ranking	Relative QM energy (kcal/mol)
1	0.00	bifurcated	3	0.76
2	0.84	bifurcated	2	0.36
3	1.15	bifurcated	38	9.65
4	1.42	bifurcated	41	10.76
5	1.43	bifurcated	17	6.51

Table 17. Reverse-docking MM energies (five lowest energies) and hydrogen bonding type in the interaction of Sigman catalyst **1** to the “SR” hetero Diels-Alder transition state model and docking energies recalculated by quantum mechanics (HF/6-31G*).

MM ranking	Relative MM energy (kcal/mol)	Hydrogen bonding pattern	QM ranking	Relative QM energy (kcal/mol)
1	0.00	cooperative	12	4.48
2	0.20	cooperative	18	5.35
3	0.54	bifurcated	19	5.57
4	0.57	cooperative	16	5.18
5	0.68	cooperative	21	5.67

Table 18. Reverse-docking MM energies (five lowest energies) and hydrogen bonding type in the interaction of Sigman catalyst **1** to the “RS” hetero Diels-Alder transition state model and docking energies recalculated by quantum mechanics (HF/6-31G*).

The results show that caution should be used when relying only on molecular mechanics for computing reverse-docking energies as, in the above demonstration, it fails to find the same lowest energy poses as quantum mechanics and in some instances molecular mechanics finds a different hydrogen bonding pattern to the rigid transition state. However, with large molecular systems one may be restricted to molecular mechanics for a computational “first pass” due to the computational cost of the quantum mechanics method followed by a recalculation of the cluster of low energy poses by more robust quantum mechanical methods (Hartree-Fock, DFT). We found though that minimization of reverse docking results using AM1 is a valuable alternative with minimal consequence on the accuracy. The semi-empirical AM1 method has a minimal computational cost and, interestingly, the ranking does not change from those predicted by HF/6-31G* (Table 19).

QM ranking	Relative QM energy (kcal/mol)	AM1 ranking	Relative QM energy (kcal/mol)
1	0.00	1	0.00
2	0.36	2	0.55
3	0.75	3	0.58
4	3.69	4	0.59
5	3.69	5	0.59

Table 19. The first five ranking AM1 minimized catalytic poses initially calculated by molecular mechanics and compared to rankings from QM calculations.

The next step in this work, which shows that quantum mechanics could be a valuable addition to the reverse docking technique, is that it should be extended to include the remaining Sigman catalysts and assess how well enantioselectivity is predicted using the molecular mechanics, quantum mechanics and AM1 methods. This system would also be a good test case for studying catalyst and transition state interaction energies, or Morokuma energies, and the relationship of the predicted interaction energies to reaction rates and enantioselectivity.

2.4 Future of organocatalyst design

2.4.1 Future work towards the rational design of an organocatalyst

The field of organocatalysis has seen several successful hydrogen bonding catalysts, many of which have been derived from thiourea, BINOL, and now squaramide. Likely as the area continues to expand, the focus will move toward the *de novo* design of

catalysts. In comparison to the organocatalysts' natural counterparts (i.e. enzymes), organocatalysts have much less selectivity and activity. However, this is not surprising considering that enzyme efficiency has evolved over hundreds of millions of years and that active site functional groups are "micro-positioned" for optimum reactivity by scaffolding within large polypeptides. Unlike enzymes where the large size and many intramolecular interactions allow micro-positioning, it is difficult to achieve in an organocatalyst given discreet bond lengths and angles permitted within the small organic molecule. It therefore cannot be expected that using an organic molecule to stabilize a transition state via hydrogen bonding that optimal stabilization will exist. Indeed fitting a catalyst to a transition state is not an easy task considering that the catalyst has to be designed and synthesized maintaining optimal positioning of the catalytic functional groups.

Precise fitting and design of a catalyst to stabilize a particular transition state would necessarily require computer-assisted *de novo* design, starting first with predicting the optimal position of the catalytic functional groups by quantum mechanics as, for example, Bronsted acids and bases were optimized around the acetaldehyde enolate depicted in Figure 62. Next, a chemical scaffold would have to be designed that would link the catalytic functional groups together maintaining the micro-positioning previously calculated. If that wasn't difficult enough, this scaffold would then have to be synthetically attainable. Until now such a design concept would be unachievable but recent advances at the Chemical Computing Group Inc. (makers of MOE) has resulted in the development of a scaffold replacement tool meant primarily for pharmaceutical

research and drug design. However, the method could be readily extended to organocatalysts design. The scaffold replacement method searches vast databases of known chemical compounds, fits them to chemical fragments fixed in position and finally scores the fit. Therefore using this tool it makes it possible to search for chemical scaffolds that would maintain the positioning of geometry optimized catalytic functional groups around a transition state. Proposed catalysts could then be synthesized and tested experimentally with final modification pending the experimental results. These modifications could include changes to the scaffold or in the case of a hydrogen bonding catalyst modifying the Bronsted acidity of the hydrogen bond donors.

With an ever-increasing interest in the field of organocatalysis the future is bright for this new field of research. Over that past 10 years many different organocatalysts have been discovered along with numerous types of reactions successfully catalyzed. The awareness that organocatalysis is not a specific mode of activation limited to a narrow reaction set but rather a general mode of activation that can be extended over many reactions has caused this area of research to grow at an ever increasing rate.

2.5 Conclusion

The work towards the rational design of a squaramide based organocatalyst led to the development of a conformational controlled hydrogen bond catalyst that showed catalytic activity when used to catalyze the Diels-Alder reaction. More significantly, work to extend the catalyst to Baylis-Hillman reaction led to the development of a squaramide monoanion and was used to catalyze the first direct aldol reaction via a Bronsted acid/base mechanism. This work lays the foundation to modify the existing squaramide catalyst or develop new catalysts with similar modes of catalytic activity to improve on both observed regio- and enantioselectivities. Also being investigated are reactions catalyzed by enzymes using a mechanism of tautomerization of a Bronsted acid/base to test the ability of squaramide monoanion to mimic these enzymes.

Extension of the reverse docking technique to use quantum mechanics shows that it can be a valuable addition to the technique for modeling catalytic poses between hydrogen bond organocatalyst and substrate. It was shown that molecular mechanics is valuable in a “first-pass” reverse-docking procedure but interesting poses should be re-evaluated using quantum mechanics to obtain more accurate molecular geometries and energies. For larger catalytic systems where quantum mechanics is not a viable alternative, semi-empirical AM1 methods could prove useful.

Chapter 3. Experimental procedures and spectral data

3.1 General

Reactions were carried out in flame dried glassware under an argon atmosphere. Tetrahydrofuran, methylene chloride, and methanol were purified by passage over neutral alumina. Toluene was purified by passage over neutral alumina followed by Q5 reactant, a copper(II) oxide oxygen scavenger. Commercial grade anhydrous ethanol was used as received. Chloroform-*d* +0.05% v/v TMS was stored over anhydrous potassium carbonate. Acetone-*d*₆ and methanol-*d*₄ stored in 1 gram ampoules were used as received. Reactions were monitored by TLC on Silicycle 60 Å F-254 plates and visualized with UV (254 nm) and KMnO₄ stain. Flash column chromatography was performed on GRACE Davison silica LC 60 Å/32-63. NMR spectra were recorded on a Varian Unity INOVA 300 at 300 MHz or a Varian Unity INOVA 400 at 400 MHz for ¹H, and 100 MHz for ¹³C and referenced from the residual solvent signal. ³¹P spectra were recorded on a Varian Unity INOVA 300 at 121 MHz. Mass spectral analysis was run on a Kratos MS-50 TS instrument. IR was obtained on a Nicolet iS10. Crystals suitable for x-ray were grown by slow evaporation using EtOAc at room temperature. Single crystals were coated with Paratone-N oil, mounted using a polyimide MicroMount and frozen in the cold nitrogen stream of the goniometer. Data was collected on a Bruker AXS P4/SMART 1000 diffractometer.

3.1.1 Conditions for the enhancement of the Diels-Alder reaction by conformationally controlled squaramides

To CDCl_3 (0.75 mL) in a NMR tube was added methyl vinyl ketone (0.075 mmol), cyclopentadiene (0.75 mmol) and squaramide (0.0075 mmol). The reaction progress was monitored by ^1H NMR for the designated time period indicated in Figure 51.

3.1.2 General procedure for aldol using Baylis-Hillman conditions

To squaramide (0.015 mmol) dissolved in CH_2Cl_2 (0.75 mL) was added enone (0.075 mmol), aldehyde (0.15 mmol), and n-butylphosphine (0.015 mmol). The reaction was stirred for 24 hrs, the solvent was evaporated under reduced pressure and the yield of aldol product determined by ^1H NMR.

3.1.3 Preparation of squaramide monoanion

Squaramide was dissolved in methanol and one equivalent of benzyltrimethylammonium (BTMA) methoxide was added. The solvent was then evaporated under reduced pressure and the residue dissolved in benzene and evaporated under reduced pressure. The residue was dissolved again in benzene and evaporated under reduced pressure and then the BTMA squaramide monoanion was immediately used.

3.1.4 Squaramide monoanion catalyzed enolization of acetone-*d*6

BTMA squaramide monoanion (0.1 mmol) was dissolved in acetone-*d*6 (0.5 mL) containing 2% v/v toluene as an internal standard. Methanol (0.05 mL) was added and the appearance of acetone-*d*5 was monitored over time by ^1H NMR.

3.1.5 General procedure for squaramide monoanion catalysis of the direct aldol reaction

BTMA squaramide monoanion (0.1 mmol) was dissolved in acetone-*d*₆ (0.5 mL) containing 2% v/v toluene and aldehyde (0.62 mmol) was added. Progress of the reaction was monitored by ¹H NMR, following the emergence of the product –CHOD signal over time.

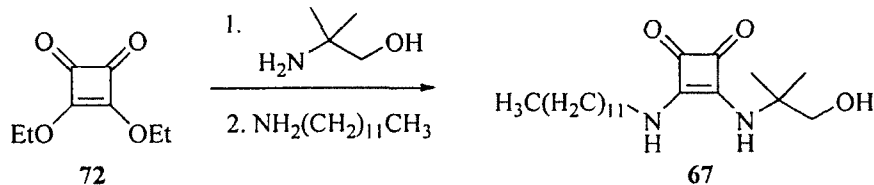
3.2 Preparation of compounds

Preparation of 25 (50 mg and 1 g scale reaction)

To a 10 mL round bottom flask (rbf) equipped with a magnetic stir bar was added dry 9-DHB (50 mg, 0.079 mmol), dried in vacuo at 110°C over P₂O₅ for 2 hrs, and PPTS (catalytic). The rbf was flushed with argon and CH₂Cl₂ was added to give a 0.03 M solution of 9-DHB. After 9-DHB and PPTS was dissolved 2.6 equivalents of cyclohexyl vinyl ether was added over 2.5 hrs and after an additional 20 minutes the reaction was quenched with pyridine (192 µl, 30 eq.). To a 10 mL rbf equipped with a magnetic stir bar was added DMP (168 mg, 5 eq.) and under argon CH₂Cl₂ was added to give a 0.2 M solution. The DMP solution was cooled to 0°C and the quenched reaction was added under argon via a canula. The reaction was warmed to room temperature and proceeded to completion after which it was diluted with diethyl ether (10 mL) and quenched with a saturated sodium bicarbonate solution containing 25% (wt/v) sodium bisulfate (10 mL). The organic layer was separated and the aqueous layer back extracted with diethyl ether (3 x 10 mL). The combined organic layers were washed with saturated aqueous ammonium chloride (2 x 10 mL), water (5 mL), and brine (5 mL) before being concentrated in vacuo and then dissolved in methanol to give a 0.01 M solution and treated with PTSA. After disappearance of starting material (observed by TLC) the methanol solution was quenched with a saturated sodium bicarbonate solution (10 mL) and extracted with ethyl acetate (3 x 10 mL). The combined organic phases were dried over MgSO₄ and concentrated in vacuo. The crude product was purified by preparative chromatography to afford the product (39.9 mg, 80.3%) as a white solid. The above procedure was repeated on a 1 g scale and afforded the product (790 mg, 79.0%) as a white powder with spectral data identical to previously reported.⁸³

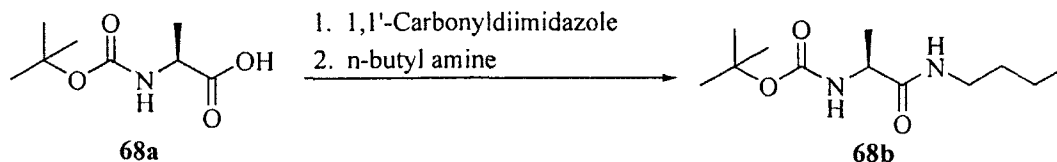
^1H NMR (300 MHz, CDCl_3 , TMS) δ 8.06 (d, 7.5 Hz, 2H), 7.61 (t, 7.5 Hz, 1H), 7.51 (t, 7.5 Hz, 2H), 6.3 (s, 1H), 6.18 (t, 9.0 Hz, 1H), 5.64 (d, 7 Hz, 1H), 4.95 (dd, 1.5, 9 Hz, 1H), 4.43 (br m, 1H), 4.3 (d, 8 Hz, 1H), 4.15 (d, 8 Hz, 1H), 3.82 (d, 7 Hz, 1H), 2.57 (m, 2H) 2.33 (s, 3H), 2.24 (s, 3H), 2.23 (m, 2H), 2.20 (s, 3H), 1.89 (s, 3H), 1.85 (m, 1H), 1.65 (s, 3H), 1.25 (s, 3H), 1.13 (s, 3H); ^{13}C NMR (100 MHz, CDCl_3) δ 205.3, 172.8, 171.6, 171.3, 168.4, 144.5, 135.2, 134.3, 131.6, 130.7, 130.2, 85.9, 82.6, 80.8, 77.9, 77.2, 76.5, 73.7, 71.2, 60.1, 47.3, 44.6, 37.2, 37.1, 28.2, 24.0, 23.0, 22.7, 22.4, 16.6, 11.0; IR (KBr, cast film) ν 3490, 2987, 2936, 2898, 1720, 1448, 1378, 1232, 1074, 1017, 979, 745, 710.

Preparation of 67



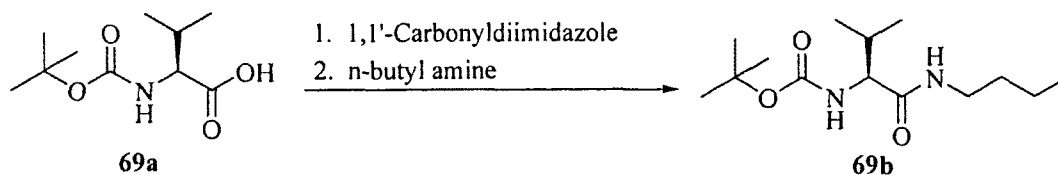
Diethyl squarate (250 mg, 1.47 mmol) was dissolved in anhydrous ethanol (10 mL) and dodecyl amine (300 mg, 1.62 mmol) was added. The reaction was stirred for 2 hrs before 2-amino-2-methyl-1-propanol (843 μ l, 8.82 mmol) was added and then refluxed for 3.5 hrs. The reaction was concentrated in vacuo, washed with diethyl ether to remove excess 2-amino-2-methyl-1-propanol and purified by flash column chromatography (10% MeOH in CH₂Cl₂) to afford the product (422 mg, 80.9%) as a white solid.

¹H NMR (400 MHz, CDCl₃, TMS) δ 7.91 (br s, 1H), 7.87 (br s, 1H), 4.64 (br s, 1H), 3.63 (br s, 4H), 1.59 (br s, 2H), 1.45 (s, 6H), 1.24 (br, 20H), 0.87 (t, 7 Hz, 3H); ¹³C NMR (100 MHz, CDCl₃) δ 182.0, 180.5, 168.8, 168.2, 70.0, 57.2, 45.0, 40.1, 31.9, 31.4, 29.6, 29.4, 29.3, 26.5, 25.5, 22.7, 14.1; IR (KBr, cast film) ν 3443, 3307, 3233, 2844, 1647, 1562, 1463, 1065.

Preparation of 68b

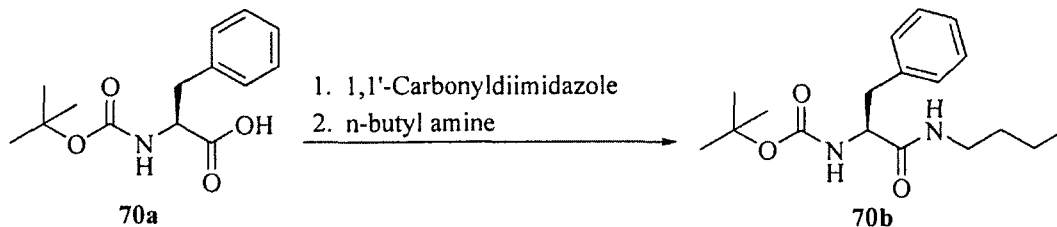
68a (2.54 g, 13.4 mmol) was dissolved in a volume of THF to give a 1 M solution to which was carefully added 1,1'-carbonyldiimidazole (1 equivalent). The mixture was stirred for 1 hr before n-butylamine (1 equivalent) was added. The reaction was stirred for a further 24 hrs and then diluted with EtOAc and washed with 10% acetic acid (3x), saturated NaHCO₃ (3x), water (1x) and brine (1x). The organic phase was dried over Na₂SO₄ and solvent evaporated under reduced pressure to afford crude product as a white solid which was used without further purification (3.0 g, 91.5%).

¹H NMR (400 MHz, CDCl₃, TMS) 6.27 (br s, 1H), 5.08 (br s, 1H), 4.12 (br t, 1H), 3.23 (q, 6.3 Hz, 2H), 1.43 (m, 2H), 1.42 (s, 9H), 1.33 (d, 7 Hz, 3H), 1.33 (m, 2H), 0.9 (t, 7.3 Hz, 3H); ¹³C NMR (100 MHz, CDCl₃) δ 172.5, 155.55, 80.0, 50.07, 39.13, 31.56, 28.28, 19.94, 18.36, 13.69; HRMS (EI): calc for C₁₂H₂₄N₂O₃, 244.1787; found m⁺/z, 244.1795.

Preparation of 69b

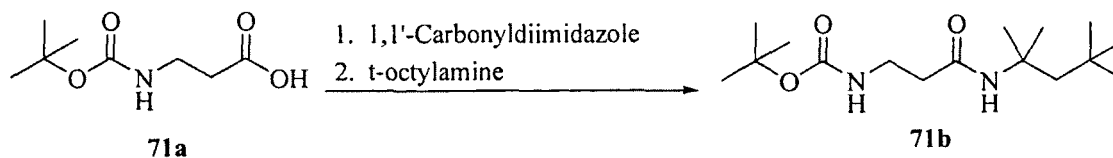
69a (3.10 g, 14.3 mmol) was dissolved in a volume of THF to give a 1 M solution to which was carefully added 1,1'-carbonyldiimidazole (1 equivalent). The mixture was stirred for 1 hr before n-butylamine (1 equivalent) was added. The reaction was stirred for a further 24 hrs and then diluted with EtOAc and washed with 10% acetic acid (3x), saturated NaHCO₃ (3x), water (1x) and brine (1x). The organic phase was dried over Na₂SO₄ and solvent evaporated under reduced pressure to afford crude product as a white solid which was used without further purification (3.44 g, 88.2%).

¹H NMR (400 MHz, CDCl₃, TMS) δ 6.08 (s, 1H), 5.11 (d, 6.8 Hz, 1H), 3.82 (dd, 2.4, 6.5 Hz, 1H), 3.24 (m, 2H), 2.09 (m, 1H), 1.47 (m, 2H), 1.43 (s, 9H), 1.32 (m, 1H), 0.92 (m, 9H); ¹³C NMR (100 MHz, CDCl₃) δ 171.48, 155.92, 60.2, 39.12, 31.59, 30.74, 28.28, 80.42, 20.0, 19.28, 17.92, 13.68; HRMS (EI): calc for C₁₄H₂₈N₂O₃, 272.2099; found m⁺/z, 272.2099.

Preparation of 70b

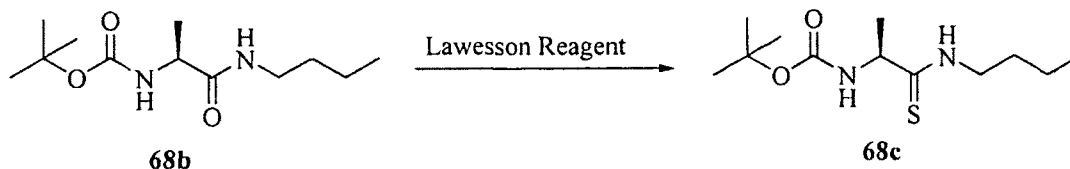
70a (2.65 g, 10.0 mmol) was dissolved in a volume of THF to give a 1 M solution to which was carefully added 1,1'-carbonyldiimidazole (1 equivalent). The mixture was stirred for 1 hr before n-butylamine (1 equivalent) was added. The reaction was stirred for a further 24 hrs and then diluted with EtOAc and washed with 10% acetic acid (3x), saturated NaHCO₃ (3x), water (1x) and brine (1x). The organic phase was dried over Na₂SO₄ and solvent evaporated under reduced pressure to afford crude product as a white solid which was used without further purification (2.80 g, 87.3%).

¹H NMR (400 MHz, CDCl₃, TMS) δ 7.31-7.20 (m, 5H), 5.62 (br s, 1H), 5.08 (br s, 1H), 4.25 (br m, 1H), 3.16-2.97 (br m, 4H), 1.34 (m, 2H), 1.27 (m, 2H), 0.86 (t, 7 Hz, 3H), 0.92 (m, 9H); ¹³C NMR (100 MHz, CDCl₃) δ 170.9, 129.3, 128.6, 126.9, 125.4, 40.1, 39.1, 38.7, 31.4, 28.3, 19.9, 13.6.

Preparation of **71b**

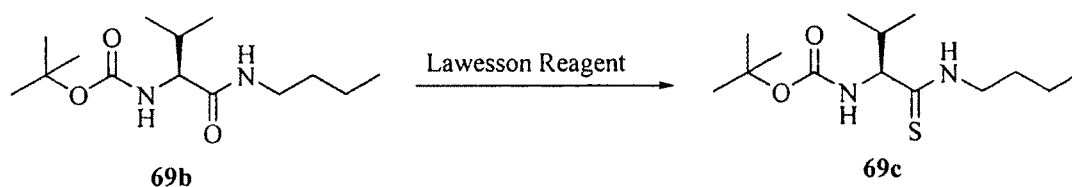
71a (952 mg, 5.03 mmol) was dissolved in CH_2Cl_2 (15 mL) to which *tert*-octylamine (500 mg, 3.87 mmol), DMAP (62 mg, 0.503 mmol), and DCC (1.04 g, 5.03 mmol) was added. The reaction was stirred for a further 24 hrs and then filtered and the precipitate rinsed with CH_2Cl_2 . The filtrate was concentrated in vacuo and purified by flash column chromatography (40% EtOAc in hexanes) to afford the product (2.80 g, 87.3%) as a white solid.

^1H NMR (400 MHz, CDCl_3 , TMS) δ 5.40 (br s, 1H), 5.20 (br s, 1H), 3.34 (q, 6 Hz, 2H), 2.29 (t, 6 Hz, 2H), 1.73 (s, 3H), 1.41 (s, 6H), 1.37 (s, 9H), 0.98 (s, 9H); ^{13}C NMR (100 MHz, CDCl_3) δ 170.4, 156.1, 79.1, 37.2, 36.7, 35.8, 32.7, 31.6, 31.4, 30.8, 29.3, 28.4, 26.2, 25.4, 25.3, 24.7.

Preparation of 68c

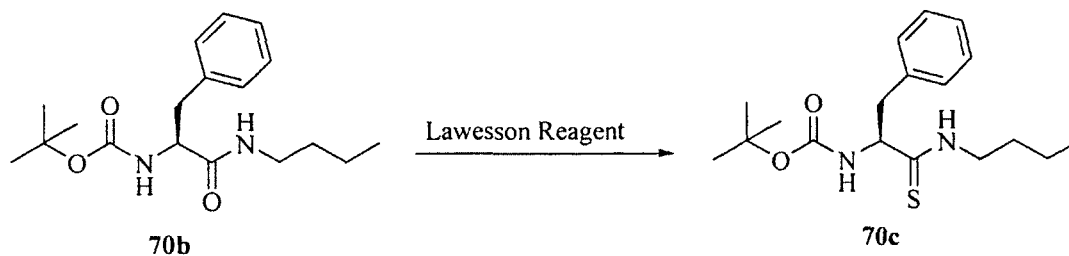
68b (2.70 g, 11.1 mmol) was dissolved in THF (40 mL) and Lawesson reagent (2.68 g, 6.64 mmol) was added. The reaction was stirred for 24 hrs and then concentrated in vacuo to afford crude product which was purified by flash column chromatography (20% EtOAc in toluene) to afford the product (2.03 g, 70.5%) as a white solid.

^1H NMR (400 MHz, CDCl_3 , TMS) δ 8.27 (br s, 1H), 5.28 (br s, 1H), 4.45 (m, 1H), 3.64 (m, 2H), 1.62 (m, 2H), 1.44 (d, 7.0 Hz, 3H), 1.43 (s, 9H), 1.37 (m, 2H), 0.93 (t, 7.2 Hz, 3H); ^{13}C NMR (100 MHz, CDCl_3) δ 204.73, 155.54, 56.18, 45.46, 29.90, 28.27, 27.89, 21.55, 20.09, 13.71; HRMS (EI): calc for $\text{C}_{12}\text{H}_{24}\text{N}_2\text{O}_2\text{S}$, 260.1558; found m/z , 260.1552.

Preparation of 69c

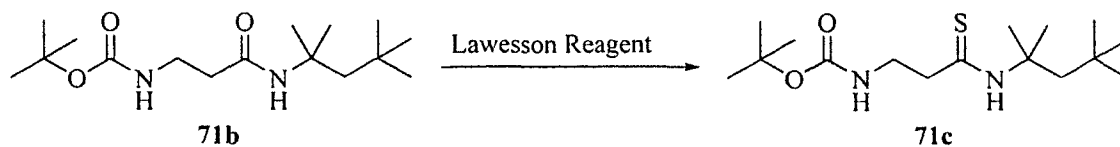
69b (3.0 g, 11.0 mmol) was dissolved in THF (40 mL) and Lawesson reagent (2.68 g, 6.64 mmol) was added. The reaction was stirred for 24 hrs and then concentrated in vacuo to afford crude product which was purified by flash column chromatography (30% EtOAc in hexanes) to afford the product (1.2 g, 38%) as a white solid.

^1H NMR (400 MHz, CDCl_3 , TMS) δ 7.94 (br s, 1H), 5.27 (br s, 1H), 3.98 (br s, 1H), 3.65 (m, 2H), 2.25 (br s, 1H), 1.63 (m, 2H), 1.43 (s, 9H), 1.37 (m, 2H), 0.94 (t, 7.4 Hz, 3H); ^{13}C NMR (100 MHz, CDCl_3) δ 155.9, 67.3, 45.3, 40.1, 32.9, 29.9, 28.3, 20.1, 19.7, 13.7.

Preparation of 70c

70b (500 mg, 1.56 mmol) was dissolved in THF (5 mL) and Lawesson reagent (379 mg, 0.936 mmol) was added. The reaction was stirred for 24 hrs and then concentrated in vacuo to afford crude product which was purified by flash column chromatography (30% EtOAc in hexanes) to afford the product (290 mg, 55.3%) as a white solid.

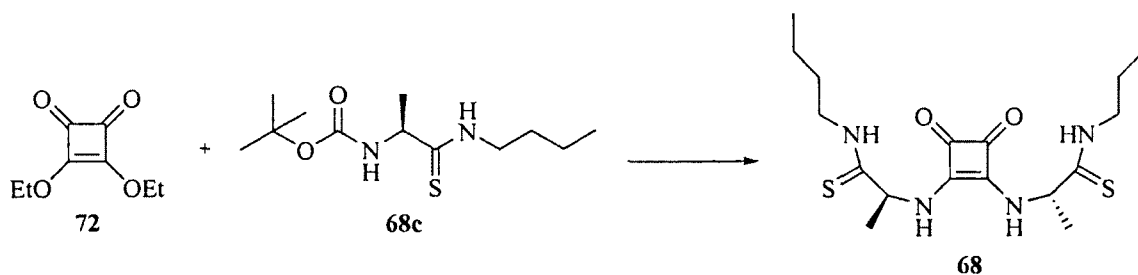
^1H NMR (400 MHz, CDCl_3 , TMS) δ 7.62 (br s, 1H), 7.31-7.19 (m, 5H), 5.52 (br s, 1H), 4.53 (q, 7.5 Hz, 1H), 3.50-3.41 (br m, 2H), 3.13 (br m, 2H), 1.40 (s, 9H), 1.37 (br m, 2H), 1.16 (br m, 2H) 0.84 (t, 7.3 Hz, 3H); ^{13}C NMR (100 MHz, CDCl_3) δ 202.5, 155.3, 136.8, 129.2, 128.6, 126.9, 62.7, 45.4, 41.9, 29.6, 28.2, 19.9, 13.6.

Preparation of 71c

71b (100 mg, 0.333 mmol) was dissolved in THF (2 mL) and Lawesson reagent (108 mg, 0.266 mmol) was added. The reaction was stirred for 24 hrs and then concentrated in vacuo to afford crude product which was purified by flash column chromatography (15% EtOAc in toluene) to afford the product (46 mg, 44%) as a white solid.

^1H NMR (400 MHz, CDCl_3 , TMS) δ 7.32 (br s, 1H), 5.09 (br s, 1H), 3.50 (q, 8 Hz, 2H), 2.70 (br t, 2H), 2.06 (s, 2H), 1.58 (s, 6H), 1.42 (s, 9H), 1.24 (s, 2H), 1.00 (s, 9H); ^{13}C NMR (100 MHz, CDCl_3) δ 200.3, 156.1, 79.9, 60.0, 49.2, 48.9, 39.4, 31.6, 31.3, 28.4, 28.3, 28.2, 25.6.

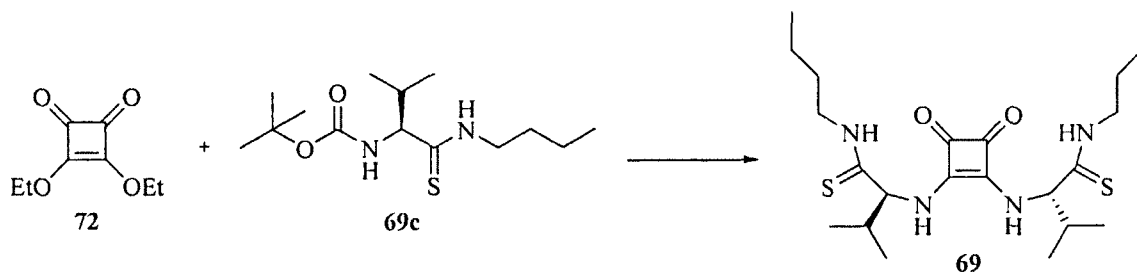
Preparation of **68**



To **68c** (139.4 mg, 0.87 mmol) was added concentrated HCl (2.5 mL) and EtOAc (7.5 mL) and the solution was stirred for 60 minutes at room temperature. The solution was then evaporated under reduced pressure and taken back up in methanol (10 mL) and evaporated under reduced pressure. The residue was taken back up in anhydrous ethanol (2 mL), diethyl squarate (50 mg, 0.29 mmol) added followed by KOH (49 mg, 0.87 mmol). The reaction was stirred for 24 hrs and then diluted with CH₂Cl₂ (20 mL) and washed with 10% acetic acid (3 x 5 mL), water (3 x 5 mL), and brine (5 mL). The organic phase was dried over Na₂SO₄ and concentrated in vacuo to afford the product (311 mg, 89.7%) as a beige solid.

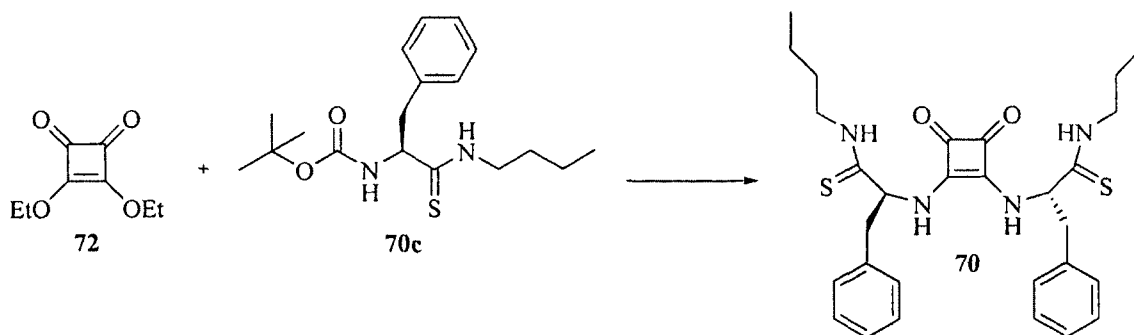
¹H NMR (400 MHz, CDCl₃, TMS) δ 8.79 (br s, 2H), 7.11 (br s, 2H), 5.07 (br s, 2H), 3.64 (m, 4H) 1.67 (m, 4H), 1.58 (d, 6.7 Hz, 6H), 1.38 (m, 4H), 0.94 (t, 7.3 Hz, 6H); ¹³C NMR (100 MHz, CDCl₃) δ 202.74, 182.70, 166.79, 58.45, 46.27, 29.81, 22.68, 20.39, 13.95; IR (KBr, cast film) ν 3234, 3006, 1660, 1581, 1511, 1460, 1270, 1258, 913; HRMS (EI): calc for C₁₈H₃₀N₄O₂S₂, 398.1810; found m⁺/z, 398.1810.

Preparation of **69**



To **69c** (288 mg, 1.0 mmol) was added concentrated HCl (2.5 mL) and EtOAc (7.5 mL) and the solution was stirred for 60 minutes at room temperature. The solution was then evaporated under reduced pressure and taken back up in methanol (10 mL) and evaporated under reduced pressure. The residue was taken back up in anhydrous ethanol (2 mL), and diethyl squarate (56 mg, 0.33 mmol) was added followed by KOH (56 mg, 1.0 mmol). The reaction was stirred for 24 hrs and then diluted with CH₂Cl₂ (20 mL) and washed with 10% aqueous acetic acid (3 x 5 mL), water (3 x 5 mL), and brine (5 mL). The organic phase was dried over Na₂SO₄ and concentrated in vacuo to afford the product (379 mg, 83.4%) as a beige solid.

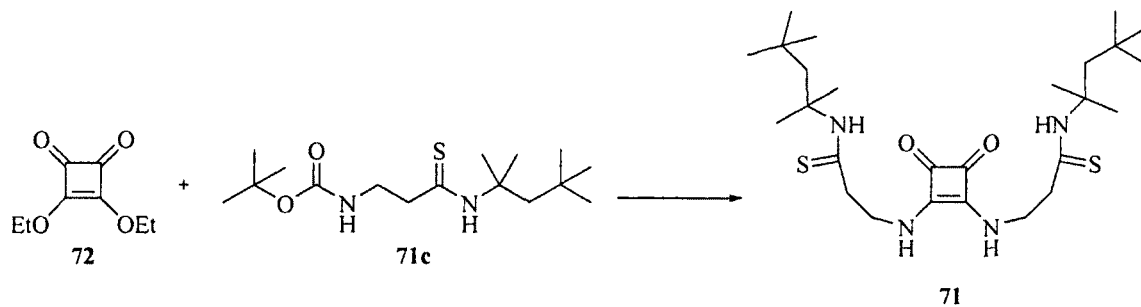
¹H NMR (400 MHz, CDCl₃, TMS) δ 8.72 (br s, 2H), 6.88 (br s, 2H), 4.57 (br s, 2H), 3.75-3.59 (m, 4H) 2.25 (m, 2H), 1.66 (m, 4H), 1.38 (m, 4H), 1.04-0.88 (m, 18H); ¹³C NMR (100 MHz, CDCl₃) δ 202.0, 182.7, 166.8, 69.1, 45.8, 33.7, 29.6, 20.2, 19.2, 18.8, 13.7; IR (KBr, cast film) ν 3212, 2961, 1651, 1584, 1511, 1464, 1403, 1093.

Preparation of 70

To **70c** (336 mg, 1.0 mmol) was added concentrated HCl (2.5 mL) and EtOAc (7.5 mL) and the solution was stirred for 60 minutes at room temperature. The solution was then evaporated under reduced pressure and taken back up in methanol (10 mL) and evaporated under reduced pressure. The residue was taken back up in anhydrous ethanol (2 mL), and diethyl squarate (56 mg, 0.33 mmol) was added followed by KOH (56 mg, 1.0 mmol). The reaction was stirred for 24 hrs and then diluted with CH₂Cl₂ (20 mL) and washed with 10% aqueous acetic acid (3 x 5 mL), water (3 x 5 mL), and brine (5 mL). The organic phase was dried over Na₂SO₄ and concentrated in vacuo to afford the product (469 mg, 85.1%) as a beige solid.

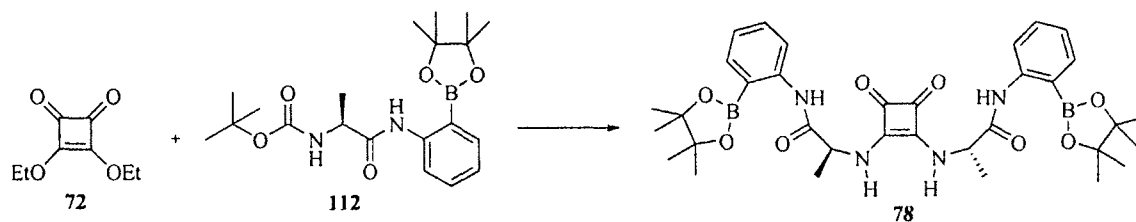
¹H NMR (400 MHz, CDCl₃, TMS) δ 8.00 (br s, 2H), 6.97 (br d, 8.5 Hz, 2H), 5.12 (br s, 2H), 3.57-3.44 (m, 4H) 3.21 (m, 4H), 1.40 (m, 4H), 1.16 (m, 4H), 0.84 (t, 7.4 Hz, 6H); ¹³C NMR (100 MHz, CDCl₃) δ 200.7, 183.0, 166.4, 135.8, 129.3, 128.7, 127.3, 64.5, 45.7, 43.1, 29.4, 19.9, 13.6; IR (KBr, cast film) ν 3246, 3012, 1663, 1581, 1518, 1451, 1404, 1274, 1252.

Preparation of 71



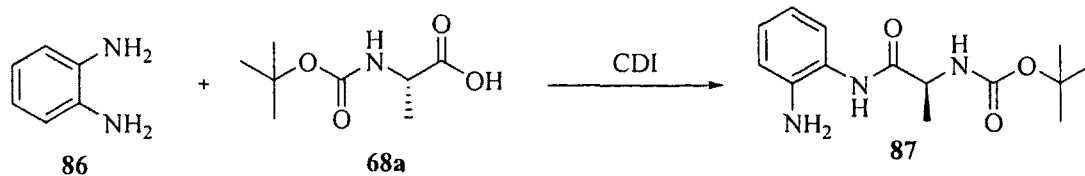
To **71c** (164 mg, 0.520 mmol) was added concentrated HCl (2.5 mL) and EtOAc (7.5 mL) and the solution was stirred for 60 minutes at room temperature. The solution was then evaporated under reduced pressure and taken back up in methanol (10 mL) and evaporated under reduced pressure. The residue was taken back up in anhydrous ethanol (2.5 mL), and diethyl squarate (29 mg, 0.17 mmol) was added followed by DBU (95 mg, 0.62 mmol). The reaction was stirred for 5 hrs and then diluted with CH₂Cl₂ (20 mL) and washed with 10% aqueous acetic acid (3 x 5 mL), water (3 x 5 mL), and brine (5 mL). The organic phase was dried over Na₂SO₄ and concentrated in vacuo to afford the product (243 mg, 91.3%) as a beige solid.

¹H NMR (400 MHz, DMSO-*d*₆) δ 9.30 (br s, 2H), 7.46 (br s, 2H), 3.82 (br m, 4H), 2.69 (m, 4H) 2.08 (s, 4H), 1.47 (s, 12H), 0.91 (s, 18H); ¹³C NMR (100 MHz, DMSO-*d*₆) δ 199.2, 183.0, 168.1, 76.8, 59.3, 47.9, 47.2, 42.7, 31.7, 31.3, 29.0.

Preparation of 78

To **112** (406 mg, 1.04 mmol) was added concentrated HCl (2.5 mL) and EtOAc (7.5 mL) and the solution was stirred for 60 minutes at room temperature. The solution was then evaporated under reduced pressure and taken back up in methanol (10 mL) and evaporated under reduced pressure. The residue was taken back up in anhydrous ethanol (5 mL), and diethyl squarate (59 mg, 0.35 mmol) was added followed by DBU (317 mg, 2.08 mmol). The reaction was stirred for 5 hrs and then diluted with CH₂Cl₂ (20 mL) and washed with 10% aqueous acetic acid (3 x 5mL), water (3 x 5 mL), and brine (5 mL). The organic phase was dried over Na₂SO₄ and concentrated in vacuo to afford the product (456 mg, 79.8%) as a beige solid.

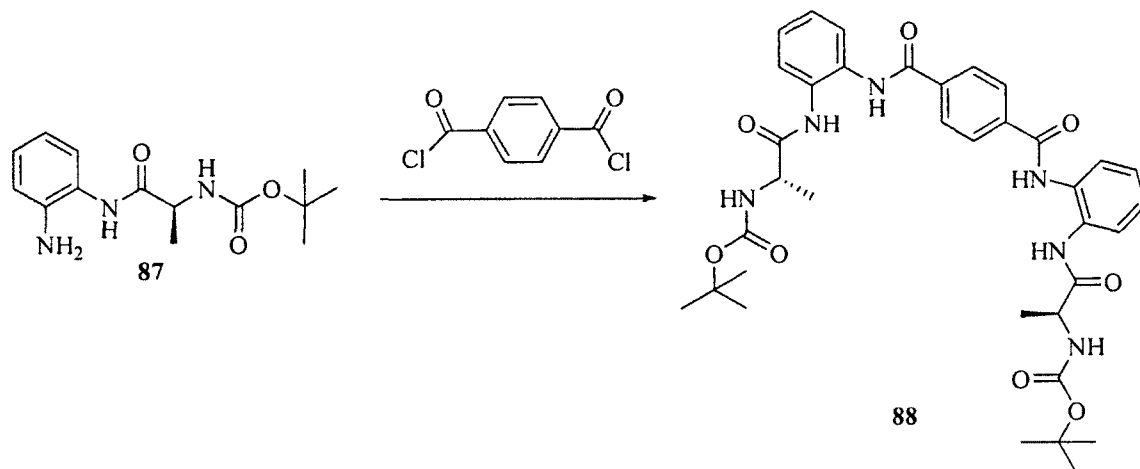
¹H NMR (300 MHz, CDCl₃, TMS) δ 9.67 (br s, 2H), 8.32 (d, 7.9 Hz, 2H), 7.78 (d, 7.6 Hz, 2H), 7.27 (m, 2H) 7.11 (m, 2H), 4.94 (br m, 4H), 1.64 (d, 7 Hz, 6H), 1.38 (s, 24H);
¹³C NMR (100 MHz, CDCl₃) δ 183.3, 170.2, 167.3, 143.3, 136.2, 132.5, 123.8, 119.6, 84.5, 53.8, 129.0 20.5; IR (KBr, cast film) ν 3265, 2974, 2926, 1679, 1574, 1524, 1445, 1350, 1137.

Preparation of **87**

To THF (10 mL) was added **68a** (2.00 g, 10.6 mmol) followed by *N,N'*-carbonyldiimidazole (1.70 g, 10.6 mmol). The mixture was stirred for 30 minutes then added under argon via a canula to **86** (2.30 g, 21.2 mmol) in THF (30 mL) and stirred overnight. The reaction was then diluted with EtOAc (50 mL) and washed with water (3 x 10 mL) and brine (10 mL). The organic phase was dried over Na₂SO₄ and concentrated in vacuo to yield a yellow oil (4.75 g) which was titrated with diethyl ether to afford the product (1.96 g, 66.2%) as a white powder.

¹H NMR (300 MHz, CDCl₃, TMS) δ 7.93 (br s, 1H), 7.27 (d, 5.5 Hz, 1H), 7.05 (dt, 1.3, 7.7 Hz, 1H), 6.80 (m, 1.3, 2H) 5.02 (br s, 1H), 4.31 (m, 1H), 3.88 (br s, 2H), 1.49 (m, 12H); ¹³C NMR (100 MHz, CDCl₃) δ 171.1, 140.6, 127.1, 125.3, 123.5, 119.1, 117.4, 50.9, 28.3, 17.6.

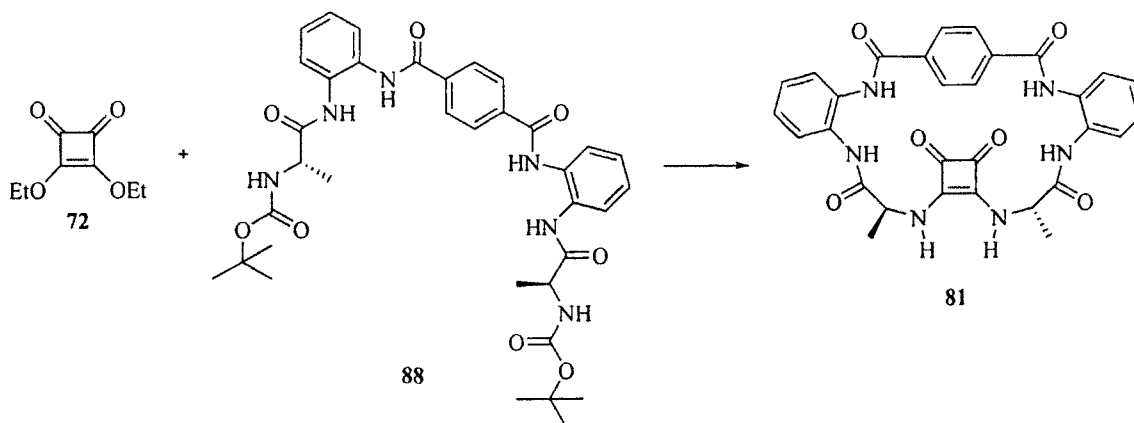
Preparation of **88**



To **87** (1.91 g, 6.80 mmol) was added toluene (50 mL), triethylamine (5.80 g, 57.6 mmol) and terephthaloyl chloride (656 mg, 3.2 mmol). The reaction was refluxed for 1.5 hrs and cooled yielding a precipitate. The precipitate was isolated by filtration and taken up in 1% MeOH/CH₂Cl₂ (100 mL) and washed with 10% acetic acid (2 x 25 mL), water (2 x 25 mL) and brine (25 mL). The organic phase was dried over Na₂SO₄ and concentrated in vacuo giving a yellow oil which was titrated with diethyl ether to afford the product (1.75 g, 79.4%) as a beige powder.

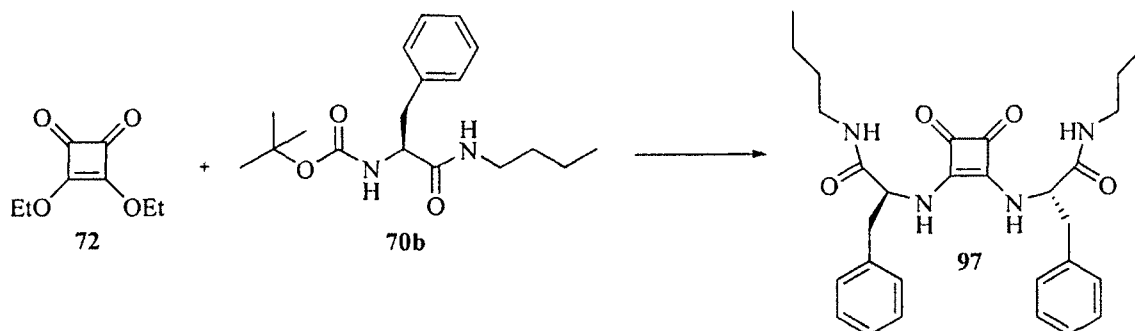
¹H NMR (300 MHz, CDCl₃, TMS) δ 9.26 (br s, 2H), 8.18 (br s, 2H), 7.89 (d, 7.8 Hz, 2H), 7.76 (s, 4H), 7.31 (m, 2H), 7.12 (m, 2H), 6.00 (br s, 2H), 4.46 (br m, 2H), 1.53 (s, 18H); ¹³C NMR (100 MHz, CDCl₃) δ 173.0, 164.3, 155.8, 136.2, 131.4, 129.2, 127.5, 126.6, 125.9, 125.7, 125.4, 80.4, 50.6, 28.4, 18.1.

Preparation of **81**



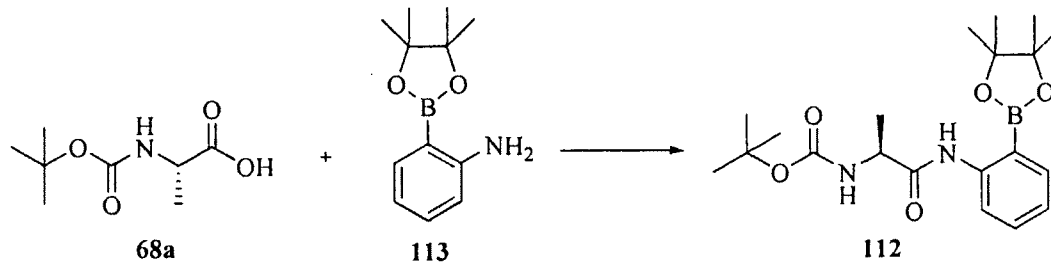
To **88** (1.68 g, 2.44 mmol) was added a 1:1 mixture of trifluoroacetic acid/ CH_2Cl_2 (5 mL) and the solution was stirred for 30 minutes at room temperature. The solution was then evaporated under reduced pressure and taken back up in methanol (10 mL) and evaporated under reduced pressure to give crude material (2.0 g). This crude (1.0 g) was suspended in water (25 mL)/ CH_2Cl_2 (50 mL) and made alkaline (pH 14). The organic phase was removed and the aqueous layer extracted with CH_2Cl_2 (50 mL). The combined organic layers were washed with brine (25 mL), dried over Na_2SO_4 and concentrated to give free diamine (578 mg) of which 388 mg (0.794 mmol) was dissolved in anhydrous ethanol (80 mL) containing diethyl squarate (135 mg, 0.794 mmol). The reaction was stirred for 60 hrs yielding a precipitate that was isolated by filtration. The precipitate was dissolved in DMSO and after addition of water yielded a white powder (yield not determined).

^1H NMR (300 MHz, $\text{DMSO}-d_6$) δ 9.48 (br s, 4H), 8.20 (br s, 2H), 8.09 (br s, 4H), 7.60 (br s, 4H), 7.25 (br s, 4H), 4.90 (br m, 2H), 1.43 (br s, 6H); MS (EI): m/z , 566.6.

Preparation of 97

To **70b** (3.20 g, 10.0 mmol) was added concentrated HCl (12.5 mL) and EtOAc (37.5 mL) and the solution was stirred for 60 minutes at room temperature. The solution was then evaporated under reduced pressure and taken back up in methanol (10 mL) and evaporated under reduced pressure. The residue was taken back up in water (10 mL) and brought to pH 12-13 with 2 M NaOH. The aqueous phase was extracted with CH₂Cl₂ (3 x 20 mL), dried over Na₂SO₄ and solvent evaporated under reduced pressure to afford the crude deprotected amine (2.04 g, 92.6%) as a yellow oil. The amine (1.12 g, 5.10 mmol) was dissolved in methanol (10 mL) and diethyl squarate (289.3 mg, 1.7 mmol) added. The reaction was stirred for 18 hrs and then the solvent evaporated under reduced pressure and the residue washed with diethyl ether to afford the product (839 mg, 95.2%) as a white solid.

¹H NMR (400 MHz, CDCl₃, TMS) δ 7.27-7.20 (m, 10H), 6.45 (br s, 2H), 4.98 (br s, 2H), 3.25-3.12 (m, 10H), 1.20-1.10 (m, 8H), 0.85 (t, 7.4 Hz, 6H); ¹³C NMR (100 MHz, CDCl₃) δ 183.2, 170.6, 167.0, 135.8, 129.5, 128.6, 127.1, 59.0, 39.6, 31.1, 19.9, 13.7; IR (KBr, cast film) ν 3250, 2958, 2870, 1657, 1591, 1524, 1454.

Preparation of **112**

To **68a** (318 mg, 1.68 mmol) was added CH₂Cl₂ (6 mL), *o*-boronate aniline **113** (283 mg, 1.29 mmol), DMAP (21 mg, 0.17 mmol) and DCC (347 mg, 1.68 mmol). The reaction was stirred for 12 hrs, filtered and concentrated in vacuo to afford crude product which was purified by flash column chromatography (40% EtOAc in hexanes) to afford the product (403 mg, 80.0%) as a white solid.

¹H NMR (300 MHz, CDCl₃, TMS) δ 9.61 (br s, 1H), 8.46 (br m, 1H), 7.76 (dd, 1.5, 7.3 Hz, 1H), 7.46 (dt, 1.5, 7.3 Hz, 1H), 7.08 (t, 7.4 Hz, 1H), 5.27 (br s, 1H) 4.35 (br s, 1H), 1.45 (m, 12H) 1.38 (s, 12H); ¹³C NMR (100 MHz, CDCl₃) δ 171.0, 144.2, 136.26, 132.9, 123.2, 119.4, 84.5, 51.2, 40.1, 28.3, 24.9, 19.4.

References

- (1) Wani, M. C.; Taylor, H. L.; Wall, M. E.; Coggon, P.; McPhail, A. T. *J. Am. Chem. Soc.* **1971**, *93*, 2325-2327.
- (2) Schiff, P. B.; Fant, J.; Horwitz, S. B. *Nature* **1979**, *277*, 665.
- (3) Nicolaou, K. C. *Chem. Commun. (Cambridge, U. K.)* **2003**, 661-664.
- (4) Kingston, D. G. I.; Hawkins, D. R.; Ovington, L. *J. Nat. Prod.* **1982**, *45*, 466-470.
- (5) Gunawardana, G. P.; Premachandran, U.; Burres, N. S.; Whittern, D. N.; Henry, R.; Spanton, S.; McAlpine, J. B. *J. Nat. Prod.* **1992**, *55*, 1686-1689.
- (6) Zamir, L. O.; Nedeia, M. E.; Bélair, S.; Sauricol, F.; Mamer, O.; Jacqmain, E.; Jean, F. I.; Garneau, F. X. *Tetrahedron Lett.* **1992**, *33*, 5173-5176.
- (7) Denis, J. N.; Greene, A. E.; Guenard, D.; Gueritte-Voegelein, F.; Mangatal, L.; Potier, P. *J. Am. Chem. Soc.* **1988**, *110*, 5917-5919.
- (8) Herranz, E.; Biller, S. A.; Sharpless, K. B. *J. Am. Chem. Soc.* **1978**, *100*, 3596-3598.
- (9) Guenard, D.; Gueritte-Voegelein, F.; Potier, P. *Acc. Chem. Res.* **1993**, *26*, 160-167.
- (10) Holton, R. A. European Patent EP0400971, **1998**.
- (11) Ojima, I. *Acc. Chem. Res.* **1995**, *28*, 383-389.
- (12) Kingston, D. G. I.; Chaudhary, A. G.; Gunatilaka, A. A. L.; Middleton, M. L. *Tetrahedron Lett.* **1994**, *35*, 4483-4484.
- (13) Gou, D. M.; Liu, Y. C.; Chen, C. S. *J. Org. Chem.* **1993**, *58*, 1287-1289.
- (14) Zamir, L. United States Patent 6222053, **2001**.
- (15) Findlay, J.; Deslongchamps, G.; Li, G. United States Patent 10/254972, 2002.
- (16) Nikolakakis, A.; Caron, G.; Cherestes, A.; Sauriol, F.; Mamer, O.; Zamir, L. O. *Bioorg. Med. Chem.* **2000**, *8*, 1269-1280.
- (17) Grob, C. A.; Baumann, W. *Helv. Chim. Acta* **1955**, *38*, 594-610.
- (18) Deslongchamps, P. *Tetrahedron* **1975**, *31*, 2463-2490.
- (19) Klein, L. L.; Li, L.; Maring, C. J.; Yeung, C. M.; Thomas, S. A.; Grampovnik, D. J.; Plattner, J. J. *J. Med. Chem.* **1995**, *38*, 1482-1492.

- (20) Plietker, B. *Org. Lett.* **2004**, *6*, 289-291.
- (21) Plietker, B. *European Journal of Organic Chemistry* **2005**, *2005*, 1919-1929.
- (22) Pfitzner, K. E.; Moffatt, J. G. *J. Am. Chem. Soc.* **1963**, *85*, 3027-3028.
- (23) Parikh, J. R.; Doering, W. v. E. *J. Am. Chem. Soc.* **1967**, *89*, 5505-5507.
- (24) Sharma, A. K.; Ku, T.; Dawson, A. D.; Swern, D. *J. Org. Chem.* **1975**, *40*, 2758-2764.
- (25) Omura, K.; Swern, D. *Tetrahedron* **1978**, *34*, 1651-1660.
- (26) Corey, E. J.; Kim, C. U. *J. Am. Chem. Soc.* **1972**, *94*, 7586-7587.
- (27) Hajos, Z. G.; Parrish, D. R. *J. Org. Chem.* **1974**, *39*, 1615-1621.
- (28) Agami, C.; Puchot, C.; Sevestre, H. *Tetrahedron Lett.* **1986**, *27*, 1501-1504.
- (29) Eder, U.; Sauer, G.; Wiechert, R. *Angewandte Chemie International Edition in English* **1971**, *10*, 496-497.
- (30) Sigman, M. S.; Jacobsen, E. N. *J. Am. Chem. Soc.* **1998**, *120*, 4901-4902.
- (31) Corey, E. J.; Grogan, M. *J. Org. Lett.* **1999**, *1*, 157-160.
- (32) Miller, S. J.; Copeland, G. T.; Papaioannou, N.; Horstmann, T. E.; Ruel, E. M. *J. Am. Chem. Soc.* **1998**, *120*, 1629-1630.
- (33) List, B.; Lerner, R. A.; Barbas, C. F. *J. Am. Chem. Soc.* **2000**, *122*, 2395-2396.
- (34) Ahrendt, K. A.; Borths, C. J.; MacMillan, D. W. C. *J. Am. Chem. Soc.* **2000**, *122*, 4243-4244.
- (35) MacMillan, D. W. C. *Nature* **2008**, *455*, 304-308.
- (36) Wittkopp, A.; Schreiner, P. R. *Chemistry - A European Journal* **2003**, *9*, 407-414.
- (37) Etter, M. C.; Panunto, T. W. *J. Am. Chem. Soc.* **1988**, *110*, 5896-5897.
- (38) Zhu, Y.; Drueckhammer, D. G. *J. Org. Chem.* **2005**, *70*, 7755-7760.
- (39) Malerich, J. P.; Hagihara, K.; Rawal, V. H. *J. Am. Chem. Soc.* **2008**, *130*, 14416-14417.
- (40) Cheon, C. H.; Yamamoto, H. *Tetrahedron Lett.* **2009**, *50*, 3555-3558.

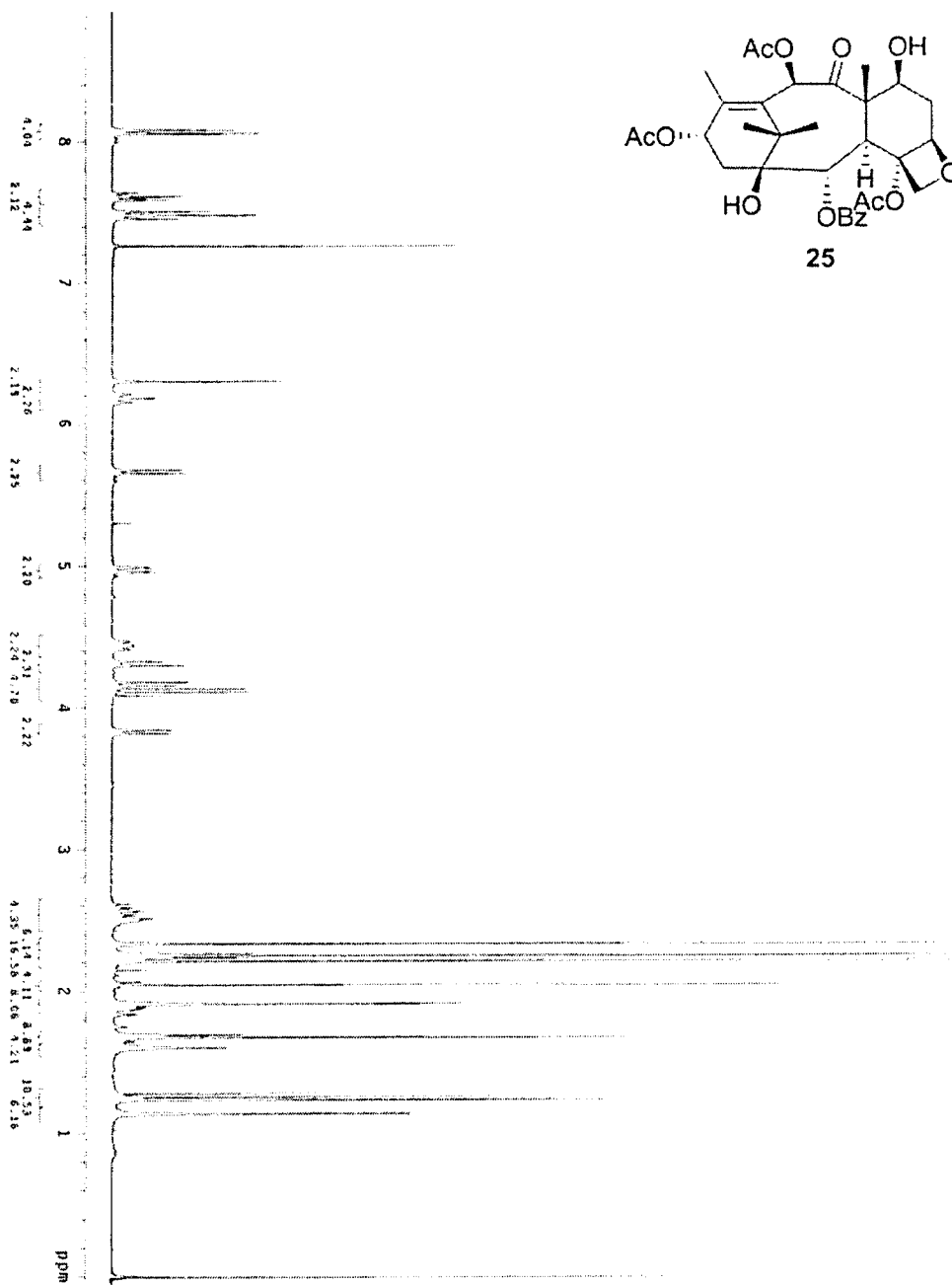
- (41) Rotger, M. C.; Pina, M. N.; Frontera, A.; Martorell, G.; Ballester, P.; Deya, P. M.; Costa, A. *J. Org. Chem.* **2004**, *69*, 2302-2308.
- (42) Pfaltz, A.; Drury, W. J. *Proceedings of the National Academy of Sciences of the United States of America* **2004**, *101*, 5723-5726.
- (43) Etter, M. C. *J. Am. Chem. Soc.* **1982**, *104*, 1095-1096.
- (44) M. R. Gholami, ; B. A. Talebi, *Journal of Physical Organic Chemistry* **2003**, *16*, 79-83.
- (45) Blake, J. F.; Lim, D.; Jorgensen, W. L. *J. Org. Chem.* **1994**, *59*, 803-805.
- (46) Alexander Wittkopp, ; Peter R. Schreiner, *Chemistry - A European Journal* **2003**, *9*, 407-414.
- (47) Muñiz, F. M.; Montero, V. A.; Fuentes de Arriba, Á. L.; Simón, L.; Raposo, C.; Morán, J. R. *Tetrahedron Lett.* **2008**, *49*, 5050-5052.
- (48) Greene, R. N. *Tetrahedron Lett.* **1972**, *13*, 1793-1796.
- (49) Anderson, S.; Anderson, H. L.; Sanders, J. K. M. *Acc. Chem. Res.* **1993**, *26*, 469-475.
- (50) Carver, F. J.; Hunter, C. A.; Shannon, R. J. *J. Chem. Soc. , Chem. Commun.* **1994**, 1277-1280.
- (51) Yamada, Y. M. A.; Ikegami, S. *Tetrahedron Lett.* **2000**, *41*, 2165-2169.
- (52) Yuan, K.; Zhang, L.; Song, H.; Hu, Y.; Wu, X. *Tetrahedron Lett.* **2008**, *49*, 6262-6264.
- (53) Sohtome, Y.; Takemura, N.; Takagi, R.; Hashimoto, Y.; Nagasawa, K. *Tetrahedron* **2008**, *64*, 9423-9429.
- (54) Berkessel, A.; Roland, K.; Neudorfl, J. M. *Org. Lett.* **2006**, *8*, 4195-4198.
- (55) Wang, J.; Li, H.; Yu, X.; Zu, L.; Wang, W. *Org. Lett.* **2005**, *7*, 4293-4296.
- (56) Sohtome, Y.; Tanatani, A.; Hashimoto, Y.; Nagasawa, K. *Tetrahedron Lett.* **2004**, *45*, 5589-5592.
- (57) Maher, D. J.; Connon, S. J. *Tetrahedron Lett.* **2004**, *45*, 1301-1305.
- (58) Shi, M.; Liu, X. *Org. Lett.* **2008**, *10*, 1043-1046.

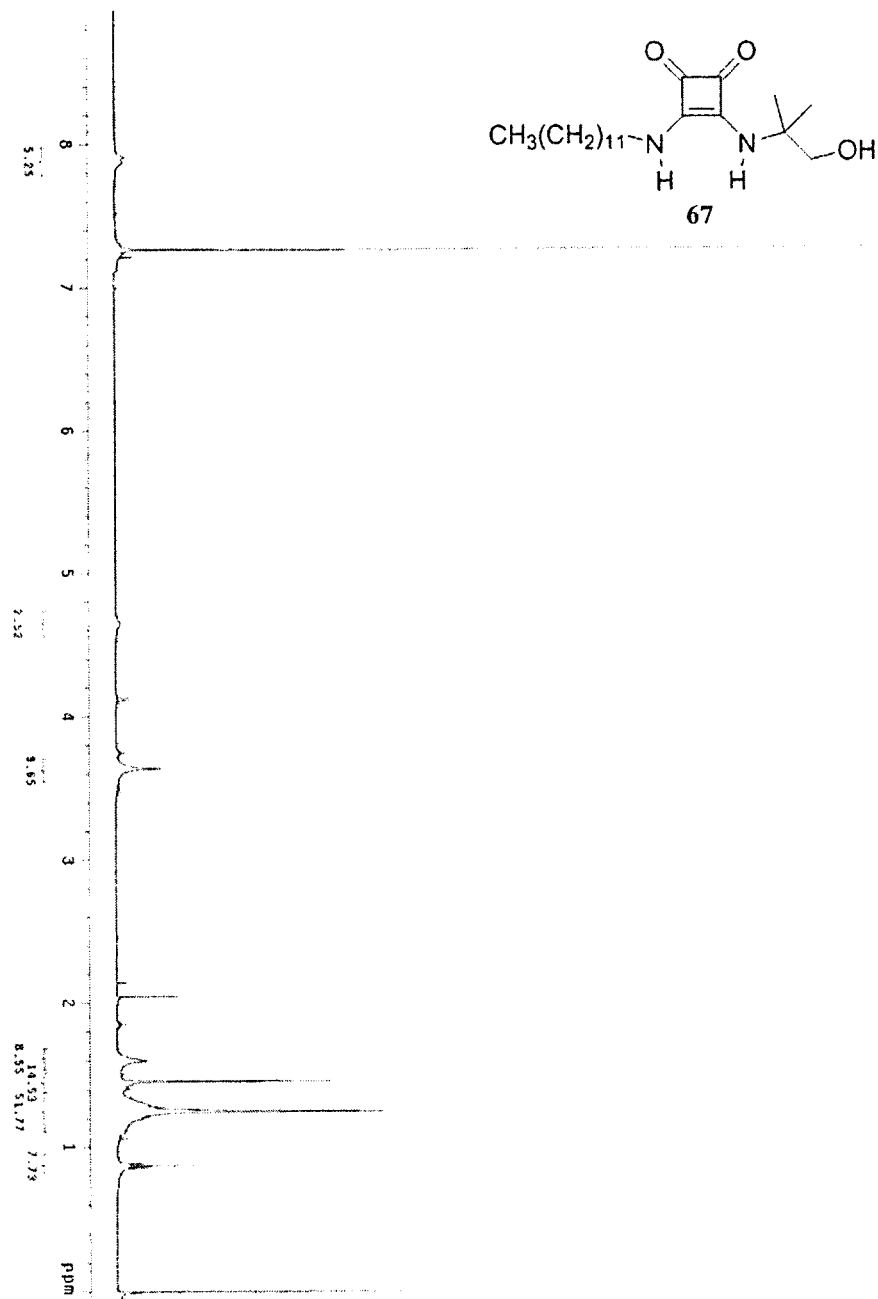
- (59) Robiette, R.; Aggarwal, V. K.; Harvey, J. N. *J. Am. Chem. Soc.* **2007**, *129*, 15513-15525.
- (60) Aggarwal, V. K.; Fulford, S. Y.; Lloyd-Jones, G. C. *Angewandte Chemie International Edition* **2005**, *44*, 1706-1708.
- (61) Shi, M.; Liu, Y. *Org. Biomol. Chem.* **2006**, *4*, 1468-1470.
- (62) Snowden, T. S.; Bisson, A. P.; Anslyn, E. V. *J. Am. Chem. Soc.* **1999**, *121*, 6324-6325.
- (63) Paradowska, J.; Rogozińska, M.; Mlynarski, J. *Tetrahedron Lett.* **2009**, *50*, 1639-1641.
- (64) Frank, A. W.; Drake, G. L. *J. Org. Chem.* **1971**, *36*, 549-552.
- (65) Li, X.; Deng, H.; Zhang, B.; Li, J.; Zhang, L.; Luo, S.; Cheng, J. *Chemistry - A European Journal* **2010**, *16*, 450-455.
- (66) Bergström, S.; Olofsson, G. *Journal of Solution Chemistry* **1978**, *7*, 497-513.
- (67) Zhong, Z.; Snowden, T. S.; Best, M. D.; Anslyn, E. V. *J. Am. Chem. Soc.* **2004**, *126*, 3488-3495.
- (68) Valenta, Z.; MaGee, D. I.; Setiadji, S. *J. Org. Chem.* **1996**, *61*, 9076-9077.
- (69) Gerlt, J. A.; Gassman, P. G. *J. Am. Chem. Soc.* **1993**, *115*, 11552-11568.
- (70) Terada, M.; Tanaka, H.; Sorimachi, K. *J. Am. Chem. Soc.* **2009**, *131*, 3430-3431.
- (71) Rankin, K. N.; Gauld, J. W.; Boyd, R. J. *The Journal of Physical Chemistry A* **2002**, *106*, 5155-5159.
- (72) Clemente, F. R.; Houk, K. N. *Angewandte Chemie International Edition* **2004**, *43*, 5766-5768.
- (73) Bahmanyar, S.; Houk, K. N. *J. Am. Chem. Soc.* **2001**, *123*, 12911-12912.
- (74) Mitsumori, S.; Zhang, H.; Ha-Yeon Cheong, P.; Houk, K. N.; Tanaka, F.; Barbas, C. F. *J. Am. Chem. Soc.* **2006**, *128*, 1040-1041.
- (75) Cheong, P. H.; Zhang, H.; Thayumanavan, R.; Tanaka, F.; Houk, K. N.; Barbas, C. F. *Org. Lett.* **2006**, *8*, 811-814.
- (76) Harriman, D. J.; Deslongchamps, G. *J. Comput. Aided Mol. Des.* **2004**, *18*, 303-308.

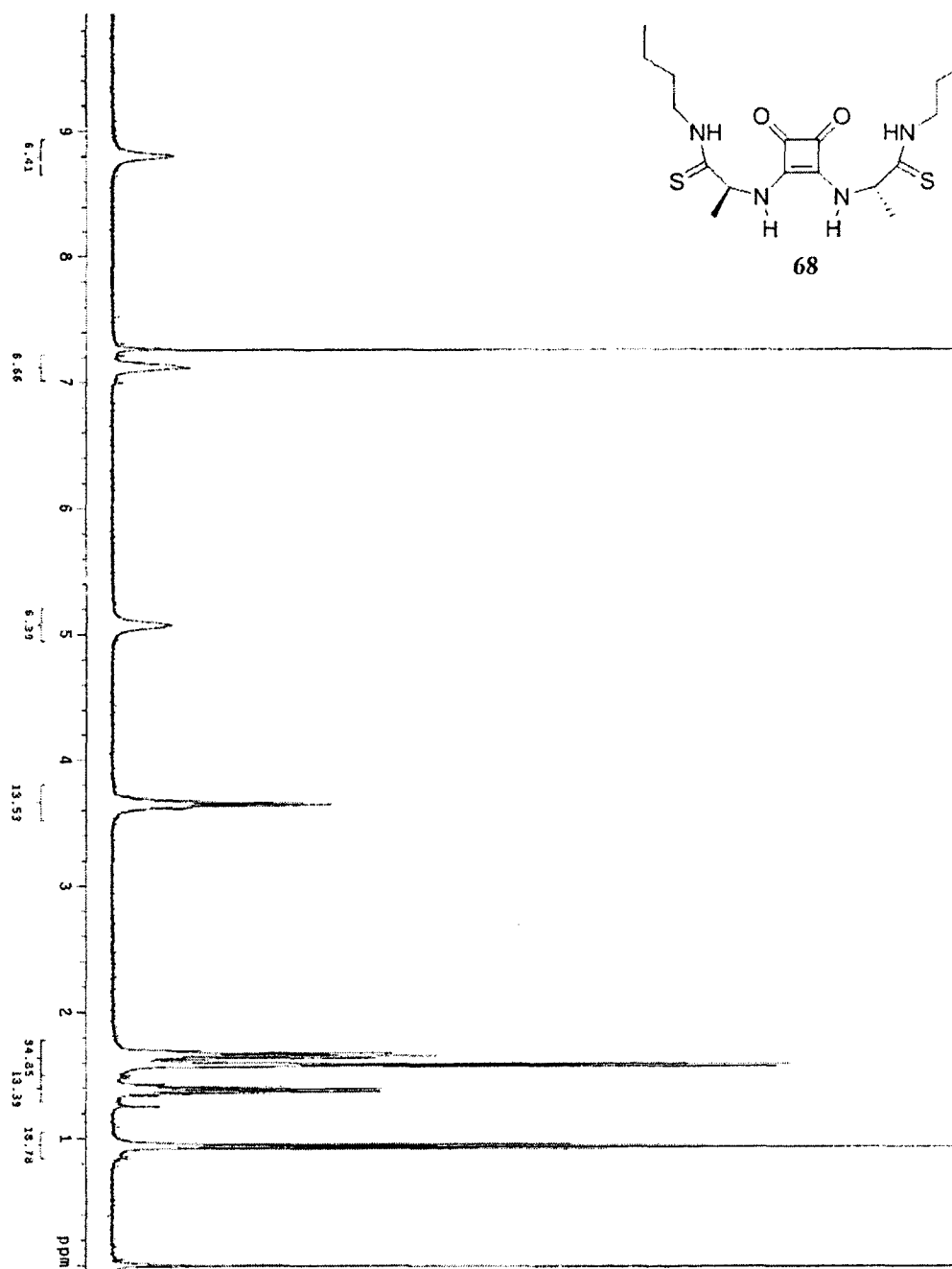
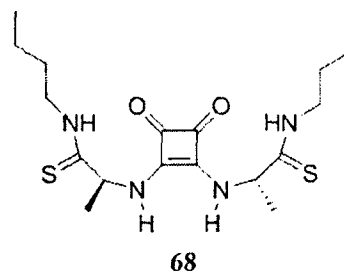
- (77) Harriman, D. J.; Lambropoulos, A.; Deslongchamps, G. *Tetrahedron Lett.* **2007**, *48*, 689-692.
- (78) Joseph Harriman, D.; Deleavey, G. F.; Lambropoulos, A.; Deslongchamps, G. *Tetrahedron* **2007**, *63*, 13032-13038.
- (79) Fleming, E. M.; Quigley, C.; Rozas, I.; Connon, S. J. *J. Org. Chem.* **2008**, *73*, 948-956.
- (80) Gordillo, R.; Dudding, T.; Anderson, C. D.; Houk, K. N. *Org. Lett.* **2007**, *9*, 501-503.
- (81) Kitaura, K.; Morokuma, K. *International Journal of Quantum Chemistry* **1976**, *10*, 325-340.
- (82) Jensen, K. H.; Sigman, M. S. *Angewandte Chemie* **2007**, *119*, 4832-4834.
- (83) Magri, N.F.; Kingston, D.G.; Jitrangsri, C.; Piccariello. *J. Org Chem.* **1986**, *51*, 3239-3242.

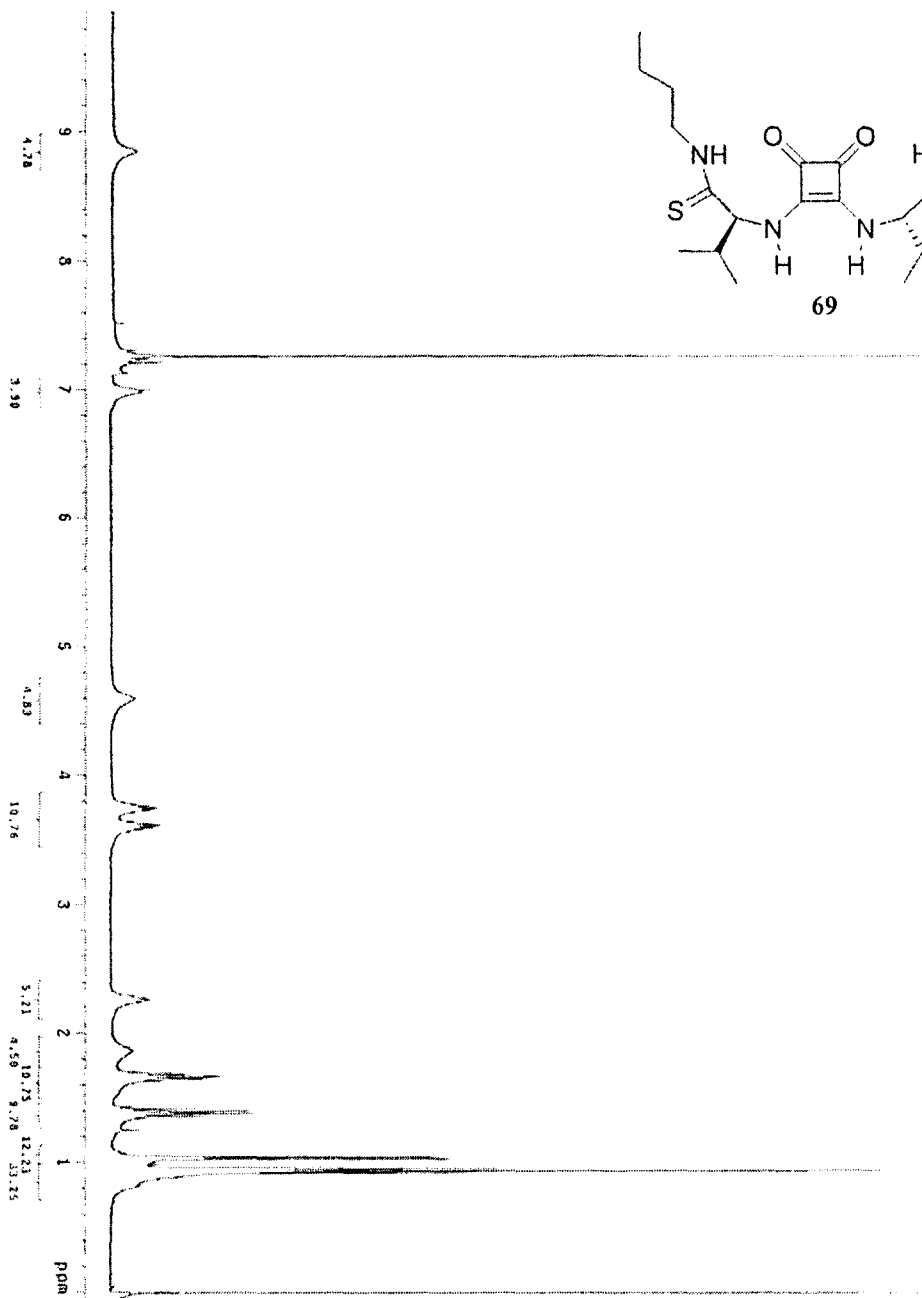
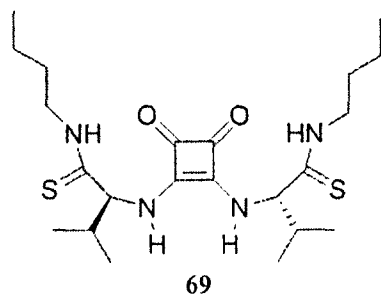
Appendix

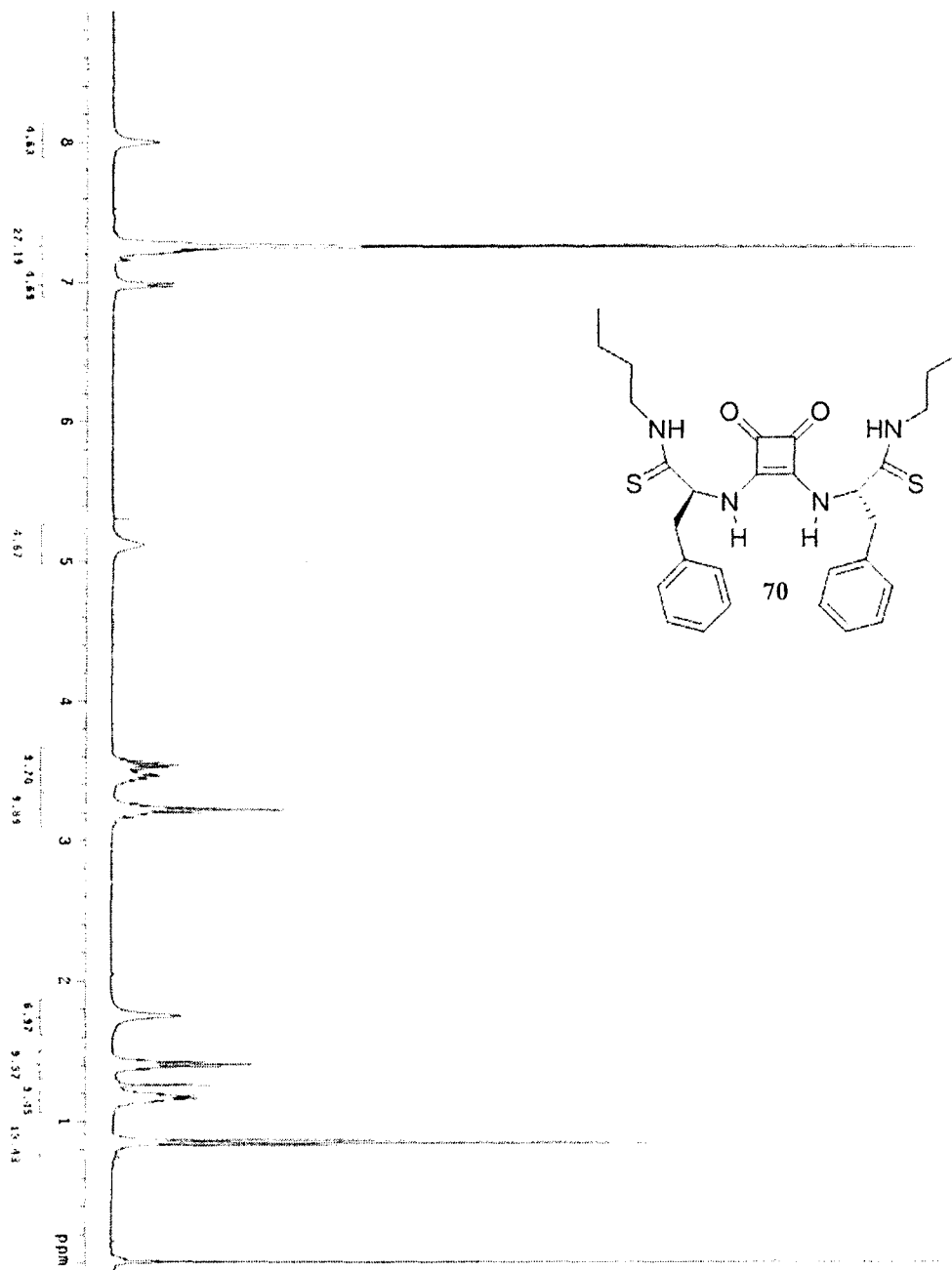
A1. ¹H NMR spectra

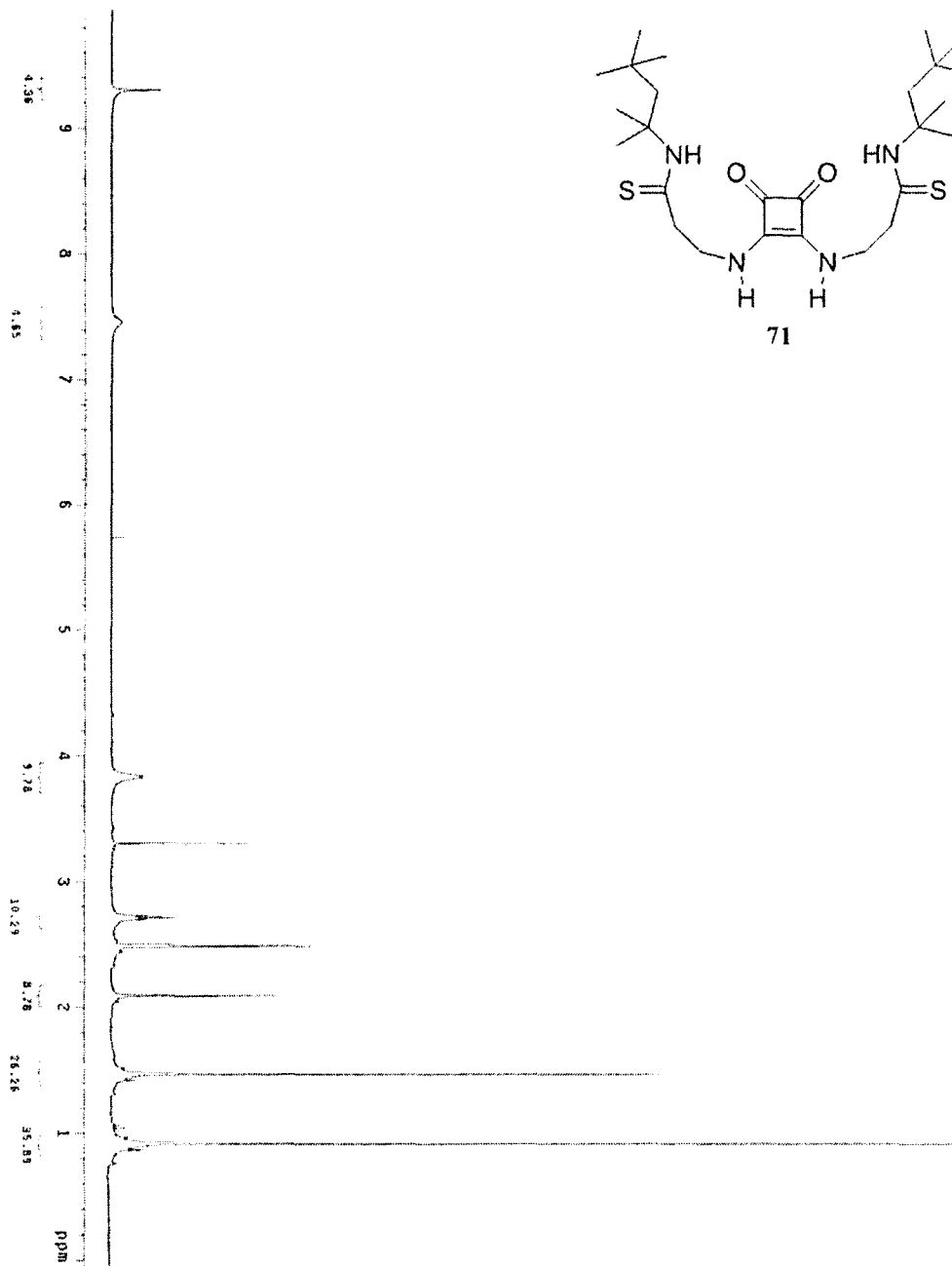
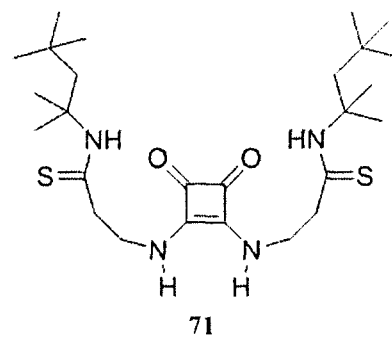


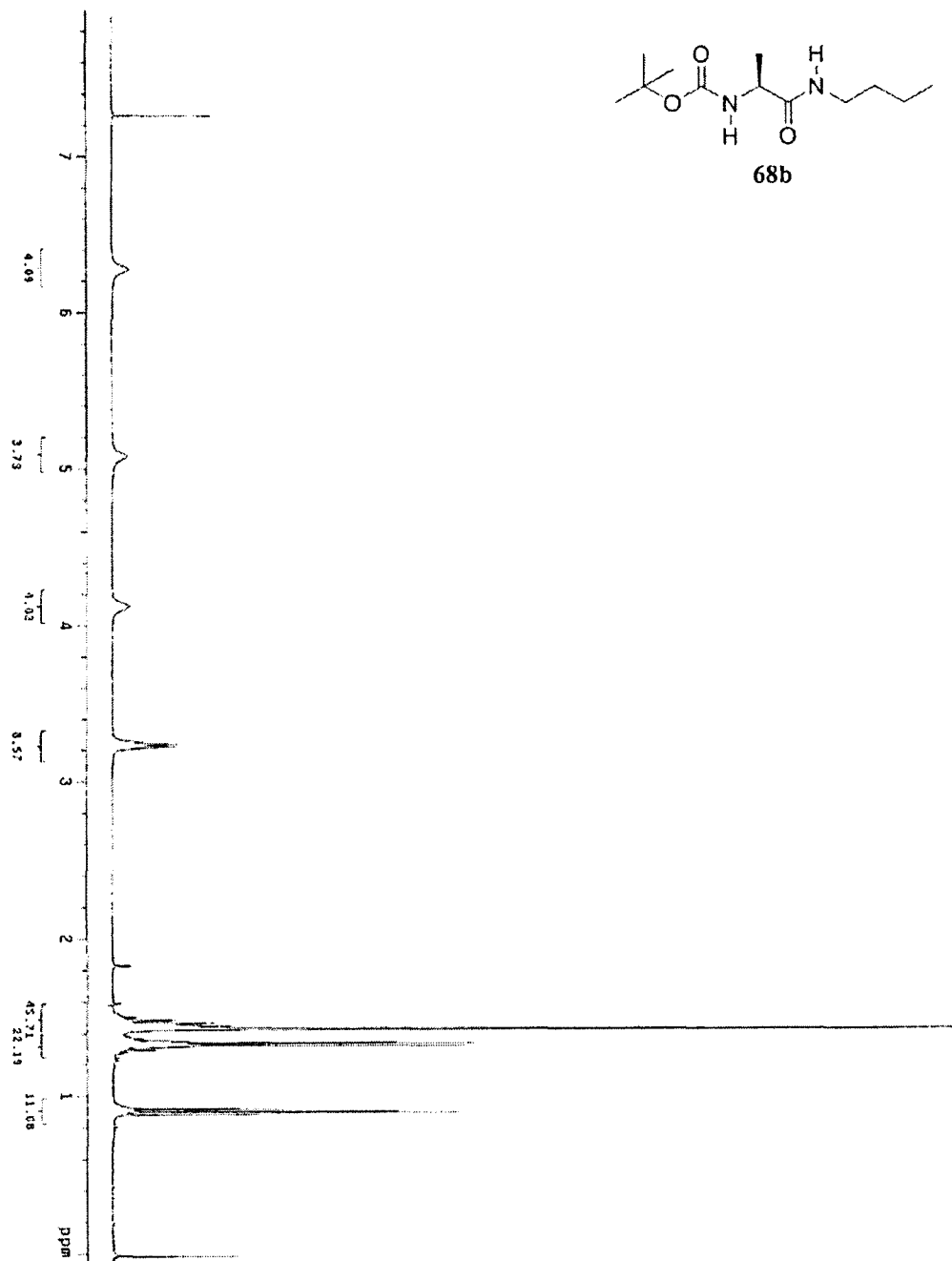
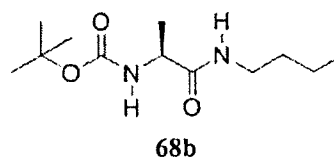


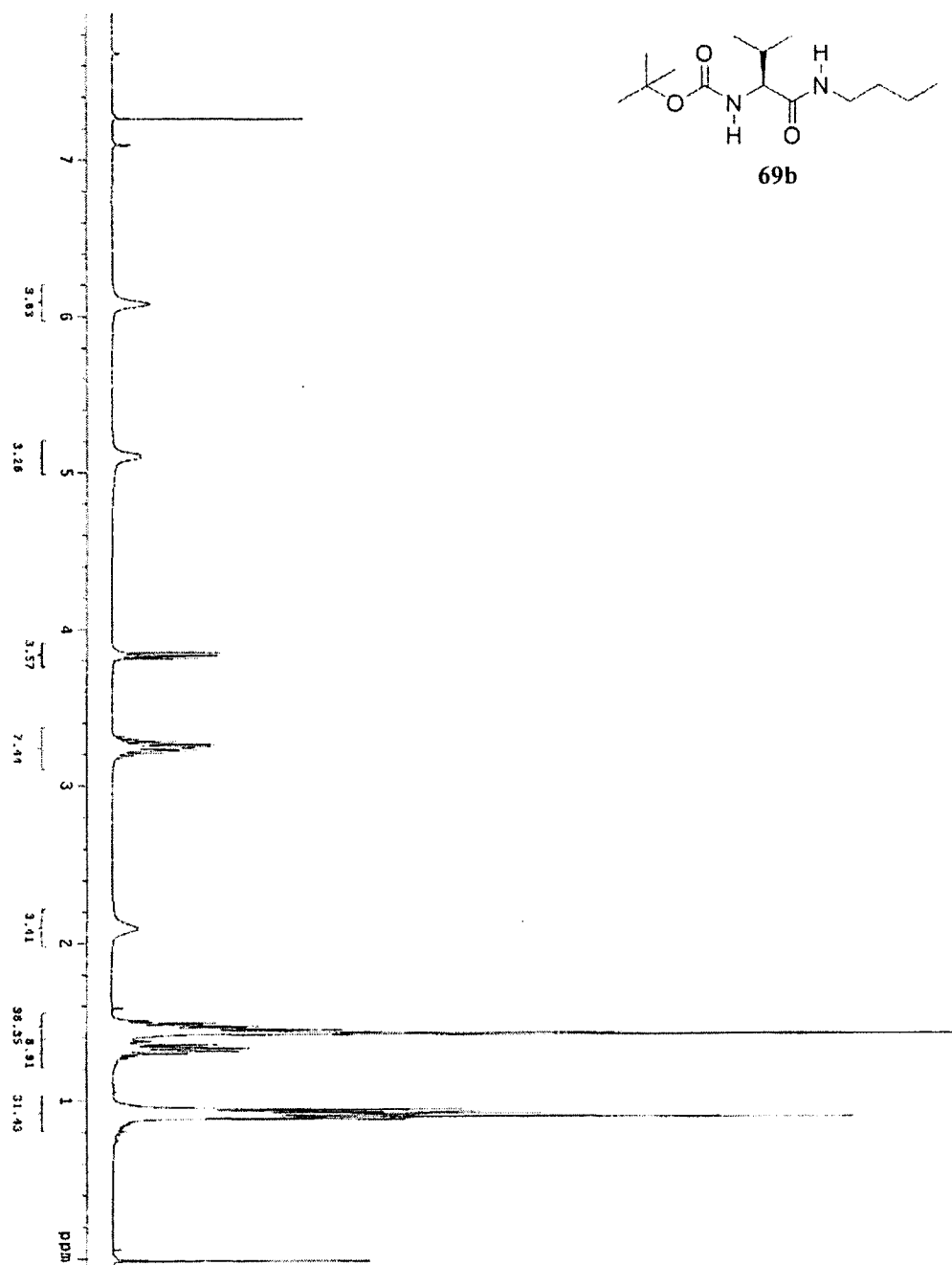
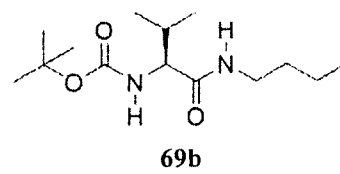


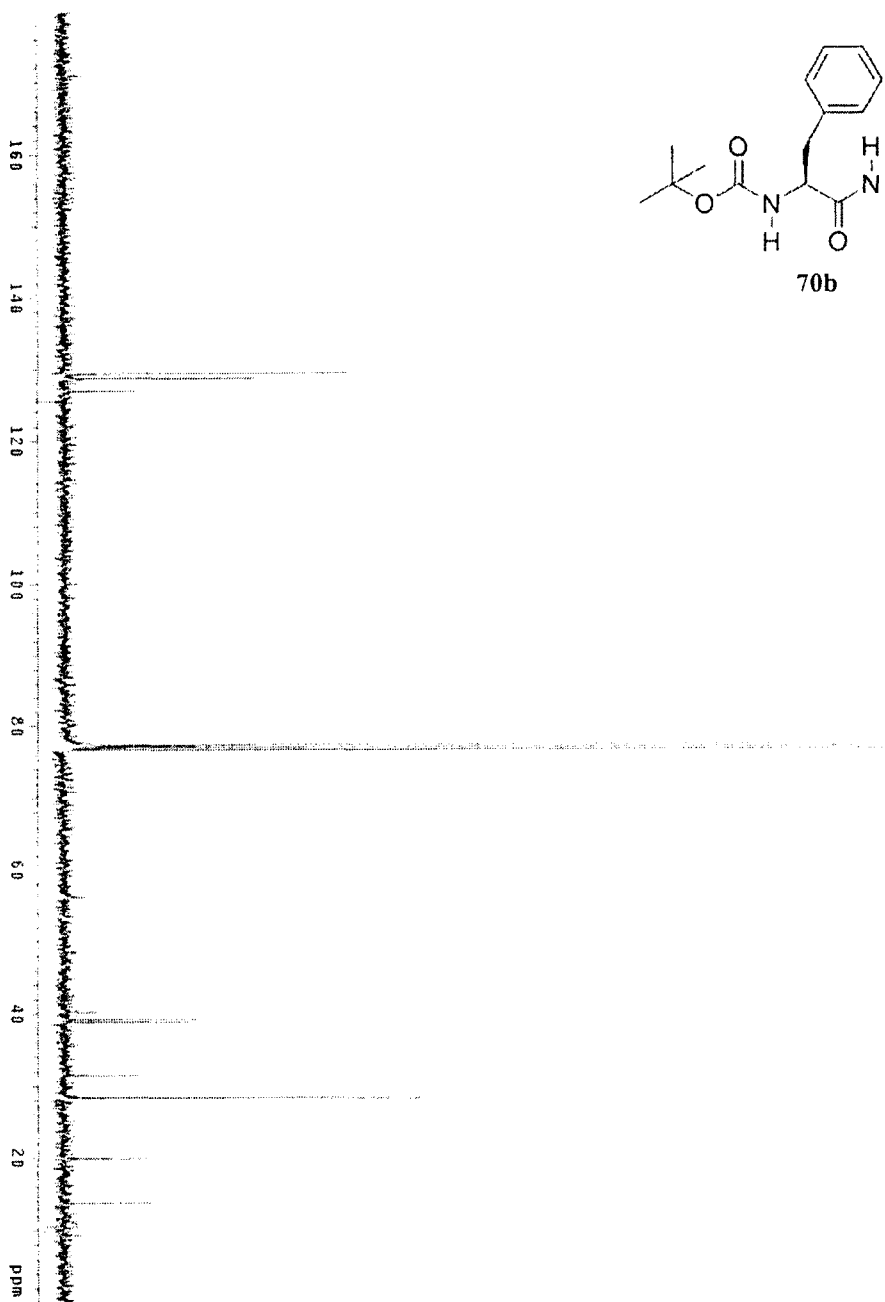
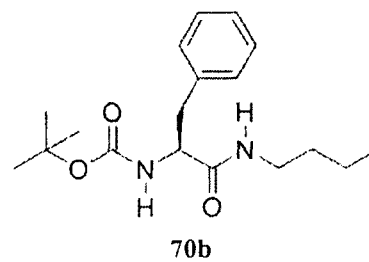


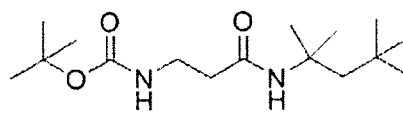




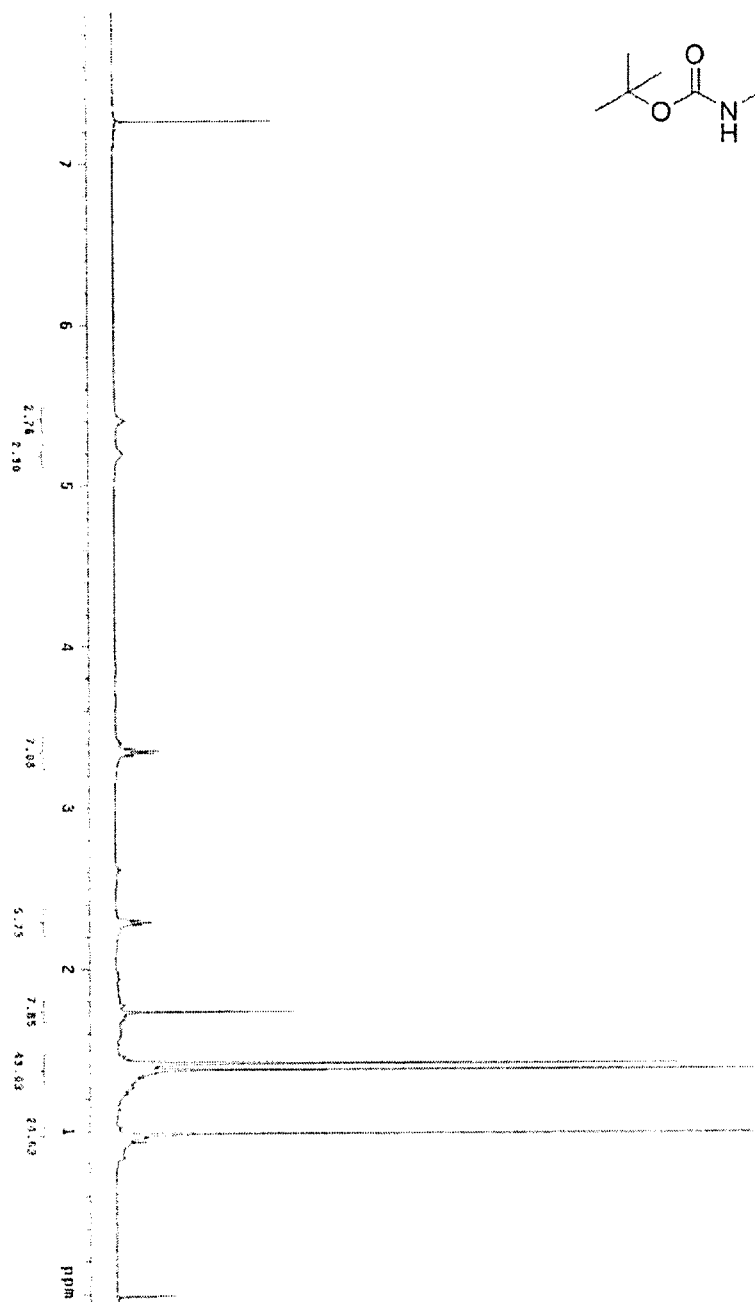


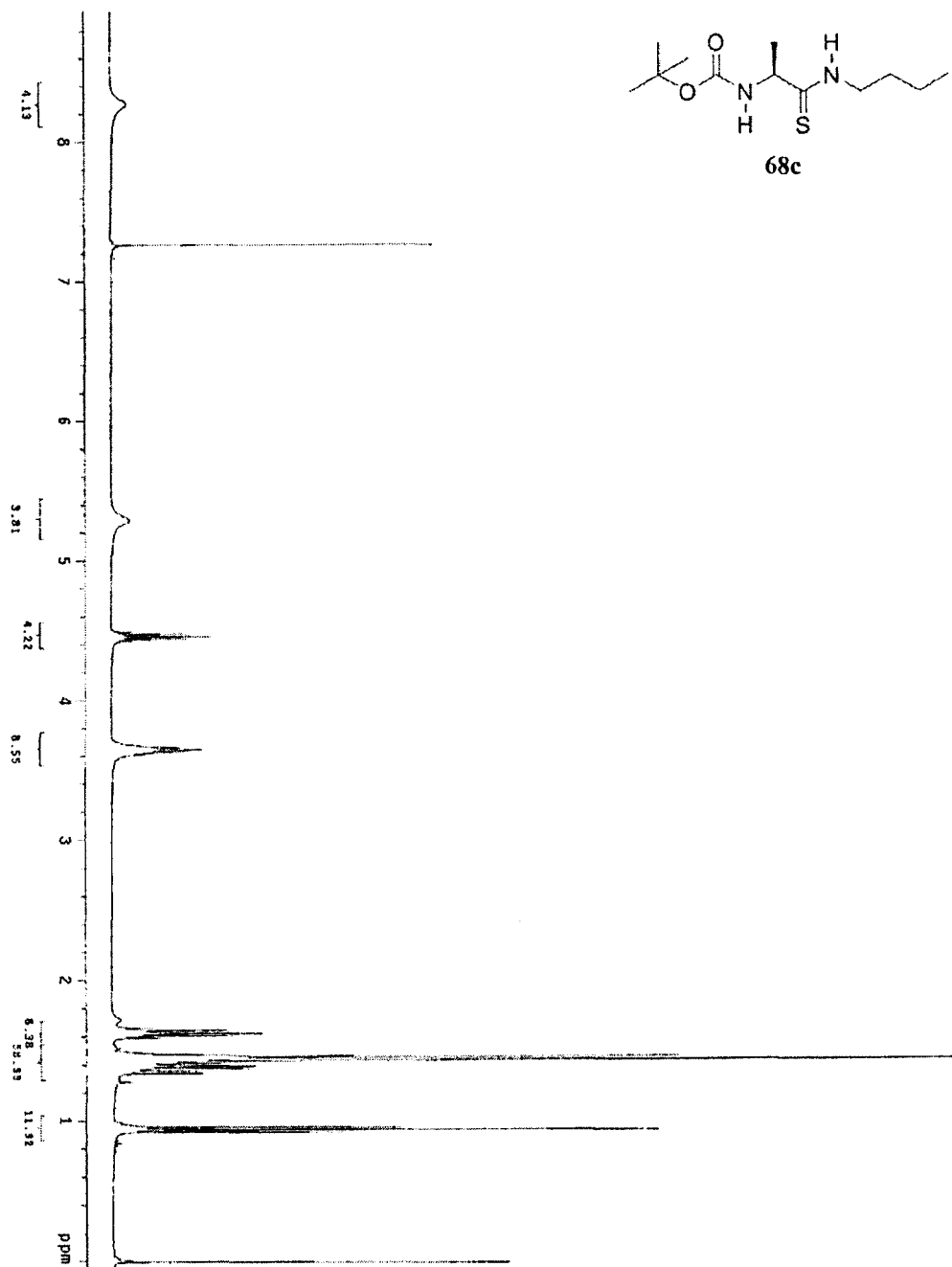
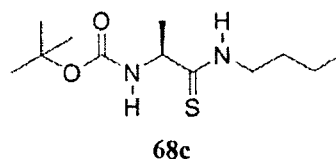


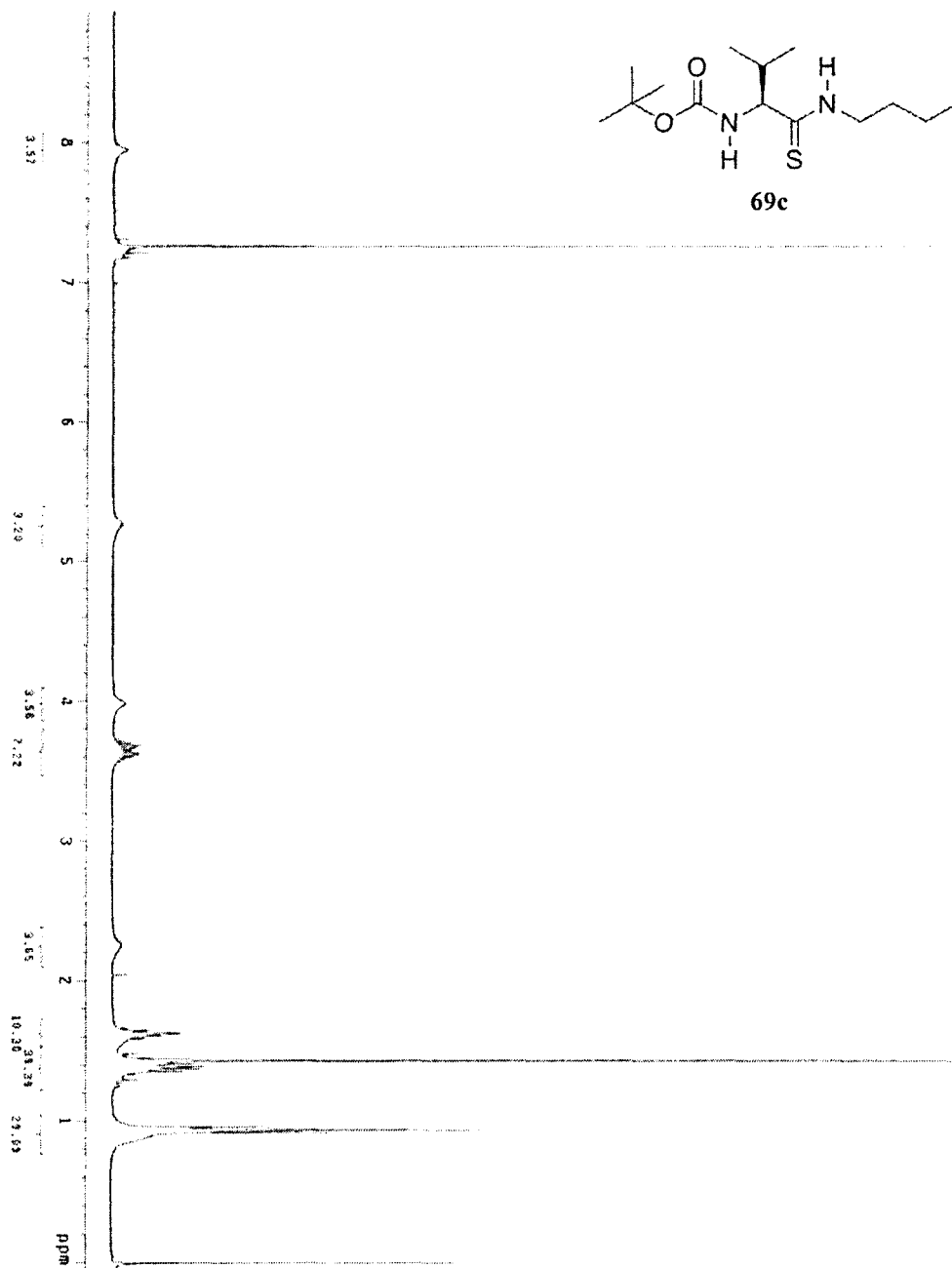
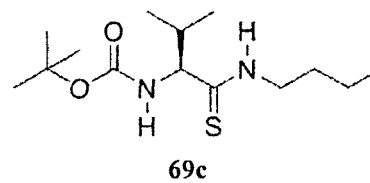


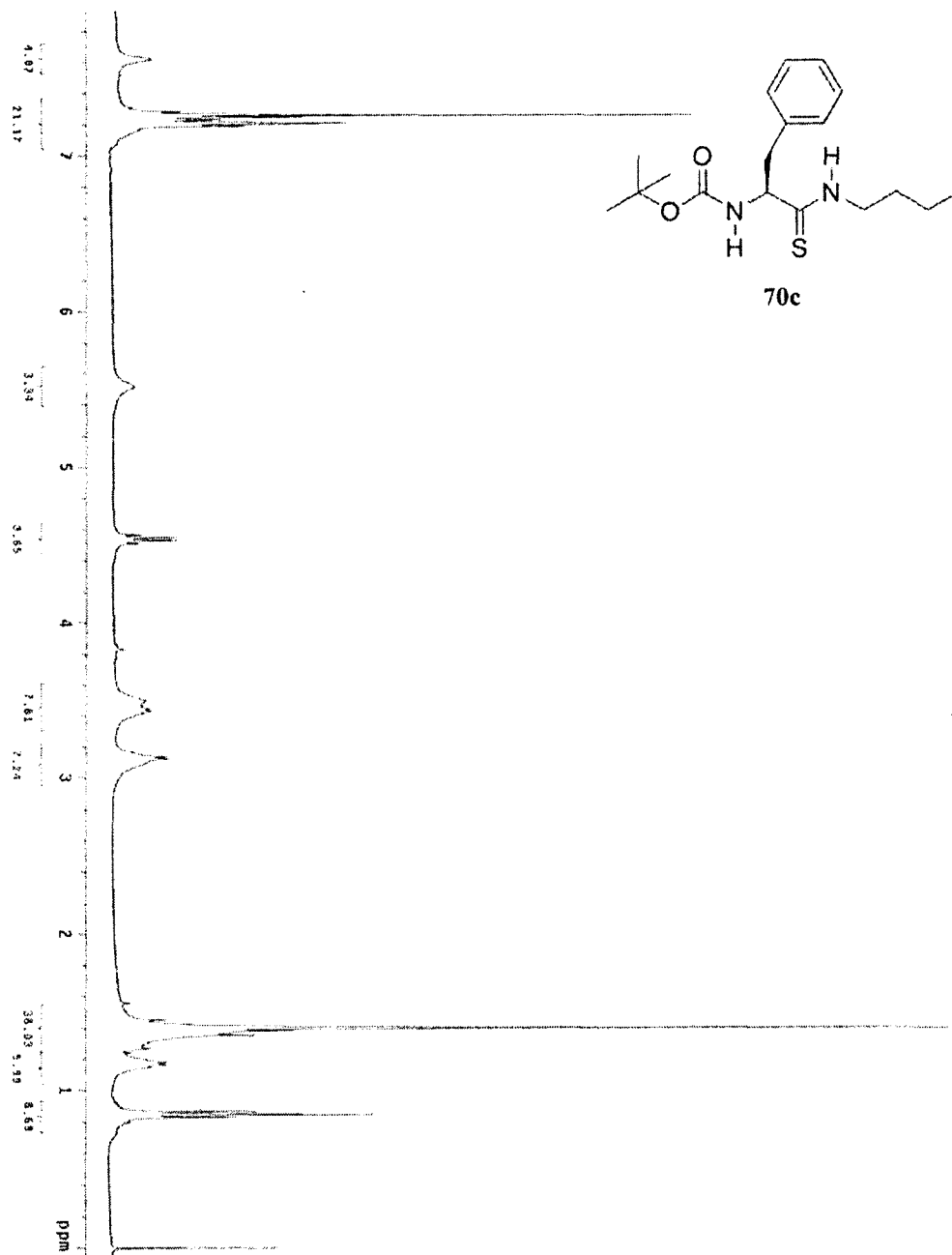


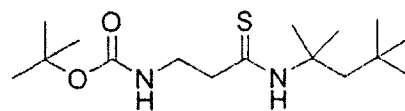
71b



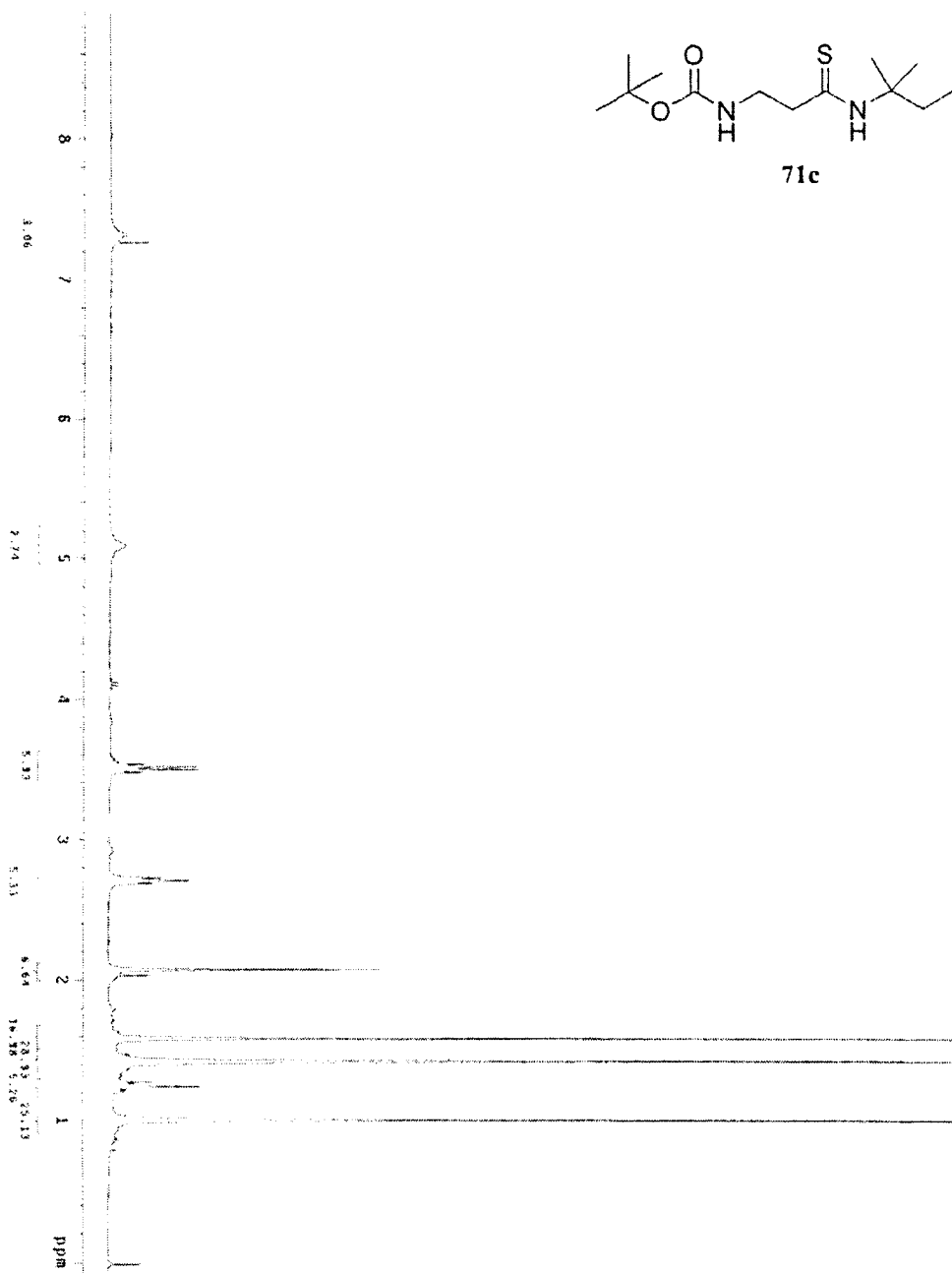


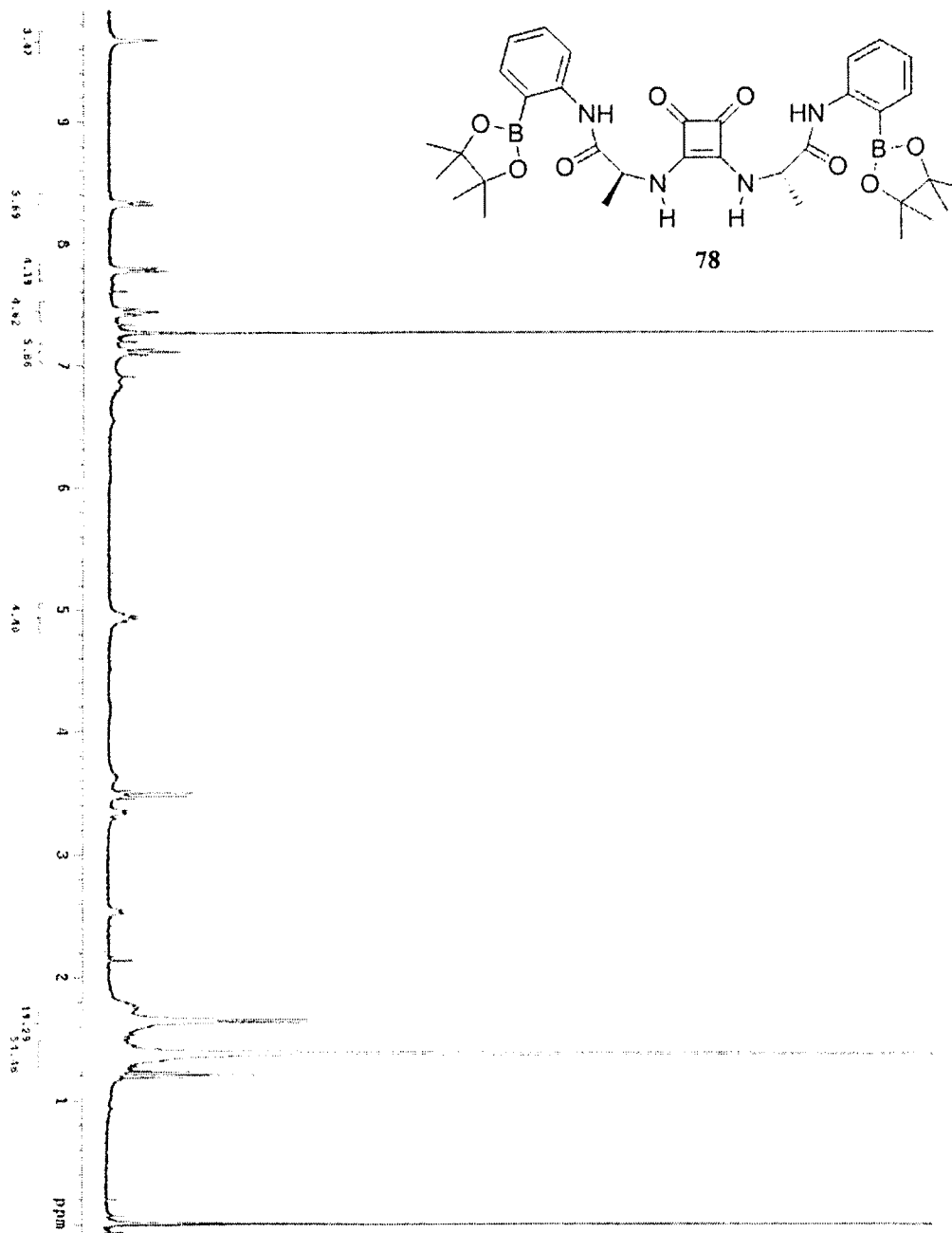


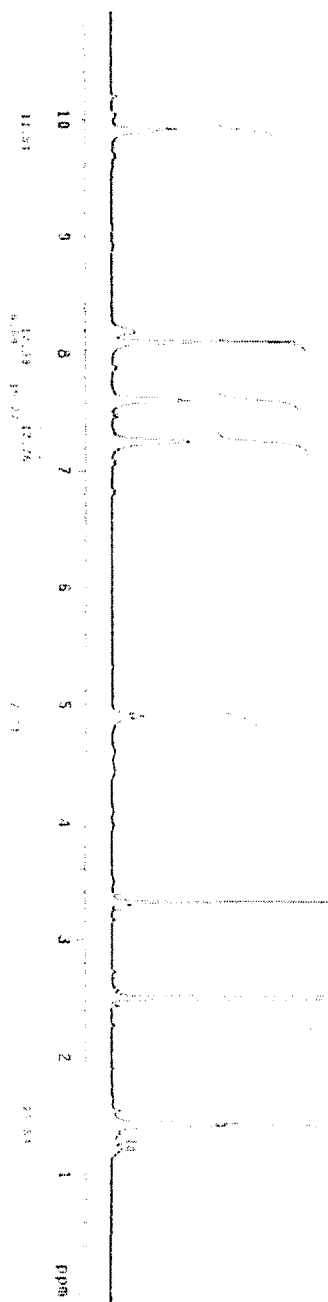
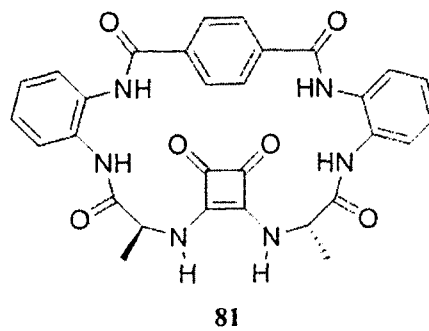


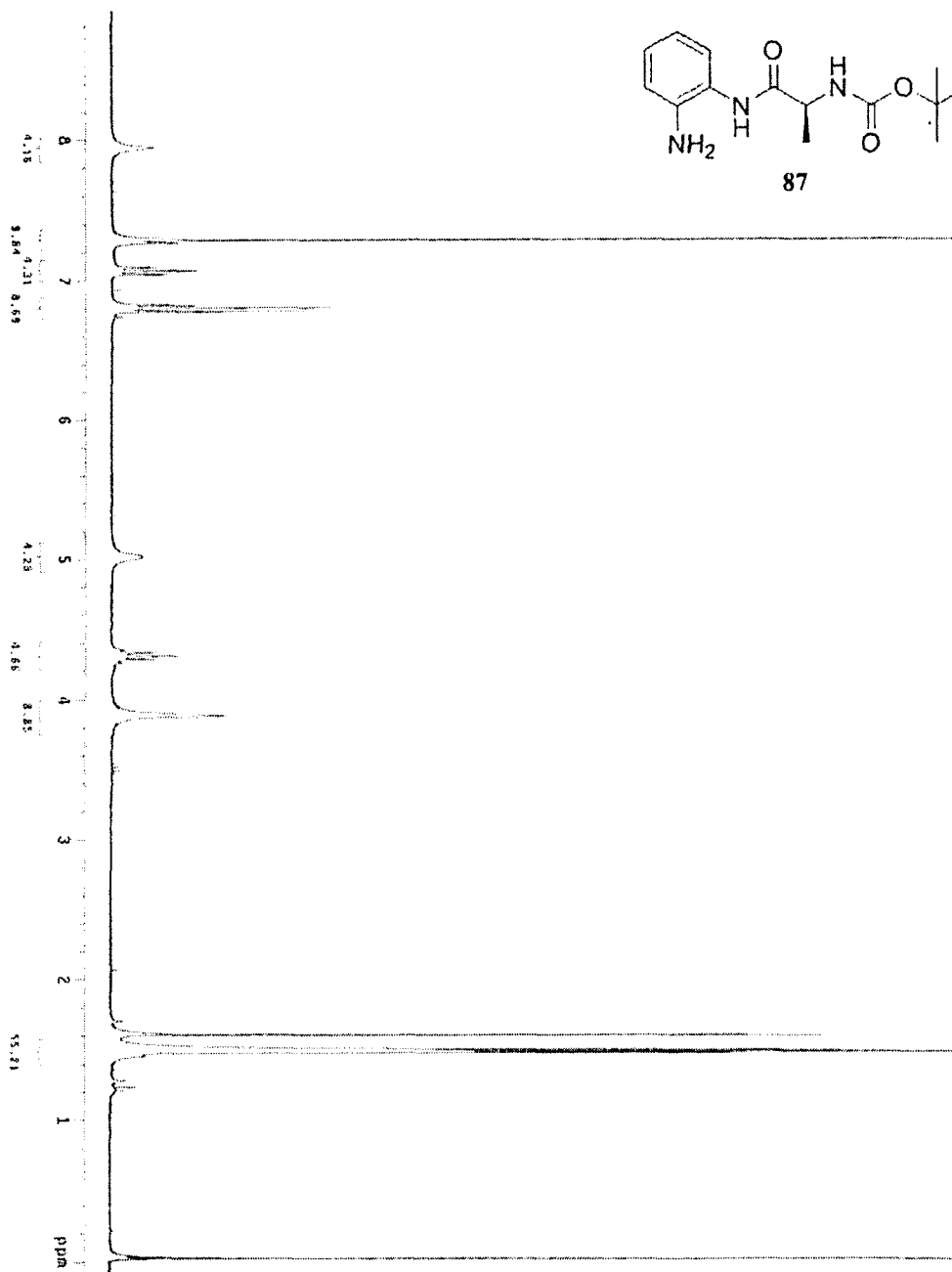
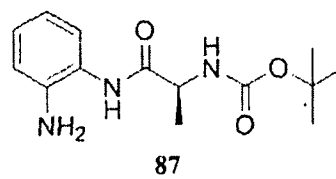


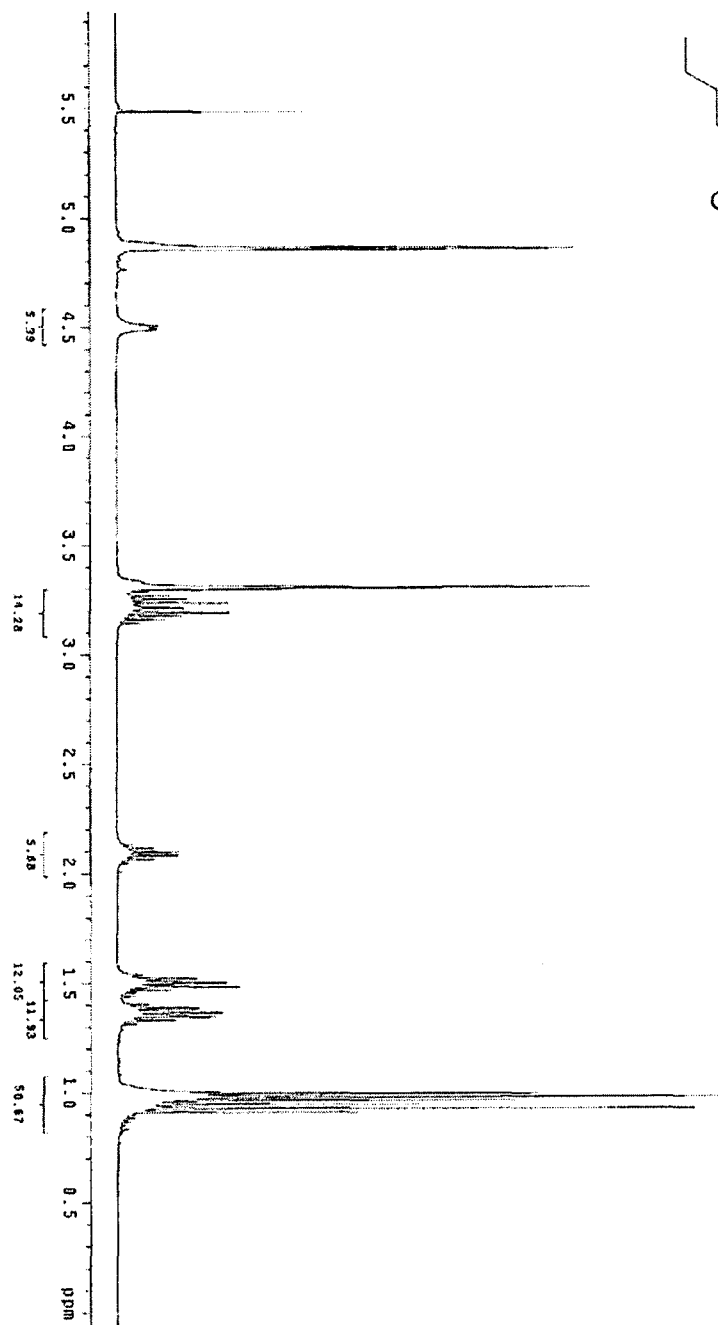
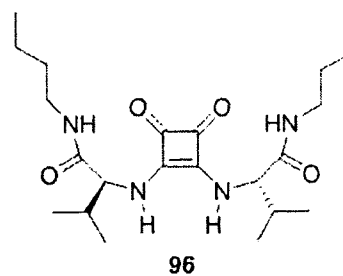
71c

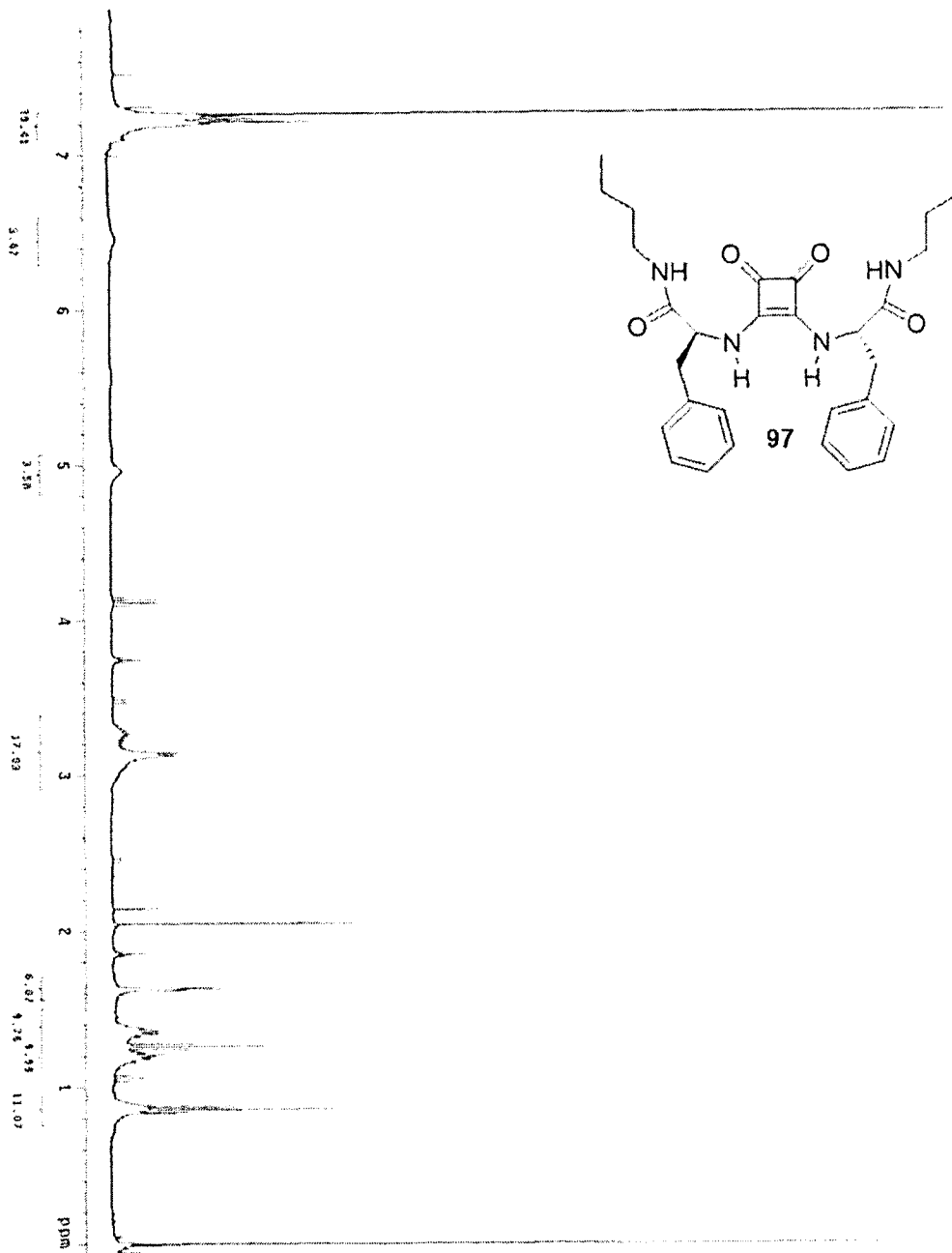


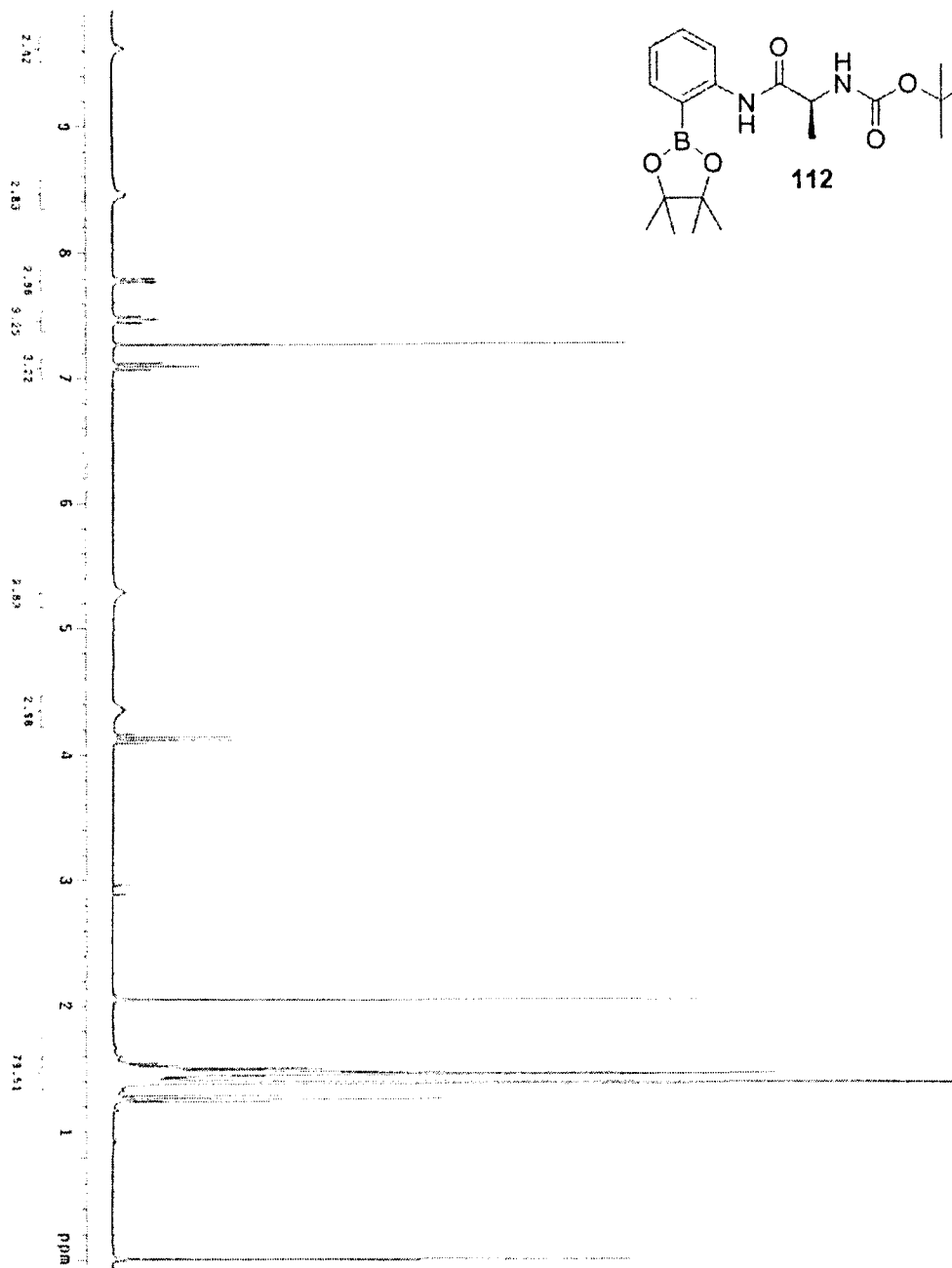
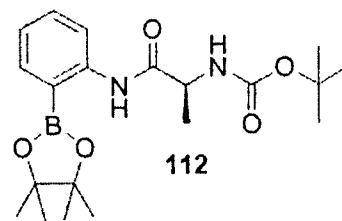




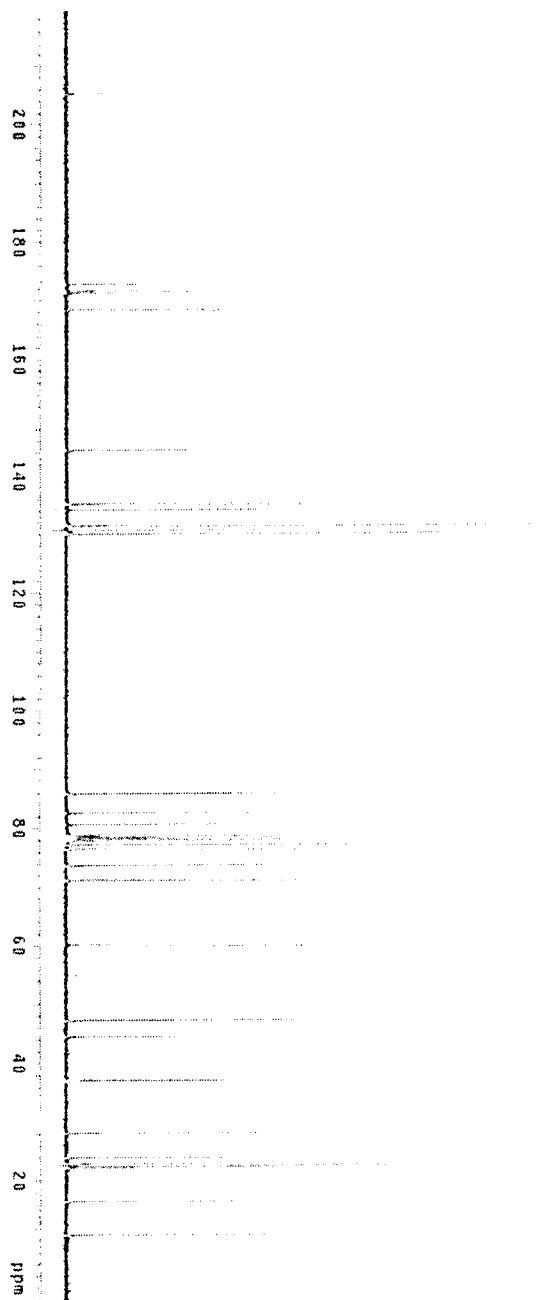
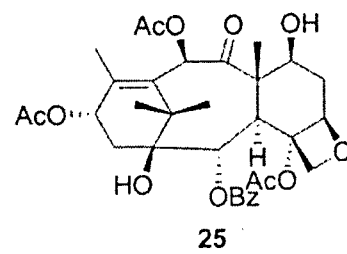


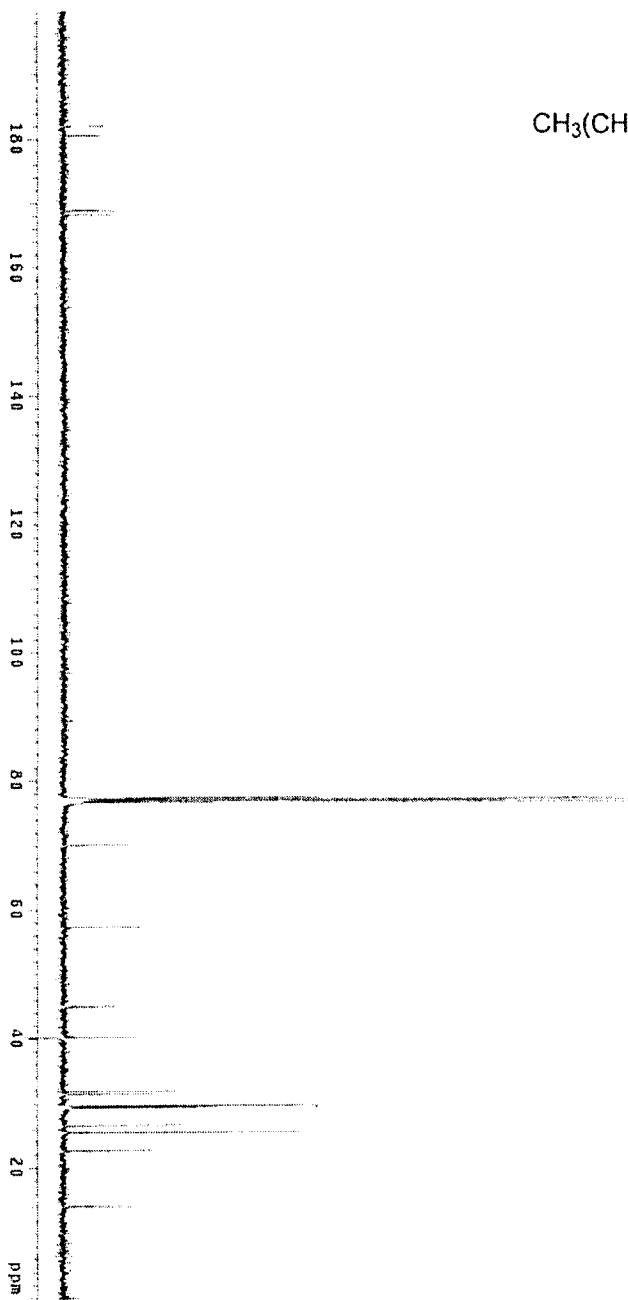
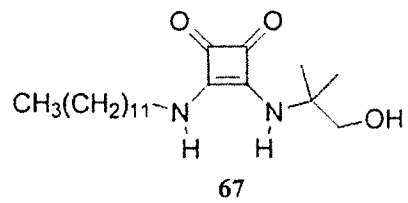


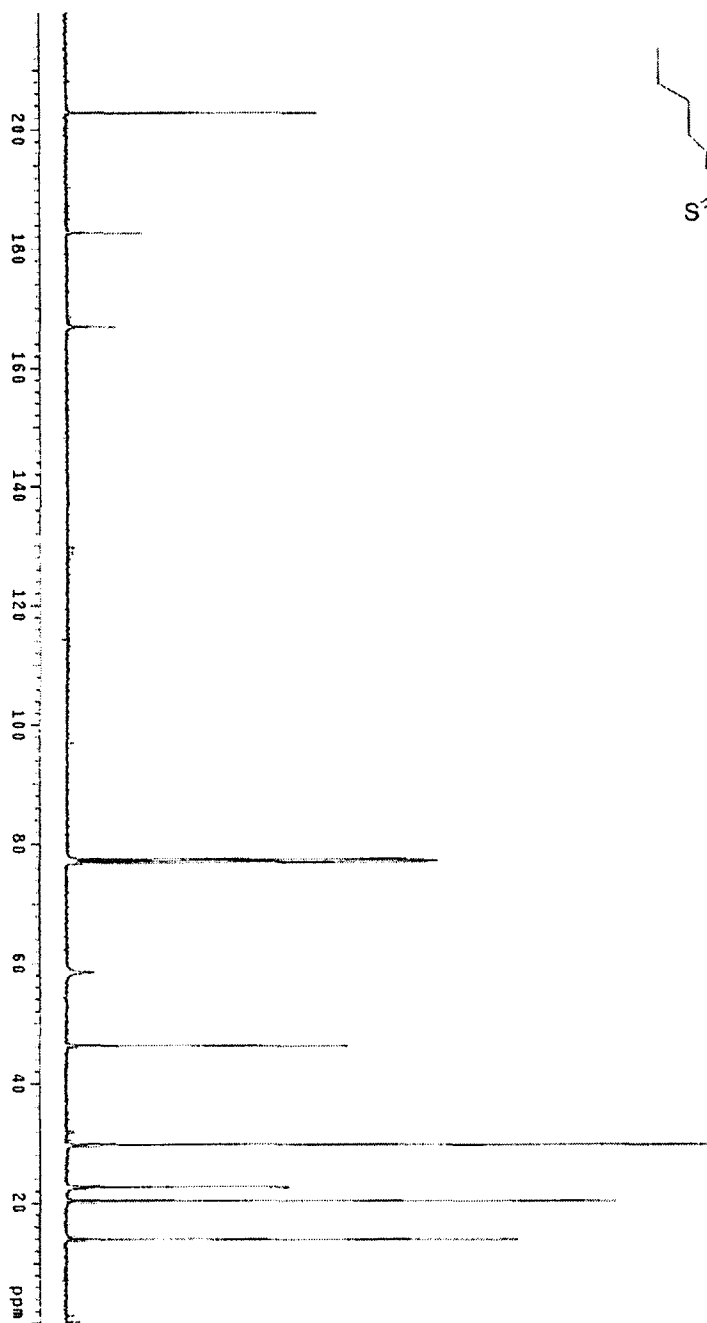
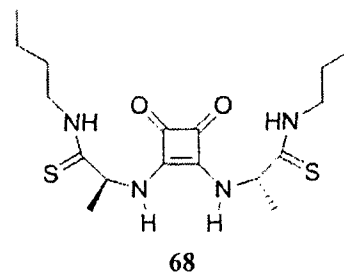


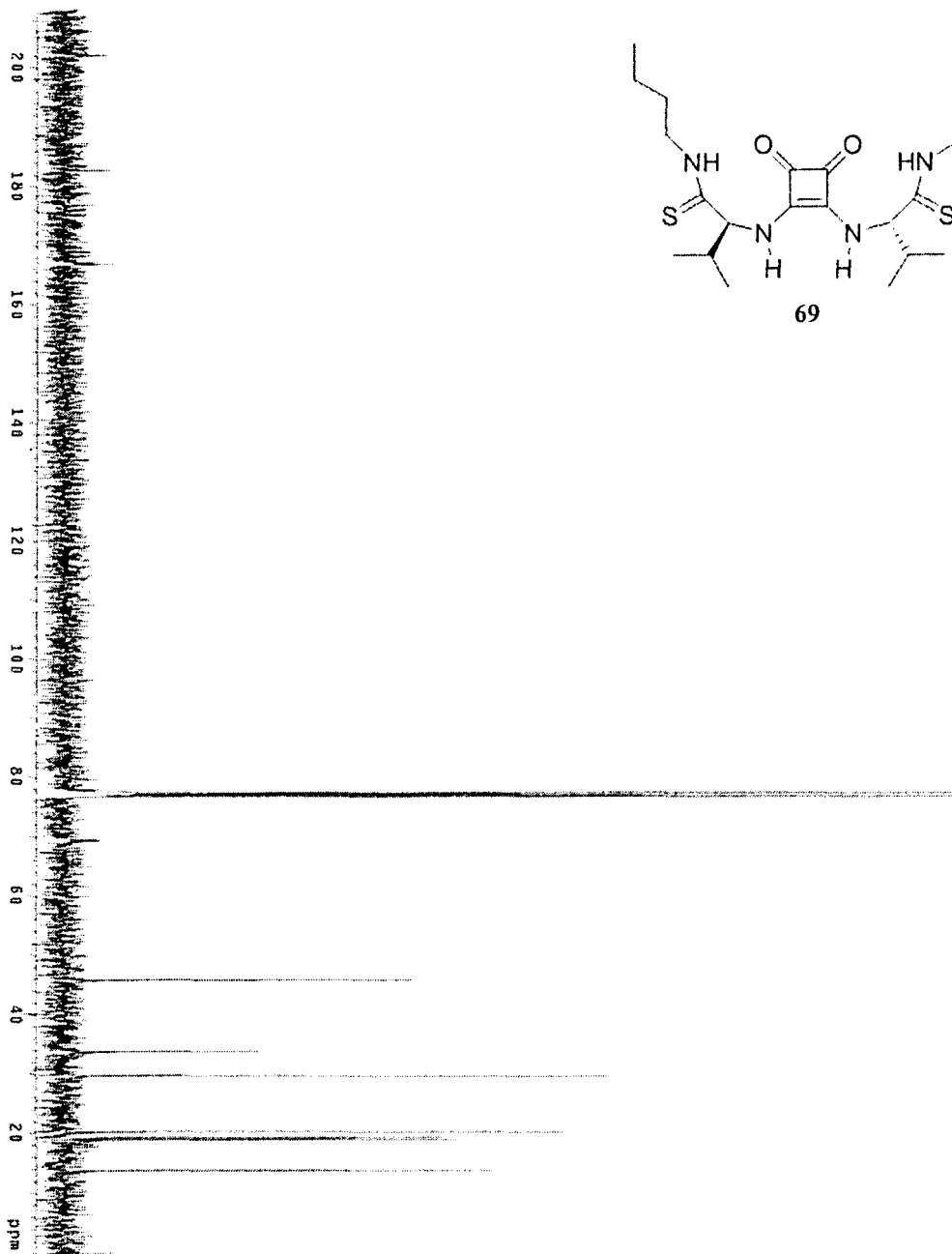


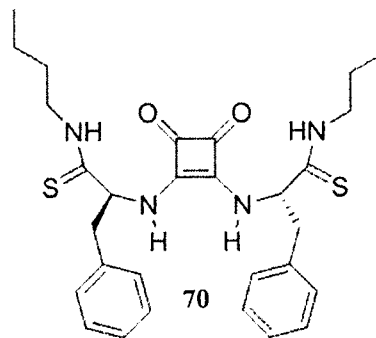
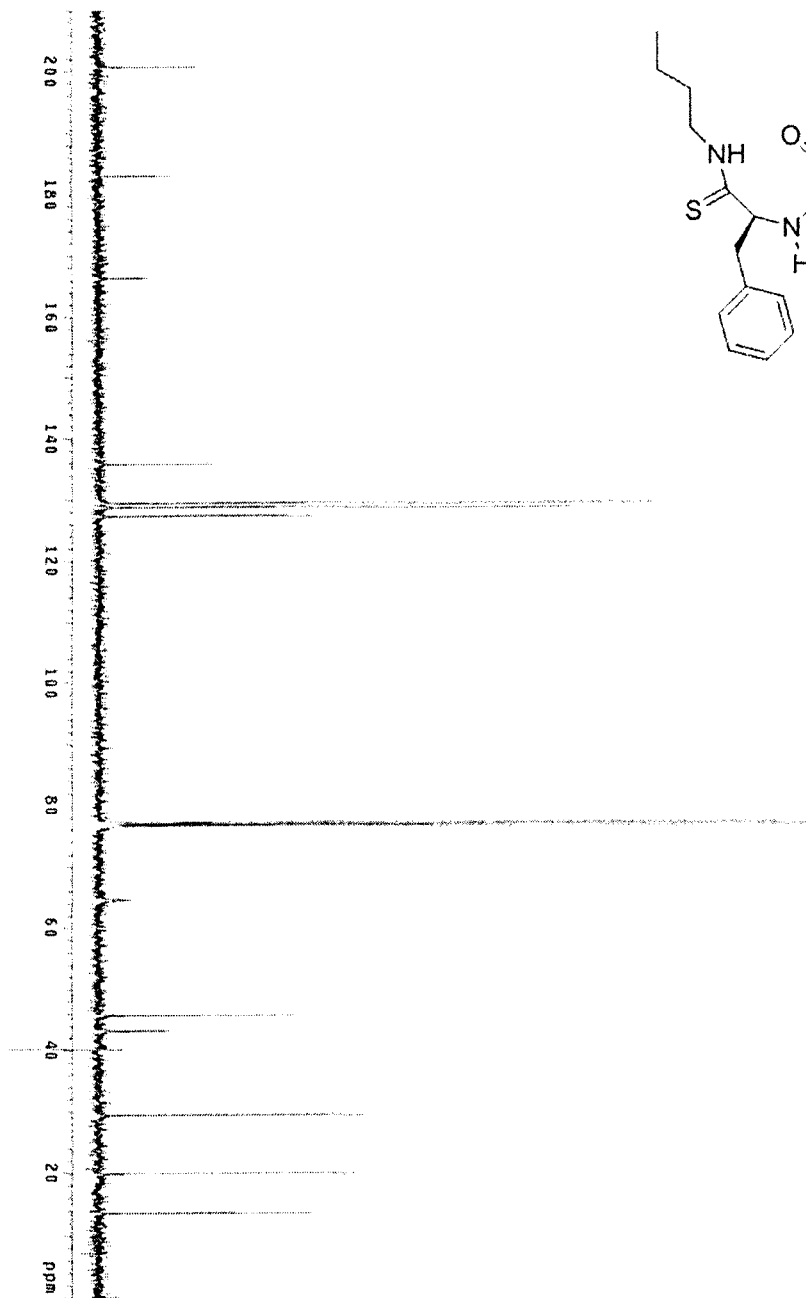
A2. ^{13}C NMR spectra

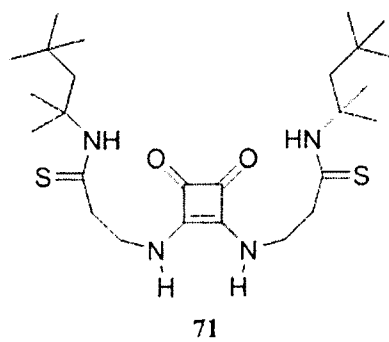


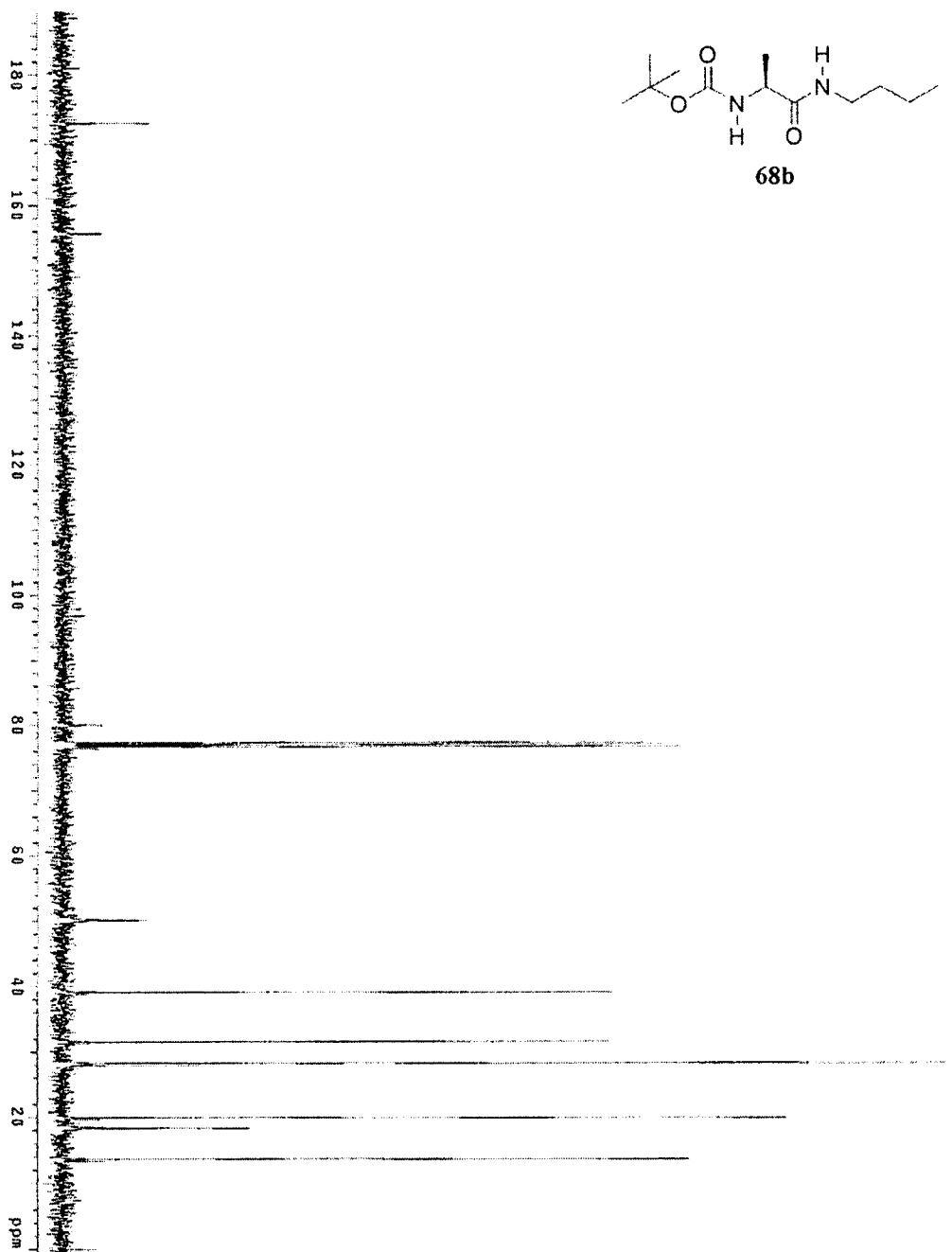
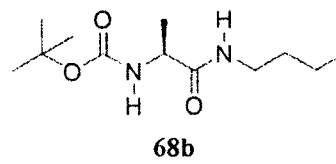


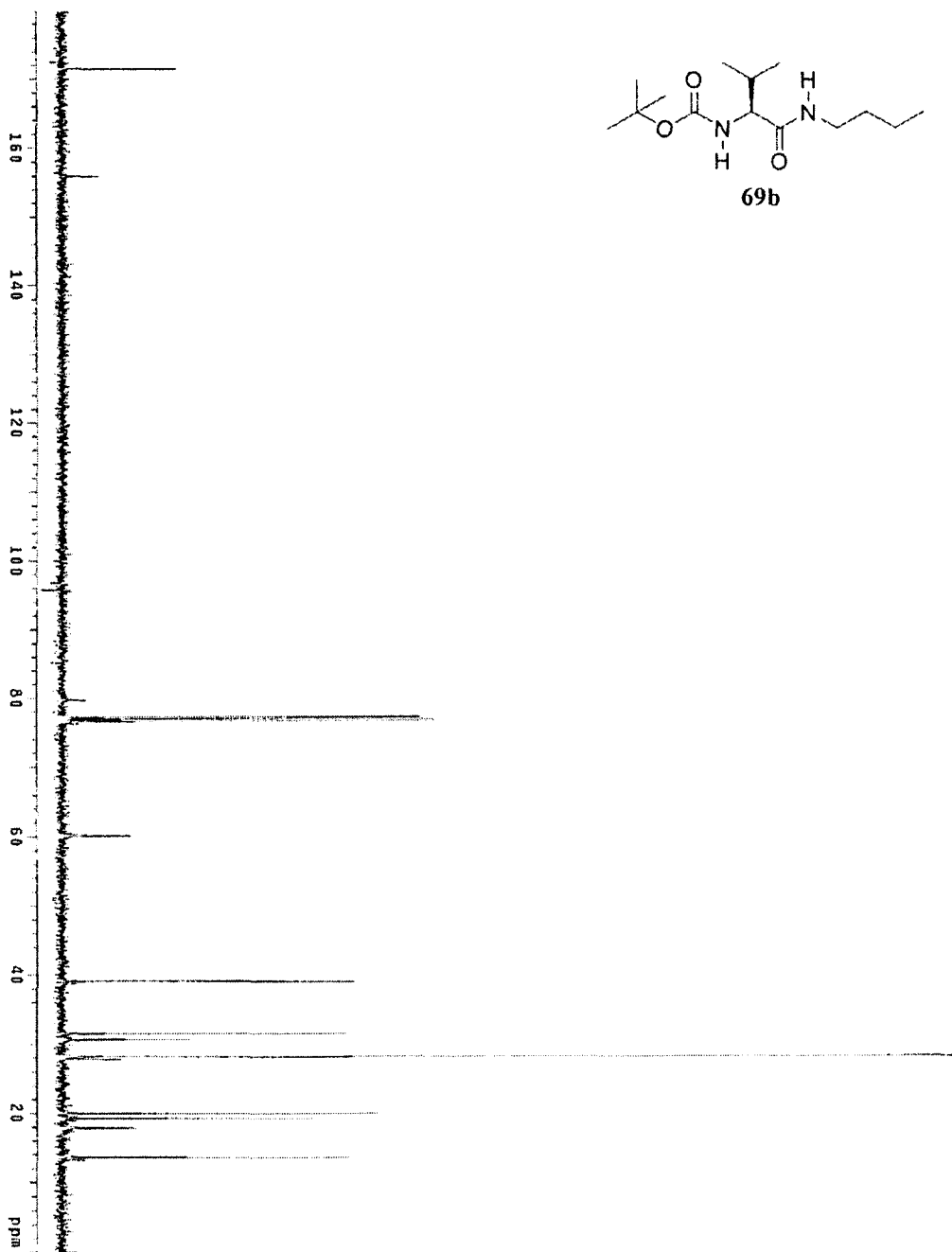
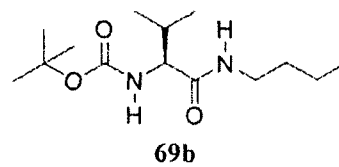


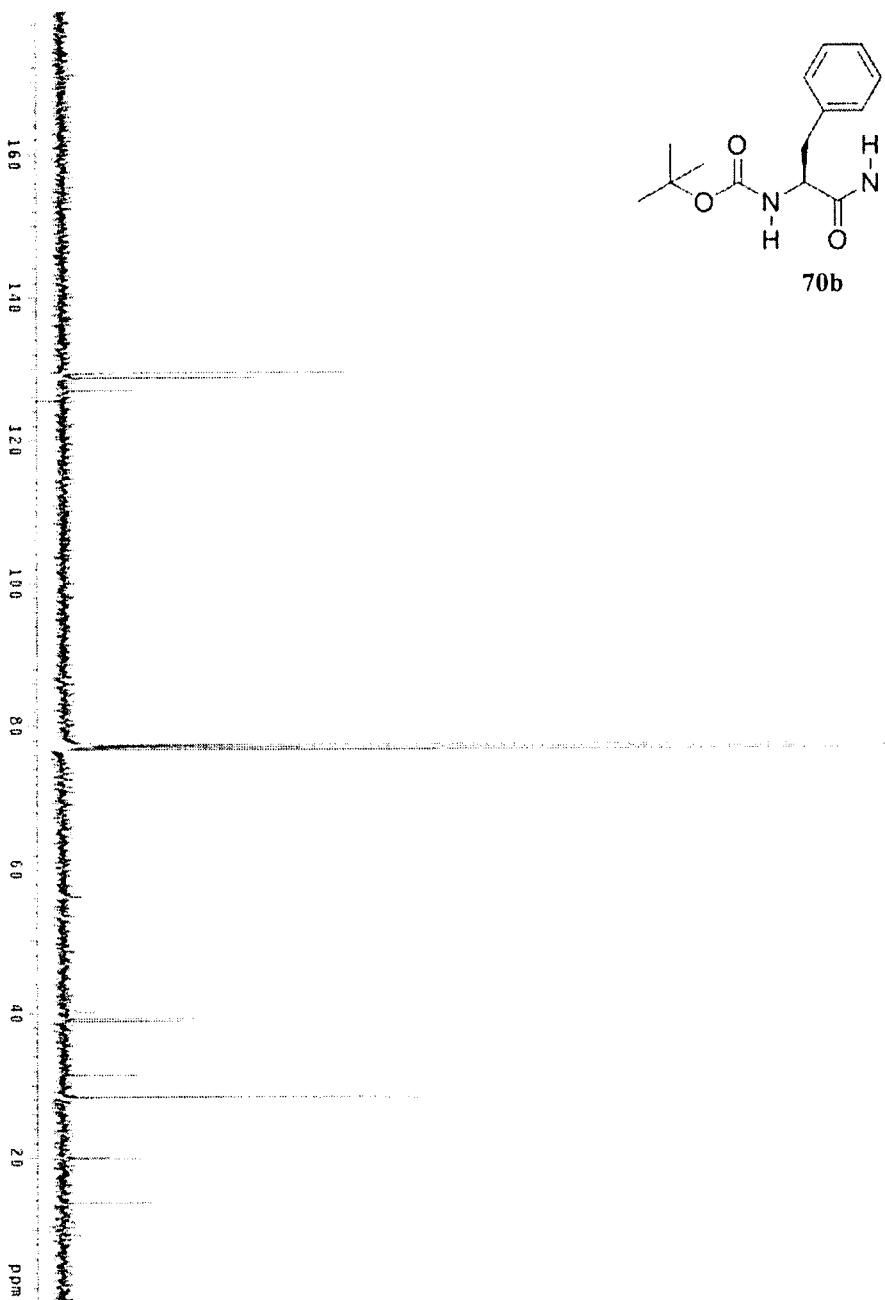
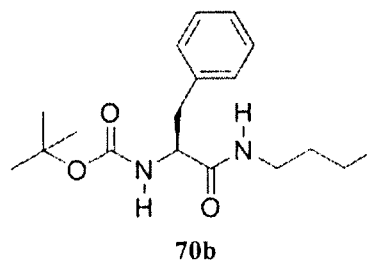


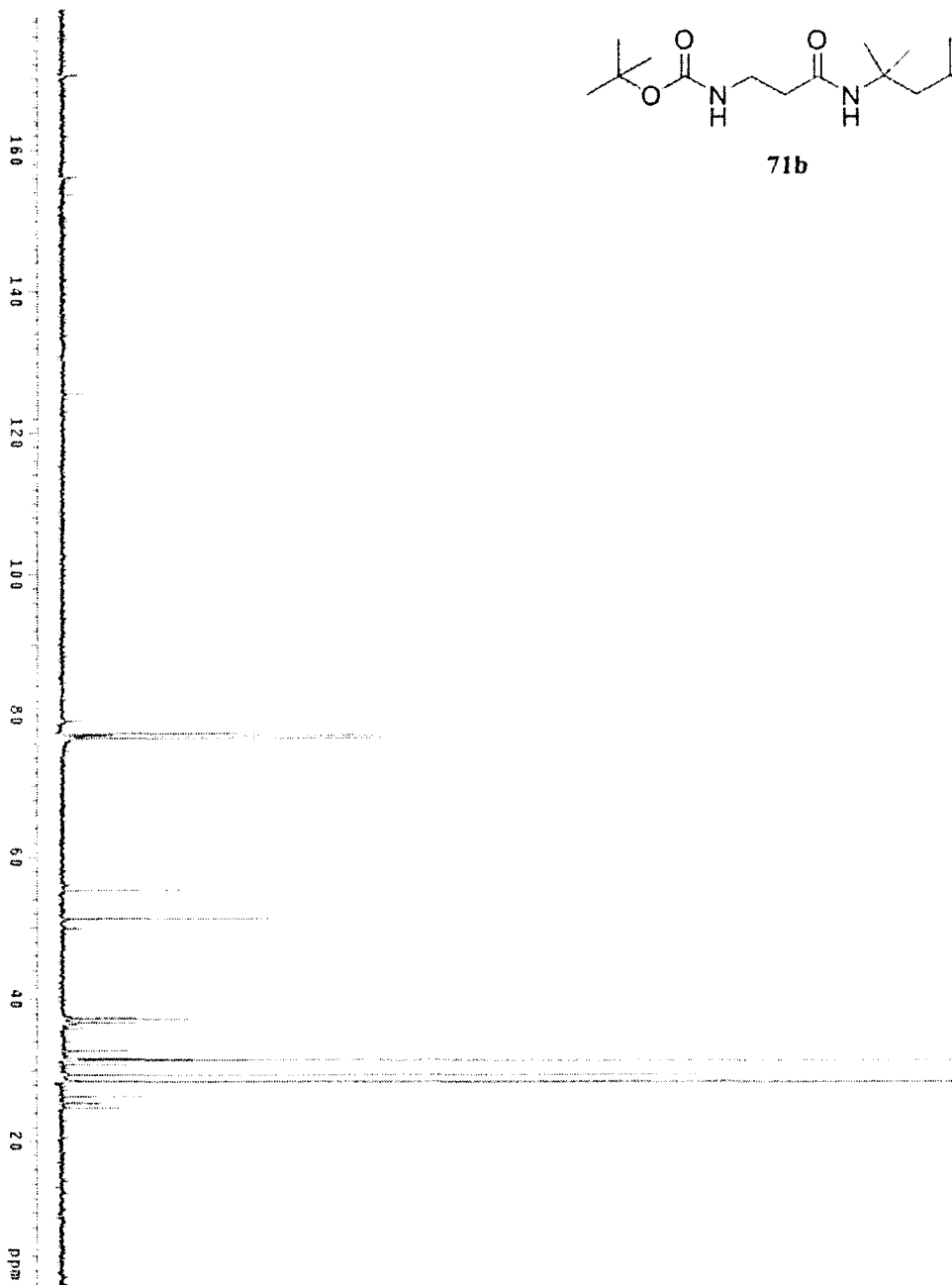
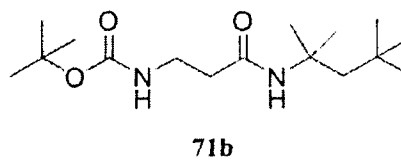


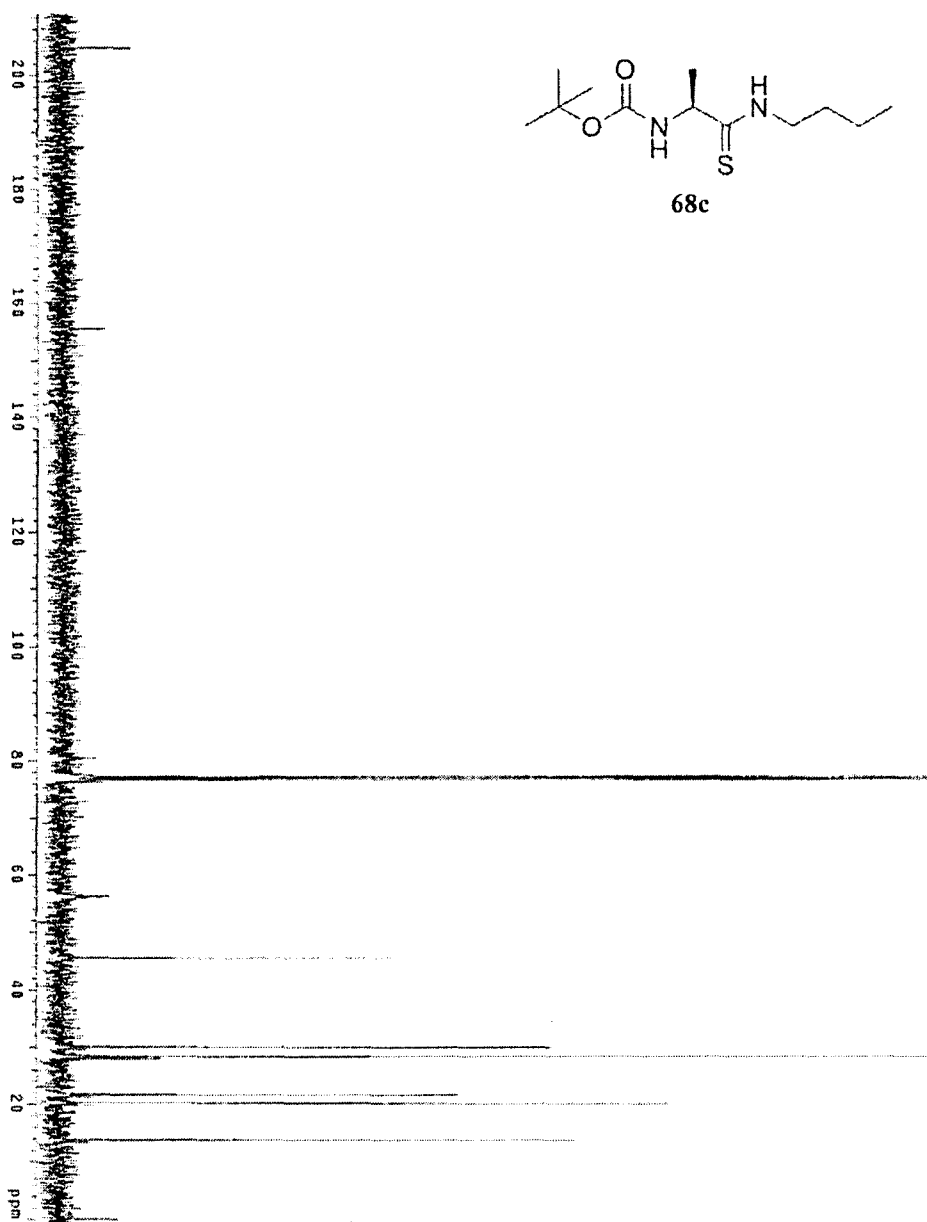
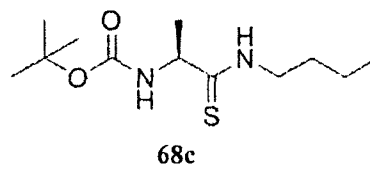


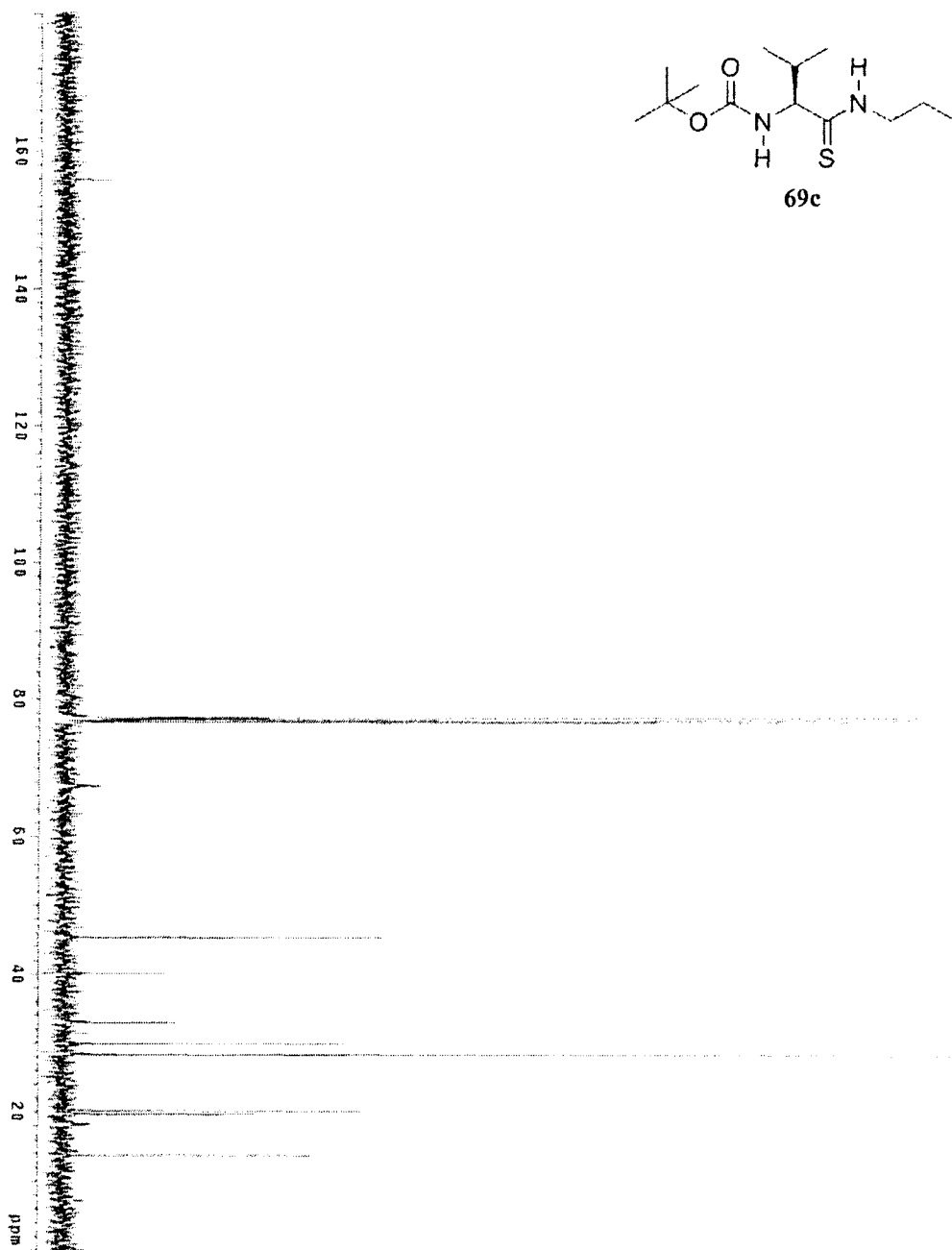
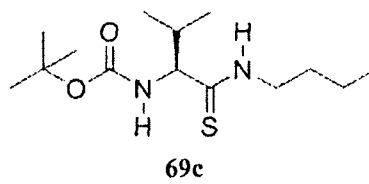


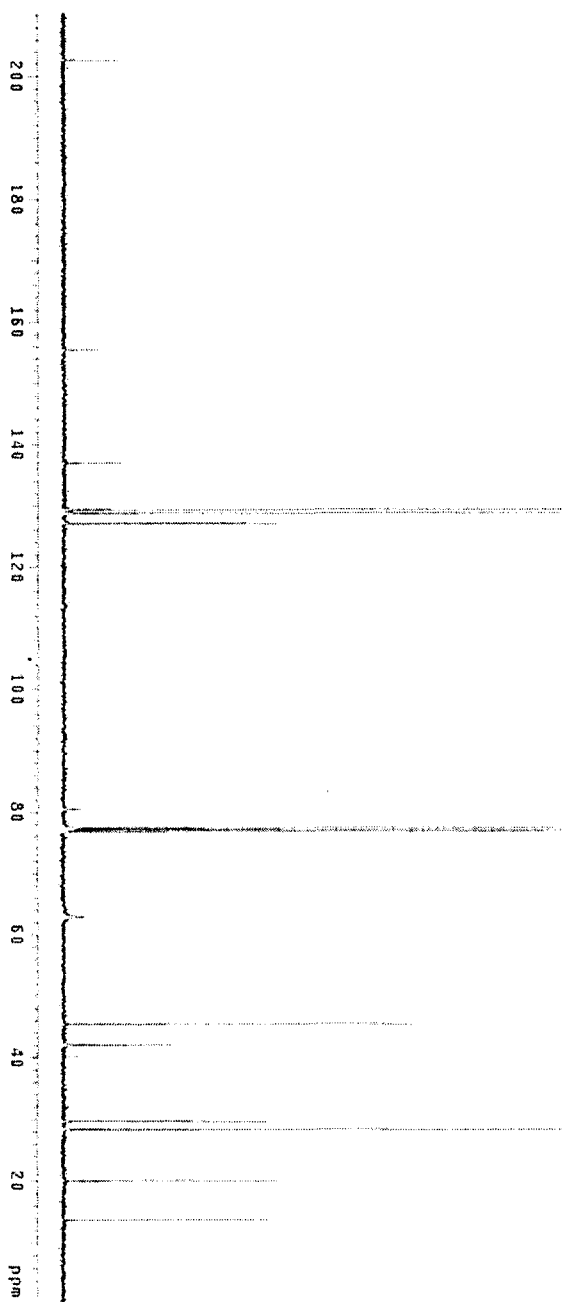
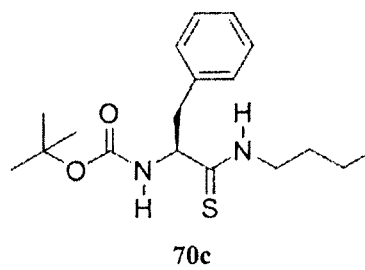


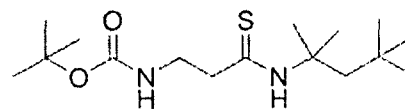




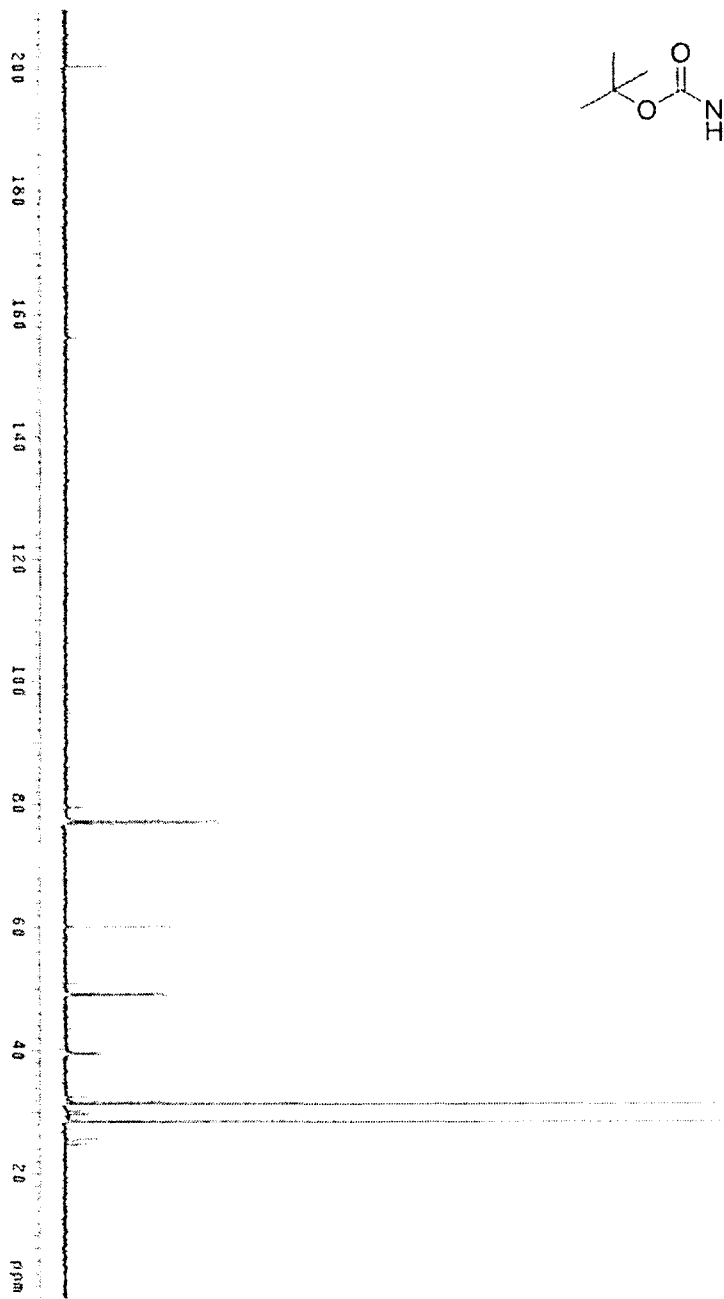


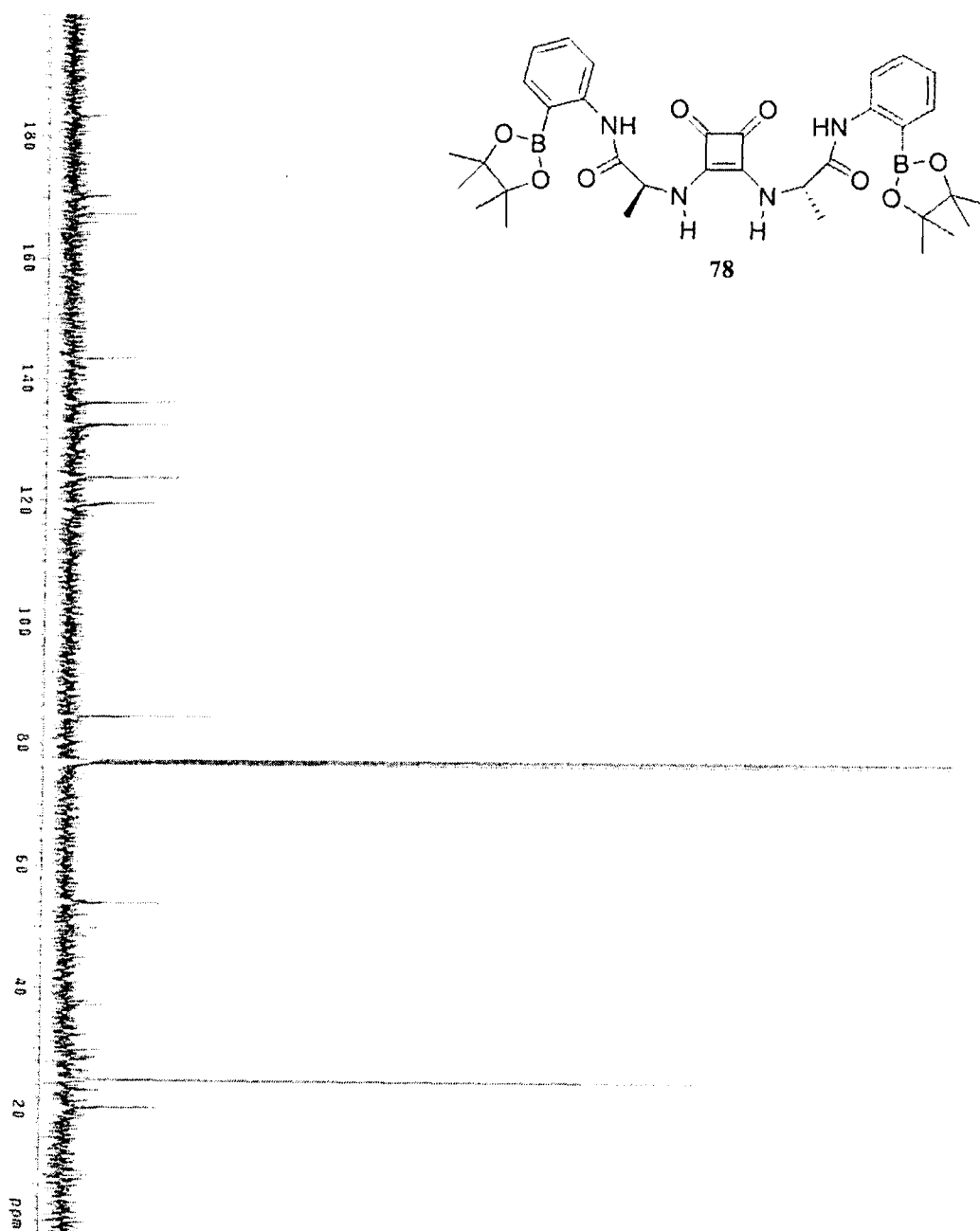


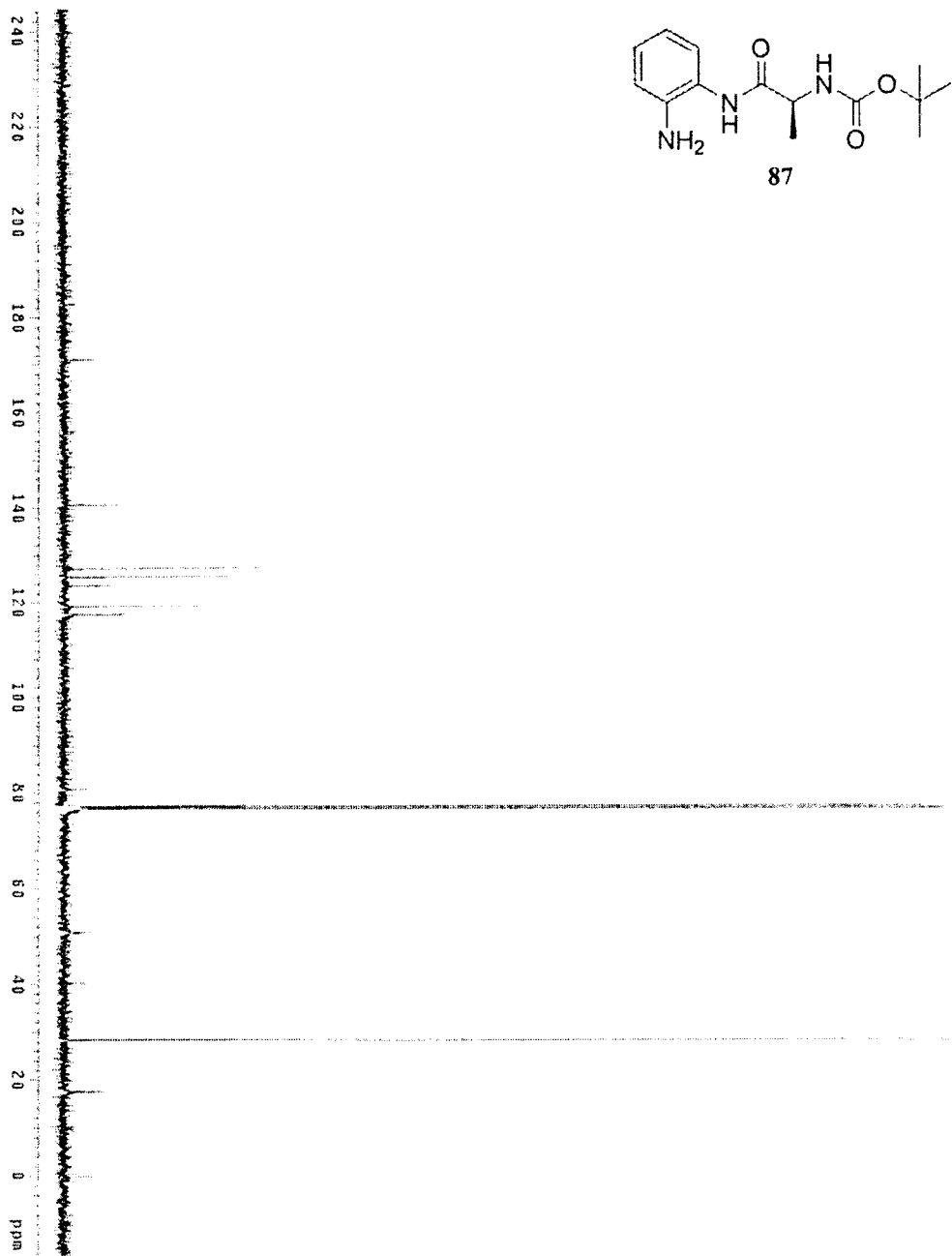
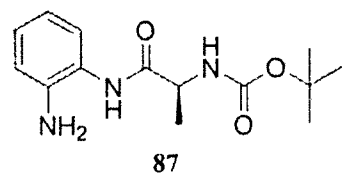


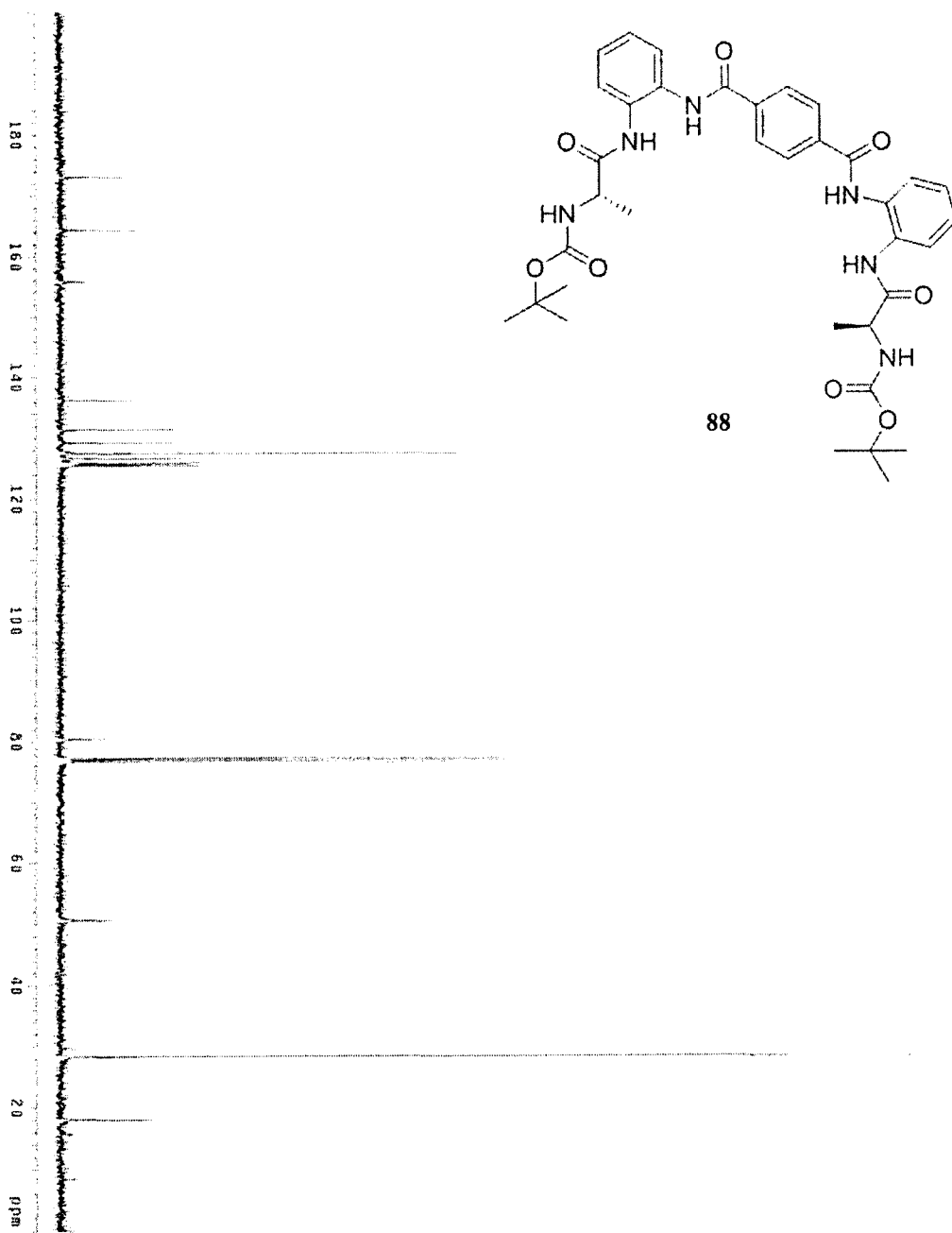


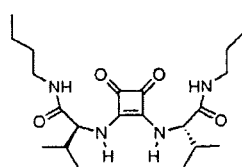
71c



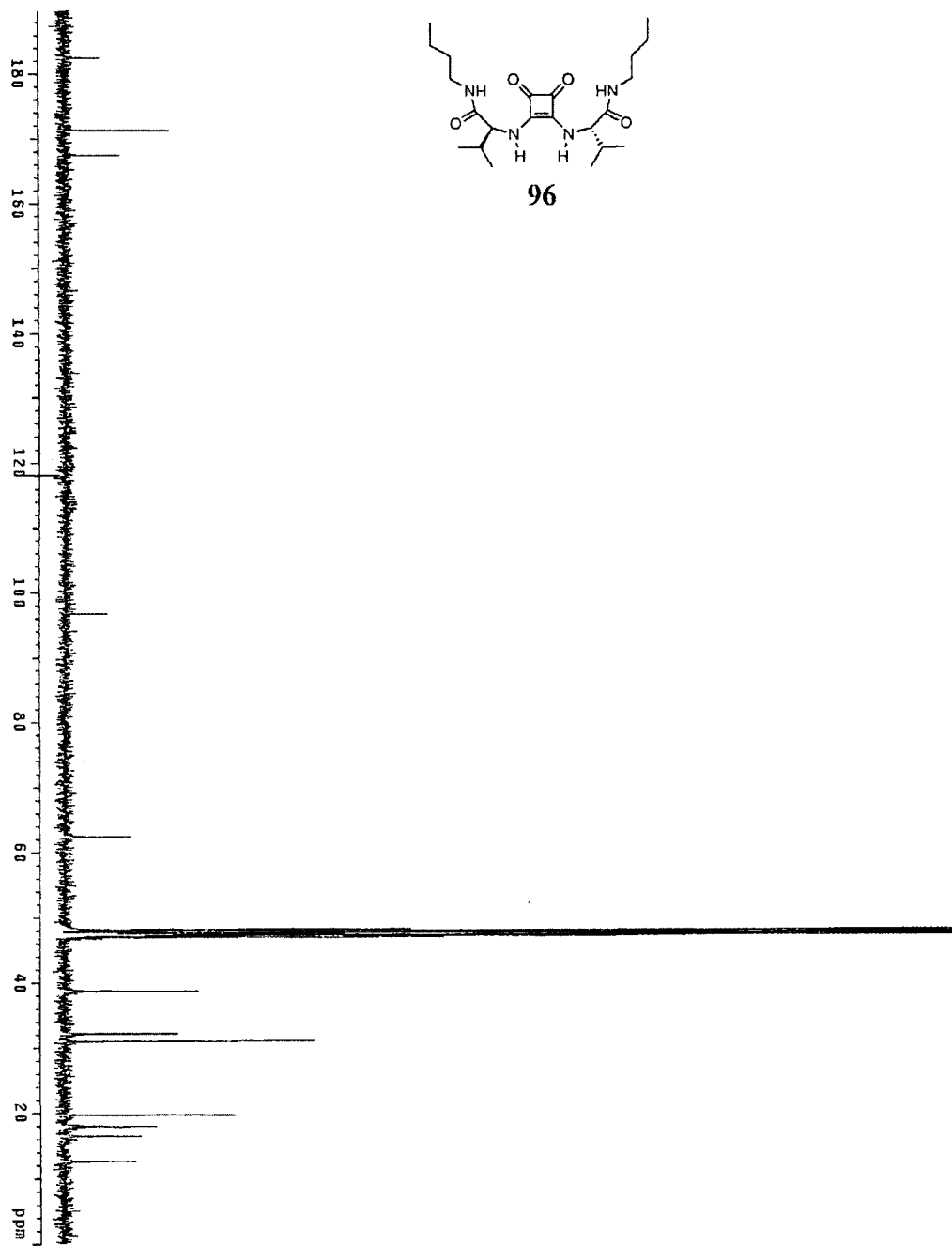


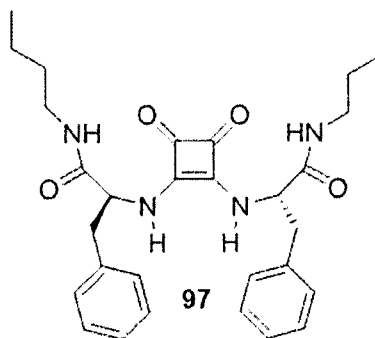
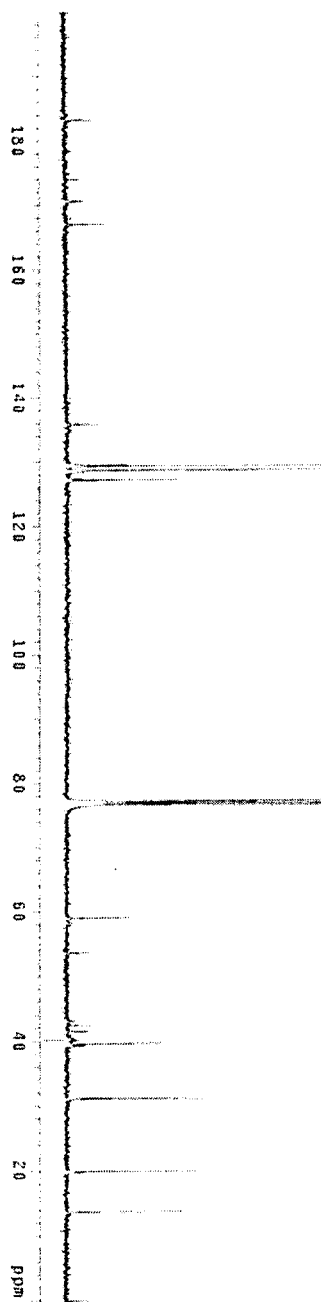


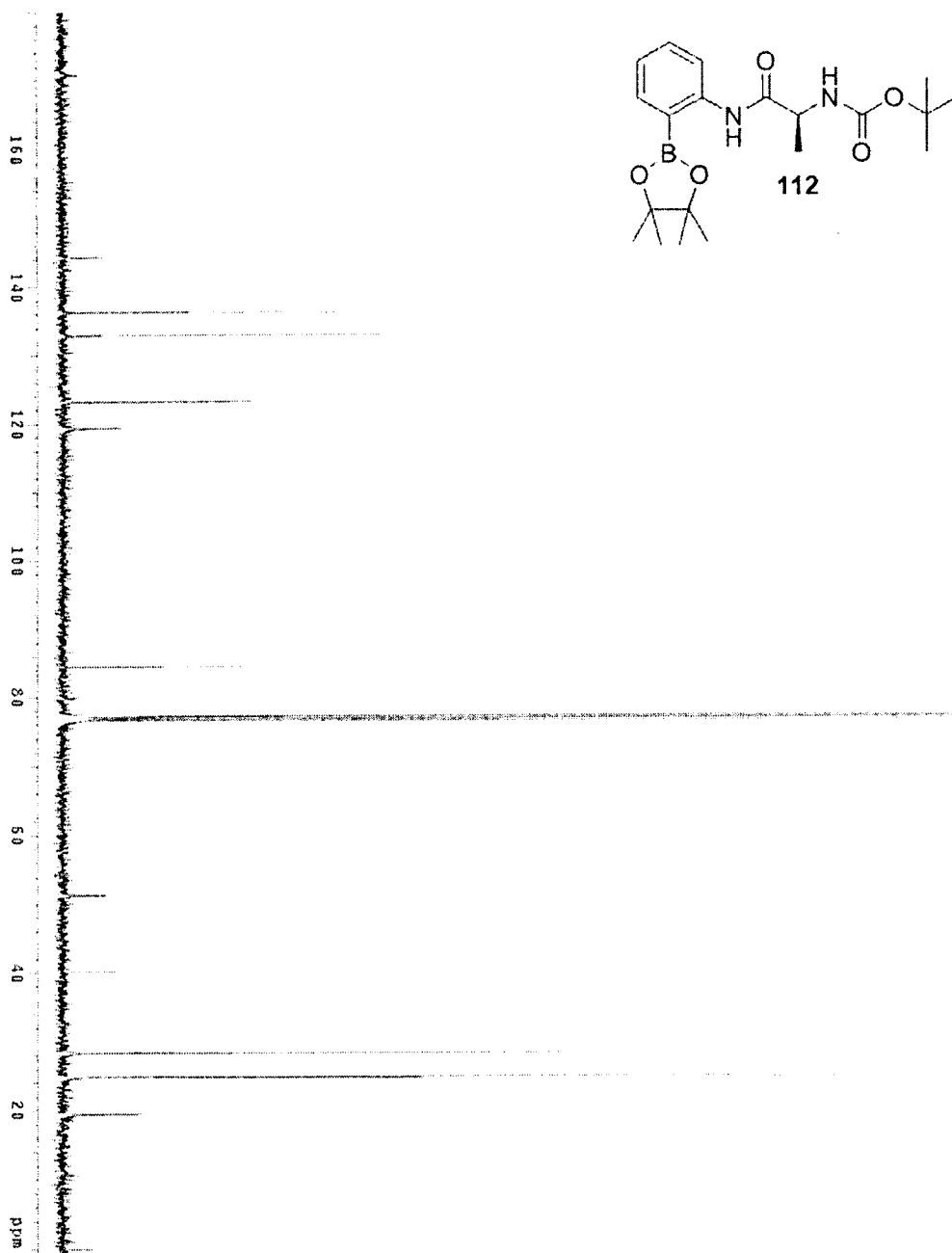




96







Curriculum Vitae

Candidate's full name: David Glen Norman

Universities attended: University of New Brunswick
Fredericton, NB, Canada
B.Sc. (Honours) Biology/Chemistry, May 2000
University of New Brunswick
Fredericton, NB, Canada
M.Sc. candidate in Biology
2001 – 2002
University of New Brunswick
Fredericton, NB, Canada
M.Sc. candidate in Organic Chemistry
2004 – 2006
University of New Brunswick
Fredericton, NB, Canada
Ph.D. candidate in Organic Chemistry
2006 – 2010

Publications: David G. Norman and Ghislain Deslongchamps,
“Squaramide monoanion is an efficient Bronsted acid/base
catalyst for enolization and the direct aldol reaction” (In
preparation).